frontiers | Research Topics

Cancer in domestic, exotic and wild animals: new horizons in tumorigenesis, diagnosis, prognosis and therapeutics through comparative oncology

Edited by
Yasunaga Yoshikawa, Isabel Pires and Leonardo Leonardi

Published in
Frontiers in Veterinary Science

FRONTIERS EBOOK COPYRIGHT STATEMENT

The copyright in the text of individual articles in this ebook is the property of their respective authors or their respective institutions or funders. The copyright in graphics and images within each article may be subject to copyright of other parties. In both cases this is subject to a license granted to Frontiers.

The compilation of articles constituting this ebook is the property of Frontiers.

Each article within this ebook, and the ebook itself, are published under the most recent version of the Creative Commons CC-BY licence. The version current at the date of publication of this ebook is CC-BY 4.0. If the CC-BY licence is updated, the licence granted by Frontiers is automatically updated to the new version.

When exercising any right under the CC-BY licence, Frontiers must be attributed as the original publisher of the article or ebook, as applicable.

Authors have the responsibility of ensuring that any graphics or other materials which are the property of others may be included in the CC-BY licence, but this should be checked before relying on the CC-BY licence to reproduce those materials. Any copyright notices relating to those materials must be complied with.

Copyright and source acknowledgement notices may not be removed and must be displayed in any copy, derivative work or partial copy which includes the elements in question.

All copyright, and all rights therein, are protected by national and international copyright laws. The above represents a summary only. For further information please read Frontiers' Conditions for Website Use and Copyright Statement, and the applicable CC-BY licence.

ISSN 1664-8714
ISBN 978-2-8325-7080-7
DOI 10.3389/978-2-8325-7080-7

Generative AI statement
Any alternative text (Alt text) provided alongside figures in the articles in this ebook has been generated by Frontiers with the support of artificial intelligence and reasonable efforts have been made to ensure accuracy, including review by the authors wherever possible. If you identify any issues, please contact us.

About Frontiers

Frontiers is more than just an open access publisher of scholarly articles: it is a pioneering approach to the world of academia, radically improving the way scholarly research is managed. The grand vision of Frontiers is a world where all people have an equal opportunity to seek, share and generate knowledge. Frontiers provides immediate and permanent online open access to all its publications, but this alone is not enough to realize our grand goals.

Frontiers journal series

The Frontiers journal series is a multi-tier and interdisciplinary set of open-access, online journals, promising a paradigm shift from the current review, selection and dissemination processes in academic publishing. All Frontiers journals are driven by researchers for researchers; therefore, they constitute a service to the scholarly community. At the same time, the *Frontiers journal series* operates on a revolutionary invention, the tiered publishing system, initially addressing specific communities of scholars, and gradually climbing up to broader public understanding, thus serving the interests of the lay society, too.

Dedication to quality

Each Frontiers article is a landmark of the highest quality, thanks to genuinely collaborative interactions between authors and review editors, who include some of the world's best academicians. Research must be certified by peers before entering a stream of knowledge that may eventually reach the public - and shape society; therefore, Frontiers only applies the most rigorous and unbiased reviews. Frontiers revolutionizes research publishing by freely delivering the most outstanding research, evaluated with no bias from both the academic and social point of view. By applying the most advanced information technologies, Frontiers is catapulting scholarly publishing into a new generation.

What are Frontiers Research Topics?

Frontiers Research Topics are very popular trademarks of the *Frontiers journals series*: they are collections of at least ten articles, all centered on a particular subject. With their unique mix of varied contributions from Original Research to Review Articles, Frontiers Research Topics unify the most influential researchers, the latest key findings and historical advances in a hot research area.

Find out more on how to host your own Frontiers Research Topic or contribute to one as an author by contacting the Frontiers editorial office: frontiersin.org/about/contact

Cancer in domestic, exotic and wild animals: new horizons in tumorigenesis, diagnosis, prognosis and therapeutics through comparative oncology

Topic editors

Yasunaga Yoshikawa — Kitasato University, Japan

Isabel Pires — University of Trás-os-Montes and Alto Douro, Portugal

Leonardo Leonardi — University of Perugia, Italy

Citation

Yoshikawa, Y., Pires, I., Leonardi, L., eds. (2025). *Cancer in domestic, exotic and wild animals: new horizons in tumorigenesis, diagnosis, prognosis and therapeutics through comparative oncology*. Lausanne: Frontiers Media SA.

doi: 10.3389/978-2-8325-7080-7

Table of contents

frontiers | Frontiers in Veterinary Science

TYPE Editorial
PUBLISHED 17 October 2025
DOI 10.3389/fvets.2025.1702872

Check for updates

OPEN ACCESS

EDITED AND REVIEWED BY
Ahmed Majeed Al-Shammari,
Mustansiriyah University, Iraq

*CORRESPONDENCE
Yasunaga Yoshikawa
✉ yyoshika@vmas.kitasato-u.ac.jp

RECEIVED 10 September 2025
ACCEPTED 06 October 2025
PUBLISHED 17 October 2025

CITATION
Yoshikawa Y, Pires I and Leonardi L (2025) Editorial: Cancer in domestic, exotic and wild animals: new horizons in tumorigenesis, diagnosis, prognosis and therapeutics through comparative oncology.
Front. Vet. Sci. 12:1702872.
doi: 10.3389/fvets.2025.1702872

COPYRIGHT
© 2025 Yoshikawa, Pires and Leonardi. This is an open-access article distributed under the terms of the Creative Commons Attribution License (CC BY). The use, distribution or reproduction in other forums is permitted, provided the original author(s) and the copyright owner(s) are credited and that the original publication in this journal is cited, in accordance with accepted academic practice. No use, distribution or reproduction is permitted which does not comply with these terms.

Editorial: Cancer in domestic, exotic and wild animals: new horizons in tumorigenesis, diagnosis, prognosis and therapeutics through comparative oncology

Yasunaga Yoshikawa[1]*, Isabel Pires[2] and Leonardo Leonardi[3]

[1]Laboratory of Veterinary Biochemistry, School of Veterinary Medicine, Kitasato University, Aomori, Japan, [2]Animal and Veterinary Research Center (CECAV) University of Trás-os-Montes and Alto Douro, Vila Real, Portugal, [3]Department of Veterinary Medicine, University of Perugia, Perugia, Italy

KEYWORDS

cancer, comparative oncology, dog, elephant (*Loxodonta africana*), giant pandas (*Ailuropoda melanoleuca*), roe deer (*Capreolus capreolus*), human, One Health

Editorial on the Research Topic
Cancer in domestic, exotic and wild animals: new horizons in tumorigenesis, diagnosis, prognosis and therapeutics through comparative oncology

Significant advances in understanding cancer biology have been made in recent years, leading to increasingly accurate and early diagnosis and specific and effective therapeutic treatments. Advances in the identification of increasingly sophisticated prognostic markers have enabled veterinarians to predict the course of many neoplastic diseases, improving the quality of clinical and therapeutic approaches and the rate of recovery for many animals affected by cancer.

Supporting these scientific advances and the fundamental and exciting findings of recent years, biomolecular and comparative studies have also been conducted across multiple animal species, including humans. These studies have allowed for the biological and genetic characterization of numerous tumors, further strengthening the importance of scientific approaches aimed at a "One Health" assessment. The comparative study of cancer in different animal species, including domestic, exotic, and wild animals, can provide valuable information of various types and degrees, with considerable potential for improving diagnostic, prognostic, and therapeutic approaches. Recent studies have shown that even particularly tumor-resistant animals, such as naked mole rats, blind mole rats, elephants, and whales, have attracted increasing attention from researchers, with the aim of characterizing the most intimate mechanisms of disease resistance in these species and breeds (1). These cancer resistance mechanisms observed in these species could offer new strategic approaches for anticancer treatments in humans, as well as in domestic and exotic animals. Therefore, by examining both tumor-prone animals closest to humans, such as dogs and cats, and tumor-resistant species, comparative oncology explores the similarities

and differences between human and animal cancers, contributing to the development of new diagnostic tools, therapies, and preventive strategies that advance both human and veterinary medicine.

These Research Topics can represent important comparative platforms in the field of oncology, representing a new intersection between medical sciences, veterinary sciences, comparative oncology, and wildlife and environmental conservation. Our goal is to create a dynamic channel for sharing cutting-edge scientific knowledge and identifying novel diagnostic, therapeutic, and preventive strategies in the largely unexplored realm of multispecies comparative oncology. This Research Topic presents a broad spectrum of contributions—three original research articles, two short reports, one clinical trial article, and six case reports—covering diverse species, including tumor-prone animals, tumor-resistant species, and wild animals. The following paragraphs summarize the key findings reported by several authors in their nine manuscripts that comprise this Research Topic.

Dogs are among the most commonly tumor-prone species in veterinary medicine. This Research Topic includes several studies focusing on canine tumors. Maniscalco et al. proposed a new scoring system that effectively distinguishes dogs with favorable-prognosis hepatoid gland tumors from those with worse prognoses, thus supporting histological diagnosis. Chu et al. evaluated treatment outcomes in dogs with transitional cell carcinoma (TCC) through a retrospective analysis and suggested that metronomic chemotherapy with chlorambucil was well-tolerated and can be considered as a single-modality treatment or as an adjunct to conventional chemotherapy. Power et al. demonstrated the potential of a novel iron-related metabolic target in canine osteoblastic osteosarcoma using pathological techniques. These results suggest that targeting iron metabolism may represent a novel therapeutic strategy. Tsumoto et al. described a recently introduced method using flow cytometry (FCM) to rapidly detect survivin expression and localization in needle biopsy specimens without anesthesia. The technology could support cancer vaccines and targeted therapies, helping to improve veterinary care through the "one-day first" program. Clinical data were also presented. Xia et al. described a clinical trial of immunotherapy with a vaccine based on dendritic cell/tumor cell fusion and demonstrated its safety. Furthermore, two case reports have indicated the utility of PET in canine cancer (Seok and Lee; Wang et al.). They would be valuable in highlighting the diagnostic and prognostic potential of PET imaging, particularly in detecting metastatic spread, guiding surgical planning, and monitoring treatment response. We also included the rare case of canine cancer. In addition, Pop et al. described a rare ossifying fibroma (OF) of the zygomatic bone in a 9-year-old Hungarian Vizsla.

This Research Topic also features studies on elephants, a non-model but cancer-resistant species that provides valuable insights into anticancer mechanisms. Kitano et al. reported on the responses of elephant cells to interstrand crosslinks in comparison with human cells.

Furthermore, we also included cancer studies focused on wild animals. Xiong et al. (a) and Xiong et al. (b) reported two clinical cases in giant pandas: one described oral fibrosarcoma and the other mandibular osteosarcoma. Vengušt et al. described a rare case of neuroendocrine carcinoma in the nasal cavity of a roe deer, highlighting its histopathological and immunohistochemical characteristics.

Overall, this Research Topic highlights current cancer research in a wide range of animal species, providing fundamental studies and diagnostic and therapeutic tools. It also focuses on comparisons between animals and humans, offering insights into recent advances in comparative oncology.

Author contributions

YY: Writing – original draft, Writing – review & editing. IP: Writing – review & editing. LL: Writing – review & editing.

Funding

The author(s) declare that financial support was received for the research and/or publication of this article. IP receives funding from the European Regional Development Fund (ERDF) through Research, Development and Innovation incentives, under the Regional Programme for Northern Portugal 2021–2027 [NORTE2030]. YY receives funding from Japan Society for the Promotion of Science KAKENHI, under Grant No. 23K05575.

Acknowledgments

We thank the editors, authors, and reviewers that contributed to this Research Topic.

Conflict of interest

The authors declare that the research was conducted in the absence of any commercial or financial relationships that could be construed as a potential conflict of interest.

Generative AI statement

The author(s) declare that Gen AI was used in the creation of this manuscript. The author(s) verify and take full responsibility for the use of generative AI (ChatGPT) in the preparation of this manuscript. Generative AI was used exclusively for language editing, and all content has been reviewed and approved by the author(s).

Any alternative text (alt text) provided alongside figures in this article has been generated by Frontiers with the support of artificial intelligence and reasonable efforts have been made to ensure accuracy, including review by the authors wherever possible. If you identify any issues, please contact us.

Publisher's note

All claims expressed in this article are solely those of the authors and do not necessarily represent those of their affiliated organizations, or those of the publisher, the editors and the reviewers. Any product that may be evaluated in this article, or claim that may be made by its manufacturer, is not guaranteed or endorsed by the publisher.

References

1. Seluanov A, Gladyshev VN, Vijg J, Gorbunova V. Mechanisms of cancer resistance in long-lived mammals. *Nat Rev Cancer.* (2018) 18:433–41. doi: 10.1038/s41568-018-0004-9

frontiers | Frontiers in Veterinary Science

TYPE Case Report
PUBLISHED 26 July 2024
DOI 10.3389/fvets.2024.1429094

Check for updates

OPEN ACCESS

EDITED BY
Yasunaga Yoshikawa,
Kitasato University, Japan

REVIEWED BY
Derek Cissell,
Invicro (United States), United States
Elissa Randall,
Colorado State University, United States

*CORRESPONDENCE
Sungin Lee
✉ sunginlee@chungbuk.ac.kr

RECEIVED 10 May 2024
ACCEPTED 11 July 2024
PUBLISHED 26 July 2024

CITATION
Seok J and Lee S (2024) Case report: Evaluation of cutaneous squamous cell carcinoma metastasized to lymph nodes using ^{18}F-fluoro-2-deoxy-D-glucose positron emission tomography/computed tomography in a dog.
Front. Vet. Sci. 11:1429094.
doi: 10.3389/fvets.2024.1429094

COPYRIGHT
© 2024 Seok and Lee. This is an open-access article distributed under the terms of the Creative Commons Attribution License (CC BY). The use, distribution or reproduction in other forums is permitted, provided the original author(s) and the copyright owner(s) are credited and that the original publication in this journal is cited, in accordance with accepted academic practice. No use, distribution or reproduction is permitted which does not comply with these terms.

Case report: Evaluation of cutaneous squamous cell carcinoma metastasized to lymph nodes using ^{18}F-fluoro-2-deoxy-D-glucose positron emission tomography/computed tomography in a dog

Jin Seok and Sungin Lee*

Department of Veterinary Surgery, College of Veterinary Medicine, Chungbuk National University, Cheongju, Republic of Korea

Introduction: 18F-fluorodeoxy-2-deoxy-D-glucose (FDG) positron emission tomography (PET) is used with high sensitivity in human medicine for initial staging and treatment planning of cutaneous squamous cell carcinoma (SCC). To the best of our knowledge, 18F-FDG PET/computed tomography (CT) has not been used for canine cutaneous SCC with lymph node metastasis.

Case presentation: A 13 year-old spayed female Maltese had rapidly growing flank SCC, which had previously recurred twice. Radiography revealed no metastases. On PET/CT imaging, increased FDG uptake was observed not only in the flank but also in the left axillary lymph node and left inguinal lymph node (standardized uptake value max [SUVmax]: 8.602, 5.354, and 1.96, respectively). Despite the evidence of metastasis, palliative skin mass resection with a 3-cm margin and lymph node dissection were performed. Histopathological examination confirmed the presence of metastases in both lymph nodes.

Discussion: 18F-FDG PET/CT is valuable for the detection of metastatic tumors in various organs. Cutaneous SCC can accumulate 18F-FDG, making it detectable on PET/CT. In this dog with flank SCC, 18F-FDG-PET/CT showed high SUVmax values, indicating its potential for tumor assessment. In veterinary medicine, SUVmax values of 2.5–3.5 are commonly used to identify metastatic lymph nodes in other cancers. Therefore, the interpretation of an SUVmax of 1.96 in an inguinal lymph node for metastatic involvement may be uncertain. Owing to the partial volume effect, 18F-FDG PET/CT has limited sensitivity in identifying LN metastases, particularly in cases of small lesions. Lower SUVmax values adjusted for smaller sizes may better distinguish between benign and malignant lymph nodes. Hence, combining differentiated SUVmax cut-offs based on lymph node size with CT assessment could enhance lymph node evaluation and assist in surgical planning.

KEYWORDS

cutaneous squamous cell carcinoma, flank, lymph node, positron emission tomography, 18F-fluorodeoxyglucose

1 Introduction

Squamous cell carcinoma (SCC) is a malignant neoplasm that originates from keratinocytes and accounts for 5% of canine skin tumors. Common predisposing factors include exposure to solar ultraviolet radiation. It predominantly affects older dogs at approximately 8 years of age. Common sites for SCC include the nail bed, scrotum, nasal planum, legs, and anus. Reports have also documented the occurrence of unpigmented flanks or abdomens in breeds such as Dalmatians and Beagles (1). The metastatic rate of cutaneous SCC in dogs remains unclear but is estimated to be approximately 5% (2). Tumors on the flank or abdomen are usually locally invasive, with low metastatic potential in the lungs or regional lymph nodes (LNs) (1).

Positron emission tomography (PET)/computed tomography (CT) is extensively used in human medicine for the diagnosis and staging of malignant tumors as well as the assessment of metastasis. This imaging technique combines CT for anatomical localization and PET for the imaging of biochemical metabolic changes. Typically, the radiopharmaceutical 18F-fluorodeoxy-2-deoxy-D-glucose (FDG) accumulates in areas of active glucose metabolism. This allows for the early detection of cancers, even those smaller than 1 cm, before visible changes occur based on biochemical abnormalities. Thus, 18F-FDG-PET/CT has a potential role in the early diagnosis and treatment planning of cutaneous SCC with high sensitivity in humans (3).

In veterinary medicine, PET/CT is used to image various tumors and provide valuable diagnostic information (2, 4, 5); however, to our knowledge, there have been no previous reports of cutaneous SCC in dogs. In one study, SCC was diagnosed in two of 14 dogs with standardized uptake value max (SUVmax) values of 12.8 and 17.1, respectively, and the location of the SCC was not mentioned (6). The novelty of this case report that it demonstrates the use of 18F-FDG PET/CT in a dog with histopathologically confirmed cutaneous SCC and regional LN metastases.

2 Case description

A 13-year-old Maltese patient visited our clinic for the evaluation of flank tumor metastases. The tumor had grown rapidly over the past 2 years. The mass initially appeared as a papilloma and was small. On February 28, 2023, the mass was surgically resected under local anesthesia at a local veterinary clinic. However, another mass subsequently recurred caudally to the surgical site and was resected using the same technique on September 22, 2023. After that, the masses recurred at both sites. No pathological diagnoses were made during either surgery. Subsequently, biopsies of both sites were performed at another local veterinary hospital, and SCC was diagnosed by histopathological examination (GreenVet, Yongin, Republic of Korea). The patient presented to our hospital with a bandage placed on the ruptured flank masses.

During physical examination, a ruptured and inflamed masses were found in the central part of the left flank, measuring 3.1 × 1.8 cm cranially and 4.5 × 2.6 cm caudally. The left axillary and inguinal LNs were palpably enlarged, particularly the left axillary node, which was approximately four times larger and significantly firmer than the left inguinal LN, measuring approximately 1 cm in diameter. Radiographs showed gallstones and nephroliths; however, there was no significant metastatic evidence related to the flank mass. Therefore, 18F-FDG PET/CT (Discovery-72 STE; General Electric Medical Systems, Waukesha, WI, USA) was planned for further metastatic evaluation. Before that, the dog underwent pre-anesthetic blood tests, including complete blood count, serum biochemical analysis, and venous blood gas analysis. Except for alkaline phosphatase (158 IU/L, reference range: 29–97 IU/L), reticulocyte count (150.8 × 10^3/μl, reference range: 10.0–110.0 × 10^3/μl), MCV (91.4, reference range: 61.6–73.5 fL), and MCHC (23.6, reference range: 32.0–37.9 g/dl), all other parameters were within normal ranges. FDG uptake may decrease when blood glucose levels exceed 200 mg/dl; however, in the present case, this patient was fasted for approximately 12 h and the glucose level was normal. Prior to the PET/CT scan, the dog was premedicated with midazolam (0.2 mg/kg; Midazolam, Bukwang Pharm. Co., Ltd., Seoul, South Korea), and a urinary catheter was placed. Anesthesia was induced using propofol and maintained with isoflurane. Before the PET scan, CT images (pre- and post-contrast) were obtained using a multidetector CT scanner with settings of 100 mAs and 120 kVp, and a slice thickness of 1.25 mm. Contrast-enhanced scans were performed after intravenous administration of iohexol at a dose of 880 mg/kg. The interval between the 18F-FDG injection and the start of scanning was 45 min, during which the patient was under anesthesia.

In 18F-FDG PET/CT scans, the region of interest was manually defined and the standardized uptake value (SUV) was calculated using the following formula: Average tissue activity concentration (MBq/mL) × body weight (g)/injected dose (MBq). This numerical value provides a semiquantitative assessment of 18F-FDG uptake and serves as an indicator of metabolic activity within the respective regions. The PET/CT scan showed increased 18F-FDG uptake in the left flank mass, the left axillary LN, and left inguinal LN. The corresponding SUVmax values were 5.354 (cranial part of the flank masses), 8.602 (caudal part of the flank masses), 7.453, and 1.961 (Figure 1). CT revealed that the depth of the left flank masses was approximately 6.56 mm. Post-contrast CT imaging showed heterogeneous enhancement in the left axillary LN, measuring 3.74 × 1.58 × 2.5 cm, with apparent invasion into the surrounding tissues (Figures 2A,B). The left inguinal LN measured 7.49 × 8.67 × 6.08 mm with subtle

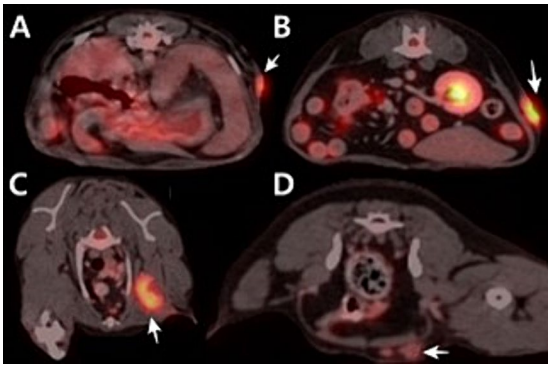

FIGURE 1
Positron emission tomography/computed tomography using 18F-fluorodeoxyglucose fusion images of the dog. **(A)** Cranial part of flank mass. SUVmax is 5.354. **(B)** Caudal part of flank mass. SUVmax is 8.062. **(C)** Axillary lymph node. SUVmax is 7.453. **(D)** Inguinal lymph node. SUVmax is 1.961.

contrast enhancement on post-contrast CT imaging (Figures 2C,D). In addition, the right axillary lymph node (LN) measured 7.65 × 3.22 × 4.63 mm, with homogeneous contrast enhancement on post-contrast CT images and an SUV max of 0.6737 on PET/CT. The right inguinal LN measured 4.49 × 5.18 × 2.59 mm, also showing homogeneous enhancement on post-contrast CT, with an SUV max of 1.526.

Despite the detection of LN metastasis on PET/CT, the patient underwent skin mass resection and a two-site lymphadenectomy for palliative purposes (Figure 3). Based on the previous histopathological examination revealing SCC and considering the high SUVmax (8.602) and history of two recurrences, the masses were deemed to be highly malignant. Therefore, the excision of the flank masses including the subcutaneous fat was planned with 3-cm margin. After premedication with midazolam (0.2 mg/kg; Midazolam, Bukwang Pharm. Co., Ltd., Seoul, South Korea), propofol (6 mg/kg; Provive, Myungmoon Pharm. Co., Ltd., Seoul, South Korea) was administered intravenously to induce anesthesia, which was maintained with isoflurane (Terrell, Piramal Critical Care, Bethlehem, PA, USA). Local infiltration anesthesia was applied on the left flank with a mixture of bupivacaine and lidocaine. Intraoperative pain control was achieved with a continuous infusion of remifentanil (5 μg/kg/min; Tivare BCWORLD Pharm. Co., Ltd., Yeojoo, South Korea).

Histopathological examination of the left flank tumors confirmed SCC extending from the dermis to the subcutis (IDEXX Laboratories, Inc., USA). Keratin pearls were observed within numerous lobules, trabeculae, and islands (Figure 4A). Anisocytosis and anisokaryosis were moderate, with mitotic counts greater than 30. The surgical margins were complete; however, extensive carcinomatous spread to both the left axillary and inguinal LNs was observed (Figures 4B,C). Moderate anisocytosis and anisokaryosis were noted, with approximately 25 mitoses per 10 high-power fields in the inguinal LN and more than 30 mitoses in the axillary LN. There were frequent areas of necrosis throughout the neoplastic tissue. Neoplastic cells were present in the angiolymphatic vessels surrounding the LNs.

On the day after surgery, subcutaneous emphysema developed on the left flank, which resolved after 1 week of compression bandaging. Sutures were removed 14 days post-surgery; no signs of inflammation, tissue edema, or seroma were observed at any surgical sites. The owner declined further metastasis assessment and requested referral to nearby local animal hospital for subsequent management. About 2 months after the surgery, the X-ray showed nodules suspected to be lung metastases, and we were informed that chemotherapy would be started at the local hospital. However, we were not given any information about the specific chemotherapy protocol.

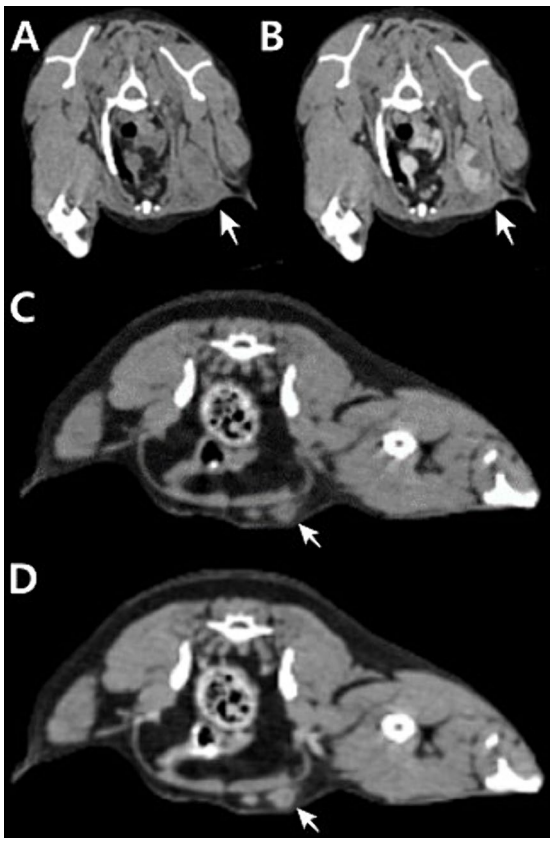

FIGURE 2
Transverse planar computed tomography (CT) images of the left axillary lymph node measuring 3.74 × 1.58 × 2.5 cm **(A,B)** and left inguinal lymph node measuring 7.49 × 8.67 × 6.08 mm **(C,D)**. Pre-contrast CT image **(A,C)**. **(B)** Post-contrast CT image showing heterogeneous enhancement with multifocal areas of necrosis and apparent invasion into the surrounding tissue. **(D)** Post-contrast CT image showing subtle contrast enhancement.

3 Discussion

Cutaneous SCC of the flank typically grows slowly and is locally invasive, with a low metastasis rate. In this case, however, the tumors had rapidly progressed over the past year. The tumors were resected thrice with incomplete margins. PET/CT revealed metastases in the left axillary and inguinal LNs, confirmed by histopathological examination. In humans, failure to completely excise cutaneous SCC increases the likelihood of local recurrence and metastasis (7). Initially, because of their papilloma-like appearance and small size, the tumors were resected with incomplete margins, and histopathological examination was omitted under the assumption that they were papilloma-like lesion. This decision was believed to have contributed to their rapid growth and metastasis. In human medicine, surgical margins for the excision of SCC are determined based on the tumor size, histological grade, and location. However, in veterinary medicine, there are no evidence-based criteria for determining the extent of surgical margins for cutaneous SCC excision, except in the nasal planum (8). In the absence of specific margin recommendations for other sites, T3 and T4 (World Health Organization's tumor-node-metastasis staging system) cases are recommended to have a minimum margin of 2 cm, which is similar to that of nasal planum SCC (9). In this case, the tumors depth exceeded 6 mm and the cranial and caudal parts were >2 cm in diameter. In addition, there was a history of recurrence and LN metastases, classifying this case as high-risk cutaneous SCC based on the human medicine criteria (10). Because obtaining a clear surgical margin is important for a good prognosis, we resected the flank masses with a wide margin of 3 cm and excised the LNs with suspected metastases (Figure 3).

18F-FDG PET/CT is a non-invasive technique that is commonly used for detecting tumor metastasis. The principle behind its use is the Warburg effect, wherein cancer cells have increased glucose utilization,

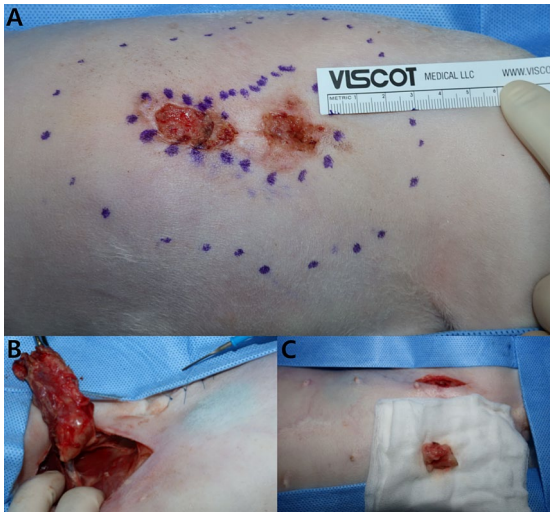

FIGURE 3
Flank skin mass resection and lymphadenectomy. **(A)** The flank mass was excised with a 3-cm margin, including the subcutaneous fat. **(B)** The left axillary lymph node infiltrating the surrounding tissues was excised, noting the mass exceeding 3 cm in size and its palpable firmness. **(C)** The left inguinal lymph node was resected together with the adjacent tissue.

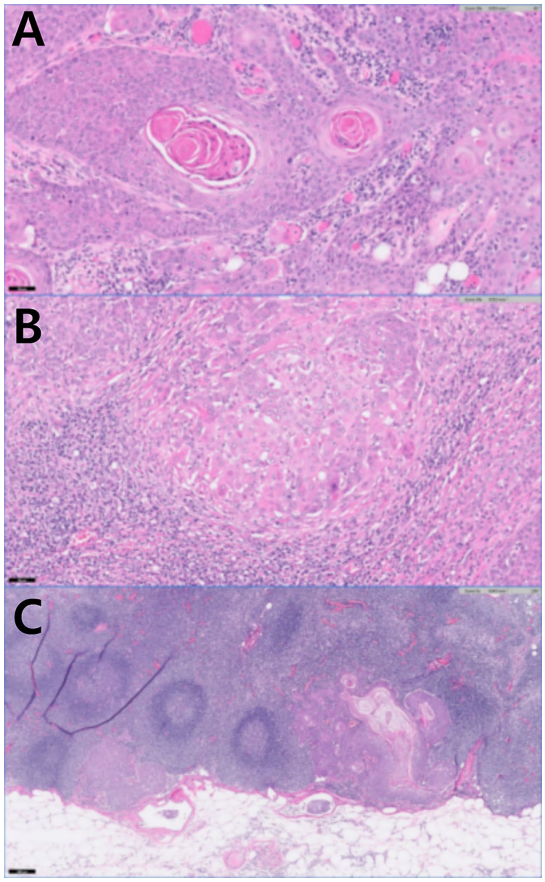

FIGURE 4
Histopathology of the left flank mass after skin mass resection and lymphadenectomy. **(A)** Keratin pearls present in squamous cell carcinoma (H&E stain, original magnification×20, scale bar 100 um). **(B)** Left axillary lymph node with squamous cell carcinoma (H&E stain, original magnification×20, scale bar 50 um). **(C)** Left inguinal lymph node with squamous cell carcinoma (H&E stain, original magnification5, scale bar 200 um).

resulting in elevated FDG uptake through the upregulated expression of GLUT-1 and hexokinase (11). Cutaneous SCC cells express GLUT-1 and can accumulate 18F-FDG (3, 12). In humans, PET/CT is predominantly used to diagnose SCC in areas such as the head, neck, oropharynx, and esophagus, with occasional use for lesions in the trunk and feet (3, 13). In a study of 23 patients diagnosed with cutaneous SCC, all had FDG-positive scans and the mean SUVmax was approximately 10.2 (3). In dogs, carcinomas have higher SUV values compared to sarcomas (SUVmax, 2.0–10.6), with reported SUVmax ranging from 7.6 to 27.0 (6). In one study, 2 of 14 dogs were identified as having SCC with SUVmax values of 12.8 and 17.1, respectively; however, their specific locations were not mentioned (6). Flank SCC in dogs, as observed in this case, had a significantly high SUVmax, indicating the potential for the evaluation of these tumors using 18F-FDG-PET/CT.

LN assessment is critical for staging and treatment planning. In dogs, the normal range of SUVmax for LNs is approximately 0.5–2.0 (14). There is no precedent for assessing LN metastasis in canine cutaneous SCC using PET/CT. Typically, an SUVmax between 2.5 and 3.5 is used as the cutoff value for identifying metastatic LNs (11, 15–17). In humans, metastatic LNs in cutaneous SCC typically exhibit SUVmax values greater than 7, distinguishing them from false-positive conditions, such as lymphadenitis. Conversely, true-negative cases have SUVmax values below 1.4 (18). Therefore, an SUVmax of 1.96 in a LN may be considered ambiguous for diagnosing metastatic involvement. The limited sensitivity of 18F-FDG in identifying LN metastasis is because of the partial volume effect, where radioactivity from small lesions under 10 mm spills into the background, leading to the underestimation of FDG uptake (19). This effect has also been reported in canine mammary gland tumors (20). Several studies have suggested the use of differential SUVmax cut-offs based on LN size, typically using thresholds of 7 or 10 mm, to enhance the sensitivity and accuracy of PET/CT in detecting metastatic LNs (19, 21, 22) and this has also been mentioned in veterinary medicine (23). In this patient, the left inguinal LN size on CT was 7.49 × 8.67 × 6.08 mm, with the longest axis being less than 10 mm. To differentiate between benign and malignant LNs, it may be more appropriate to apply a lower SUVmax that is tailored to smaller LNs. CT is commonly used to show enlarged lymph nodes as an indication of metastasis. However, it is generally accepted that normal-sized lymph nodes can also contain metastases, while enlarged lymph nodes may sometimes be free of metastasis. The evaluation of CT scans with differentiated SUVmax cut-off values based on LN size may provide a more accurate assessment of LN status and assist in selecting biopsy sites during surgery.

In conclusion, this case demonstrates, for the first time, that flank cutaneous SCC metastasizes to regional LNs in dogs with high FDG uptake on PET/CT. Therefore, diagnosing cutaneous SCC and assessing metastasis in dogs is a feasibility of PET/CT, similar to its application in humans. In veterinary medicine, although there are no defined SUVmax cutoff values for malignant LNs, it is important

to consider that LNs smaller than 10 mm may have an FDG uptake lower than the SUVmax of 2.5, even when histopathologically confirmed as malignant metastatic LNs. Although further studies are needed, the interpretation of a lower SUVmax value as the cut-off for LNs <10 mm could enhance the sensitivity of the detection of LN metastasis.

Data availability statement

The original contributions presented in the study are included in the article/supplementary material, further inquiries can be directed to the corresponding author.

Ethics statement

Ethical approval was not required for the studies involving animals in accordance with the local legislation and institutional requirements because this is the case report of a clinical patient, not an experimental research. Written informed consent was obtained from the owners for the participation of their animals in this study.

Author contributions

JS: Writing – review & editing, Writing – original draft, Data curation, Conceptualization. SL: Writing – review & editing, Writing – original draft, Supervision, Funding acquisition, Data curation, Conceptualization.

Funding

The author(s) declare that financial support was received for the research, authorship, and/or publication of this article. This work was supported by the National Research Foundation of Korea (NRF) grant funded by the Korea government (MSIT; RS-2023-00253736) and also supported by "Regional Innovation Strategy (RIS)" through the National Research Foundation of Korea (NRF) funded by the Ministry of Education (MOE; 2024RIS-001).

Acknowledgments

The authors thank the owners of the dog included in this study.

Conflict of interest

The authors declare that the research was conducted in the absence of any commercial or financial relationships that could be construed as a potential conflict of interest.

Publisher's note

All claims expressed in this article are solely those of the authors and do not necessarily represent those of their affiliated organizations, or those of the publisher, the editors and the reviewers. Any product that may be evaluated in this article, or claim that may be made by its manufacturer, is not guaranteed or endorsed by the publisher.

References

1. Vail DM, Thamm DH, Liptak JM. Withrow and MacEwen's small animal clinical oncology-E-book. Amsterdam: Elsevier Health Sciences (2019).

2. Seiler SM, Baumgartner C, Hirschberger J, Beer AJ, Brühschwein A, Kreutzmann N, et al. Comparative oncology: evaluation of 2-Deoxy-2-[18F]fluoro-D-glucose (FDG) positron emission tomography/computed tomography (PET/CT) for the staging of dogs with malignant tumors. *PLoS One*. (2015) 10:e0127800. doi: 10.1371/journal.pone.0127800

3. Mahajan S, Barker CA, Singh B, Pandit-Taskar N. Clinical value of 18F-FDG-PET/CT in staging cutaneous squamous cell carcinoma. *Nucl Med Commun*. (2019) 40:744–51. doi: 10.1097/MNM.0000000000001029

4. Leblanc AK, Jakoby BW, Townsend DW, Daniel GB. 18FDG-PET imaging in canine lymphoma and cutaneous mast cell tumor. *Vet Radiol Ultrasound*. (2009) 50:215–23. doi: 10.1111/j.1740-8261.2009.01520.x

5. Lee D, Yun T, Koo Y, Chae Y, Chang D, Yang MP, et al. 18F-FDG PET/CT image findings of a dog with adrenocortical carcinoma. *BMC Vet Res*. (2022) 18:15. doi: 10.1186/s12917-021-03102-6

6. Hansen AE, McEvoy F, Engelholm SA, Law I, Kristensen AT. FDG PET/CT imaging in canine cancer patients. *Vet Radiol Ultrasound*. (2011) 52:201–6. doi: 10.1111/j.1740-8261.2010.01757.x

7. Roel E, Marsidi N, Michi M, Henny EP, Goeman JJ, Van Kester MS. Incomplete excision of cutaneous squamous cell carcinoma; systematic review of the literature. *Acta Derm Venereol*. (2020) 100:adv00084. doi: 10.2340/00015555-3441

8. Kudnig ST, Séguin B. *Veterinary surgical oncology*. Hoboken, NJ: John Wiley & Sons (2022).

9. Tobias KM, Johnston SA. *Veterinary surgery: Small animal-e-book: 2-volume set*. St. Louis, MO: Elsevier Health Sciences (2013).

10. Jambusaria-Pahlajani A, Miller CJ, Quon H, Smith N, Klein RQ, Schmults CD. Surgical monotherapy versus surgery plus adjuvant radiotherapy in high-risk cutaneous squamous cell carcinoma: a systematic review of outcomes. *Dermatologic Surg*. (2009) 35:574–84. doi: 10.1111/j.1524-4725.2009.01095.x

11. Lin EC, Alavi A. *PET and PET/CT. A clinical guide*. 3rd ed. New York: Thieme (2009).

12. Abdou AG, Eldien MM, Elsakka D. GLUT-1 expression in cutaneous basal and squamous cell carcinomas. *Int J Surg Pathol*. (2015) 23:447–53. doi: 10.1177/1066896915589968

13. Wl W, Chevretton EB, McGurk M, Hussain K, Davis J, Beaney R, et al. A prospective study of PET-FDG imaging for the assessment of head and neck squamous cell carcinoma. *Clin Otolaryngol Allied Sci*. (1997) 22:209–14. doi: 10.1046/j.1365-2273.1997.00852.x

14. Randall EK. PET-computed tomography in veterinary medicine. *Vet Clin North Am Small Anim Pract*. (2016) 46:515–33. doi: 10.1016/j.cvsm.2015.12.008

15. Willcox JL, Spriet M, Zwingenberger AL, Phillips KL, Burton JH, Skorupski KA, et al. Evaluation of accuracy for 18 F-FDG positron emission tomography and computed tomography for detection of lymph node metastasis in canine oral malignant melanoma. *Vet Comp Oncol*. (2021) 19:463–72. doi: 10.1111/vco.12651

16. Bassett CL, Daniel GB, Legendre AM, Bochsler PN, Smith GT. Characterization of uptake of 2-deoxy-2-[18F] fluoro-D-glucose by fungal-associated inflammation: the standardized uptake value is greater for lesions of blastomycosis than for lymphoma in dogs with naturally occurring disease. *Mol Imaging Biol*. (2002) 4:201–7. doi: 10.1016/S1536-1632(02)00002-1

17. Çaylaklı F, Yılmaz S, Özer C, Reyhan M. The role of PET-CT in evaluation of cervical lymph node metastases in oral cavity squamous cell carcinomas. *Turk Arch Otorhinolaryngol*. (2015) 53:67–72. doi: 10.5152/tao.2015.608

18. Fujiwara M, Suzuki T, Takiguchi T, Fukamizu H, Tokura Y. Evaluation of positron emission tomography imaging to detect lymph node metastases in patients with high-risk cutaneous squamous cell carcinoma. *J Dermatol*. (2016) 43:1314–20. doi: 10.1111/1346-8138.13403

19. Bae SU, Won KS, Song BI, Jeong WK, Baek SK, Kim HW. Accuracy of F-18 FDG PET/CT with optimal cut-offs of maximum standardized uptake value according to size for diagnosis of regional lymph node metastasis in patients with rectal cancer. *Cancer Imaging*. (2018) 18:32. doi: 10.1186/s40644-018-0165-5

20. Sánchez D, Romero L, López S, Campuzano M, Ortega R, Morales A, et al. 18F-FDG-PET/CT in canine mammary gland tumors. *Front Vet Sci*. (2019) 6:280. doi: 10.3389/fvets.2019.00280

21. Murakami R, Uozumi H, Hirai T, Nishimura R, Shiraishi S, Ota K, et al. Impact of FDG-PET/CT imaging on nodal staging for head-and-neck squamous cell carcinoma. *Int J Radiat Oncol Biol Phys*. (2007) 68:377–82. doi: 10.1016/j.ijrobp.2006.12.032

22. Bianchini C, Caracciolo M, Urso L, Ciorba A, Bonsembiante A, Migliorelli A, et al. Role of 18F-FDG PET/CT in evaluating lymph node status in patients with head and neck squamous cell carcinoma. *Acta Otorhinolaryngol Ital*. (2023) 43:235–44. doi: 10.14639/0392-100X-N2370

23. Randall E, Kraft S, Yoshikawa H, LaRue S. Evaluation of 18F-FDG PET/CT as a diagnostic imaging and staging tool for feline oral squamous cell carcinoma. *Vet Comp Oncol*. (2016) 14:28–38. doi: 10.1111/vco.12047

frontiers | Frontiers in Veterinary Science

TYPE Clinical Trial
PUBLISHED 20 August 2024
DOI 10.3389/fvets.2024.1397518

Check for updates

OPEN ACCESS

EDITED BY
Leonardo Leonardi,
University of Perugia, Italy

REVIEWED BY
Serenella Silvestri,
Centre for Haemato-Oncology Research (CREO), Italy
Cristina Massoco,
University of São Paulo, Brazil

*CORRESPONDENCE
Jih-Jong Lee
✉ jacklee@ntu.edu.tw

RECEIVED 07 March 2024
ACCEPTED 05 August 2024
PUBLISHED 20 August 2024

CITATION
Xia Y-Y, Liao AT, Liu R-M, Yang S-Y, Kuo C-C, Ke C-H, Lin C-S and Lee J-J (2024) Immunotherapeutic allogeneic dendritic cell and autologous tumor cell fusion vaccine alone or combined with radiotherapy in canine oral malignant melanoma is safe and potentially effective.
Front. Vet. Sci. 11:1397518.
doi: 10.3389/fvets.2024.1397518

COPYRIGHT
© 2024 Xia, Liao, Liu, Yang, Kuo, Ke, Lin and Lee. This is an open-access article distributed under the terms of the Creative Commons Attribution License (CC BY). The use, distribution or reproduction in other forums is permitted, provided the original author(s) and the copyright owner(s) are credited and that the original publication in this journal is cited, in accordance with accepted academic practice. No use, distribution or reproduction is permitted which does not comply with these terms.

Immunotherapeutic allogeneic dendritic cell and autologous tumor cell fusion vaccine alone or combined with radiotherapy in canine oral malignant melanoma is safe and potentially effective

Yuan-Yuan Xia[1,2], Albert TaiChing Liao[1], Ru-Min Liu[1], Shu-Ya Yang[1], Chien-Chun Kuo[1], Chiao-Hsu Ke[1], Chen-Si Lin[1] and Jih-Jong Lee[2,3]*

[1]Department of Veterinary Medicine, School of Veterinary Medicine, National Taiwan University, Taipei, Taiwan, [2]Graduate Institute of Veterinary Clinical Science, School of Veterinary Medicine, National Taiwan University, Taipei, Taiwan, [3]National Taiwan University Veterinary Hospital, National Taiwan University, Taipei, Taiwan

Introduction: Immunotherapy represents a promising breakthrough in cancer management and is being explored in canine melanomas. Dendritic cells (DCs) play a crucial role in priming T-cell-mediated immune reactions through the antigen-presenting function. Combining immunotherapy and radiation therapy may generate more substantial anti-cancer efficacy through immunomodulation.

Objectives: Our research reported a preliminary result of the safety and outcome of a kind of immunotherapy, the allogeneic dendritic cell and autologous tumor cell fusion vaccine, alone or in combination with hypofractionated radiation therapy, in canine oral malignant melanoma.

Methods: Two groups of dogs with histopathological diagnoses of oral malignant melanoma were recruited. In group 1 (DCRT), dogs received a combination of DC fusion vaccine and radiotherapy. In group 2 (DC), dogs received DC fusion vaccine alone. DC vaccination was given once every 2 weeks for four doses. Radiotherapy was performed weekly for five fractions. Dogs that received carboplatin were retrospectively collected as a control group (group 3).

Results: Five dogs were included in group 1 (two stage II, three stage III), 11 in group 2 (three stage I/II, eight stage III/IV), and eight (two stage I/II, six stage III/IV) in the control group. Both DC and DCRT were well-tolerated, with only mild adverse events reported, including mucositis, gastrointestinal discomfort, and injection site reactions. The median progression-free intervals in groups 1, 2, and 3 were 214 (95% CI, NA, due to insufficient data), 100 (95% CI, 27–237), and 42 days (95% CI, NA-170), respectively, which were not significantly different. The 1-year survival rates were 20, 54.5, and 12.5% in groups 1, 2, and 3. Dogs in the DCRT group exhibited significantly higher TGF-β signals than the DC group throughout the treatment course, indicating a possible higher degree of immunosuppression.

Conclusion: The manuscript demonstrated the safety of dendritic cell/tumor cell fusion vaccine immunotherapy, alone or in combination with radiotherapy. The results support further expansion of this immunotherapy, modification

of combination treatment and protocols, and investigation of combining DC vaccine with other treatment modalities.

Clinical trial registration: Preclinical Trials, PCTE0000475.

KEYWORDS

canine oral melanoma, immunotherapy, dendritic cell fusion vaccine, radiotherapy, immunotherapy combined with radiation

1 Introduction

Canine oral malignant melanoma (OMM) is the most common tumor in the canine oral cavity and its management remains challenging due to its propensity for local invasion and distant metastasis (1). Surgery and radiation therapy (RT) provide the most effective tumor controls which primarily target local tumor invasion. Hypofractionated radiation, as reported in several studies, has been commonly used in canine OMM, demonstrating an overall 81–100% tumor response rate with tolerable side effects. Reported median survival times of dogs with OMM undergoing RT alone range from 171 to 307 days, while additional systemic treatments appeared to have minimal impact on survival (2–5). Considering the high rate of distant metastasis, systemic treatment against canine OMM is imperative. Conventional chemotherapy utilizing platinum-based agents, however, only offered a modest 28–37% response rate (6, 7). In our department, using chemotherapy in dogs with OMM lacking wide-margin surgery resulted in a 12.5% response rate and a median overall survival of 6 months (8). Evidence of therapeutic effects in canine OMM is also limited for tyrosine kinase inhibitors (TKIs) (9, 10). On the other hand, immunotherapy, aiming to activate and modulate the immune system, is the fourth pillar in both human and veterinary cancer management.

At the time of this manuscript preparation, two commercialized immunotherapeutic drugs were approved for treating canine malignant melanoma. The first is the US FDA and USDA-approved DNA vaccine Oncept®, which expresses xenogeneic human tyrosinase and is applied for dogs with stage II/III oral melanoma after surgical control since 2007. Theoretically, the DNA product was designed to induce an immunostimulatory function, but the clinical experiences were controversial (11, 12). Although some long-term survivors were observed, and it remained an option due to the vaccine's general safety, more solid evidence of efficacy was required. The second, the immune checkpoint inhibitor (ICI), represents a promising immunotherapeutic breakthrough in human and canine cancer fields. In late 2023, the commercialized canine anti-programmed cell death receptor-1 (PD-1) antibody Gilvetmab was conditionally approved by the USDA for canine mast cell tumor and malignant melanoma treatment, and further clinical studies are underway to investigate its toxicity and efficacy. Other research on canine ICIs showed some survival benefits in end-stage OMM dogs. In the study conducted by Igase et al. (13) the anti-PD-1 treatment induced a 26.5% response rate. And Maekawa et al. (14) reported that the anti-PD-ligand-1 (PD-L1) treatment resulted in a significantly prolonged survival of 143 days compared to a historical control.

Our team has constructed a cancer immunotherapeutic vaccine by fusing autologous cancer cells with allogeneic dendritic cells (DCs) and re-injecting the fusion product subcutaneously into tumor-bearing dogs. This approach aimed to capitalize on the great antigen-presenting and processing ability of DCs, to prime a specific anti-tumor immune response involving both CD4 and CD8 T cells (15). Previously, Gyorffy et al. (16) reported a successful generation of autologous bone-marrow-derived DCs (BMDCs) from three melanoma dogs and a healthy dog. After infection with the human xenoantigen gp100, the DC-product was re-injected into dogs, with a combination of RT. Although the case number was low, two out of three melanoma dogs lived for over 20 months. However, because the DC function might be defective during tumor proliferation process (15), an allogeneic DC source from healthy young adult dogs was preferred by our team. Based on this conception, the allogeneic BMDC/autologous tumor cells fusion vaccine was conducted by our team and re-injected into transmissible venereal tumor (TVT)-inoculated beagles. The vaccination significantly slowed tumor growth rate and induced earlier self-regression without significant side effects. Increased MHC expression on tumor cells, enhanced TVT-specific cytotoxicity and natural killer cell activity, as well as increased interferon (IFN)-γ production, were observed in the vaccinated group (17). The DC generation method in this experiment was successfully repeated in serial studies, as confirmed by morphology and cell phenotypes (18, 19). Another team used allogeneic or autologous DCs and fused them with canine mammary gland tumor cell lines to develop fusion vaccine products. The two kinds of vaccines were injected into laboratory beagles, resulting in cytotoxic T-lymphocyte reaction and specific anti-tumor IgG detection, respectively (20, 21). These previous basic and clinical data support us in further investigating the clinical efficacy of DC-based vaccines in cancer-bearing dogs.

While we treat cancer using the above strategies separately, whether those therapies could be combined to enhance treatment efficacy was asked. Combinatorial therapies have already been applied in chemotherapy and RT (22), as some chemotherapy agents are radiosensitizers. Combining immunotherapy and RT is gaining attention in recent cancer research. Radiation can induce both local and systemic anti-tumor immune reactions, and there were occasional reports of the "abscopal effect" in humans, describing the phenomenon of regression of unirradiated lesions (23). However, RT also causes the accumulation of several immunosuppressive cells and cytokines, resulting in a negative impact on the immune system (23, 24). Many pre-clinical and clinical studies are working on combining RT and immunotherapy using ICIs, with some encouraging pre-clinical evidence and some controversial clinical experiences (23–29). To further explore the clinical efficacy, more issues about the exact treatment sequence, RT fractionation and treatment resistance, should be addressed. In veterinary research, only a few published studies focused on this topic. Canter et al. (30) applied RT and subsequent intra-tumoral natural-killer (NK) cell transfer in a canine

osteosarcoma mouse model and clinical patients. Delayed tumor growth and enhanced NK cell homing to the tumor were observed in the mouse model. Fifty percent of clinical osteosarcoma dogs were metastasis-free after 6 months, with acceptable side effects (30). Deguchi et al. (31) retrospectively analyzed dogs with stage IV OMM being treated with anti-PD-L1 and hypofractionated RT, and a 55.6% clinical benefit rate was reported in dogs receiving RT ≤ 8 weeks before anti-PD-L1 treatment, which was significantly higher than the group of dogs having ICIs alone. Boss et al. (32) recruited dogs with spontaneous tumors and treated them with stereotactic body radiotherapy (SBRT) alone or combinatorial OX40/TLR immunotherapy. The latter group of dogs had decreased tumor-infiltrating regulatory T cells (Tregs) and tumor macrophages, as well as a significantly increased serum interleukin (IL)-7 concentration (32). Besides, Magee et al. (33) employed a kind of immune-radiotherapy composed of external beam radiotherapy, intra-tumoral cytokine and targeted radionuclide. The treatment was well-tolerated and could induce tumor microenvironment modulations (33). As dogs are great animal models in cancer research, more studies are warranted exploring the immunotherapy and RT combinational treatment modality.

Based on the information above, our manuscript outlines a pilot clinical study investigating the use of the DC/tumor fusion vaccine alone or in combination with RT in dogs with OMM. The study aimed to address two questions: (1) the safety of the DC fusion vaccine alone and in combination with RT, and (2) the outcome of the DC fusion vaccine and the combinatorial treatment.

2 Materials and methods

2.1 Study design and patient recruitment

The study was executed at National Taiwan University Veterinary Hospital Animal Cancer Treatment Center, and was a single-center, open-label pilot study. Client-owned dogs were enrolled into Group 1 (DCRT) or Group 2 (DC), which was decided by the owners based on the clinicians' suggestions on possible treatment options.

Group 1 (DCRT): due to the COVID-19 pandemic, radiation therapy for small animals has been unavailable in our area since 2020. Therefore, only dogs from 2019 to 2020 that received concurrent radiation therapy and dendritic cell immunotherapy were recruited. Dogs in this group should have histopathological diagnoses of oral malignant melanoma. Dogs were not required to be treatment-naïve but should fail previous treatment. For surgical procedures, either tumor debulking or biopsy, or wide-margin surgery (e.g., partial or total maxillectomy or mandibulectomy) was acceptable. Whether to perform a regional lymphadenectomy was determined by the clinician. Dogs should be clinically staged based on the WHO TNM staging system (Table 1). Dogs in stage I-III were included because surgery and RT would not be strongly recommended by clinicians for stage IV dogs considering the cost and risks of repeated anasthesia. During the staging process, tumor size was measured by caliper or by head computed tomography (CT) scan. The ipsilateral mandibular lymph nodes or any enlarged mandibular or retropharyngeal lymph nodes were defined as regional lymph nodes (RLNs), and metastasis was surveyed through histopathology or cytology, or was suspected by radiologists through CT. Pulmonary metastasis was screened by thoracic CT and soft tissue attenuation lesions would be presumed to be metastasis without further cytology or pathology confirmation. Basic blood tests, including a complete blood count (CBC) and biochemistry, were obtained before enrollment. Dogs with severe liver or renal insufficiency or autoimmune disease were not eligible to be included. Other examinations, such as urinalysis and abdominal ultrasound, were not required in each patient but were determined by the attending clinician. Concurrent use of steroids was not allowed. The study was fully reviewed and approved by the National Taiwan University Institutional Animal Care and Use Committee (approval no. NTU-109-EL-00106). All the owners were informed of the study details before enrollment, and informed consent was obtained.

TABLE 1 WHO-based TNM clinical staging system of canine oral malignant melanoma.

T: Primary tumor		N: Regional lymph nodes		M: Distant metastasis	
T1	Tumor ≤2 cm in diameter	N0	No evidence of regional node involvement	M0	No evidence of distant metastasis
T2	Tumor 2–4 cm in diameter	N1	Histologic/ cytologic evidence of regional node involvement	M1	Evidence of distant metastasis
T3	Tumor >4 cm in diameter	N2	Fixed nodes		
Stage I = T1 N0 M0					
Stage II = T2 N0 M0					
Stage III = T3 N0 M0 or T2 N1 M0					
Stage IV = Any T, any N, and M1					

Group 2 (DC): dogs that received dendritic cell immunotherapy without RT were recruited from 2019 to 2022. The diagnosis criteria, surgical procedures, examination of primary oral mass and definition of RLN, decisions on regional lymphadenectomy, staging criteria, and exclusion criteria were the same as in Group 1. During the initial staging process, if the initial chest X-ray survey revealed evidence of pulmonary metastasis, the dog would be excluded because surgical procedures would not be strongly suggested. If the pulmonary metastatic lesion was tiny and could only be detected by a CT, the dog was still allowed to be enrolled. Therefore, dogs in stage I-III and early stage IV were included. Similarly, baseline CBC and biochemistry were obtained before enrollment, and other clinical examinations were not required but were determined by the clinician. Concurrent use of steroids was not allowed. The study was fully reviewed and approved by the National Taiwan University Institutional Animal Care and Use Committee (approval no. NTU-110-EL-00134). All the owners were informed of the study details before enrollment, and informed consent was obtained.

Control group: because neither radiotherapy nor commercialized Oncept immunotherapy is available in our area currently, a group of dogs (Group 3) with histopathologically diagnosed OMMs who received carboplatin in our department was used as a control group (data of this population was reported as a part of our previous work) (8), to compare the treatment efficacy preliminarily. Patients' information, treatment, and outcome details were recorded. Evaluation criteria for clinical stage, RLN, and distant metastasis were the same as

those in groups 1 and 2. None of the dogs received wide-margin surgery or RT. All of the patients had maximum-tolerated-dose carboplatin, treatment dose and interval were determined by the attending clinician.

2.2 Dendritic cell immunotherapy manufacturing

The dendritic cell immunotherapy utilized autologous tumor cells and allogeneic dendritic cells, which were fused *in vitro* into a vaccine product. A detailed process was described previously (17, 34).

Tumor cell preparation: freshly biopsied or removed tumor tissue was suspended and was mechanically crushed and separated into single cells in a sterile stainless steel mesh, with phosphate-buffered saline (Simply, GeneDireX, Taipei, Taiwan) solution with 5% antibiotics of Penicillin–Streptomycin-Amphotericin B (P/S/A, Simply, GeneDireX, Taipei, Taiwan). At least a 1*1*1 cm tumor sample was requested to obtain sufficient tumor cells, but it was encouraged to be as large as possible. The total cell count should be at least 4×10^7, and the cells were preserved in cryogenic tubes. Each tube contains around 1×10^7 cells. All the cells were checked microscopically to ensure no bacterial or fungal infection and were then stored in nitrogen liquid until vaccine preparation.

Dendritic cell generation: peripheral blood was collected from healthy dog donors. Mononuclear cells (PBMCs) were isolated by gradient centrifugation using Ficoll–Hypaque (density 1.077, Cytiva, Uppsala, Sweden) at 400 g for 35 min at room temperature. The buffy coat was extracted and centrifugated at 500 g for 15 min at 16°C and was washed twice using PBS. The obtained PBMCs were cultured in RPMI 1640 medium (Simply, GeneDireX, Taipei, Taiwan) with 10% donor dog serum and 1% P/S/A for 24 h (day 1) for cell adherence. From the second day to the seventh day, the culture medium was changed to RPMI 1640 with 10% fetal bovine serum (FBS, Gibco, Thermo Fisher Scientific, Massachusetts, United States), 1% P/S/A, and IL-4, GM-CSF and Flt-3 L (all from R&D System, Minnesota, United States) to induce immature dendritic cell differentiation. On day 8, additional lipopolysaccharide (LPS, Merck KGaA, Darmstadt, Germany) was added to stimulate dendritic cell maturation. On day 11, the mature dendritic cells were harvested and every 1×10^7 cell was preserved in a cryogenic tube and stored in nitrogen liquid until vaccine preparation.

Fusion vaccine preparation: 1×10^7 tumor cells and 1×10^7 dendritic cells were thawed and recovered 1 day before cell fusion. The tumor cells and dendritic cells were mixed and fused by adding 1 mL of polyethyleneglycol (PEG, Jena Bioscience GmbH, Jena, Germany) to the resuspended cell pellet during 2-min stirring. Based on previous studies, the fusion rate could reach 60%. The fusion product was cultured in RPMI 1640 with 10% FBS, 1% P/S/A, IL-4, and GM-CSF for 3 days before treatment. On the treatment day, the fusion product was treated with 15 ug/mL mitomycin (BOC Science, New York, United States) and was then resuspended in 400 µL 0.9% normal saline. The fresh fusion vaccine product should only be valid for use on the same day.

2.3 Radiation therapy

A hypofractionated radiation therapy protocol was used and dogs were treated weekly. Radiation was delivered by a 6 MV linear accelerator (Synergy, 500 MU/min, Elekta, Stockholm, Sweden). Pre-treatment cone-beam CT (Discovery CT 590, GE, 16 slices) was performed 1 week before treatment for treatment planning. Patient positioning for the CT scan was determined by the attending clinician, and a thermoplastic facial mask was used for immobilization. Gross tumor volume (GTV) was defined as primary tumor volume. Whether to include RLNs in the treatment field was determined by the attending clinician. For the primary tumor, radiation therapy was prescribed with 8–8.5 Gy per fraction, for a total of 40–42.5 Gy. While for the RLN, the dosage was 7–8 Gy per fraction. General anesthesia was performed by clinical veterinarians from the National Taiwan University Veterinary Hospital. A follow-up CT scan was arranged 1 month after finishing treatment.

2.4 Treatment protocol and schedule

The freshly harvested dendritic cell/tumor cell fusion vaccine was given subcutaneously at the lateral cervical region ipsilateral to the tumor, between mandibular and prescapular lymph nodes.

For the group 1/DCRT group, the treatment schedule is summarized in Figure 1. Briefly, the primary tumor sample was biopsied for vaccine preparation, and the patient would receive CT planning in the same week. RT would be started next week and proceeded weekly for five treatments. The DC vaccine would be given 2–3 days after the second RT treatment due to the time needed for manufacturing. The DC vaccine would be prescribed every 2 weeks for a total of four doses. A follow-up CT scan was arranged 4 weeks after the fifth RT, and would be in the same week as the last DC vaccination.

For the group 2/DC group, patients had their tumors removed or biopsied for vaccine preparation. Patients would receive the DC vaccine 1–2 weeks after surgery once the surgical wound healed well. The vaccination would be prescribed once every 2 weeks, and a total of four doses were planned.

2.5 Response and adverse event evaluation

Tumor response was evaluated based on the Veterinary Cooperative Oncology Group Response Evaluation Criteria in Solid Tumors v1.0 (35) and was defined as complete remission (CR), partial remission (PR), stable disease (SD) and progressive disease (PD). If the best response was SD, the duration should be at least 4 weeks. A clinical benefit rate was calculated as the percentage of patients who achieved CR/PR/SD. The response rate was defined as the percentage of dogs achieving CR and PR.

Radiation toxicity was evaluated based on the toxicity criteria of the veterinary radiation therapy oncology group (36) and was assessed and graded at each treatment and recheck. Radiation side effects were defined as acute (within 6 months) or delayed (>6 months). If acute mucositis occurred and affected the patient's quality of life, nonsteroidal anti-inflammatory drugs were prescribed to alleviate clinical signs.

Immunotherapy toxicity was evaluated based on clinical signs, physical examination, blood, and imaging examinations. Physical examination was performed at each treatment and recheck. Essential CBC and biochemistry, and 3-view chest radiographs were checked before the first and third vaccinations, and 1 month after the fourth

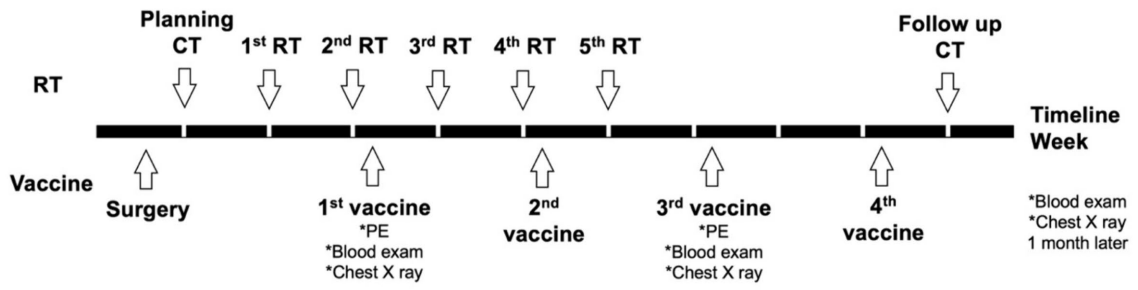

FIGURE 1
Planning treatment schedule of the dogs in the DCRT group. Briefly, surgery was performed for DC vaccine sampling and debulking, and CT planning for RT was performed in the same week of surgery. The first RT started 1 week after CT planning; the first DC vaccination started 2 days after the second RT. RT was scheduled weekly for a total of five treatments; the DC vaccine was given every other week for a total of four doses. PE, physical examination.

vaccination. To classify the adverse events more specifically, the Veterinary Cooperative Oncology Group—Common Terminology Criteria for Adverse Events (VCOG-CTCAE) v1.1 and v2 (37, 38) were used as reference criteria, which were also used for chemotherapy-caused adverse event evaluation.

Patient follow-up and re-staging examinations were arranged monthly for 3 months and every 3 months after.

2.6 Peripheral blood plasma cytokine concentration analysis

In group 1 and group 2, blood samples from individual patients were collected in EDTA tubes before the first and third vaccination, and 4 weeks after the fourth vaccination. Plasma was preserved at −20°C until analysis. The plasma cytokine analysis was proceeded by using the commercial ProcartaPlex Dog Cytokine/Chemokine Panel 11 plex (including IFN-γ, IL-10, IL-12, IL-2, IL-6, IL-8, MCP-1, SCF, TNF-α, VEGF-A, NGF-β) and ProcartaPlex Dog TGF-beta-1 Simplex kit and analyzer (Invitrogen, Thermo Fisher Scientific, Massachusetts, United States).

2.7 Statistical analysis

Patient's signalment, tumor information (oral tumor size, location, bony invasion), RLN status, clinical stage, mitotic count under histopathological evaluation, surgical procedure, residue tumor status before DCRT or DC treatment, tumor response during treatment (i.e., PD or not), and other anti-cancer treatments before enrollment or after disease progression (i.e., chemotherapy, targeted therapy, other immunotherapies), were recorded. Progression-free interval (PFI) and overall survival (OST) were recorded. PFI was calculated from the day the studied treatment started to the day of disease progression or other treatment initiation. OST was defined as disease-specific survival and was calculated from the start of treatment to the time of tumor-related death. For patients who received additional treatments after PD or due to their owners' insistence, the OST would be recorded from the day the studied treatment started to the time the other treatments were initiated, and then the data would be censored from survival analysis. If disease progression was not confirmed, or the death was unrelated to melanoma, the data would still be recorded but would be censored from PFI or OST analysis. Local recurrence was defined as a cytologically or histologically diagnosed melanoma that recurred at the original site or RLNs after treatment. Distant metastasis was detected by radiography or ultrasonography. Categorical variables were compared using Fisher's exact test. Continuous variables were analyzed by the Mann–Whitney test. Cytokines at different time points within a single group were analyzed by the Wilcoxon test. Cytokines at different time points between the DCRT and DC groups were analyzed by multiple Mann–Whitney tests with an adjusted p-value by using the Holm-Sidak method (setting $\alpha = 0.05$) to control the type I error rate when performing the multiple comparisons. PFI and OST were described by Kaplan–Meier curves with 95% confidence interval obtained directly from the graphs, and were compared by Log-rank test. All statistical analyses were performed by GraphPad Prism (RRID: SCR_002798), version 10.0, GraphPad Software, San Diego, California United States.[1] A $p < 0.05$ was considered statistically significant.

3 Results

3.1 Patients' characteristics

Group 1/DCRT group: five dogs were prospectively enrolled. Detailed patient characteristics are summarized in Table 2. The median age of the five dogs was 12 years old (interquartile range/IQR, 11–13). The median body weight was 5.8 kg (IQR, 4.3–13). The median oral tumor size was 3.0 cm (IQR, 2.5–3.4). Two dogs (40%) had mandibular tumors while the other three (60%) had maxillary tumors. Two dogs were stage II (40%), and three were stage III (60%). Four out of five (80%) dogs had metastatic RLNs. Before enrollment, four dogs were treatment-naïve; one had received metronomic chemotherapy for 2 weeks with macroscopic disease, without obvious

1 www.graphpad.com

10.3389/fvets.2024.1397518

TABLE 2 Patients' characteristics and tumor information of the five dogs in the DCRT group.

No.	Age (y/o)	Breed	Sex	Weight (kg)	Tumor diagnosis	Tumor location	Clinical stage	Mass size (cm)[1]	Lymph node metastasis	MC	Bone invasion	Treatments before enrollment	Surgical procedure after enrollment
1	13	Maltese	Fs	2.64	AMM	Lt. maxilla	II	3.4	Yes/path	2/HPF	Yes	Yes, chemo[2]	Biopsy
2	14	Shiba	Mi	13	MM	Lt. mandible	III	3.0	Presumed yes/imaging	6/10 HPF	No	No	Biopsy
3	8	Welsh Corgi	Mc	16.5	MM	Rt. mandible	III	2.1	Yes/cytology	1/HPF	No	No	Biopsy
4	11	Dachshund	Mi	5.8	MM	Lt. maxilla	III	2.5	Yes/path	8/10 HPF	No	No	Biopsy
5	12	Miniature poodle	Mi	4.3	MM	Lt. maxilla	II	4.1	No/path	NR	Yes	No	Biopsy

[1]Maximum diameter was recorded. [2]Metronomic chemotherapy was prescribed for 2 weeks before DCRT treatment. Fs, female spayed; Mc, Male castrated; Mi, Male intact; AMM, amelanotic malignant melanoma; MM, malignant melanoma; HPF, high power field; path, histopathology; MC, mitotic count; NR, not reported.

response. None of the dogs received wide-margin surgery. All the dogs had macroscopic disease when they received DCRT.

Group 2/DC group: 11 dogs were prospectively included. Detailed patient information is summarized in Table 3. The median age of the 11 dogs was 13 years old (IQR, 10–14). The median body weight was 6.8 kg (IQR, 5.7–19). The median oral tumor size was 2.3 cm (IQR, 1.8–3.7). Five dogs (45%) had maxillary tumors, three (27%) had mandibular tumors, and three (27%) had lingual tumors. Three dogs (27%) were stage I/II, and eight (73%) were stage III/IV. Five dogs (45%) had metastatic tumor cells in the RLNs. The median mitotic count was 12/10 high-power fields (HPFs) (IQR, 8–34), ranging from 4 to 102/10 HPFs. Before enrollment, seven dogs (64%) were treatment-naïve; two (18%) had marginal excision but the tumor recurred within 4 weeks; one (9%) received marginal excision and metronomic chemotherapy for 8 weeks then the tumor recurred; one (9%) received metronomic chemotherapy for 6 weeks without clinical benefit. When receiving the DC vaccine, five dogs (45%) had macroscopic disease, either in the oral cavity or the lung parenchyma.

Group 3: eight dogs were retrospectively collected. Detailed patient information is summarized in Table 4. The median age of dogs in this group was 13.5 years old (IQR, 11.8–14). The median body weight was 9.0 kg (IQR, 7.6–10.4). The median oral tumor size was 2.8 cm (IQR, 3.4–3.1). Four dogs (50%) had mandibular tumors, three (37.5%) had maxillary tumors and one (12.5%) had a tonsil melanoma. Two dogs (25%) were in clinical stage I/II and six (75%) were in stage III/IV. Four dogs (50%) had metastatic RLNs. Two dogs had tumor debulking surgery before receiving carboplatin while the other six dogs were treated in macroscopic disease status. Neither of the dogs in this group received other systemic treatments before carboplatin. None of them received wide-margin surgery or radiotherapy during their disease course.

Patient characteristics between the three groups were not significantly different.

3.2 Treatment response and adverse events

Group 1/DCRT group: results of the five dogs are summarized in Table 5. Four dogs received DCRT following the planned schedule and protocol. One patient (No. 4) received RT on schedule but started the DC vaccination after the third radiation because, under histopathological exam, only rare cells contained pigments, and additional immunohistochemistry stains were required to confirm the melanoma diagnosis. All dogs responded to radiation therapy, two had CR and three had PR as the best response. Regarding RT toxicity, only mild and self-limited acute side effects were observed, including grade 1 alopecia and grade 2 mucositis. For the DC vaccination, three dogs did not report any side effects, one dog had a tiny, self-recovered injection site subcutaneous nodule that was too small and deep to perform a fine-needle aspiration (FNA), and the other had grade 1 hyporexia. No aggressive medical intervention was needed in this group.

Group 2/DC group: results are summarized in Table 6. All 11 dogs had sufficient tumor cell counts and were scheduled to receive four vaccination doses. Nine dogs finished the full protocol, and two of them extended the treatment to a total of five doses, as the owners required. Two dogs (patients No. 4 and 10) did not finish the treatment because of tumor progression, after receiving two and three doses of

TABLE 3 Patients' characteristics and tumor information of the 11 dogs in the DC vaccine group.

No.	Age (y/o)	Breed	Sex	Weight (kg)	Tumor diagnosis	Tumor location	Clinical stage	Mass size (cm)[1]	Lymph node metastasis	MC/10HPF	Bone invasion	Treatments before enrollment	Surgical procedure after enrollment
1	14	Shi Tzu	Mc	5.5	MM	Lt. mandible	IV	2.7	Yes/path	37	Yes	No	Oral mass debulking
2	13	Miniature poodle	Fs	5.8	MM	Lt. caudal maxilla	III	4	Yes/path	8	Yes	No	Oral mass partial debulking[2]
3	14	Schnauzer	Fs	6.5	MM	Rt. maxilla	II	2.3	Not reported	12	Yes	No	Oral mass debulking
4	13	Mixed breed	Mc	20	MM	Lingual	III	3.4	Yes/path	15	No	No	Oral mass debulking
5	10	Mixed breed	Mc	21	MM	Lingual	IV	2	No/path	Not reported	No	Marginal excision	Oral mass debulking
6	11	Miniature poodle	Mc	2.8	MM	Lt. maxilla	IV	0.7	No/path	8	Yes	Marginal excision	Partial maxillectomy
7	10	Mixed breed	Mc	20	MM	Lingual and lip	I	1.6	No/path	34	No	No	Glossectomy, lip mass debulking
8	15	Mixed breed	Fs	18.5	MM	Rostral maxilla	III	2.1	Yes/path	Hard to evaluate[3]	No	No	Oral mass debulking
9	14	Mixed breed	Fs	15	AMM	Lt. mandible	III	4	No/path	4	No	Metronomic chemotherapy	Oral mass debulking
10	10	Dachshund	Mi	6.8	MM	Rostral maxilla	III	5	Yes/path	102	Yes	Metronomic chemotherapy	Biopsy
11	8	Miniature poodle	Fi	2.5	MM	Rostral mandible	I	1.3	No/cytology	7	Yes	No	Rostral mandibulectomy

[1]Maximum diameter of the oral tumor; [2]Oral mass partial debulking: patient No. 2 had the tumor invade the orbital and retrobulbar area, which was not able to be surgically removed. [3]According to the histopathological report, the mitotic count was difficult to observe due to the obscurations by large numbers of cytoplasmic granules. Fs, female spayed; Fi, female intact; Mc, male castrated; Mi, male intact; MM, malignant melanoma; AMM, amelanotic malignant melanoma; path, histopathology; MC, mitotic count; HPF, high power field.

10.3389/fvets.2024.1397518

10.3389/fvets.2024.1397518

TABLE 4 Patients' characteristics and tumor information of the eight dogs in the carboplatin control group.

No.	Age (y/o)	Breed	Sex	Weight (kg)	Tumor diagnosis	Tumor location	Clinical stage	Mass size (cm)[1]	Lymph node metastasis	MC	Bone invasion	Treatments before enrollment	Surgical procedure
1	14	Schnauzer	Mi	6.9	MM	Lt. mandible	III	2.5	Yes/path	30/10 HPF	No	Marginal excision	Oral mass debulking
2	14	Schnauzer	Mc	9.1	MM	Rt. Mandible	II	3.6	No/cytology	8–10/10 HPF	Yes	Marginal excision	No
3	14	Dachshund	Fs	8.8	MM	Rt. Maxilla	I	2.0	No/cytology	0-2/HPF	Not reported	Marginal excision	No
4	11	Schnauzer	Mc	6.3	MM	Maxilla/soft palate	III	4.5	Yes/cytology	0-2/HPF	Not reported	No	No
5	15	Beagle	Mi	20	MM	Rt. Maxilla	IV	1.5	Not reported	Not reported	Not reported	Marginal excision	No
6	13	Scottish terrier	Mi	13	MM	Tonsil	IV	2.6	Yes/path	5-8/HPF	No	No	No
7	10	Schnauzer	Fs	7.8	MM	Rt. Mandible	IV	3.0	No/cytology	5-7/HPF	Yes	Marginal excision	No
8	12	Shiba	Mi	9.5	MM	Rt. Mandible	III	3.0	Yes/imaging	Rare	No	No	Oral mass debulking

[1]Maximum diameter of the oral tumor; Fs, female spayed; Mc, male castrated; Mi, male intact; MM, malignant melanoma; path, histopathology; MC, mitotic count; HPF, high power field.

DC vaccine, respectively. No dog responded to the treatment, while eight dogs achieved stable disease (three were stable with macroscopic lesions, five were progression-free with microscopic tumor cells) during vaccination treatment, resulting in a clinical benefit rate of 73%. Two of the three stage IV dogs could maintain stable disease during treatment and survived for over a year. Nine dogs did not report any adverse events during the whole treatment process. One dog had a 1-cm injection site nodule and FNA revealed predominantly neutrophils and macrophages. This patient had a self-recovery without medical intervention. The other dog reported grade 2 gastrointestinal toxicities, including hyporexia, vomiting and diarrhea, which could be managed by supportive treatments.

Group 3: results are presented in Table 7. The median carboplatin initiation dosage of all eight patients was 250 mg/m^2 (IQR, 250–262.5) and the median dose of injections was 2 (IQR, 1–3). One dog had a partial response to carboplatin, and four maintained stable disease, leading to a 12.5% response rate and 62.5% clinical benefit rate. Side effects were reported in five dogs which were mainly grade 1–2 and self-limited gastrointestinal discomfort.

3.3 Outcome

All dogs in Groups 1 and 2 had died by the time of this manuscript preparation.

In the DCRT group, three dogs died because of tumor-related reasons (two died of local disease, one was due to distant metastasis), and two of them received other kinds of treatments (other immunotherapies, metronomic chemotherapy) after tumor progression. One dog (No. 3) survived 22 months and died of liver failure with neurological signs. No local recurrence or pulmonary metastasis was observed before death; however, whether the liver or brain had melanoma metastasis, or the dog developed primary liver diseases, was not confirmed. Treatment-related reasons were less likely due to the long duration from treatment to death, and no adverse events were reported during treatment. The other dog (patient No. 4) had a sudden death 28 days after treatment finished, without any evidence of disease progression at the last visit. However, tumor-related reasons could not be excluded because the dog had occasional vomiting and coughing 2 weeks before death. Although the activity, appetite and respiratory rate were normal, melanoma metastasis or tumor emboli were possible causes of death. Treatment-related reasons were less likely because no abnormal radiation-induced or immuno-dysregulation signs were noted. Other diseases, including cardiopulmonary or gastrointestinal problems, were not excluded either, but no more clinical signs were reported. No necropsy was performed.

In the DC group, all 11 dogs had died. Four (36%) deaths were because of local tumor progression, six dogs (55%) died of distant melanoma metastasis; one dog (patient No. 8) developed a rapidly enlarged Rt. forelimb mass around 19 months after DC finished, and became anorexia and died within 2 months. The owner declined diagnostic exams of the Rt. forelimb mass, therefore, whether the mass was a melanoma metastasis or a second malignancy was undetermined, or if there were other comorbidities leading to the patient's death. Six dogs received other treatments after disease progression (other immunotherapies, chemotherapy, or TKIs). After the DC treatments were finished, two dogs received other

TABLE 5 Treatment protocol, adverse events and outcomes of the five dogs in the DCRT group.

No.	RLN removal	RT (oral mass)	RT (RLN)	DC doses	Best response	Adverse events (RT/DC)	PFI (days)	TLP (days)	TDM (days)	OST (days)	Other treatments after PD	Outcome
1	Yes	8.5 Gy*5	No	Regular, 4 doses	CR	Grade 2 mucositis, grade 1 skin/NR	79	79	No	113	No	Spontaneous death; local disease
2	No	8 Gy*5	7.5 Gy*5	Regular, 4 doses	PR	Grade 2 mucositis/NR	62	102	62; pulmonary	62	Metronomic chemotherapy	Spontaneous death; pulmonary metastasis
3	No	8 Gy*5	7 Gy*5	Regular, 4 doses	CR	Grade 1 skin/ Injection site nodule	630[2]	No	Unsure	630	Progression was not confirmed	Spontaneous death; liver failure, neurological signs
4	Yes	8 Gy*5	8 Gy*5	started after 3rd RT, 4 doses[1]	PR	Grade 1 skin/ Grade 1 hyporexia	101[2]	Unsure	Unsure	101	Progression was not confirmed	Sudden death; undetermined cause
5	Yes	8 Gy*5	7 Gy*5	Regular, 4 doses	PR	Grade 1 skin/NR	214	214	No	214	Adoptive NK cell therapy	Spontaneous death; local disease
Median PFI (days)						214 (95% CI, NA)						
Median OST (days)						Not reached due to insufficient event numbers						

1: the patient started DC vaccination after the third radiation because additional immunohistochemistry stains were required to confirm the final melanoma diagnosis. 2: patient No. 3 died of liver failure and neurological signs without evidence of local tumor recurrence or pulmonary metastasis, but liver or brain metastasis could not be ruled out; patient No. 4 died of undetermined cause, the patient developed occasional vomiting and coughing around two weeks before death (four weeks after treatment finished), a tumor-related death could not be excluded but was not confirmed. The data were recorded as durations from treatment to death. RLN, regional lymph node; NR, not reported; PFI, progression-free interval; TLP, time to local progression since treatment started; TDM, time to distant metastasis since treatment started; OST, overall survival time; NK cell, natural killer cell.

10.3389/fvets.2024.1397518

TABLE 6 Treatment protocol, adverse events and outcomes of the 11 dogs enrolled in the DC vaccine group.

No.	RLN removal	DC doses	Residue tumor before DC vaccination	Best response	Adverse events	PFI (days)	TLP (days)	TDM (days)	OST (days)	Treatments after PD	Outcome
1	Yes	4	Macroscopic/lung	SD	NR	161	No	161; pulmonary PD	161	Chemotherapy; ACT	Euthanasia; pulmonary metastasis
2	Yes	5	Macroscopic / retrobulbar	SD	Injection site nodule	70	70	141; pulmonary	70	ACT; surgery	Euthanasia; local disease
3	No	5	Microscopic	SD/PF	NR	117[2]	177	204; pulmonary	117	ACT; TKI; chemotherapy	Spontaneous death; Local lymphadenomegaly; SIRS, AKI
4	Yes	2	Microscopic	PD	NR	14	14	21; pulmonary	23	No	Euthanasia; diffuse metastasis
5	Yes	4	Macroscopic/lung	SD	grade 2 GI signs[1]	100[2]	333	366; pulmonary PD	100	ACT	Spontaneous death; pulmonary metastasis
6	Yes	4	Macroscopic /lung	PD	NR	31	31	31; pulmonary PD	51	No	Euthanasia; diffuse metastasis
7	Yes	4	Microscopic	SD/PF	NR	418	No	418; pulmonary	525	No	Euthanasia; pulmonary metastasis; UB mass, hematuria; liver and splenic mass; anemia;
8	Yes	4	Microscopic	SD/PF	NR	686[3]	No	No	686	No	Spontaneous death; anorexia; Rt. forelimb mass
9	Yes	4	Microscopic	SD/PF	NR	60	60	No	60	TKI	Euthanasia; local tumor, AKI, cachexia;
10	Yes	3	Macroscopic /oral	PD	NR	27	27	No	44	No	Euthanasia; local disease;
11	No	4	Microscopic	SD/PF	NR	237	No	237; subcutaneous 316; pulmonary	237	Chemotherapy; TKI	Spontaneous death; diffuse distant metastasis
Median PFI (days)					100 (95% CI, 27–237)						
Median OST (days)					525 (95% CI, 44-NA)						

[1]Gastrointestinal (GI) signs, including hyporexia, vomiting, and diarrhea. [2]Patients did not have disease progression at this time. Owners insisted on continuing with other treatments, so the PFIs were recorded as the duration from DC vaccination to initiation of other treatments. [3]Patient No. 8 had a rapidly enlarged Rt. forelimb mass 19 months after DC finished and died within 2 months, without evidence of tumor progression. Melanoma-related death could not be ruled out but was not confirmed. The data was recorded as the duration from treatment to death. RLN, regional lymph node; PF, progression-free; NR, not reported; PFI, progression-free interval; TLP, time to local progression since treatment started; TDM, time to distant metastasis since treatment started; OST, overall survival time; ACT: adoptive natural killer cell therapy; TKI, tyrosine kinase inhibitor; SIRS, systemic inflammatory response syndrome; AKI, acute kidney injury; UB, urinary bladder.

10.3389/fvets.2024.1397518

TABLE 7 Treatment protocol, adverse events and outcome of the eight dogs in the carboplatin control group.

No.	RLN removal	Residue tumor before chemotherapy	Chemotherapy	Best response	Adverse events	PFI (days)	TLP (days)	TDM (days)	OST (days)	Treatments after PD	Outcome
1	Yes	Microscopic	Carboplatin; 250 mg/m^2; 3 cycles	SD	Grade 1–2 GI[1]	169	176	169	211	No	Spontaneous death; pulmonary metastasis
2	No	Macroscopic	Carboplatin; 250 mg/m^2; 2 cycles	SD	Grade 1–2 GI[1]	44	44	No	197	No	Euthanasia; local disease
3	No	Microscopic	Carboplatin; 250 mg/m^2; 3 cycles	PF	Grade 1–2 GI[1]; grade 2 ALT elevation	PF	PF	PF	Alive	No	Follow up: > 960 days without progression
4	No	Macroscopic	Carboplatin; 250 mg/m^2; 1 cycle	PR	NR	42	42	No	42	No	Spontaneous death; local disease
5	No	Macroscopic	Carboplatin; 300 mg/m^2; 1 cycle	NA	NA	21	NA	NA	21	NA	Unsure; died 21 days after chemotherapy
6	Yes	Macroscopic	Carboplatin; 300 mg/m^2; 3 cycles	SD	NR	31	31	98	100	No	Spontaneous death; pulmonary metastasis
7	No	Macroscopic	Carboplatin; 300 mg/m^2; 1 cycle	PD	Grade 1 GI[1]	14	14	14	81	No	Spontaneous death; pulmonary metastasis, anorexia
8	No	Macroscopic	Carboplatin; 250 and 300 mg/m^2	PD	Grade 1 creatinine elevation	28	28	No	28	Immunotherapy	Spontaneous death; local disease
Median PFI (days)				42 (95% CI, NA-170)							
Median OST (days)				148.5 (95% CI, NA)							

[1]Gastrointestinal (GI) signs, including hyporexia, vomiting, and diarrhea. RLN, regional lymph node; PF, progression-free; NA, not assessed; NR, not reported; PFI, progression-free interval; TLP, time to local progression since treatment started; TDM, time to distant metastasis since treatment started; OST, overall survival time.

10.3389/fvets.2024.1397518

immunotherapies without disease progression due to the owners' insistence. The PFIs in these two dogs were recorded as the duration from the day DC vaccination started to the time of other treatment initiation. Among the three stage IV dogs, patient No. 1's pulmonary lesion was solitary and 0.3 cm in diameter, and could only be detected on thoracic CT. The nodule progressed 5 months later after DC vaccination. The patient then received other treatments (immunotherapy, chemotherapy) and survived another 8 months, and died of extensive pulmonary metastasis. Patient No. 5, with stage 4 lingual melanoma, also had a stable solitary pulmonary lesion, and the owner wanted to continue with another immune cell therapy using autologous natural killer cells after finishing DC vaccination. The pulmonary lesion achieved PR after cell therapy. However, the patient developed local recurrence 8 months later, and the pulmonary metastasis deteriorated 9 months later. Patient No. 6 had two tiny pulmonary nodules measured about 0.2 cm on thoracic CT before treatment, and presented with an extensive miliary to nodular pulmonary metastatic pattern on chest X-ray before the third DC treatment. The patient also developed suspected brain metastasis and was euthanized 2 months later. Patient No. 11 developed diffuse subcutaneous masses around 8 months after treatment started, and the masses were confirmed to be melanoma by histopathology. The patient then received chemotherapy (carboplatin, doxorubicin) and targeted therapy and survived 5 months more.

In Group 3, six dogs died because of tumor progression (three died of local disease, three died of pulmonary metastasis); one dog (patient No. 5) died 21 days after treatment, the cause was undetermined and either rapid tumor progression or treatment-related fatal adverse events were possible reasons. Seven dogs had carboplatin as their sole systemic treatment, while one dog received immunotherapy after carboplatin failure but no obvious response was observed. Patient No. 3 was still alive without tumor recurrence at the time of data collection (follow-up time, 960 days).

For survival analysis, in the DCRT group, patients No. 3 and 4 were censored from PFI analysis because tumor progression was not confirmed, leaving the PFI of 79, 62 and 214 days in the other three dogs; the median PFI was 214 days (95% CI, NA). Regarding the overall survival, patients No. 3 and 4 were censored from OST analysis because of undefined causes of death, and patients No. 2 and 5 were censored because they received other treatments after failing DCRT; survival times of these dogs were recorded (Table 5) but median OST could not be reached due to insufficient uncensored data. Overall, the 1-year survival rate was 20% in the DCRT group. In the DC group, patient No. 8 was censored from PFI analysis, resulting in a median PFI of 100 days (95% CI, 27–237). Seven dogs were censored from OST analysis because of unidentified tumor-related death (patient No. 8) or receiving other treatments after tumor progression (patients No. 1, 2, 3, 5, 9, 11). The median OST was 525 days (95% CI, 44-NA), and the 1-year survival rate was 54.5%. In the carboplatin group, two dogs were censored from PFI analysis (patient No. 3 was alive, and patient No. 5 had an undetermined cause of death), resulting in a median PFI of 42 days (95% CI, NA-170). Three dogs were censored from OST analysis (patients No. 3, 5, and 8), leading to a median OST of 148.5 days (95% CI, NA); the 1-year survival rate was 12.5%. The PFI and OST are presented by the Kaplan–Meier curves in Figure 2. The survival curves were not significantly different by the Log-rank test.

3.4 Cytokine analysis

All patients in the DCRT group and six in the DC group had sufficient plasma collection at different time points for cytokine analysis. Some concentrations of the evaluated cytokines were too low to be detected. After discussing with the product specialist, we decided to use both concentration and median fluorescent intensity (MFI) for those cytokines with detectable concentration values, while for those the concentration values were non-detected, MFI was used for analysis.

No clear association between cytokine changes and clinical evolution was found. In the DCRT group, no cytokine changed significantly before or after treatment. While in the DC group, although no cytokine revealed significant change, the MCP-1 increased after treatment ($p = 0.06$), and the VEGF-A decreased ($p = 0.06$).

Between the two groups, the TGF-β and IFN-γ MFIs were significantly higher in the DCRT group. The TGF-β MFI was higher in the DCRT group before DC vaccination ($p = 0.004$), and remained higher during ($p = 0.016$) and post-vaccination ($p = 0.036$), compared to the DC group. While the IFN-γ MFI was significantly higher during ($p = 0.016$) and after vaccination ($p = 0.018$) in the DCRT group.

4 Discussion

The current manuscript reported a pilot study investigating the safety and efficacy of dendritic cell/tumor cell fusion vaccine immunotherapy, alone or in combination with radiotherapy, in treating canine oral malignant melanoma. Safety evaluation was the primary study aim, which indicated that both DC and DCRT were well-tolerated, with only mild gastrointestinal and injection site adverse events recorded. Overall, dogs that received the DC vaccine achieved a median PFI of 100 days (95% CI, 27–237), while dogs in the DCRT group had a median PFI of 214 days (95% CI, NA). Dogs in the DC group seemed to live longer and had a higher 1-year survival rate (54.5 vs. 20%). However, compared to the retrospectively collected control group composed of dogs receiving carboplatin without wide-margin surgery or RT, treating with DC or DCRT did not generate significantly superior survivals. But at least the general safety of DC vaccination preliminarily supported further exploration of this treatment in a more rigorously constructed clinical trial to assess its efficacy. It is to be noted that chemotherapy is not a standard of care in dogs with malignant melanoma. The authors chose this group because of the current treatment dilemma of lacking RT and other immunotherapies in our area, resulting in the necessity of investigations on treatments other than surgery. In addition, the authors did not enroll dogs receiving only surgery as a control group because those dogs in our department were predominantly in clinical stage I-II, which might carry an inherently better prognosis than dogs in the DCRT or DC group. As for dogs receiving only RT, the medical records were not as complete as we required.

The PFI is the appropriate statistic to evaluate treatment efficacy. Median PFI was only 100 days in the DC group. However, two patients switched to another immunotherapy after completing the DC vaccination without disease progression, potentially underestimating the actual PFI. Notably, two of the three stage IV dogs (patients No. 1 and 5) survived for over a year and could maintain stable disease

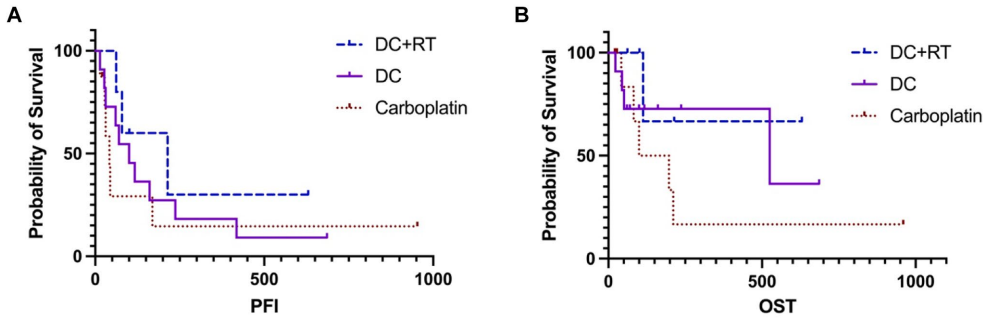

FIGURE 2
The Kaplan–Meier curves of PFI **(A)** and OST **(B)** survivals in the DCRT and DC groups. Neither revealed significant differences. The censored data were presented as vertical tick marks.

during DC vaccination. The pulmonary metastases were solitary and small in these two dogs, which might facilitate the immunotherapy to work, as the tumor burden was relatively not heavy. Moreover, in patient No. 5, the subsequent adoptive natural killer cell therapy after DC vaccination resulted in partial remission of the pulmonary metastasis, but we did not design a study to explore the exact mechanism and efficacy of combining the two immunotherapies. Lacking wide-margin surgery and RT resulted in inadequate local control in most dogs in the DC group. Only patient No. 8 had the least tumor burden by removing the primary oral tumor and two metastatic lymph nodes and survived 23 months without additional treatments. Patient No. 2 had mild orbital invasions that could not be removed by surgery and had a modest survival time; patient No. 10 carried an invasive primary oral mass and experienced a worse outcome; patient No. 4 had the most aggressive tumor that progressed dramatically despite treatment intervention. A future clinical study of using DC vaccination as an adjuvant therapy could be considered.

However, the clinical outcome of the DCRT group did not meet our expectations. Firstly, although the case number was low, the percentage of dogs with RLN metastasis was numerically higher in the DCRT group, indicating a possible poorer prognosis. Besides, in theory, radiation can induce tumor cell death, leading to tumor-antigen release and subsequent antigen-presenting process, alteration in tumor surface markers (e.g., MHC-I, FAS ligand, immune checkpoint molecules) expression, production of cytokines and chemokines, and recruitment of CD8 T cells and tumor-infiltrating lymphocytes, all of which exerts the immune-stimulation facility. Meanwhile, radiation also has an immunosuppressive impact by increasing Treg infiltration, TGF-β and IL-10 excretion, and myeloid-derived suppressor cells (MDSCs) recruitment (23, 24). Therefore, our initial hypothesis for this inferior DCRT outcome is the potential RT-induced immunosuppressive environment, as we found that compared to the DC group, the MFI of TGF-β in the DCRT group was significantly higher throughout the treatment course. The MFI of IFN-γ was also significantly higher in the DCRT group after treatment. Radiation-induced IFN-γ production can activate APCs and T cells and promote a tumor-killing process; on the other hand, IFN-γ can also induce PD-L1 expression and stimulate tumor prosurvival mechanisms (23). We should not use this data to draw a conclusion, as changes in immune function and the correlated immunotherapeutic clinical outcomes should not be interpreted using a single parameter or a simple combination. However, further exploration of those cytokines' functions in a larger group is worthwhile, as well as using a comprehensive complex of immune response patterns consisting of lymphocyte recirculation and subpopulation activations, APCs' function changes, along with the cytokines profiles, to elucidate the correlations between immune pattern changes and clinical outcomes.

The DCRT treatment sequence should be investigated. In our protocol, due to the DC vaccine manufacturing process and some force majeure related to RT, we overlapped RT and DC vaccination, as the vaccination started after the second radiation fraction. It is not clearly understood which treatment sequence is optimal or at what exact time point immunotherapy should be inducted. A study by Deguchi et al. (31) was the only one that compared different treatment schedules of ICI and RT in dogs (31), and they found that the best outcome was achieved in the previous RT group (dogs treated with RT within 8 weeks prior to the first ICI dose) rather than the concurrent RT group (ICI was given within 1 week of the first RT). Although most of the current studies focus on a combination of ICIs and RT, and the different mechanisms of ICIs and the DC vaccine require different evaluations of treatment sequence, it is still possible that our DCRT protocol was suboptimal. Because we gave the DC vaccination after the second RT, some dogs exhibiting partial responses to the first RT may have less tumor antigen release and an inferior antigen-presenting process in the second RT. Further studies could be designed to give the DC vaccine on the same day as the first RT, to see if there is a better outcome.

Besides, at the time we designed our DCRT protocol, there was not much study discussing the regional lymph node impact, and the inclusion of RLNs in the radiation field was determined by each clinician. Recently, studies in mouse models with head and neck tumors have shown that elective lymph node irradiation ablated the combinatorial efficacy of SBRT and immunotherapy and reduced antigen-experienced T cell expansion (39). Similar findings were also observed in dogs with nasal tumors, that nodal irradiation reduced the CD4 and CD8 T cell counts in the nasal cavity, reduced gene expressions in antigen presentation and T cell activation, and increased immunosuppressive gene expressions (39). Another team reported similar findings that lymphablation was deleterious to ICI response and overall survival in mouse models, and the DCs in draining lymphatics were necessary for the ICI response (40). In light of these results, we found that four out of five dogs in our DCRT group had regional lymph nodes included in their RT fields. Although we did not irradiate all the draining lymph nodes but only

included one or two of the RLNs, it may still impact the immunotherapeutic effect adversely but failed to be significantly presented due to the small case number. However, canine OMM has a higher nodal metastatic rate than sinonasal tumors. For those RLNs that have abundant metastases and are structurally effaced by tumor cells, whether to spare these nodes during RT may need further evaluation, as the nodal microenvironment and immune cell composition might differ. Alternatively, the metastatic RLNs could be preserved initially to generate immune responses during RT and immunotherapy, and be removed later. According to Darragh et al. (39) study, sentinel lymphadenectomy after treatment completion led to a decreased local metastatic rate and had no impact on systemic immunity. More clinical trials are warranted regarding these questions.

The DC generation and fusion vaccine preparation methodology followed established protocols (18, 19), with clear functional and immunophenotypic evaluation. Based on the previous studies, the morphology of the PBMC-generated DCs was similar to typical DCs; the phenotypic expressions of CD80, CD83, CD86, CD1a, CD11c, CD40, and MHC II were observed in mature DCs, as were productions of IL-1b, IL-10, IL-12p40, IL-13, and TNF-α. Similar to previous studies, the DC generation rate in the current study was calculated as $3–4 \times 10^7$ mature DCs per 100 mL of peripheral blood and was uniform among different generating processes. Therefore, we did not repeat the function and expression analyses, and only confirmed the DCs' morphology microscopically. Our previous experiments also showed that treating dogs with OMM with the BMDC/tumor cell fusion vaccine and surgery significantly prolonged survival, decreased circulating Tregs and increased melanoma-specific cytotoxicity were also observed (34). Allogeneic DCs and autologous tumor cell fusion products can stimulate immune reactions directly or via cross-presentation through the expressions of DC-derived MHC-I, DC-derived MHC-II loading with tumor antigen, and tumor-derived MHC-I loaded with tumor antigen (15). Cross-presentation of allogeneic DCs to the host could allow antigens to be presented by the host's antigen-presenting cells, priming the immune response (21). Although different epitopes from allogeneic DCs can stimulate allorecognition, it has been suggested that the MHC molecules should be partially shared between donor and host to generate antigen-specific T-cell responses (15, 41). In this manuscript, we did not analyze the MHC allele similarity between our patients and donor dogs. Thus, mismatches may exist, potentially leading to a lack of tumor antigen-specific immunostimulation and weakened DC vaccination efficacy. Nevertheless, we still chose to use allogenic sources because autologous DCs from cancer-bearing patients may be defective; besides, dogs in our study were predominantly small to medium-sized populations, and it was harmful to collect 50 or 100 mL of peripheral blood or perform a bone-marrow aspiration to generate sufficient mononuclear cells for DC vaccine preparation. Moreover, by recognizing and presenting the MHCs of allogeneic DCs, as well as the MHCs of tumor-bearing dogs in the fusion cells, it was theoretically reasonable that T-lymphocytes could still be stimulated by this method, generating the expected immune response.

Except for the questions mentioned above, several limitations exist in this manuscript. First, the sample size was small. One of the obstacles in patient recruitment was an inherent feature of using autologous tumor cells. Because we harvested primary tumors from canine oral cavities, it was unsurprising that bacterial pollution existed during the cell culture process, rendering an exclusion from the treatment.

Furthermore, the treatment outcome could not be rigorously compared because this was not a double-blind random prospective clinical trial, and some deviations existed in the patient recruitment and treatment process. For example, the clinical stage inclusion criteria were mildly different between DC and DCRT groups, because RT was not strongly suggested if the patient was in stage IV, but the early pulmonary metastasis, which was detected by CT, was allowed in the DC group. Besides, at the time of DCRT patient enrollment, there was no consensus among our clinicians regarding the RLN removal or RLN inclusion in the RT field, resulting in inconsistent decisions in the studied population. Thirdly, as a pilot study, we allowed patients who were previously treated to enroll, and patients who failed DC or DCRT to switch to other therapies, which was also a confounder on efficacy evaluation and resulted in a largely censoring process on OST analysis. Specifically speaking, before starting DC or DCRT, three dogs had metronomic chemotherapy with a duration from 2 weeks to 2 months. As metronomic chemotherapy can generate antineoplastic effects through inhibitions on angiogenesis and Tregs accumulation, and induction of tumor dormancy (42), whether these three dogs had immune modulations which then affected the treatment efficacy, was undetermined. In addition, although the DC protocols in the two groups were generally uniform as designed, one dog in the DCRT group started DC vaccination before the third RT, and two dogs in the DC group extended to five doses as owners required. Whether those deviations affected outcomes was also unknown. Lastly, examinations of the abdominal cavity and urinalysis were not routinely required, leading to a possible underdiagnosis; and some histological characteristics, such as the mitotic figures, were not consistently calculated by 10 HPFs in the DCRT group. However, a prognostic cut-off value was ≥4/10 HPFs (43), and most of our patients had mitotic counts exceeding this value, or in those with unmentioned or calculated mitoses per HPF, metastatic disease was diagnosed, indicating a poorer prognosis in general.

5 Conclusion

The allogeneic DC and autologous tumor cell fusion vaccine immunotherapy alone and in combination with local radiotherapy reported in this manuscript were well-tolerated in dogs with oral melanoma. Receiving the DC vaccine alone or the combinatorial DCRT did not demonstrate a survival difference but the cytokine analysis revealed a higher TGF-β signal in the DCRT group, indicating a potential immunosuppressive status. Given the general safety and the limitations of the study design, the current manuscript supports the further need for a more well-constructed clinical trial on an expanded scale, to investigate the actual efficacy of DC and DCRT in dogs. Studies on treatment sequence and protocol modification in the DCRT group, as well as analysis of the peripheral blood immune cells and cytokines, are also warranted.

Data availability statement

The original contributions presented in the study are included in the article/supplementary material, further inquiries can be directed to the corresponding author.

Ethics statement

The animal studies were approved by the National Taiwan University Institutional Animal Care and Use Committee. The studies were conducted in accordance with the local legislation and institutional requirements. Written informed consent was obtained from the owners for the participation of their animals in this study.

Author contributions

Y-YX: Data curation, Investigation, Writing – original draft, Formal analysis. AL: Conceptualization, Funding acquisition, Investigation, Methodology, Supervision, Writing – review & editing. R-ML: Investigation, Writing – review & editing. S-YY: Investigation, Writing – review & editing. C-CK: Investigation, Writing – review & editing. C-HK: Investigation, Writing – review & editing. C-SL: Investigation, Writing – review & editing. J-JL: Conceptualization, Funding acquisition, Methodology, Project administration, Supervision, Writing – review & editing.

Funding

The author(s) declare that financial support was received for the research, authorship, and/or publication of this article. This study was supported by a grant from the National Science Council, Taipei, Taiwan (MOST 111-2313-B-002-019).

Conflict of interest

The authors declare that the research was conducted in the absence of any commercial or financial relationships that could be construed as a potential conflict of interest.

Publisher's note

All claims expressed in this article are solely those of the authors and do not necessarily represent those of their affiliated organizations, or those of the publisher, the editors and the reviewers. Any product that may be evaluated in this article, or claim that may be made by its manufacturer, is not guaranteed or endorsed by the publisher.

References

1. Bergman PJ, Selmic LE, Kent MS. 20- Melanoma In: DM Vail, DH Thamm and JM Liptak, editors. Withrow and MacEwen's small animal clinical oncology. *6th* ed. St. Louis, MO: W.B. Saunders (2020). 367–81.

2. Freeman KP, Hahn KA, Harris FD, King GK. Treatment of dogs with oral melanoma by hypofractionated radiation therapy and platinum-based chemotherapy (1987-1997). *J Vet Intern Med*. (2003) 17:96–101. doi: 10.1111/j.1939-1676.2003.tb01329.x

3. Proulx DR, Ruslander DM, Dodge RK, Hauck ML, Williams LE, Horn B, et al. A retrospective analysis of 140 dogs with oral melanoma treated with external beam radiation. *Vet Radiol Ultrasound*. (2003) 44:352–9. doi: 10.1111/j.1740-8261.2003.tb00468.x

4. Cunha SCS, Corgozinho KB, Silva FBF, Silva KVGC, Ferreira AMR. Radiation therapy for oral melanoma in dogs: a retrospective study. *Ciência Rural*. (2018) 48:e20160396. doi: 10.1590/0103-8478cr20160396

5. Baja AJ, Kelsey KL, Ruslander DM, Gieger TL, Nolan MW. A retrospective study of 101 dogs with oral melanoma treated with a weekly or biweekly 6 Gy x 6 radiotherapy protocol. *Vet Comp Oncol*. (2022) 20:623–31. doi: 10.1111/vco.12815

6. Rassnick KM, Ruslander DM, Cotter SM, Al-Sarraf R, Bruyette DS, Gamblin RM, et al. Use of carboplatin for treatment of dogs with malignant melanoma: 27 cases (1989-2000). *J Am Vet Med Assoc*. (2001) 218:1444–8. doi: 10.2460/javma.2001.218.1444

7. Brockley LK, Cooper MA, Bennett PF. Malignant melanoma in 63 dogs (2001-2011): the effect of carboplatin chemotherapy on survival. *N Z Vet J*. (2013) 61:25–31. doi: 10.1080/00480169.2012.699433

8. Xia Y, Liao AT, Lee J. A retrospective study of chemotherapeutic effect without wide-margin surgery or radiation therapy in dogs with oral malignant melanoma. *Can Vet J*. (2024) 65:343–50.

9. Tani H, Miyamoto R, Noguchi S, Kurita S, Nagashima T, Michishita M, et al. A canine case of malignant melanoma carrying a KIT c.1725_1733del mutation treated with toceranib: a case report and in vitro analysis. *BMC Vet Res*. (2021) 17:147. doi: 10.1186/s12917-021-02864-3

10. Giuliano A, Dobson J. Prospective clinical trial of masitinib mesylate treatment for advanced stage III and IV canine malignant melanoma. *J Small Anim Pract*. (2020) 61:190–4. doi: 10.1111/jsap.13111

11. Bergman PJ, McKnight J, Novosad A, Charney S, Farrelly J, Craft D, et al. Long-term survival of dogs with advanced malignant melanoma after DNA vaccination with xenogeneic human tyrosinase: a phase I trial. *Clin Cancer Res*. (2003) 9:1284–90.

12. Pellin MA. The use of Oncept melanoma vaccine in veterinary patients: a review of the literature. *Vet Sci*. (2022) 9:597. doi: 10.3390/vetsci9110597

13. Igase M, Nemoto Y, Itamoto K, Tani K, Nakaichi M, Sakurai M, et al. A pilot clinical study of the therapeutic antibody against canine PD-1 for advanced spontaneous cancers in dogs. *Sci Rep*. (2020) 10:18311. doi: 10.1038/s41598-020-75533-4

14. Maekawa N, Konnai S, Nishimura M, Kagawa Y, Takagi S, Hosoya K, et al. PD-L1 immunohistochemistry for canine cancers and clinical benefit of anti-PD-L1 antibody in dogs with pulmonary metastatic oral malignant melanoma. *NPJ Precis Oncol*. (2021) 5:10. doi: 10.1038/s41698-021-00147-6

15. Koido S. Dendritic-tumor fusion cell-based Cancer vaccines. *Int J Mol Sci*. (2016) 17:828. doi: 10.3390/ijms17060828

16. Gyorffy S, Rodriguez-Lecompte JC, Woods JP, Foley R, Kruth S, Liaw PC, et al. Bone marrow-derived dendritic cell vaccination of dogs with naturally occurring melanoma by using human gp100 antigen. *J Vet Intern Med*. (2005) 19:56–63. doi: 10.1111/j.1939-1676.2005.tb02659.x

17. Pai CC, Kuo TF, Mao SJ, Chuang TF, Lin CS, Chu RM. Immunopathogenic behaviors of canine transmissible venereal tumor in dogs following an immunotherapy using dendritic/tumor cell hybrid. *Vet Immunol Immunopathol*. (2011) 139:187–99. doi: 10.1016/j.vetimm.2010.10.013

18. Wang YS, Chi KH, Chu RM. Cytokine profiles of canine monocyte-derived dendritic cells as a function of lipopolysaccharide-or tumor necrosis factor-alpha-induced maturation. *Vet Immunol Immunopathol*. (2007) 118:186–98. doi: 10.1016/j.vetimm.2007.05.010

19. Wang YS, Chi KH, Liao KW, Liu CC, Cheng CL, Lin YC, et al. Characterization of canine monocyte-derived dendritic cells with phenotypic and functional differentiation. *Can J Vet Res*. (2007) 71:165–74.

20. Bird RC, Deinnocentes P, Church Bird AE, van Ginkel FW, Lindquist J, Smith BF. An autologous dendritic cell canine mammary tumor hybrid-cell fusion vaccine. *Cancer Immunol Immunother*. (2011) 60:87–97. doi: 10.1007/s00262-010-0921-2

21. Bird RC, Deinnocentes P, Lenz S, Thacker EE, Curiel DT, Smith BF. An allogeneic hybrid-cell fusion vaccine against canine mammary cancer. *Vet Immunol Immunopathol*. (2008) 123:289–304. doi: 10.1016/j.vetimm.2008.02.013

22. Hume KR, Johnson JL, Williams LE. Adverse effects of concurrent carboplatin chemotherapy and radiation therapy in dogs. *J Vet Intern Med*. (2009) 23:24–30. doi: 10.1111/j.1939-1676.2008.0224.x

23. Weichselbaum RR, Liang H, Deng L, Fu YX. Radiotherapy and immunotherapy: a beneficial liaison? *Nat Rev Clin Oncol*. (2017) 14:365–79. doi: 10.1038/nrclinonc.2016.211

24. Sharabi AB, Lim M, DeWeese TL, Drake CG. Radiation and checkpoint blockade immunotherapy: radiosensitisation and potential mechanisms of synergy. *Lancet Oncol*. (2015) 16:e498–509. doi: 10.1016/S1470-2045(15)00007-8

25. Twyman-Saint Victor C, Rech AJ, Maity A, Rengan R, Pauken KE, Stelekati E, et al. Radiation and dual checkpoint blockade activate non-redundant immune mechanisms in cancer. *Nature*. (2015) 520:373–7. doi: 10.1038/nature14292

26. Luo LY, O'Hara MH, Mitchell TC, Vonderheide RH, Wherry EJ, Minn AJ, et al. Combining radiation with immunotherapy: the University of Pennsylvania experience. *Semin Radiat Oncol*. (2020) 30:173–80. doi: 10.1016/j.semradonc.2019.12.007

27. Arina A, Gutiontov SI, Weichselbaum RR. Radiotherapy and immunotherapy for Cancer: from "systemic" to "multisite". *Clin Cancer Res*. (2020) 26:2777–82. doi: 10.1158/1078-0432.CCR-19-2034

28. Qin R, Olson A, Singh B, Thomas S, Wolf S, Bhavsar NA, et al. Safety and efficacy of radiation therapy in advanced melanoma patients treated with Ipilimumab. *Int J Radiat Oncol Biol Phys*. (2016) 96:72–7. doi: 10.1016/j.ijrobp.2016.04.017

29. Hiniker SM, Reddy SA, Maecker HT, Subrahmanyam PB, Rosenberg-Hasson Y, Swetter SM, et al. A prospective clinical trial combining radiation therapy with systemic immunotherapy in metastatic melanoma. *Int J Radiat Oncol Biol Phys*. (2016) 96:578–88. doi: 10.1016/j.ijrobp.2016.07.005

30. Canter RJ, Grossenbacher SK, Foltz JA, Sturgill IR, Park JS, Luna JI, et al. Radiotherapy enhances natural killer cell cytotoxicity and localization in pre-clinical canine sarcomas and first-in-dog clinical trial. *J Immunother Cancer*. (2017) 5:98. doi: 10.1186/s40425-017-0305-7

31. Deguchi T, Maekawa N, Konnai S, Owaki R, Hosoya K, Morishita K, et al. Enhanced systemic antitumour immunity by Hypofractionated radiotherapy and anti-PD-L1 therapy in dogs with pulmonary metastatic Oral malignant melanoma. *Cancers*. (2023) 15:3013. doi: 10.3390/cancers15113013

32. Boss MK, Watts R, Harrison LG, Hopkins S, Chow L, Trageser E, et al. Immunologic effects of stereotactic body radiotherapy in dogs with spontaneous tumors and the impact of intratumoral OX40/TLR agonist immunotherapy. *Int J Mol Sci*. (2022) 23:826. doi: 10.3390/ijms23020826

33. Magee K, Marsh IR, Turek MM, Grudzinski J, Aluicio-Sarduy E, Engle JW, et al. Safety and feasibility of an in situ vaccination and immunomodulatory targeted radionuclide combination immuno-radiotherapy approach in a comparative (companion dog) setting. *PLoS One*. (2021) 16:e0255798. doi: 10.1371/journal.pone.0255798

34. Chuang T-F. Immunotherapy and imaging diagnosis of canine cancers. PhD Dissertion. Taipei: National Taiwan University (2011).

35. Nguyen SM, Thamm DH, Vail DM, London CA. Response evaluation criteria for solid tumours in dogs (v1.0): a veterinary cooperative oncology group (VCOG) consensus document. *Vet Comp Oncol*. (2015) 13:176–83. doi: 10.1111/vco.12032

36. Ladue T, Klein MK. Toxicity criteria of the veterinary radiation therapy oncology group. *Vet Radiol Ultrasound*. (2001) 42:475–6. doi: 10.1111/j.1740-8261.2001.tb00973.x

37. Group VCOO. Veterinary cooperative oncology group - common terminology criteria for adverse events (VCOG-CTCAE) following chemotherapy or biological antineoplastic therapy in dogs and cats v1.1. *Vet Comp Oncol*. (2016) 14:417–46. doi: 10.1111/vco.283

38. LeBlanc AK, Atherton M, Bentley RT, Boudreau CE, Burton JH, Curran KM, et al. Veterinary cooperative oncology group-common terminology criteria for adverse events (VCOG-CTCAE v2) following investigational therapy in dogs and cats. *Vet Comp Oncol*. (2021) 19:311–52. doi: 10.1111/vco.12677

39. Darragh LB, Gadwa J, Pham TT, Van Court B, Neupert B, Olimpo NA, et al. Elective nodal irradiation mitigates local and systemic immunity generated by combination radiation and immunotherapy in head and neck tumors. *Nat Commun*. (2022) 13:7015. doi: 10.1038/s41467-022-34676-w

40. Saddawi-Konefka R, O'Farrell A, Faraji F, Clubb L, Allevato MM, Jensen SM, et al. Lymphatic-preserving treatment sequencing with immune checkpoint inhibition unleashes cDC1-dependent antitumor immunity in HNSCC. *Nat Commun*. (2022) 13:4298. doi: 10.1038/s41467-022-31941-w

41. Fabre JW. The allogeneic response and tumor immunity. *Nat Med*. (2001) 7:649–52. doi: 10.1038/89008

42. Gaspar TB, Henriques J, Marconato L, Queiroga FL. The use of low dose metronomic chemotherapy in dogs-insight into a modern cancer field. *Vet Comp Oncol*. (2018) 16:2–11. doi: 10.1111/vco.12309

43. Smedley RC, Bongiovanni L, Bacmeister C, Clifford CA, Christensen N, Dreyfus JM, et al. Diagnosis and histopathologic prognostication of canine melanocytic neoplasms: a consensus of the oncology-pathology working group. *Vet Comp Oncol*. (2022) 20:739–51. doi: 10.1111/vco.12827

frontiers | Frontiers in Veterinary Science

TYPE Case Report
PUBLISHED 10 January 2025
DOI 10.3389/fvets.2024.1497077

Check for updates

OPEN ACCESS

EDITED BY
Leonardo Leonardi,
University of Perugia, Italy

REVIEWED BY
Robert Michael Baratt,
Salem Valley Veterinary Clinic, United States
Aurelian-Sorin Pasca,
Iasi University of Life Sciences (IULS), Romania

*CORRESPONDENCE
Alexandru-Flaviu Tăbăran
✉ alexandru.tabaran@usamvcluj.ro

RECEIVED 16 September 2024
ACCEPTED 04 December 2024
PUBLISHED 10 January 2025

CITATION
Pop R, Tăbăran A-F, Vasiu I, Milgram J and Ober CA (2025) Surgical management of ossifying fibroma in a 9-year-old Hungarian Vizsla: a case report and review of the literature. *Front. Vet. Sci.* 11:1497077. doi: 10.3389/fvets.2024.1497077

COPYRIGHT
© 2025 Pop, Tăbăran, Vasiu, Milgram and Ober. This is an open-access article distributed under the terms of the Creative Commons Attribution License (CC BY). The use, distribution or reproduction in other forums is permitted, provided the original author(s) and the copyright owner(s) are credited and that the original publication in this journal is cited, in accordance with accepted academic practice. No use, distribution or reproduction is permitted which does not comply with these terms.

Surgical management of ossifying fibroma in a 9-year-old Hungarian Vizsla: a case report and review of the literature

Romelia Pop[1], Alexandru-Flaviu Tăbăran[1]*, Iosif Vasiu[2], Joshua Milgram[3] and Ciprian Andrei Ober[2]

[1]Department of Pathology, Faculty of Veterinary Medicine, University of Agricultural Sciences and Veterinary Medicine of Cluj-Napoca, Cluj-Napoca, Romania, [2]Department of Anesthesiology and Surgery, University of Agricultural Sciences and Veterinary Medicine, Cluj-Napoca, Romania, [3]Department of Small Animal Surgery, The Koret School of Veterinary Medicine, The Hebrew University of Jerusalem, Rehovot, Israel

Ossifying fibroma (OF) is a rare, benign fibro-osseous neoplasm that primarily originates from membranous bones. While most frequently documented in equines, OF has also been reported in other species, including dogs, though it remains uncommon. The condition poses significant diagnostic challenges due to its ambiguous presentation, often requiring differentiation from other benign and malignant intraosseous lesions. This case report describes an ossifying fibroma localized to the zygomatic bone in a 9-year-old Hungarian Vizsla. A zygomatic arch ostectomy was successfully performed, and long-term follow-up was excellent. This is only the second documented case of zygomatic localization of OF in a dog, highlighting the rarity of this presentation. The discussion emphasizes the importance of distinguishing OF from other proliferative fibro-osseous lesions, such as fibrous dysplasia (FD) and cemento-osseous dysplasia (COD), and considering the potential for malignancies, such as low-grade osteosarcoma (LG-OSA), to mimic these benign growths. This case contributes valuable insights to the limited veterinary literature on ossifying fibroma, particularly regarding its atypical presentations in canine patients.

KEYWORDS

fibroma, ossifying, zygomatic, radiology, histopathology, dog

1 Introduction

Ossifying fibroma (OF) represents a rare and benign fibro-osseous neoplasm (1) that primarily arises from membranous bones (2). Its infrequent occurrence and ambiguous clinical presentation pose significant diagnostic and therapeutic challenges in veterinary medicine. OF is most commonly found in equines, particularly horses (3–7), but it can also be observed in other species such as dogs (1, 8, 9) and cats (10). Rare instances have been reported in rabbits (11), llamas (12), and canaries (13) (see Table 1). In humans, according to the World Health Organization (WHO), the most frequent localization of ossifying fibroma is in the posterior mandible (14). Similarly, literature on canine cases indicates that the most common sites of ossifying fibroma are the mandible and maxilla (see Figure 1). This case report details the occurrence of ossifying fibroma in a 9-year-old Hungarian Vizsla with zygomatic localization. Through this detailed case study, we aim to contribute to the limited veterinary literature on ossifying fibroma, providing valuable insights for clinicians encountering similar cases in their practice. To the authors' knowledge, this is

TABLE 1 Documented cases of ossifying fibroma in dogs: breed, age, and localization.

No.	Breed	Age (years)	Localization	References
1.	Pembroke Welsh corgi	1.8	Zygomatic arch	(15)
2.	Mixed breed	15	Left hemimandible	(9)
3.	Pembroke Welsh corgi	3	C6 cervical vertebra	(8)
4.	Australian Terrier	6	Left calvarium	(18)
5.	NS	7.5	Left caudal maxilla	(1)
6.	NS	13	Left rostral maxilla	(1)
7.	NS	12	Left caudal mandible	(1)
8.	Kelpie cross	10	Frontal sinus	(19)
9.	NS	NS	Maxilla (no specific location mentioned)	(20)
10.	NS	NS	Maxilla (no specific location mentioned)	(20)
11.	NS	NS	Mandible (no specific location mentioned)	(20)
12.	NS	NS	Mandible (no specific location mentioned)	(20)
13.	Golden retriever	9	Right mandible	(21)

NS, not specified.

the second report of an ossifying fibroma with zygomatic bone localization in this species, the first one being described by Best, E. in a Corgi (15).

2 Case description

2.1 Clinical examination

A 9.4-year-old male Hungarian Vizsla was referred to the Department of Surgery and Intensive Care for evaluation of a slow-growing zygomatic arch mass near the right eye, present for 2 years (see Figure 2A). Upon examination, the mass measured ~2.5 cm in diameter, with a multilobulated, firm, non-mobile, and non-painful consistency upon palpation. Occasional signs included blepharospasm, photosensitivity, hyperemic conjunctiva, and purulent epiphora. Non-contrast computed tomography (CT) revealed a focal, round, expansile bone lesion on the right zygomatic arch, measuring 2.0 × 2.3 × 1.5 cm (L, H, W) (see Figure 3). The inner bone structure, nasolacrimal duct, and teeth were unaffected, and no lymphadenopathy was noted. Thoracic CT showed no evidence of metastasis. Given the lesion's slow growth, the owner opted for an excisional biopsy. Cefazolin (22 mg/kg IV) was administered preoperatively. The surgical approach was well documented (16), and the cosmetic outcome was excellent following the zygomatic arch ostectomy. The procedure involved an incision of the skin and temporalis muscle aponeurosis along

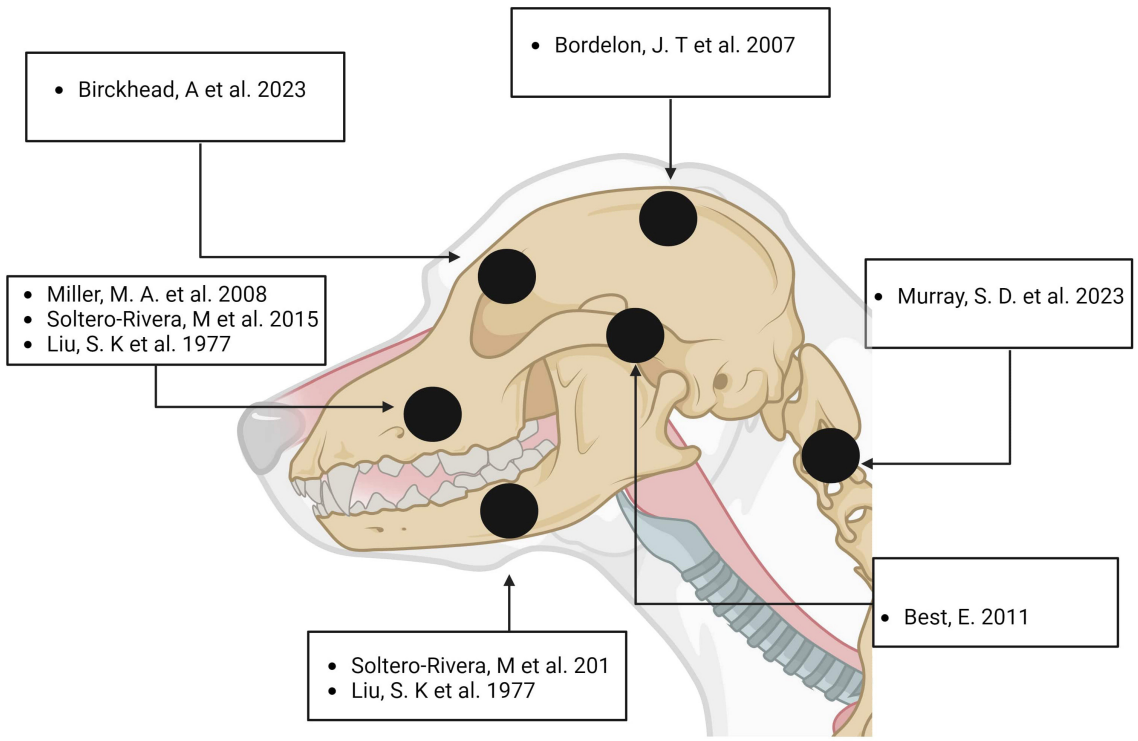

FIGURE 1
Distribution of Ossifying Fibroma in the Cranio-Cervical Region of Dogs. Created with Biorender.

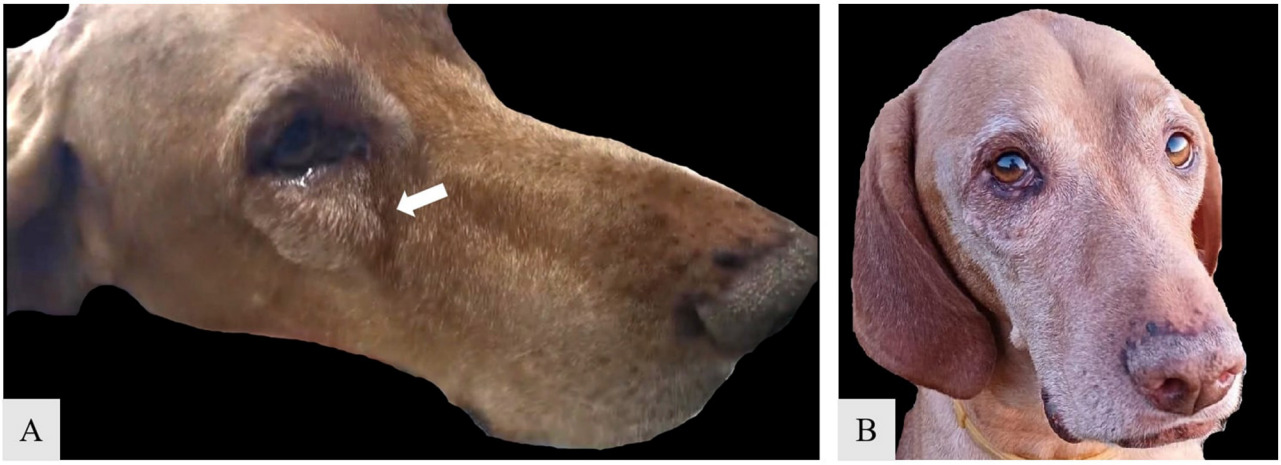

FIGURE 2
Preoperative appearance of neoplastic growth on the zygomatic arch in male Hungarian Viszla [**(A)** white arrow]; Ten-months postoperative aspect of the zygomatic area **(B)**.

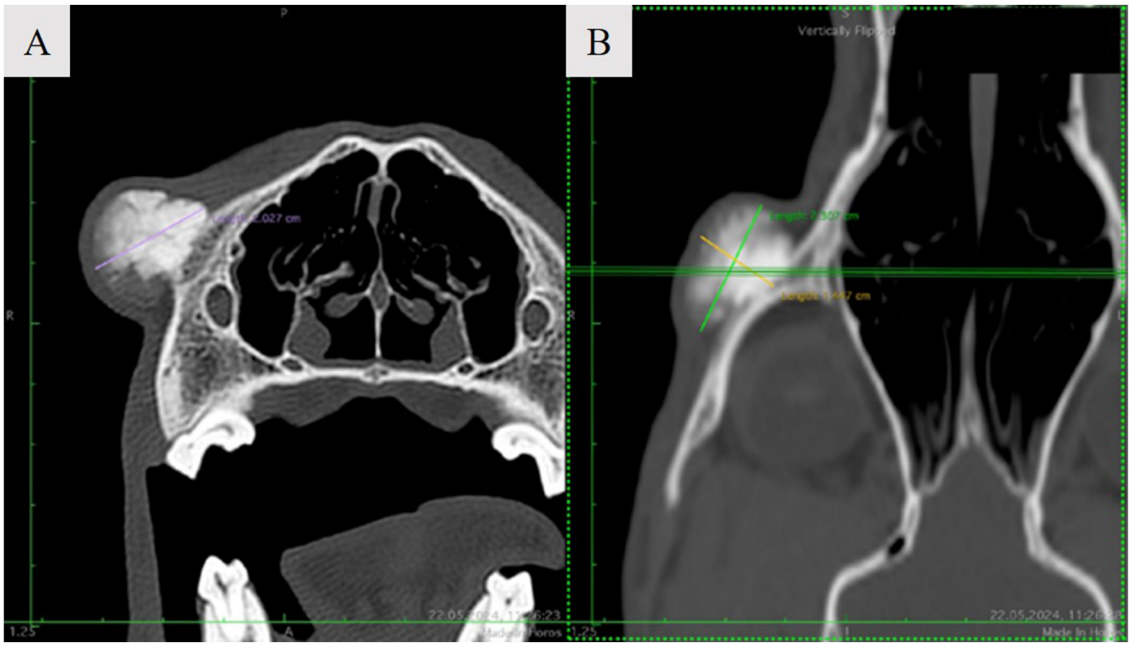

FIGURE 3
Noncontrast axial **(A)** and dorsal **(B)** CT image demonstrating a focal, round, expansile bone cortical lesion of the right zygomatic arch.

the dorsal margin of the zygomatic arch. Both cranial and caudal osteotomies were performed with an oscillating saw, preserving the orbital ligament. Histopathological analysis of the excised tissue confirmed the diagnosis of ossifying fibroma. The dog's recovery from surgery and anesthesia was uneventful. Postoperative pain management was maintained using a constant rate infusion (CRI) of lidocaine (20 μg/kg/h) combined with ketamine (10 μg/kg/h) and metamizole (25 mg/kg IV every 8 h). The dog was discharged with robenacoxib (2 mg/kg SC every 24 h). The owner was advised to provide a soft kibble diet, avoid toys or mouth play, and restrict the dog's exercise to short-lead walks for two weeks.

2.2 Histopathological examination

For histological analysis, the mass was fixed in 10% neutral buffered formalin (NBF) for 24 h, followed by decalcification in a rapid decalcifier for 5 days. The tissue was then routinely

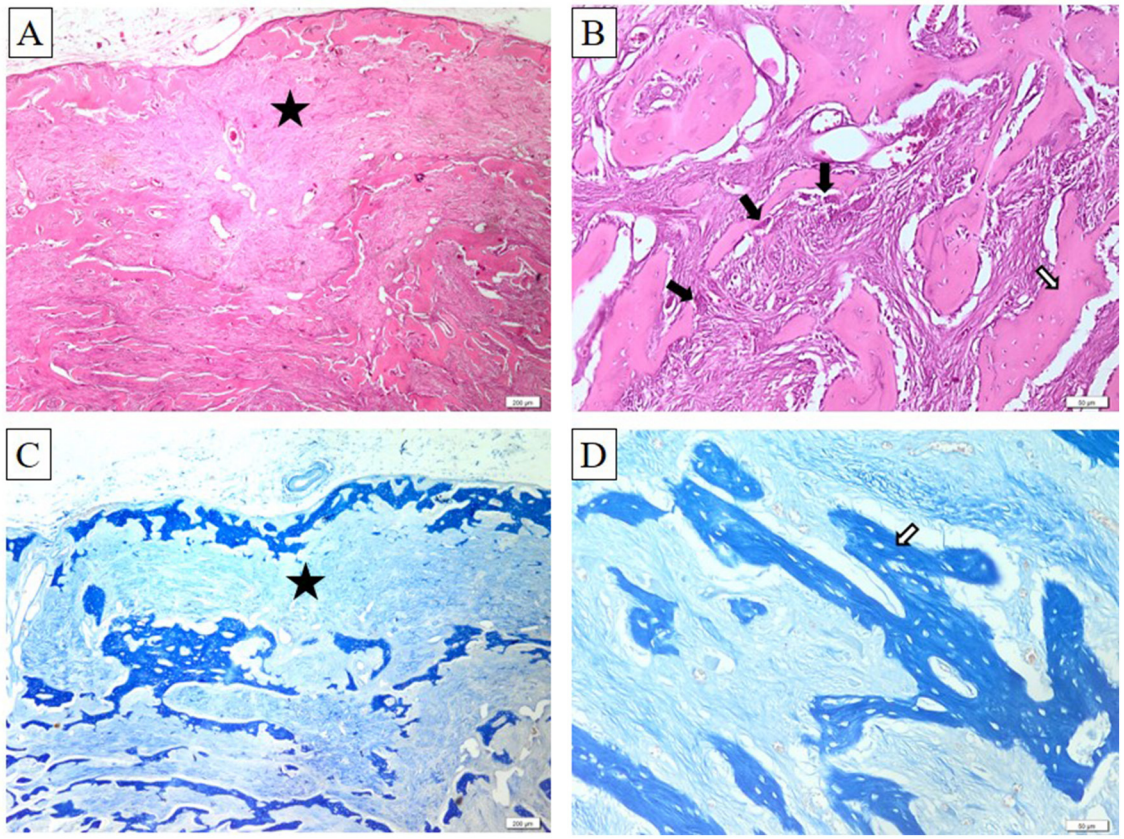

FIGURE 4
Ossifying fibroma. Bony trabeculae (white arrows) bordered by a single layer of osteoblasts (black arrows) and embedded within abundant fibrous connective tissue (black asterisk). Within this connective tissue, numerous well-differentiated spindle-shaped fibroblasts are dispersed. H&E stain **(A, B)**, Masson's trichrome stain **(C, D).** Ob. ×4 **(A, C)** and ob. ×20 **(B, D)**. Barr 50 μm **(B, D)** and 200 μm **(A, C)**.

processed for paraffin embedding. Sections, 2 micrometers thick, were cut and stained with hematoxylin and eosin (H&E). Histopathological examination revealed a well-demarcated mass composed of a fibrous component consisting of spindle-shaped fibroblasts arranged in a whorled or storiform pattern, embedded within a collagenous stroma. Interspersed throughout the fibrous stroma were varying amounts of mineralized material, including woven bone, lamellar bone, and cementum-like calcifications. The mineralized component often appeared as trabeculae of osteoid and mature bone, occasionally rimmed by osteoblasts. These trabeculae were typically surrounded by osteoclast-like giant cells involved in bone remodeling. The transition between the fibrous tissue and the mineralized material was gradual, with no signs of anaplasia or atypia. The presence of well-formed bone trabeculae within a cellular fibroblastic stroma is characteristic of ossifying fibroma. Additionally, areas of hemorrhage and cystic degeneration were observed in some cases (see Figure 4).

2.3 Follow-up

Two weeks after discharge, the incision site showed proper healing, with a good cosmetic outcome. The owner reported normal prehension and behavior. The dog was bright, alert, tolerated food and water well, and was walked daily on a leash. Monthly follow-ups were conducted via telephone, and the owner was instructed to return for in-person evaluations at three-month intervals during the first year post-surgery. At 10 months after the procedure, a clinical examination revealed no signs of tumor recurrence (Figure 2B), and the owner reported no changes in the dog's eating, drinking, or behavior. Twelve months after surgery, the owner was very satisfied with the cosmetic appearance and the comfort of the right eye.

3 Discussion

Ossifying fibroma (OF) is a rare, benign fibro-osseous neoplasm that requires careful differentiation from other benign intraosseous proliferative fibro-osseous lesions (PFOLs). PFOLs are characterized by the replacement of normal bone with a fibrous matrix containing varying degrees of mineralization and ossification (1). In humans, this category includes conditions such as ossifying fibroma (OF), fibrous dysplasia (FD), and cemento-osseous dysplasia (COD) (17). It is important to recognize that some malignant lesions, like low-grade osteosarcoma (LG-OSA), can mimic these benign growths, especially in the skull.

A review of the literature highlights the rarity of ossifying fibroma across species, with most cases documented in equines, particularly horses (3–7). In small animals, reports are limited, although ossifying fibroma has been observed in dogs (1, 8, 9, 18–21) and cats (10). This limited occurrence poses challenges in diagnosis and treatment, particularly when the lesion arises in atypical locations, such as the zygomatic bone, as in the case presented here. The uniqueness of this case—only the second report of such localization in a dog—emphasizes the need for continued documentation and study of these rare cases to enhance understanding and management of OF in veterinary practice.

In veterinary medicine, other potential differential diagnoses for intraosseous lesions, besides true PFOLs like OF and FD, include osteoma, osteitis/osteomyelitis, fibrous osteodystrophy, conventional osteosarcoma (OSA), and multilobular tumor of bone (MLTB). FD is a rare benign condition in which fibrous tissue replaces normal bone, leading to deformities and swelling. It commonly affects young animals, with expansile growth potentially causing decreased bone strength and pathologic fractures, often in the skull and jawbones. Radiographically, fibrous dysplasia typically presents a more homogeneous "ground glass" appearance, lacking the well-defined margins characteristic of ossifying fibroma (17). Cemento-osseous dysplasia (COD) primarily affects the jawbones (maxilla and mandible) and is characterized by a disorganized mixture of fibrous tissue, irregular bone, and cementum-like material (22). However, in our case, the lesion was uniquely located in the zygomatic bone, underscoring the importance of careful diagnostic evaluation to distinguish ossifying fibroma from other intraosseous lesions. Given the rarity of OF in dogs and its variable presentation, this case report contributes valuable insights to the limited veterinary literature. The zygomatic localization presents a unique diagnostic challenge, requiring a comprehensive understanding of potential differential diagnoses. Since the literature primarily documents ossifying fibroma in the mandible and maxilla of dogs (1), this case highlights the importance of considering less common sites when diagnosing PFOLs in small animals. Continued reporting and review of such cases are critical to refining diagnostic and therapeutic approaches for ossifying fibroma and similar lesions in veterinary practice.

Data availability statement

The original contributions presented in the study are included in the article/supplementary material, further inquiries can be directed to the corresponding author.

Ethics statement

The animal studies were approved by University Ethics Committee, The Bioethics Subcommittee for Experiments on Animals, Plants, or Human Subjects. University of Agriculture Science and Veterinary Medicine Cluj-Napoca, Romania. The studies were conducted in accordance with the local legislation and institutional requirements. Written informed consent was obtained from the owners for the participation of their animals in this study.

Author contributions

RP: Conceptualization, Methodology, Writing – original draft. A-FT: Investigation, Supervision, Validation, Visualization, Writing – review & editing. IV: Conceptualization, Methodology, Writing – original draft. JM: Methodology, Supervision, Validation, Writing – review & editing. CO: Investigation, Supervision, Validation, Writing – review & editing.

Funding

The author(s) declare financial support was received for the research, authorship, and/or publication of this article. The University of Agriculture Science and Veterinary Medicine Cluj-Napoca, Romania.

Conflict of interest

The authors declare that the research was conducted in the absence of any commercial or financial relationships that could be construed as a potential conflict of interest.

Publisher's note

All claims expressed in this article are solely those of the authors and do not necessarily represent those of their affiliated organizations, or those of the publisher, the editors and the reviewers. Any product that may be evaluated in this article, or claim that may be made by its manufacturer, is not guaranteed or endorsed by the publisher.

References

1. Soltero-Rivera M, Engiles JB, Reiter AM, Reetz J, Lewis JR, Sánchez MD. Benign and malignant proliferative fibro-osseous and osseous lesions of the oral cavity of dogs. *Vet Pathol.* (2015) 52:894–902. doi: 10.1177/0300985815583096

2. Thompson KG, Dittmer KE. Tumors of Bone. In: Meuten DJ, editors. *Tumors in Domestic Animals*. Hoboken, NJ: John Wiley & Sons, Inc (2016). p. 356–424. doi: 10.1002/9781119181200.ch10

3. Crijns CP, Vlaminck L, Verschooten F, van Bergen T, De Cock HE, Huylebroek F, et al. Multiple mandibular ossifying fibromas in a yearling B elgian D raught horse filly. *Equine Vet Educ.* (2015) 27:11–5. doi: 10.1111/eve.12246

4. Puff C, Ohnesorge B, Wagels R, Baumgärtner W. An unusual mucinous osteoma with features of an ossifying fibroma in the nasal cavity of a horse. *J Comp Pathol.* (2006) 135:52–5. doi: 10.1016/j.jcpa.2006.02.008

5. Kodaira K, Muranaka M, Naito Y, Ode H, Oku K, Nukada T, et al. Histopathological characteristics of an ossifying fibroma formed in the maxilla of a racehorse. *J Equine Sci.* (2010) 21:7–10. doi: 10.1294/jes.21.7

6. Turek B, Górski K, Drewnowska O, Buczkowska R, Kozłowska N, Sapierzyński R. Ossifying fibroma in the nasal cavity of a 2-year-old horse. *Animals.* (2021) 11:317. doi: 10.3390/ani11020317

7. Morse CC, Saik JE, Richardson DW, Fetter AW. Equine juvenile mandibular ossifying fibroma. *Vet Pathol.* (1988) 25:415–21. doi: 10.1177/030098588802500603

8. Murray SD, Cameron S, Tolliver SE, Cole CY, Aschenbroich SA. Ossifying fibroma in the cervical vertebra of a dog. *Can Vet J.* (2023) 64:367–71.

9. Miller MA, Towle HAM, Heng HG, Greenberg CB, Pool RR. Mandibular ossifying fibroma in a dog. *Vet Pathol.* (2008) 45:203–6. doi: 10.1354/vp.45-2-203

10. Turrel JM, Pool RR. Primary bone tumors in the cat: a retrospective study of 15 cats and a literature review. *Vet Radiol.* (1982) 23:152–66. doi: 10.1111/j.1740-8261.1982.tb01099.x

11. Whitten KA, Popielarczyk MM, Belote DA, McLeod GC, Mense MG. Ossifying fibroma in a miniature rex rabbit (*Oryctolagus cuniculus*). *Vet Pathol.* (2006) 43:62–4. doi: 10.1354/vp.43-1-62

12. McCauley CT, Campbell GA, Cummings CA, Drost WT. Ossifying fibroma in a llama. *J Vet Diagn Invest.* (2000) 12:473–6. doi: 10.1177/104063870001200517

13. Razmyar J, Dezfoulian O, Peighambari SM. Ossifying fibroma in a canary (*Serinus canaria*). *J Avian Med Surg.* (2008) 22:320–2. doi: 10.1647/2007-027.1

14. Thompson LDR. World Health Organization classification of tumours: pathology and genetics of head and neck tumours. *Ear Nose Throat J.* (2006) 85:74. doi: 10.1177/014556130608500201

15. Best E. *Ossifying fibroma of the zygomatic arch in a 20-month-old male corgi.* (2011). Available at: https://www.vettimes.co.uk/app/uploads/wp-post-to-pdf-enhanced-cache/1/ossifying fibroma of the zygomatic arch in a 20 month old male corgi.pdf (accessed December 1, 2024).

16. Dörner J, Oberbacher S, Dupré G. Comparison of three surgical approaches for zygomatic sialoadenectomy in canine cadavers. *Vet Surg.* (2021) 50:564–70. doi: 10.1111/vsu.13589

17. Alawi F. Benign fibro-osseous diseases of the maxillofacial bones: a review and differential diagnosis. *Pathol Patterns Rev.* (2002) 118:S50–70. doi: 10.1309/NUXA-JUT9-HA09-WKMV

18. Bordelon JT, Rochat MC. Use of a titanium mesh for cranioplasty following radical rostrotentorial craniectomy to remove an ossifying fibroma in a dog. *J Am Vet Med Assoc.* (2007) 231:1692–5. doi: 10.2460/javma.231.11.1692

19. Birckhead A, Carstens A, Geiss E, Yap F, Huizing X. Computed tomographic characteristics of frontal sinus ossifying fibroma in a dog. *Vet Radiol. Ultrasound.* (2023) 64:E60–3. doi: 10.1111/vru.13285

20. Liu S, Dorfman HD, Hurvitz AI, Patnaik AK. Primary and secondary bone tumours in the dog. *J Small Anim Pract.* (1977) 18:313–26. doi: 10.1111/j.1748-5827.1977.tb05890.x

21. Speltz MC, Pool RR, Hayden DW. Pathology in practice. *J Am Vet Med Assoc.* (2009) 235:1283–5. doi: 10.2460/javma.235.11.1283

22. Veltrini VC, Figueira JA, Santin GC, de Sousa SCOM, de Araújo NS. Can non-collagenous proteins be employed for the differential diagnosis among fibrous dysplasia, cemento-osseous dysplasia and cemento-ossifying fibroma? *Pathol-Res Pract.* (2019) 215:152450. doi: 10.1016/j.prp.2019.152450

frontiers | Frontiers in Veterinary Science

TYPE Case Report
PUBLISHED 04 February 2025
DOI 10.3389/fvets.2024.1500679

Check for updates

OPEN ACCESS

EDITED BY
Yasunaga Yoshikawa,
Kitasato University, Japan

REVIEWED BY
Carlos Rodriguez,
VSNT, United States
Serpil Dağ,
Kafkas University, Türkiye

*CORRESPONDENCE
Desheng Li
lidesheng_ccrcgp@163.com
Zhengli Chen
chzhli75@163.com

†These authors have contributed equally to this work

RECEIVED 23 September 2024
ACCEPTED 16 December 2024
PUBLISHED 04 February 2025

CITATION
Xiong Z, Ling S, Li C, Deng L, He M, Wang C, Li D and Chen Z (2025) Case report: A study on the pathological diagnosis of oral fibrosarcoma in a giant panda.
Front. Vet. Sci. 11:1500679.
doi: 10.3389/fvets.2024.1500679

COPYRIGHT
© 2025 Xiong, Ling, Li, Deng, He, Wang, Li and Chen. This is an open-access article distributed under the terms of the Creative Commons Attribution License (CC BY). The use, distribution or reproduction in other forums is permitted, provided the original author(s) and the copyright owner(s) are credited and that the original publication in this journal is cited, in accordance with accepted academic practice. No use, distribution or reproduction is permitted which does not comply with these terms.

Case report: A study on the pathological diagnosis of oral fibrosarcoma in a giant panda

Zongliang Xiong[1†], Shanshan Ling[2†], Caiwu Li[2†], Linhua Deng[2], Ming He[2], Chengdong Wang[2], Desheng Li[2*] and Zhengli Chen[1*]

[1]Experimental Animal Disease Model Research Laboratory, School of Veterinary Medicine, Sichuan Agricultural University, Chengdu, China, [2]Key Laboratory of State Forestry and Grassland Administration on the Giant Panda, China Conservation and Research Center for the Giant Panda, Chengdu, China

A female giant panda presented with a large, hard mass on the right cheek, which was investigated at the Dujiangyan Base of the China Conservation and Research Center for the Giant Panda with computed tomography (CT) scans and biopsy of the oral mass, as well as venous blood sampling. Hematological tests revealed elevated levels of the tumor marker CA724, along with infectious disease, anemia, hepatic damage, and renal failure. Imaging studies identified a soft tissue mass in the right cheek area. Macroscopic pathological changes, histopathological features, and immunohistochemical analysis were consistent with a low-grade malignant fibrosarcoma within the oral cavity, indicating malignant potential. This case represents the first report of an oral tumor in a giant panda, providing valuable data for future clinical diagnoses of neoplasms in this species.

KEYWORDS

case report, giant panda, oral fibrosarcoma, pathology diagnostic research, biopsy

Introduction

The giant panda (*Ailuropoda melanoleuca*), the only mammal within the order Carnivora, family Ursidae, subfamily Ailuropodinae, and genus Ailuropoda, is an endangered and rare animal, affording it first-class state protection in China. It is referred to as a "living fossil" and "Chinese national treasure", and research into its diseases, as well as prevention and control, have garnered significant attention. With the enhancement of animal protection measures, the life expectancy of giant pandas has increased, and the occurrence of tumors has risen correspondingly. Consequently, research on tumors in giant pandas has gained increasing significance. There are relatively few reports documenting giant panda tumor cases. At present, the documented cases include only types such as ovarian cancer, pancreatic ductal adenocarcinoma, seminoma, cutaneous hemangioma, and conjunctival angiosarcoma (1–5). This results in a scarcity of clinical diagnostic data pertaining to giant panda tumors, with a particular deficiency in detection data and reports from live sampling.

This report concentrates on a case of neoplasm in an aged giant panda identified during clinical feeding and management procedures. The preliminary diagnosis was informed by hematology, serum biochemistry, and oncologic blood markers. Subsequent diagnostic workups, including imaging and histopathological examination, facilitated further diagnosis of biopsied samples obtained from the living panda, resulting in a confirmed diagnosis of oral fibrosarcoma. Oral fibrosarcoma is a highly invasive malignant neoplasm, characterized by an insidious onset and limited initial lesion size. In veterinary oncology, oral fibrosarcoma is frequently diagnosed in dogs, cats, and various other

species. Oral tumors and tumor-like lesions in dogs and cats are often categorized as proliferative, inflammatory, or benign conditions, typically affecting middle-aged animals, without gender predisposition. The most common lesion in dogs is gingival hyperplasia, followed by peripheral odontogenic fibroma, and in cats, the most prevalent condition is lymphoplasmacytic stomatitis. The oral tumor in this report of a giant panda is presumed to originate from oral bleeding induced by consuming bamboo sticks. Chronic irritation led to the growth of specific tumors within the oral cavity, ultimately progressing to low-grade malignant fibroma. Consequently, this case report establishes a reasonably standardized and systematic diagnostic approach for oral tumors in giant pandas, offering a tangible benchmark for early detection and diagnosis of such tumors in giant pandas moving forward.

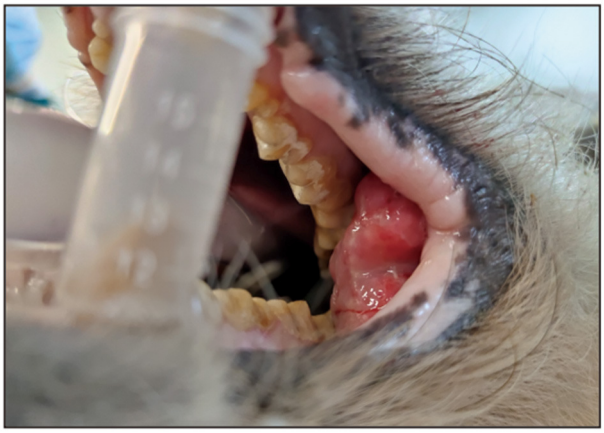

FIGURE 1
Oral growths in afflicted giant pandas.

Case description

Medical history investigation

Upon reviewing the medical records at the Dujiangyan Base of the China Conservation and Research Center for the Giant Panda, we obtained insights into the giant panda's clinical presentations and medical history. The detailed information is as follows: Ye Ye, a female giant panda, was born on September 25, 1999. At the age of 20, a physical examination detected a mass, measuring approximately 1 cm × 1 cm × 1 cm, beneath the mucosa of her right cheek. Subsequently, at age 21, she was transferred from the Shenshuping Base to the Dujiangyan Base, with no significant changes noted during this interval. Two years post-transfer, oral bleeding was observed, and examination identified a large, hard mass on her right cheek. Four months subsequent to this discovery, tissue from Ye Ye's oral mass and venous blood were collected for further diagnostic analysis.

Clinical examination

Routine examinations, including live sample collection, were conducted: with a body temperature of 37.3°C, a respiratory rate of 20 breaths/min, and a heart rate of 80 beats/min. Clinical examination revealed that the lesion was located beneath the buccal mucosa within the oral cavity. There were no signs of excessive salivation, exophthalmos, facial edema or deformity, epistaxis, weight loss, halitosis, dysphagia, or oral pain, nor was there cervical lymph node enlargement, or loose teeth. A smooth-surfaced, firm, multi-lobed tumor was visualized inside the oral cavity (Figure 1).

Results

Hematology tests

Routine hematological analysis: the leukocyte count (WBC) is unremarkable, whereas neutrophil percentage (Neu%) and count (Neu) are elevated. Conversely, lymphocyte percentage (Lym%) and count (Lym#) are reduced, and eosinophil percentage (Eos%) and count (Eos) are likewise decreased. These findings suggest a potential infectious or neoplastic process in the giant panda Ye Ye, supported by indicators of lymphatic tissue compromise. The erythrocyte count (RBC) for Ye Ye is stable; however, decrements in hemoglobin (HGB), hematocrit (HCT), mean corpuscular volume (MCV), mean corpuscular hemoglobin (MCH), red cell distribution width standard deviation (RDW-SD), and mean platelet volume (MPV) are consistent with a diagnosis of nutritional anemia. Furthermore, a marked increase in the platelet count (PLT) suggests a possible link to malignancy (Table 1). Blood biochemical analysis reveals elevated activities of alanine aminotransferase (ALT) and aspartate aminotransferase (AST), with reduced albumin (ALB) levels and elevated globulin (GLO) levels. Additionally, total bilirubin (TBil) levels are diminished, γ-glutamyltransferase (GGT) levels are increased, and alkaline phosphatase (ALP) levels are elevated. These findings collectively suggest liver tissue pathology and hepatocellular damage in the giant panda Ye Ye. Elevated serum creatinine (CREA) and reduced uric acid (UA) levels indicate impaired renal function, specifically a decline in glomerular filtration rate, in the giant panda Ye Ye (Table 1). Coagulation profile reveals: Prothrombin time (PT) is prolonged, and fibrinogen concentration (Fbg) is reduced. Fibrinogen, identified as coagulation factor I, is a principal protein in the coagulation cascade. An elevated thrombin time (TT) suggests potential liver dysfunction, infection, or malignancy in the giant panda Ye Ye (Table 1). Serum tumor marker analysis: carbohydrate antigen 72-4 (CA724) levels were elevated, a marker for epithelial neoplasms. Hence, the presence of an epithelial tumor in the giant panda Ye Ye is suggested (Table 1).

Given the findings from the hematological tests, it is tentatively concluded that the giant panda Ye Ye may have a neoplastic condition and may additionally be experiencing infectious diseases, anemia, hepatic impairment, renal dysfunction, among other conditions.

Imaging assessment

The computed tomography (CT) scan disclosed a soft tissue mass within the right cheek region of the panda, measuring

TABLE 1 Hematology test of the giant panda called YeYe.

Test type	Test Item	Results	Units of Measurement	Range
Routine blood test	WBC	8.84	10e9/L	3.5–9.5
	Neu%	84.8	%	50–70
	Lym%	11.4	%	20–40
	Mon%	3.3	%	3.0–8
	Eos%	0.2	%	0.5–5.
	Bas%	0.3	%	0–1.0
	Neu#	7.5	10e9/L	2.00–7.00
	Lym#	1.01	10e9/L	1.1–3.2
	Mon#	0.29	10e9/L	0.10–0.60
	Eos#	0.01	10e9/L	0.02–0.52
	Bas#	0.03	10e9/L	0.00–0.10
	RBC	5.05	10e12/L	4.0–5.5
	HGB	86	g/L	120–160
	HCT	25.1	%	35.0–45.0
	MCV	49.8	fL	82.0–100.0
	MCH	17	pg	27.0–34.0
	MCHC	342	g/L	316–354
	RDW-CV	14.4	%	11.0–16.0
	RDW-SD	30.1	fL	39.0–53.9
	PLT	638	10e9/L	80–300
	MPV	5	fL	9.4–12.5
	PDW	14.4	fL	9.8–16.2
	PCT	0.319	%	0.16–0.38
Blood biochemistry test	ALT	175	U/L	5–40
	AST	122	U/L	8–40
	ALT/AST	0.7		0.8–2.0
	TP	62.9	g/L	60–85
	ALB	21.8	g/L	35–55
	GLO	41.1	g/L	20–40
	A/G	0.5		1.5–2.5
	TBil	1.69	umol/L	3.4–20.5
	DBil	1.61	umol/L	0–6.8
	IBi1	0.08	umol/L	0–15
	GGT	52	u/L	11–50
	ALP	386	u/L	40–150
	TBA	31.2	umol/L	0–10
	PA	7	mg/L	200–400
	CHE	580	u/L	4,000–11,000
	BUN	8.11	mmol/L	2.86–8.2
	CREA	112.06	umol/L	21.5–104
	UA	48	umol/L	208–428
	CYS-C	0.04	mg/L	0.51–1.09
	GLU	2.65	mmol/L	2.75–22
	TC	3.12	mmol/L	0–5.2
	TG	1.99	mmol/L	0–1.7
	HDL	1.95	mmol/L	0.83–1.96
	LDL	1.08	mmol/L	0–3.12
	ApoA1	0.01	g/L	1–1.6
	ApoB	0.02	g/L	0.6–1.10
	eGFR	1750.89	mL/min/1	
Coagulation test	PT	23.2	Sec	10–40
	APTT	32.5	Sec	20–40
	Fbg	1.84	g/L	45,326
	TT	24.7	Sec	14–21
	INR	2.09		0.8–1.25
Blood tumor marker detection	AFB	0.16	ng/mL	0–9
	CEA	0.06	ng/mL	0–5
	CA153	0	U/mL	0–14
	CA19-9	<0.8	U/mL	0–25
	CA125	1.1	U/mL	0–35
	CA724	30.19	U/mL	0–6.9

The values marked in blue are below the reference range, and those marked in red above it.

approximately 9.2 cm × 5.0 cm. The mass exhibited uneven density, punctuated by areas of calcification and gas shadows. The demarcation of the lesion was indistinct (Figure 2A), and the cortical bone adjacent to the lesion was hypertrophied and irregular, with significant edema of the surrounding soft tissues (Figure 2B). Sinusitis was also observed (Figure 2C).

Pathological examination

Following the aforementioned diagnostics, a biopsy of the oral mass was performed on the giant panda to obtain tissue samples. The procured samples were photographed, macroscopically observed, measured, and subsequently fixed in PFA solution. Subsequently, histopathological evaluation was conducted via paraffin sectioning, HE staining, and immunohistochemical assays. Macroscopic examination revealed a large tumor, measuring approximately 12 cm × 9 cm × 5 cm. It was situated beneath the buccal mucosa within the oral cavity, appearing as a large, firm plaque with a multinodular, gelatinous surface and rubbery consistency (Figures 3A–C). Histological analysis post paraffin embedding and HE staining revealed that the tumor was composed of numerous neoplastic cells organized in fascicular or storiform arrangements. The neoplastic cells varied in size, exhibiting a spindle or oval morphology, with infrequent

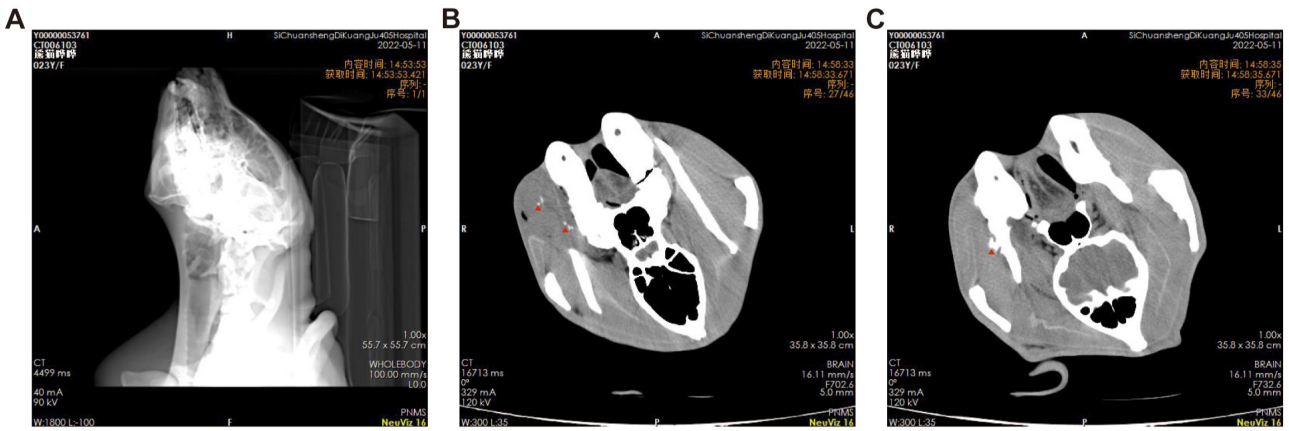

FIGURE 2
(A–C) Cross-sectional computed tomography images of the giant panda's head, the red triangle indicates the location of tumor calcification.

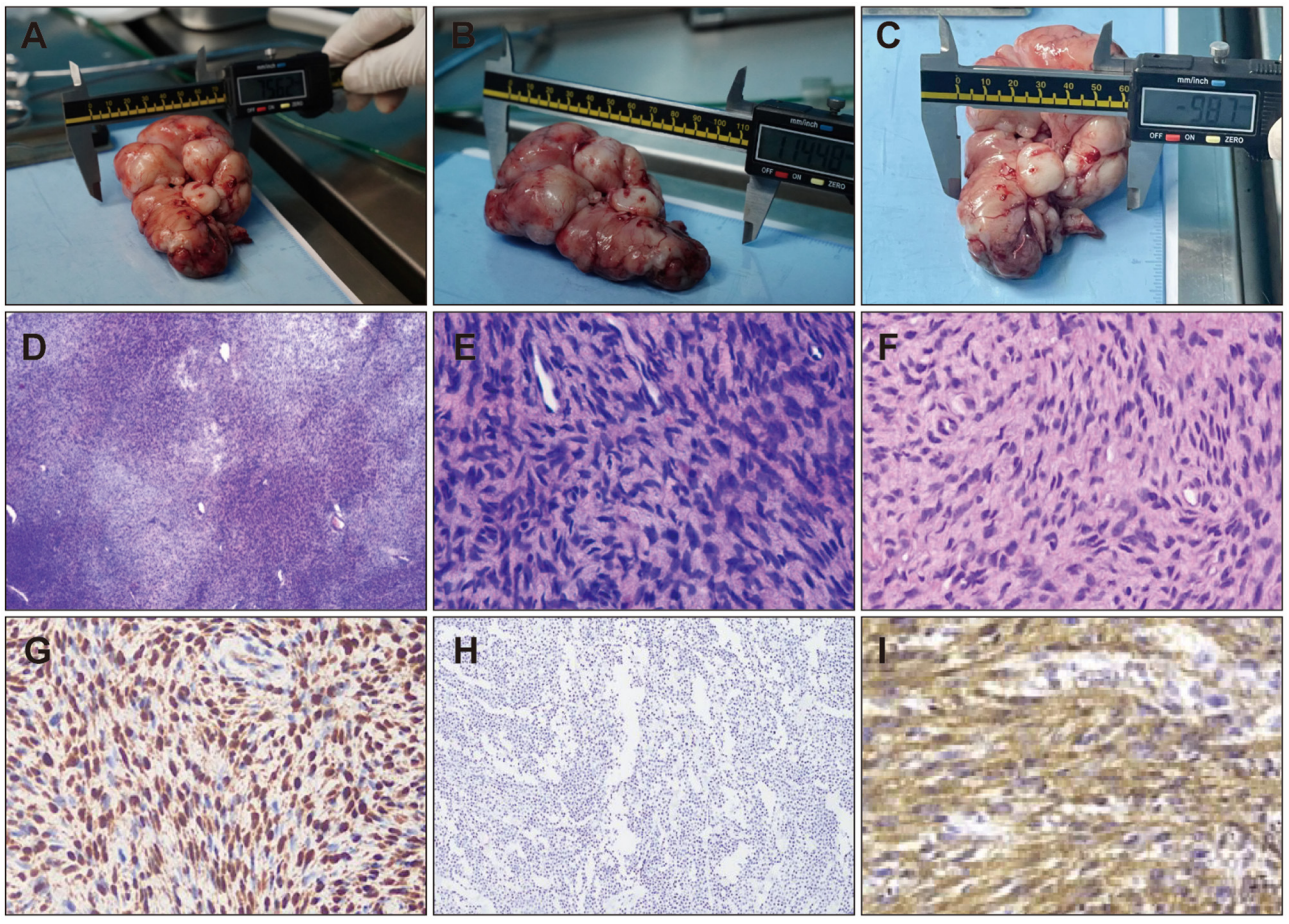

FIGURE 3
Histopathological Features of Oral Tumor Lesions from Living Giant Pandas. Pathological characteristics of oral tumors collected from living giant pandas **(A–C)**. **(D)** HE staining of tumor tissue (40X), **(E)** HE staining of tumor tissue (100X), **(F)** HE staining of tumor tissue (100X). Immunohistochemical staining of cavitary tumors, **(G)** Positive expression of S100 by immunohistochemistry. **(H)** Positive expression of Vimentin by immunohistochemistry. **(I)** Negative expression of CD34 by immunohistochemistry.

mitotic figures, and numerous small blood vessels were noted within the tumor's core (Figures 3D–F). Microscopically, the case demonstrated characteristic features of low-grade malignancy, aligning with a diagnosis of low-grade fibrosarcoma. Further differential diagnosis was conducted using immunohistochemical assays. The immunohistochemical results indicated positive

staining for Vimentin (++), focal S100 (+), with negative results for AE1/AE3, EMA, CK7, SMA, CD34, CD31, Desmin, Calponin, CD99, and a low Ki67 labeling index of approximately 1%. Consistent with the immunophenotypic profile of low-grade malignant fibrosarcoma, only Vimentin is expressed in immunohistochemistry; SMA may show positive expression in instances of myofibroblastic differentiation; Desmin, CK, EMA, and CD34 were non-reactive. The immunohistochemical findings corroborate the histopathological diagnosis of low-grade malignant fibrosarcoma (Figures 3G–I).

Discussion

Due to their unique characteristics, giant pandas can live for decades in artificial breeding environments, resulting in a longer lifespan compared to their wild counterparts. With the extension of the life cycle, the incidence of tumors rises, posing a threat to the lives of geriatric giant pandas. However, the scarcity of early clinical samples hinders effective monitoring of tumor occurrence in geriatric giant pandas. Our report demonstrates that tumor occurrence can be inferred by detecting blood-based tumor markers (PLT and CA724 in this study). Consequently, upon detecting abnormal blood indicators during health assessments, it is imperative to conduct more comprehensive examinations and initiate treatment for tumors at an early stage. This approach can help maintain the population of geriatric giant pandas to a significant extent, while also enriching the clinical data available, thereby aiding in the conservation and growth of the giant panda population.

The typical locations for oral fibrosarcoma in animals include the hard palate and maxillary gingiva (6–8). It presents as a firm, well-circumscribed tumor. The tumor exhibits a nodular, lobulated, or irregular morphology. It is clearly demarcated from the surrounding tissues, and sometimes encapsulated; the consistency is slightly firmer than that of normal tissue; the sectioned surface is pink or off-white, and uniform in appearance (9). Fibrosarcoma tumor cells exhibit size variation, with frequent occurrence of giant cells; the tumor cells display a range of shapes and are markedly pleomorphic; the nuclei of tumor cells are intensely pigmented and frequently exhibit mitotic figures (9); there is a preponderance of tumor cells with a sparse presence of collagen fibers. Diagnosis should be informed by the animal's age, breed, gender, and location characteristics, alongside X-rays and CT scans. However, a definitive diagnosis requires histopathological examination of the excised tissue (9–11). Fibrosarcoma typically shows resistance to radiotherapy and chemotherapy, and is characterized by a high recurrence rate (9, 11, 12). Postoperatively, treatments included injections of cyclophosphamide and cytarabine; however, a recurrence was observed within 14 days (13, 14). Given the unique nature of this case, no additional treatments were administered to the giant panda. The majority of the giant panda's oral bleeding episodes were associated with the consumption of bamboo poles; therefore, the feeding regimen was modified to utilize bamboo shoots in place of poles, aiming to diminish the frequency of bleeding. Following the adjustment, there was a noticeable reduction in the frequency of bleeding. Significant improvements were observed, leading to an enhanced quality of life.

This case report documents the first instance of low-grade oral fibrosarcoma in giant pandas. It has established a standardized and systematic diagnostic protocol, offering valuable data and a reference framework for the diagnosis and prevention of diseases in giant pandas.

Data availability statement

The original contributions presented in the study are included in the article/supplementary material, further inquiries can be directed to the corresponding authors.

Ethics statement

The animal study was approved by Sichuan Agricultural University. The study was conducted in accordance with the local legislation and institutional requirements.

Author contributions

ZX: Formal analysis, Writing – original draft, Writing – review & editing. SL: Methodology, Writing – original draft. CL: Supervision, Validation, Writing – original draft. LD: Resources, Supervision, Writing – original draft. MH: Methodology, Project administration, Writing – original draft. CW: Formal analysis, Writing – original draft. DL: Resources, Writing – original draft. ZC: Funding acquisition, Writing – review & editing.

Funding

The author(s) declare financial support was received for the research, authorship, and/or publication of this article. This project was supported by the China Youth Development Foundation Mercedes-Benz Star Fund.

Conflict of interest

The authors declare that the research was conducted in the absence of any commercial or financial relationships that could be construed as a potential conflict of interest.

Publisher's note

All claims expressed in this article are solely those of the authors and do not necessarily represent those of their affiliated organizations, or those of the publisher, the editors and the reviewers. Any product that may be evaluated in this article, or claim that may be made by its manufacturer, is not guaranteed or endorsed by the publisher.

References

1. Lopez M, Talavera C, Rest JR, Taylor D. Haemangiosarcoma of the conjunctiva of a giant panda. *Vet Rec.* (1996) 138:24.

2. Mauroo NF, Rourke NL, Chan WK. Cutaneous hemangioma in a giant panda (*Ailuropoda melanoleuca*). *J Zoo Wildl Med.* (2006) 37:59–60. doi: 10.1638/04-098.1

3. Yijiao C, Junhui A, Rong H, Yuliang L, Donghui W, Songrui L, et al. Single-cell mRNA sequencing of giant panda (*Ailuropoda melanoleuca*) seminoma reveals the cellular and molecular characteristics of tumour cells. *Vet Med Sci.* (2024) 10:e1348. doi: 10.1002/vms3.1348

4. Wang Y, Xia M, Li X, Guo X, Lu Y, Zhao S, et al. A rare case of giant panda cancer: pancreatic ductal adenocarcinoma. *Animal Model Exp Med.* (2022) 5:582–6. doi: 10.1002/ame2.12269

5. Gao Q, Wang C, Li D, Zhang H, Deng L, Li C, et al. A case of giant panda ovarian cancer diagnosis and histopathology. *BMC Vet Res.* (2018) 14:311. doi: 10.1186/s12917-018-1630-x

6. Satthathum C, Srisampane S, Jariyarangsrirattana P, Anusorn P, Sattasathuchana P, Thengchaisri N. Characteristics of canine oral tumors: Insights into prevalence, types, lesion distribution. *J Adv Vet Anim Res.* (2023) 10:554–62. doi: 10.5455/javar.2023.j709

7. Gardner H, Fidel J, Haldorson G, Dernell W, Wheeler B. Canine oral fibrosarcomas: a retrospective analysis of 65 cases (1998-2010). *Vet Comp Oncol.* (2015) 13:40–7. doi: 10.1111/vco.12017

8. Miwa Y, Nakata M, Takimoto H, Chambers JK, Uchida K. Spontaneous oral tumours in 18 rabbits (2005-2015). *J Small Anim Pract.* (2021) 62:156–60. doi: 10.1111/jsap.13082

9. Scott SM, Reiman HM, Pritchard DJ, Ilstrup DM. Soft tissue fibrosarcoma. A clinicopathologic study of 132 cases. *Cancer.* (1989) 64:925–31.

10. Folpe AL. Fibrosarcoma: a review and update. *Histopathology.* (2014) 64:12–25. doi: 10.1111/his.12282

11. Harvey HJ. Oral tumors. *Vet Clin North Am Small Anim Pract.* (1985) 15:493–500. doi: 10.1016/S0195-5616(85)50052-2

12. Martano M, Iussich S, Morello E, Buracco P. Canine oral fibrosarcoma: changes in prognosis over the last 30 years? *Vet J.* (2018) 241:1–7. doi: 10.1016/j.tvjl.2018.09.005

13. Rueda Domínguez A, Olmos Hidalgo D, Viciana Garrido R, Torres Sánchez E. Liposomal cytarabine (DepoCyte) for the treatment of neoplastic meningitis. *Clin Transl Oncol.* (2005) 7:232–8. doi: 10.1007/BF02710168

14. Salehi B, Selamoglu Z, Mileski SK, Pezzani R, Redaelli M, Cho WC, et al. Liposomal cytarabine as cancer therapy: from chemistry to medicine. *Biomolecules.* (2019) 9:773. doi: 10.3390/biom9120773

frontiers | Frontiers in Veterinary Science

TYPE Case Report
PUBLISHED 05 February 2025
DOI 10.3389/fvets.2025.1535432

Check for updates

OPEN ACCESS

EDITED BY
Yasunaga Yoshikawa,
Kitasato University, Japan

REVIEWED BY
Andrew F. Rich,
International Zoo Veterinary Group,
United Kingdom
Marco Rondena,
Private Veterinary Clinic San Marco Srl, Italy

*CORRESPONDENCE
Gorazd Vengušt
✉ gorazd.vengust@vf.uni-lj.si

RECEIVED 27 November 2024
ACCEPTED 20 January 2025
PUBLISHED 05 February 2025

CITATION
Vengušt G, Vengušt DŽ, Cantile C, Gombač M, Tekavec K and Švara T (2025) Case report: Neuroendocrine carcinoma of the nasal cavity in a roe deer (*Capreolus capreolus*).
Front. Vet. Sci. 12:1535432.
doi: 10.3389/fvets.2025.1535432

COPYRIGHT
© 2025 Vengušt, Vengušt, Cantile, Gombač, Tekavec and Švara. This is an open-access article distributed under the terms of the Creative Commons Attribution License (CC BY). The use, distribution or reproduction in other forums is permitted, provided the original author(s) and the copyright owner(s) are credited and that the original publication in this journal is cited, in accordance with accepted academic practice. No use, distribution or reproduction is permitted which does not comply with these terms.

Case report: Neuroendocrine carcinoma of the nasal cavity in a roe deer (*Capreolus capreolus*)

Gorazd Vengušt[1]*, Diana Žele Vengušt[1], Carlo Cantile[2], Mitja Gombač[1], Kristina Tekavec[1] and Tanja Švara[1]

[1]Institute of Pathology, Wild Animals, Fish and Bees, Veterinary Faculty, University of Ljubljana, Ljubljana, Slovenia, [2]Department of Veterinary Sciences, University of Pisa, Pisa, Italy

Neuroendocrine tumors of the nasal cavity are rare in both animals and humans. This report describes the macroscopic, histopathological and immunohistochemical characteristics of a neuroendocrine tumor in a three-year-old female roe deer (*Capreolus capreolus*) that was shot due to a facial deformity caused by an oval, firm, exophytic lesion effacing the left frontal and parietal regions. Longitudinal sectioning of the skull revealed a nasal cavity tumor that had invaded the cribriform plate, the rostral bones of the skull, the rostral aspect of the cranial cavity and the frontal sinuses and extended through the lacrimal, sphenoid and zygomatic bones into the subcutaneous tissue. Histopathologically, the tumor consisted of neoplastic cells forming sheets, nests, trabecular and cribriform structures separated by a delicate fibrovascular stroma. Mitoses were rare. Based on the histopathological and immunohistochemical findings, a neuroendocrine carcinoma was diagnosed. Based on thorough database searches, this is the first known case of a nasal neuroendocrine carcinoma in a roe deer.

KEYWORDS

roe deer, nasal cavity, neuroendocrine carcinoma, tumor, immunohistochemistry

1 Introduction

Tumors in the nasal cavity or paranasal sinuses (i.e., sinonasal tumors) are uncommon in animals. Among the epithelial tumors, adenocarcinomas predominate, whereas chondrosarcoma is the most common malignant mesenchymal tumor (1). Sinonasal tumors with neuroendocrine differentiation, such as neuroendocrine carcinomas (NECs) and olfactory neuroblastomas (ONBs) (formerly known as esthesioneuroblastoma) have been occasionally reported in animals. Namely, NECs have been reported in dogs (*Canis lupus familiaris*) (2), horses (*Equus ferus caballus*) (3) and free-living Japanese raccoon dog (*Nyctereutes procyonoides viverrinus*) (4), whereas ONBs have been described in cats (*Felis catus*) and dogs (2, 5–10), horse (11), cattle (*Bos taurus*) (12), axolotl (*Ambystoma mexicanum*) (13, 14) and goldfish (*Carassius auratus*) (15).

During passive disease surveillance of roe deer in Switzerland (16), Slovenia (17), Sweden (18) and in the Netherlands (19), tumors were detected in 32, 19, 19 and four cases, respectively. The most frequently diagnosed tumor in Slovenia (17) was a fibropapilloma, in Switzerland and Sweden a lymphoma (16, 18), while reports from other researchers suggest that liver neoplasms are the most common tumors in roe deer (20, 21). Other neoplasms of various origins have been described in several case reports, such as pulmonary adenocarcinoma (22), mandibular ossifying fibroma and oral papillomas (23), leukemia (24), neuroblastoma (25), oral squamous cell carcinoma (26), cutaneous teratoma (27), suggesting that this species is particularly prone to developing neoplastic diseases (16).

This report describes the macroscopic, histopathological and immunohistochemical findings of an NEC in a three-year-old female roe deer (*Capreolus capreolus*).

2 Case description

A three-year-old female roe deer was shot by a local hunter in June 2023 in Nova vas in the Inner Carniola hunting area in southern Slovenia, Europe (45°45′42.89 "N, 14°30′11.43 "E), due to a facial deformity. The age of the animal was estimated by hunter and authorized hunting committees during the mandatory annual inspection of hunted ungulates at the end of the year. Eruption patterns and tooth wear were used to estimate the age of the animal. The animal was submitted to the Veterinary Faculty of the University of Ljubljana for necropsy. At necropsy, the animal was in good body condition (19.5 kg), defined by normally developed skeletal muscles and adequate subcutaneous and internal fat reserves. Gross examination of the head revealed an oval, apparently well-circumscribed, firm lesion in the left frontal and parietal region of the head (Figures 1A,B), which was covered with intact skin. Examination of the cut surface of the head revealed a poorly circumscribed, unencapsulated, oval, grey-white tumor mass measuring 14 × 11.5 × 13 cm, which originated from the ethmoid region of the left nasal cavity and had invaded and destroyed the cribriform plate and the rostral bones of the skull. The tumor occupied the rostral part of the cranial cavity and affected the frontal lobe of the brain. The tumor mass also occupied the frontal sinuses, invaded the frontal, lacrimal, sphenoid and zygomatic bones and grew into the subcutis of the frontal and parietal regions (Figure 1). As a result of the ingrowth of the tumor mass into the orbit, proptosis of the left eye occurred. No metastases and no other lesions were detected at necropsy.

For histopathology, several samples of the tumor were collected, immediately fixed in 10% buffered formalin and routinely embedded in paraffin. For light microscopic examination, 4 µm thick sections were stained with hematoxylin and eosin and with the modified Grimelius stain (28). Histopathological examination revealed predominantly a well-demarcated, partially encapsulated tumor that was multifocally infiltrative and was composed of sheets, nests, trabeculae, rosettes, and cribriform structures separated by a small to moderate amount of fibrovascular stroma. The neoplastic cells were polygonal, with indistinct cell borders and small to moderate amounts of eosinophilic non-granular cytoplasm demonstrating mild anisocytosis. The modified Grimelius staining revealed numerous dark cytoplasmic granules within the neoplastic cells. Single round to oval nuclei were evident, exhibiting mild anisokaryosis and up to one small nucleolus (Figures 2A,B). Three mitoses per 10 high-power fields (2.37 mm^2) were counted. Multifocally, small to medium sized necrotic foci, hemorrhages and lytic bone fragments were present within the neoplasm. Invasion of blood and lymph vessels was not observed.

Immunohistochemistry was performed to confirm the origin of the neoplastic cells. The procedure was performed on selected 4 µm thick paraffin sections, which were first deparaffinized. The antigens were retrieved by boiling the slides in EDTA buffer (pH 9.0) in a microwave oven for 10 min [for immunolabeling of neuron-specific enolase (NSE), chromogranin A, synaptophysin, and microtubule-associated protein 2 (MAP-2)] or in citrate buffer for 10 min [for immunolabeling of neurofilament H (NFH)] or 20 min [for immunolabeling of cytokeratins, S-100 protein, glial fibrillary acidic protein (GFAP) and calcitonin]. The slides were then incubated with the primary antibodies for 1 h at room temperature in a humidified chamber (Table 1). The remaining immunohistochemistry was performed according to a previously described protocol (29). Tissues from the roe deer without lesions were used as positive controls: pancreas served as a positive control for immunoreactivity for cytokeratins, synaptophysin, chromogranin A, and NSE; thyroid gland served as a positive control for calcitonin; and brain tissue was used for S-100 protein, GFAP, NFH and MAP-2.

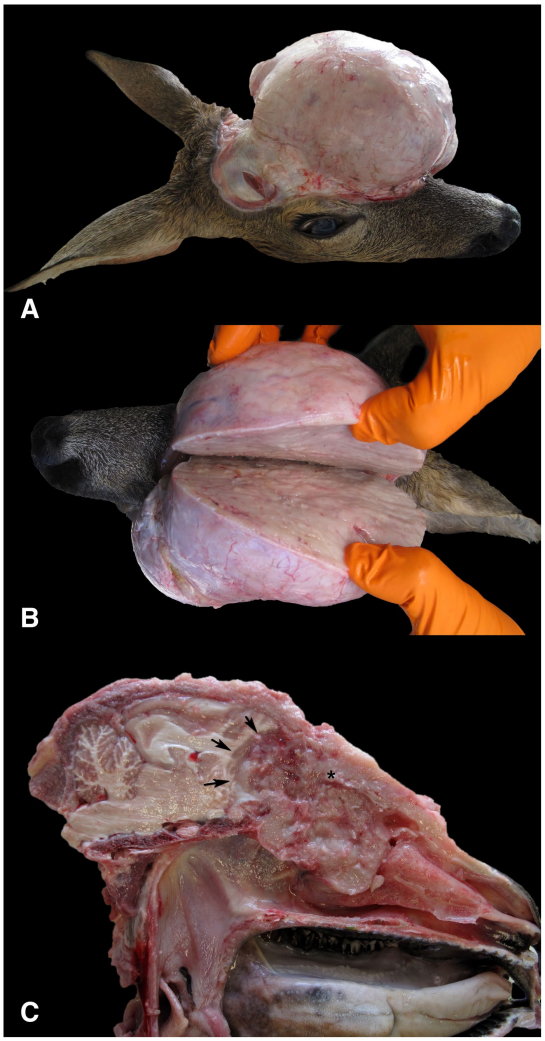

FIGURE 1
Gross findings in a female roe deer (*Capreolus capreolus*) with neuroendocrine carcinoma. **(A)** The surface of the tumor mass after removal of the skin showed a highly exophytic, grey-white, firm mass. **(B)** The cut surface of the tumor mass was grey-white, smooth and moderately bulged. **(C)** The tumor, which originated from the ethmoidal region of the left nasal cavity (*), had invaded and destroyed the cribriform plate and the rostral bones of the skull. The tumor occupied the rostral part of the cranial cavity and affected the frontal lobe of the brain (arrows). The exophytic portion of the tumor, which protruded above the parietal and nasal regions, was removed.

10.3389/fvets.2025.1535432

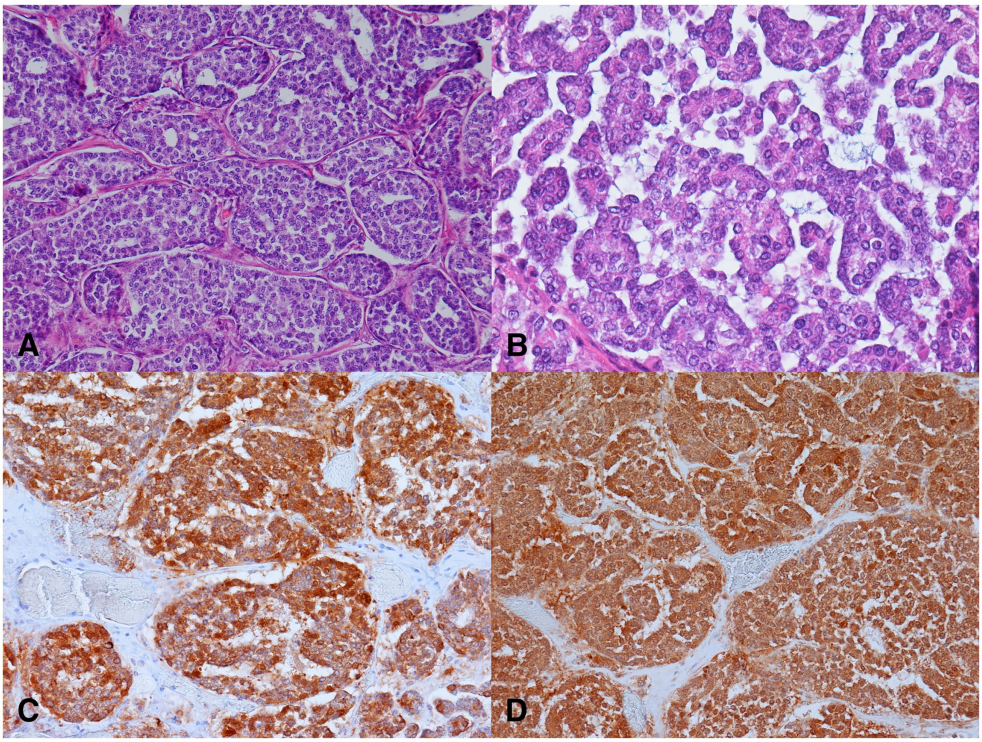

FIGURE 2
Microscopic findings of the neuroendocrine carcinoma in a female roe deer (*Capreolus capreolus*). **(A)** Nests of neoplastic cells separated by delicate fibrovascular stroma. H&E, 200x. **(B)** Nests of small to medium sized neoplastic cells exhibiting mild anisocytosis and anisokaryosis. H&E, 400x. **(C)** Neoplastic cells demonstrated strong cytoplasmic immunolabeling for cytokeratins. Pancytokeratin AE1/AE3 immunohistochemistry (IHC), 200x. **(D)** Neoplastic cells exhibited strong cytoplasmic immunolabeling for neuron specific enolase (IHC), 200x.

TABLE 1 **Details of immunohistochemistry reagents and results of immunolabeling.**

Antibody	Clonality	Concentration	Incubation	Manufacturer	Immunolabeling in neoplastic cells
Cytokeratin	AE1/AE3	1:100	60 min	DAKO	100%
Cytokeratin	MNF116	1:100	60 min	DAKO	–
Neuron specific enolase		1:100	60 min	DAKO	100%
Synaptophysin		1:100	60 min	DAKO	–
Chromogranin A		1:500	60 min	DAKO	–
Calcitonin		1:1600	60 min	DAKO	–
S-100 protein		1:800	60 min	DAKO	–
GFAP		1: 2000	60 min	DAKO	–
Neurofilament H		1:200	60 min	Millipore	–
Microtubule-associated protein 2 (MAP-2)	HM-2	1:500	60 min	Sigma	–

Most of the neoplastic cells were immunoreactive for cytokeratin AE1/AE3, and NSE. The immunolabeling was intense and localized in the cytoplasm (Figures 2C,D). The neoplastic cells were negative for cytokeratin MNF116, synaptophysin, chromogranin A, calcitonin, S-100 protein, GFAP, and NFH.

Based on the gross, histopathological and immunohistochemical features of the tumor, a nasal NEC was diagnosed.

3 Discussion

Based on thorough database searches (PubMed Central, Google Scholar, CAB Abstract) covering the years (1950–2024), and using mixed keyword combinations of "neuroendocrine," "tumor," "neoplasm," "neoplasia," "carcinoma," "roe deer," and "*Capreolus capreolus*," this is the first description of NEC in a roe deer and the

second reported case in wild animals. The first case was previously described in a raccoon dog (4).

Histologically, the neuroendocrine differentiation of the tumor was suspected based on the architecture of the tumor and the morphology of the tumor cells, which were consistent with an endocrine tumor (1). This was confirmed by histochemical and immunohistochemical stainings. The tumor cells showed argyrophilic staining and expressed NSE and cytokeratins. The Grimelius stain is a silver stain that shows neuroendocrine granules with specific peptide hormones and biogenic amines. Although it stains almost all neuroendocrine tumors with few exceptions, it is not specific for a single neuroendocrine tumor type (30). Immunohistochemistry is valuable for the confirmation of tumors of neuroendocrine origin in both humans and animals (2, 4, 31, 32). Cytokeratins, synaptophysin, NSE, and chromogranin A are usually expressed in sinonasal tumors with neuroendocrine differentiation (3, 32). In addition, tumor cells can also express somatostatin, vasoactive intestinal polypeptide (VIP), protein gene product 9.5 (PGP 9.5) (2), and S-100 (4).

In this case, two differential diagnoses were considered: NEC and ONB, based on histopathologic and immunohistochemical confirmation of neuroendocrine differentiation in the tumor cells. Their phenotypic characteristics overlap considerably, which makes differentiation and diagnosis difficult (5, 33).

Grossly, ONB often grows more invasively and causes more extensive destruction of adjacent bony structures (34, 35). Extension of the neoplasm into the olfactory bulb and orbital wall causing proptosis has been described in a cattle with ONB (12). Compression of the olfactory bulb and frontal lobe with caudal displacement of both cerebral hemispheres and the cerebellum has been described in a dog with ONB (36), and osteolysis of the cribriform plate and extension of the tumor into the brain was observed in two dogs and one cat with ONB (7). In the axolotl, the tumor replaced part of the maxillary bone tissue (13). On the other hand, there have been some other cases of ONB in dogs, cats, and horses, in which the tumor showed no invasive growth into the bone and/or brain cavity (6, 11, 37).

In a case of NEC in a Japanese raccoon dog, Kubo et al. (4) reported destruction of the maxilla, extension of the tumor to the subcutis leading to swelling of the ridge of the nose, and extrusion of the eyeball. Sako et al. (2) found neoplastic infiltration of the nasal septum and frontal sinus in two dogs, and osteolysis of the maxilla and frontal bone in two of the ten dogs with NEC included in the study (2). Three horses with NEC were also found to have exophthalmos (3). In the case described here, the tumor also invaded the frontal sinuses, frontal bone, lacrimal bone, sphenoid bone and zygomatic bone as well as the rostral part of the cranial cavity and the orbit, resulting in proptosis of the left eye.

Both NEC and ONB form microscopic rosettes (1), and electron microscopic or immunohistochemical examination is often necessary to differentiate between them. In contrast to NEC, ONB has cell extensions that contain microtubules (1, 4). While the WHO classification requires electron microscopy for a definitive diagnosis in humans (37), these ultrastructural features have not yet been clearly demonstrated in animals (2, 5, 38).

The immunohistochemical findings of NEC and ONB also overlap considerably, and some researchers have even suggested that these two tumors are different manifestations of the same entity (11). Cytokeratins, chromogranin, and synaptophysin, as well as several peptides such as calcitonin and VIP, which are more regularly expressed in NEC (1) and the lack of immunolabeling for some cytoskeletal proteins such as neurofilament, class III beta-tubulin isotype and MAP-2 in human NEC are suggested to be the main differences between NEC and ONB (2, 39). In a study, cytokeratin AE1/AE3 was expressed in all 10 cases of NEC in the nasal cavity of dogs (2). Expression of MAP-2 has been shown to be a potentially reliable and sensitive marker for ONB in dogs and cats, as all but one case of ONB in cats were immunoreactive for MAP-2 (5). MAP-2 expression has also been described in case of ONB in horse (11).

NSE expression is used to support the diagnosis of ONB in human pathology and has also been described in cases of ONB in animals (5, 10). However, in animals, NSE is also expressed in NEC (2).

4 Conclusion

In conclusion, NEC in a roe deer was diagnosed based on the histopathological and immunohistochemical characteristics of the tumor. The tumor cells expressed NSE and cytokeratin AE1/AE3, but were immunohistochemically negative for synaptophysin, chromogranin A, calcitonin, S-100 protein, GFAP, NFH, and MAP-2, which in our opinion supports the diagnosis of NEC.

Data availability statement

The original contributions presented in the study are included in the article/supplementary material, further inquiries can be directed to the corresponding author.

Ethics statement

Ethical approval was not required for the study involving animals in accordance with the local legislation and institutional requirements as all samples were taken post-mortem.

Author contributions

GV: Conceptualization, Data curation, Investigation, Writing – original draft. DV: Data curation, Investigation, Writing – original draft. CC: Data curation, Investigation, Writing – review & editing. MG: Data curation, Investigation, Writing – review & editing. KT: Data curation, Investigation, Writing – review & editing. TŠ: Data curation, Investigation, Supervision, Writing – original draft, Writing – review & editing.

Funding

The author(s) declare that financial support was received for the research, authorship, and/or publication of this article. This research was funded by the Slovenian Research and Innovation Agency (research core funding No. P4-0092 'Animal health, environment and food safety'), Administration of the Republic of Slovenia for Food Safety, Veterinary Service and Plant Protection, and Hunting Association of Slovenia (No. 403–114/2024).

Acknowledgments

The authors would like to thank the Slovenian Research Agency (program P4-0092), hunters, Administration of the Republic of Slovenia for Food Safety, Veterinary Service and Plant Protection and the Slovenian Hunting Association for supporting the research.

Conflict of interest

The authors declare that the research was conducted in the absence of any commercial or financial relationships that could be construed as a potential conflict of interest.

Generative AI statement

The authors declare that no Gen AI was used in the creation of this manuscript.

Publisher's note

All claims expressed in this article are solely those of the authors and do not necessarily represent those of their affiliated organizations, or those of the publisher, the editors and the reviewers. Any product that may be evaluated in this article, or claim that may be made by its manufacturer, is not guaranteed or endorsed by the publisher.

References

1. Meuten DJ. Tumors in domestic animals In: DJ Meuten, editor. Tumors in domestic animals. *4th* ed. Ames: John Wiley & Sons, Ltd (2016)

2. Sako T, Shimoyama Y, Akihara Y, Ohmachi T, Yamashita K, Kadosawa T, et al. Neuroendocrine carcinoma in the nasal cavity of ten dogs. *J Comp Pathol*. (2005) 133:155–63. doi: 10.1016/j.jcpa.2005.04.002

3. Van Maanen C, Klein WR, Dik KJ, Van Den Ingh TSGAM. Three cases of carcinoid in the equine nasal cavity and maxillary sinuses: histologic and immunohistochemical features. *Vet Pathol*. (1996) 33:92–5. doi: 10.1177/030098589603300114

4. Kubo M, Matsuo Y, Okano T, Sakai H, Masegi T, Asano M, et al. Nasal neuroendocrine carcinoma in a free-living Japanese raccoon dog (*Nyctereutes procyonoides viverrinus*). *J Comp Pathol*. (2009) 140:67–71. doi: 10.1016/j.jcpa.2008.09.007

5. Brosinski K, Janik D, Polkinghorne A, Von Bomhard W, Schmahl W. Olfactory neuroblastoma in dogs and cats – a histological and Immunohistochemical analysis. *J Comp Pathol*. (2012) 146:152–9. doi: 10.1016/j.jcpa.2011.06.002

6. Parker VJ, Morrison JA, Yaeger MJ. Olfactory neuroblastoma in a cat. *J Feline Med Surg*. (2010) 12:867–71. doi: 10.1016/j.jfms.2010.09.009

7. Söffler C, Hartmann S, Gorgas D, Ludewig E, Von Pückler K, Kramer M, et al. Magnetic resonance imaging features of esthesioneuroblastoma in three dogs and one cat. *Tierarztl Prax Ausg K Kleintiere Heimtiere*. (2016) 44:333–40. doi: 10.15654/TPK-150963

8. Church ME, Veluvolu SM, Durham AC, Woolard KD. Clinical outcomes, ultrastructure and immunohistochemical features of canine high-grade olfactory neuroblastoma. *Vet Comp Oncol*. (2019) 17:578–84. doi: 10.1111/vco.12512

9. Romano AM, Frank CB. Olfactory ganglioneuroblastoma in a dog: case report and literature review. *J Vet Diagn Invest*. (2021) 33:1013–7. doi: 10.1177/10406387211022864

10. Martí-García B, Priestnall SL, Holmes E, Suárez-Bonnet A. Olfactory neuroblastoma in a domestic cat and review of the literature. *Vet Clin Pathol*. (2023) 52:521–6. doi: 10.1111/vcp.13255

11. Yamate J, Izawa T, Ogata K, Kobayashi O, Okajima R, Kuwamura M, et al. Olfactory neuroblastoma in a horse. *J Vet Med Sci*. (2006) 68:495–8. doi: 10.1292/jvms.68.495

12. Anderson BC, Cordy DR. Olfactory neuroblastoma in a heifer. *Vet Pathol*. (1981) 18:536–40. doi: 10.1177/030098588101800411

13. Shioda C, Uchida K, Nakayama H. Pathological features of olfactory neuroblastoma in an axolotl (*Ambystoma mexicanum*). *J Vet Med Sci*. (2011) 73:1109–11. doi: 10.1292/jvms.11-0105

14. Modesto F, Nicolier A, Hurtrel C, Benoît J. Excisional biopsy and radiotherapy for management of an olfactory neuroblastoma in an axolotl (*Ambystoma mexicanum*). *J Am Vet Med Assoc*. (2021) 260:436–41. doi: 10.2460/javma.20.09.0498

15. Vigliano FA, Marcaccini AJ, Sarradell J, Bermúdez R, Quiroga MI. First description of an olfactory neuroblastoma in goldfish *Carassius auratus*: a case report. *Dis Aquat Org*. (2011) 96:61–8. doi: 10.3354/dao02383

16. Pewsner M, Origgi FC, Frey J, Ryser-Degiorgis MP. Assessing fifty years of general health surveillance of roe deer in Switzerland: a retrospective analysis of necropsy reports. *PLoS One*. (2017) 12:e0170338. doi: 10.1371/journal.pone.0170338

17. Žele Vengušt D, Kuhar U, Jerina K, Vengušt G. Twenty years of passive disease surveillance of roe deer (*Capreolus capreolus*) in Slovenia. *Animals*. (2021) 11:407. doi: 10.3390/ani11020407

18. Aguirre AA, Bröjer C, Mörner T. Descriptive epidemiology of roe deer mortality in Sweden. *J Wildl Dis*. (1999) 35:753–62. doi: 10.7589/0090-3558-35.4.753

19. Hoekman ED. Dutch roe deer (*Capreolus capreolus*), review of cases presented at the Dutch wildlife health Centre. Utrecht, The Netherlands: Facultad de Veterinaria (2013).

20. Munro R, Youngson RW. Hepatocellular tumours in roe deer in Britain. *Vet Rec*. (1996) 138:542–6. doi: 10.1136/vr.138.22.542

21. Brunk R. Wildpathologische Untersuchungen der Jahre 1939 bis 1959. *Z Für Jagdwiss*. (1960) 6:121–85. doi: 10.1007/BF01890162

22. Bednarski M, Wimonć M, Kolenda R, Wlekliński E, Król D, Houszka M. Primary pulmonary adenocarcinoma in roe deer-a case report. *Med Weter*. (2019) 75:6206–2019. doi: 10.21521/mw.6206

23. Zürcher-Giovannini S, Ruder TD, Pool R, Erdelyi K, Origgi FC. Mandibular ossifying fibroma and multiple oral papillomas in a roe deer (*Capreolus capreolus*). *Front Vet Sci*. (2020) 7:166. doi: 10.3389/fvets.2020.00166

24. Elvestad K, Henriques UV. Leukaemic neoplasia in free-living mammals in Denmark. *Acta Vet Scand*. (1985) 26:61–71. doi: 10.1186/BF03546564

25. Kleinschmidt S, Peters M, Wohlsein P. Central nervous system neuroblastoma in a wild deer (*Capreolus capreolus*). *J Comp Pathol*. (2012) 146:283–7. doi: 10.1016/j.jcpa.2011.07.001

26. Domenis L, Campanella C, Rubini D, Parovel E, Orusa R, Robetto S. Oral squamous cell carcinoma in a free-ranging roe deer (*Capreolus capreolus*). *J Vet Med Animal Sci*. (2020) 3:1024.

27. Barlow AM, Couper D. Cutaneous teratoma in a wild roe deer (*Capreolus capreolus*) in the UK. *Vet Rec*. (2006) 159:211–2. doi: 10.1136/vr.159.7.211

28. Lack EE, Mercer L. A modified Grimelius argyrophil technique for neurosecretory granules. *Am J Surg Pathol*. (1977) 1:275–8. doi: 10.1097/00000478-197709000-00009

29. Cociancich V, Švara T, Pogačnik M. Malignant mesenchymoma of the aortic valve in a dog. *Slov Vet Res*. (2013) 50:83–8.

30. Grimelius L. Methods in neuroendocrine histopathology, a methodological overview. *Ups J Med Sci*. (2008) 113:243–60. doi: 10.3109/2000-1967-238

31. Kulke MH, Mayer RJ. Carcinoid tumors. *N Engl J Med*. (1999) 340:858–68. doi: 10.1056/NEJM199903183401107

32. Kuwata K, Shibutani M, Kemmochi Y, Taniai E, Morita R, Ogawa B, et al. A neuroendocrine carcinoma of undetermined origin in a dog. *J Toxicol Pathol*. (2010) 23:151–5. doi: 10.1293/tox.23.151

33. Ninomiya F, Suzuki S, Tanaka H, Hayashi S, Ozaki K, Narama I. Nasal and paranasal adenocarcinomas with neuroendocrine differentiation in dogs. *Vet Pathol*. (2008) 45:181–7. doi: 10.1354/vp.45-2-181

34. Pickuth D, Heywang-Köbrunner SH. Imaging of recurrent esthesioneuroblastoma. *Br J Radiol*. (1999) 72:1052–7. doi: 10.1259/bjr.72.863.10700820

35. Siudak K, Klingler M, Schmidt MJ, Herden C. Metastasizing Esthesioneuroblastoma in a dog. *Vet Pathol*. (2015) 52:692–5. doi: 10.1177/0300985814559402

36. Hara K, Shimada A, Morita T, Sawada M, Umemura T. Olfactory neuroepithelioma in a dog: an immunohistochemical and electron microscopic study. *J Vet Med Sci*. (2002) 64:391–3. doi: 10.1292/jvms.64.391

37. Dungworth DL, Donald L. Histological classification of tumors of the respiratory system of domestic animals. Washington, DC: Armed Forces Institute of Pathology (1999).

38. Döpke C, Gröne A, Borstel MV, Oppen TV, Boéve MH, Baumgärtner W. Metastatic esthesioneuroblastoma in a horse. *J Comp Pathol*. (2005) 132:218–22. doi: 10.1016/j.jcpa.2004.07.003

39. Frierson HF, Ross GW, Mills SE, Frankfurter A. Olfactory neuroblastoma. Additional immunohistochemical characterization. *Am J Clin Pathol*. (1990) 94:547–53. doi: 10.1093/ajcp/94.5.547

frontiers | Frontiers in Veterinary Science

TYPE Original Research
PUBLISHED 05 February 2025
DOI 10.3389/fvets.2025.1451510

Check for updates

OPEN ACCESS

EDITED BY
Isabel Pires,
University of Trás-os-Montes and Alto Douro, Portugal

REVIEWED BY
Vittoria Castiglioni,
IDEXX Laboratories, Germany
Erik Teske,
Utrecht University, Netherlands

*CORRESPONDENCE
Lorella Maniscalco
✉ lorella.maniscalco@unito.it

†These authors have contributed equally to this work and share first authorship

‡These authors have contributed equally to this work and share last authorship

RECEIVED 19 June 2024
ACCEPTED 22 January 2025
PUBLISHED 05 February 2025

CITATION
Maniscalco L, Olimpo M, Parisi L, Buracco P, Mazzone E, Martinelli G, Martano M, Iussich S and Morello E (2025) A novel scoring system proposal to guide treatment of dogs with hepatoid gland tumors.
Front. Vet. Sci. 12:1451510.
doi: 10.3389/fvets.2025.1451510

COPYRIGHT
© 2025 Maniscalco, Olimpo, Parisi, Buracco, Mazzone, Martinelli, Martano, Iussich and Morello. This is an open-access article distributed under the terms of the Creative Commons Attribution License (CC BY). The use, distribution or reproduction in other forums is permitted, provided the original author(s) and the copyright owner(s) are credited and that the original publication in this journal is cited, in accordance with accepted academic practice. No use, distribution or reproduction is permitted which does not comply with these terms.

A novel scoring system proposal to guide treatment of dogs with hepatoid gland tumors

Lorella Maniscalco[1*†], Matteo Olimpo[1†], Lorenza Parisi[1], Paolo Buracco[1], Eugenio Mazzone[1], Greta Martinelli[1], Marina Martano[2], Selina Iussich[1‡] and Emanuela Morello[1‡]

[1]Department of Veterinary Sciences, University of Turin, Grugliasco, Italy, [2]Department of Veterinary Medical Sciences, University of Parma, Parma, Italy

Hepatoid perianal gland tumors are relatively common in dogs, accounting for 25% of all skin tumors. However, the specific factors involved in their development are still not completely clear. It has been established that hormonal influences can impact the formation of these tumors. The prognosis for dogs with perianal tumors depends largely on histology (benign vs. malignant) and, in case of malignancy, it has been suggested that the stage of the disease is important, with a more favorable outcome in dogs having small (under 5 cm in diameter), *non*-metastatic adenocarcinomas which are surgically removed with non-infiltrated margins. Nevertheless, there is a paucity of studies which thoroughly relate hepatoid gland histotypes to their prognosis; therefore, it is possible that a well-differentiated adenocarcinoma could be misclassified. Based on a retrospective review of 76 dogs with hepatoid gland tumors having clinical follow-up, the aims of this study were (1) to establish a histological grading system capable of potentially predicting prognosis and (2) to explore the role of Ki67 as a potential prognostic marker. Based on histopathological features only, the proposed grading system effectively differentiated tumors with a favorable prognosis from those with a worse prognosis to support histological diagnosis. The evaluation of the Ki67 index was not useful to predict prognosis in this study.

KEYWORDS

dogs, neoplasm grading system, Ki67 antigen, perianal glands tumor, hepatoid tumors

1 Introduction

Tumors of the perianal/hepatoid glands are quite prevalent in dogs, constituting 25% of all skin tumors (1). Hepatoid gland adenomas account for most canine perianal tumors in dogs (58–96%), while adenocarcinoma is rare (3–21%) (2–4). An influence of sexual hormones on the growth of adenomas, and even of differentiated adenocarcinomas, has been shown (5, 6). Adenoma occurs more frequently in intact male dogs (3, 7). In particular, intact male dogs over 10 years of age are 5.6 times more likely to develop hepatoid gland tumors than neutered male and spayed female dogs (6, 8).

The mechanisms involved in the development of hepatoid tumors are not completely understood (8–10).

The prognosis of malignant hepatoid perianal tumors, apart from histological features, depends on the clinical stage of the disease [TNM; (11)]. In fact, it has been reported to be favorable in dogs with a minimally invasive adenocarcinoma, less than 5 cm in diameter and without regional metastasis at presentation (12); additionally, it has also been suggested that prognosis may be influenced by the excision margin status (13). The prognosis for benign hepatoid perianal tumors is favorable, and castration and marginal surgical excision are

curative, being the local recurrence rate very low; although it has been reported that an incomplete surgical resection may be a risk factor for recurrence (2, 14). Local regrowth after surgery in a neutered male is suggestive of tumor malignancy (3).

In the case of hepatoid malignancy, clinical stage (11) is the only prognostic factor identified; dogs bearing tumors larger than 5 cm in diameter have an 11-fold higher risk of death (12). According to the 1990 study byVail et al., dogs with stage 1 and stage 2 tumors had a disease-free interval of 2 years while a 1-year survival rate of 75% was recorded in dogs with T1 tumors and of 60% in dogs with T2 tumors. Median survival time for stage 3 and 4 was 6–12.5 months (12). Metastases are rare and are mostly found at the level of the sublumbar lymph nodes (15%); however, they can also occur in the lungs, liver, and spleen (12).

Regarding the histological morphology of perianal adenomas and epitheliomas, the most recent classifications agree that both entities have little or no nuclear atypia (2, 15). However, in contrast to epitheliomas, perianal adenomas usually consist of ordered lobules of well-differentiated hepatoid cells which form islands, cords and trabeculae. Adenocarcinomas are composed of disorganized, poorly differentiated, hepatoid cells with pleomorphic nuclei, prominent nucleoli, and vacuolated cytoplasm, having an elevated degree of nuclear atypia and an elevated mitotic rate in both the hepatoid and the reserve cell population (2, 15, 16). Thus, while the older textbooks considered the possibility of adenocarcinomas having a different degree of differentiation (17), the most recent classifications incorporate them into a single category characterized by frank malignant criteria (15). Well-differentiated adenocarcinomas were previously differentiated from adenomas by the presence of signs of tissue invasion, and a crowded or sloppy architecture (17); however, they are no longer mentioned in the new reference texts (15).

There are only a few prognostic immunohistochemical studies including Ki67 (14), COX-2 (15) and p53 (18). Adenocarcinomas showed a higher proliferation rate as compared to epitheliomas and adenomas grouped together, and a higher Ki-67 index was related to recurrence of perianal gland adenocarcinoma (14).

The aims of this study were to evaluate a novel histological grading for hepatoid perianal tumors, single and non-metastatic at presentation, capable of predicting prognosis, and of investigating the Ki67 index as an additional prognostic factor.

2 Materials and methods

2.1 Case selection and inclusion/exclusion criteria

The cases studied were retrieved from dogs treated at the Veterinary Teaching Hospital (VTH) of the Department of Veterinary Sciences of the University of Turin (Italy) between January 2006 and December 2021, confirmed to be a hepatoid gland tumor based on the histology performed on the surgical specimens. At the time of admission, informed consent was obtained from the dogs' owners for both the clinical and surgical procedures and the potential use of the results for clinical research studies.

The study included only those dogs with a hepatoid gland tumor, clinically single at presentation that was surgically excised, and staged T1-T3/N0/M0 (11); in addition, complete survey data and a tissue specimen of adequate quality had to be available. Therefore, the exclusion criteria included the presence of distant metastases, an incomplete clinical report and a follow-up time of less than 6 months. Dogs clinically bearing multiple hepatoid nodules or those with sublumbar lymphadenopathy at admission were also excluded.

2.2 Histopathology

Archived paraffin-embedded tissues were retrieved, sectioned (4 µm), and stained with hematoxylin and eosin (HE). The histological slides were reviewed independently by 2 pathologists (L.M. and S.I.). They were blinded to the original histological diagnosis, clinicopathological data and clinical outcome; all the discordant results were reviewed by the 2 pathologists with a multiheaded microscope to reach a consensus based on the criteria established by the latest classification (19).

The tumor features were evaluated for all cases, regardless of diagnosis. To standardize the assessment, numerical values were assigned to the characteristics shown in Table 1. The mitotic count was assessed in areas of 2.37 mm2 for all cases, searching for the zones of the highest proliferative activity, which were then expressed as an arithmetic average of the counts reported by the two pathologists (20).

TABLE 1 Tumor features evaluated.

	Evaluation		
Capsule or pseudocapsule	Absent	Present	/
Calcific or mineralized intralesional foci	Absent	Present	/
Ulceration	Absent	Present	/
Loss of lobular/trabecular architecture	No	Yes (more than 50%)	/
Sebaceous differentiation	Absent	Present	/
Ductal differentiation	Absent	Present	/
Tumor infiltrating lymphocytes	Absent	Present	/
Infiltrative growth	Absent	Present	/
Multinucleated cells	Absent	Present	/
Cellular pleomorphism	Regular, uniform cells having small nuclei with occasional small nucleoli	Moderate degree of variation in nuclear size and shape with nucleoli which can be prominent	Notable variation in nuclear size and more

Finally, the values were reported in an Excel chart (Microsoft® Excel® 2016 MSO.).

2.3 Establishment of histological grading

A novel grading system was created for hepatoid gland tumors using prognostic histological characteristics, such as weighted sums. This indicated that all the categorical features (given as binary values, 0/1) were summed up together after being weighted by their hazard ratios which were derived from a survival regression model measuring their association with time to recurrence. The grading was created as follows:

$$Grading(x) = \{high,\ \sum_i Hz_i x_i > 10\ low,\ \sum_i Hz_i x_i \leq 10$$

where x is the list of the canine patient's characteristics and Hz is the relative hazard ratio.

2.4 Ki67 immunohistochemical staining and automated evaluation

Immunohistochemical staining for Ki-67 was carried out on additional sections obtained from formalin fixed paraffin embedded (FFPE) samples. Briefly, four µm sections of FFPE tissue were cut, mounted on positively charged slices (Menzel-Gläser Superfrost plus. Thermo scientific), deparaffinized in xylene, rehydrated in graded ethanol and rinsed in distilled water. Endogenous peroxidases were blocked by incubating sections for 20 min in 0.3% hydrogen peroxide diluted in distilled water.

Antigens retrieval was performed placing sections in a microwave-resistant container with a solution of tris-EDTA (pH 9.0) and heating 3 times (3 min each) at 700 W. The sections were left to cool at room temperature for 15 min and were next immersed in phosphate buffer saline solution (pH 7.4) for 5 min.

Tissue sections were subsequently incubated with Blocking serum (Vector® Vectastain Elite ABC kit) for 20 min in a humidified chamber, then incubated with the monoclonal mouse anti-human Ki-67 antibody (clone MIB-1, M7240, Dako, Glostrup, Denmark) diluted 1:200 in a PBS solution, in a humidified chamber for 120 min.

After incubation, tissue sections were washed in PBS-tween20 diluted 1:1000 and then incubated with biotinylated secondary antibody (Vector® Vecstain Elite ABC kit, Anti-Mouse IgG/Rabbit IgG) in a humidified chamber, for 30 min.

Avidin-biotin system (Vecstain®) was used for immunolabeling, and reactions were visualized with 3′3′-diaminobenzidine (DAB, Peroxidase Substrate Cat. No. SK-4100). QuPath software was used for assessing the Ki67, following the guidelines provided by Pai et al. (21) and checking step by step that the cell selection provided by the software was correct (21). Briefly, for each case prepared, 3 fields were evaluated from Ki67-labeled slides in Ki67 hotspots (areas of the greatest immunolabeling of the tumor cells for this proliferation marker). The fields were photographed at 20x with a camera (Leica ICC50, Leica®, Germany), placed on an optical microscope (Leica DM750, Leica® Germany) and acquired as images on a personal computer using dedicated software (Leica Application Suite X 5.1.0.25593, Leica®, Germany). The settings used are summarized in Supplementary File S1.

2.5 Follow-up

The owners or referring veterinarians were contacted to update the follow-up of the dogs included in the study to ascertain whether the tumor had recurred, whether the dog was still alive, or had died and the cause of death. Overall survival (OS) was considered as the number of days from surgery to death, while the disease-free interval (DFI) was considered as the number of days from surgery to tumor recurrence, and/or evidence of regional (cytologically confirmed) or distant metastasis. The cases were censored using right censoring (22, 23).

2.6 Statistical analysis

A grid search was used to identify the cut-off values to apply when using clinical prediction models to assign triage levels to the canine patients. This was carried out using a grid search to optimize the difference between both the median estimated OS and the DFI using the data uncovered by the newly found cut-offs. After having set an appropriate cut-off point for each continuous feature in order to reduce the degrees of freedom of the dataset, the prognostic relevance of each feature was accessed using a univariate regression model (survreg). The features having a *p*-value under the chosen statistical threshold of 0.05 were acknowledged to be independently relevant, requiring additional analysis.

The statistically significant parameters emerging from the univariate analysis regarding DFI were used to generate a scoring system. This score was defined as the sum of the hazard ratios associated with the presence of each characteristic. Finally, a suitable cut-off approximation was carried out regarding the newly designed score to divide (non-censored) canine patients into two categories (good and bad prognosis). The cut-off was then validated on both OS and DFI using the regression model. Clinical and pathological results were grouped into contingency tables and analyzed using Fisher's exact or Chi square tests. All the analyses were carried out in an R environment (R Software v.4.3.1).

3 Results

A total of 76 hepatoid perianal gland tumors were retrieved from an equal number of dogs. Of the canine population examined, 66 were male (85.0%) of which 11 were neutered (16.6%), and 10 were female (15.0%) of which 6 were spayed (6.0%). There were 30 mixed-breed dogs (39.0%) and 46 purebred dogs (61.0%). The mean age was 11.4 years (SD ± 2.4 years). The mean weight was 18.4 kg (SD ± 13.4 kg). Regarding the surgical procedure, tumor excision with a 5–10 mm margin was attempted in all cases and was combined with castration in 45 cases (59.2%). In 31 dogs (40.8%), the tumor excision was not combined with neutering; 10 intact male dogs out of 55 (18.0%) were not castrated at owners' request. The mean tumor size was 2.5 cm (SD ± 2.2 cm). Of the

45 dogs which underwent castration, histopathology revealed a testicular neoplasm in 18 dogs (40%). In particular, 9 dogs (50.0%) had a seminoma, 2 dogs (11.0%) a seminoma and a Leydig cell tumor, 1 dog (5.5%) a seminoma and a Sertoli cell tumor, 3 dogs (17.0%) a Sertoli cell tumor, 1 dog (5.5%) a Sertoli cell tumor and a Leydig cell tumor, and 2 dogs (11.0%) a Leydig cell tumor only. The perianal tumors were histologically classified as adenomas (19 cases, 25.0%), adenocarcinomas (50 cases, 65.8%) and epitheliomas (7 cases, 9.2%). The median mitotic count was 9.27 ± 10.49. The hepatoid tumors were histologically completely resected in all cases. The overall recurrence rate was 13%. Among the 10 dogs that showed signs of local recurrence, all were diagnosed with adenocarcinoma, and they included 1 female (10%), 2 neutered males (20%), and 7 intact males (70%); the latter had all been neutered during the excision of the hepatoid tumor. The metastatic rate was 9.2%; metastases developed in the regional sacral lymph nodes in 7 cases, lungs in 2 cases and liver in 1 case. The dogs with metastases were 2 spayed female and 5 male dogs neutered at the time of the tumor excision. Fifty-four of 76 cases were censored as these dogs died from tumor-unrelated causes or were lost during the follow-up period. The median overall DFI and OS was 730 days. The clinical and histological results were compared with the follow-up data and are summarized in Table 2.

The histological features were recorded and analyzed, considering those parameters which better correlated with prognosis (Supplementary File S2). Such features included anisocytosis, anisokaryosis, mitotic count, presence of tumor-infiltrating lymphocytes (TILs), sebaceous differentiation (the presence of cytoplasmic lipidisation), existence of a capsule, calcifications, infiltrative growth, ductal differentiation (squamous metaplasia), loss of lobular/trabecular architecture, ulceration and multinucleated cells.

A grading system was assessed including low and high grade (Table 3) based on whether they were associated with low or high probability of having a worse prognosis, respectively, and was applied by the two pathologists (L.M.; S.I.).

According to this novel histological grading, a total of 38/76 cases were classified as low grade (50%) and 38/76 cases as high grade (50%) malignancy. Regarding the original diagnosis, of the

TABLE 2 Clinical and histological results in comparison with the follow up data.

Variable		Median DFI (days)	Median OS (days)	*p* value DFI	*p* value OS
Sex	Male	303	498	$p > 0.05$	$p > 0.05$
	Female	1963	1981		
	Neutered male	/	899		
	Spayed female	345	498		
Weight	≤7 kg	254	570	$p > 0.05$	$p > 0.05$
	>7 kg	1963	1,542		
Tumor size	T1	1963	1,460	$p > 0.05$	$p > 0.05$
	T2	630	1,121		
	T3	287	662		
Testicular tumors	Absent	700	899	$p > 0.05$	$p > 0.05$
	Present	303	–		
Mitotic count	≤11	1963	1,542	$p = 0.003$*	$p > 0.05$
	>11	303	735		
Multinucleated cells	Absent	1963	1,542	$p = 0.002$*	$p > 0.05$
	Present	303	498		
Loss of lobular/trabecular architecture	No (Figure 1A)	1963	1981	$p = 0.0009$*	$p = 0.003$*
	Yes (Figure 1B)	324	570		
Sebaceous differentiation	Absent	1963	1,542	$p = 0.02$*	$p > 0.05$
	Present (Figure 1C)	345	635		
Calcific foci	Absent	700	1,460	$p > 0.05$	$p > 0.05$
	Present	630	899		
Infiltrative growth	Absent	1963	1,542	$p > 0.05$	$p > 0.05$
	Present	324	700		
Ductal differentiation	Absent (Figure 1D)	1963	1,542	$p = 0.015$*	$p = 0.04$*
	Present	324	570		
Cellular pleomorphism	Regular (Figure 1E)	2045	1,246	$p = 0.002$*	$p = 0.01$*
	Moderate	1,286	617		
	Severe (Figure 1F)	1,081	351		

*statistically significant association.

10.3389/fvets.2025.1451510

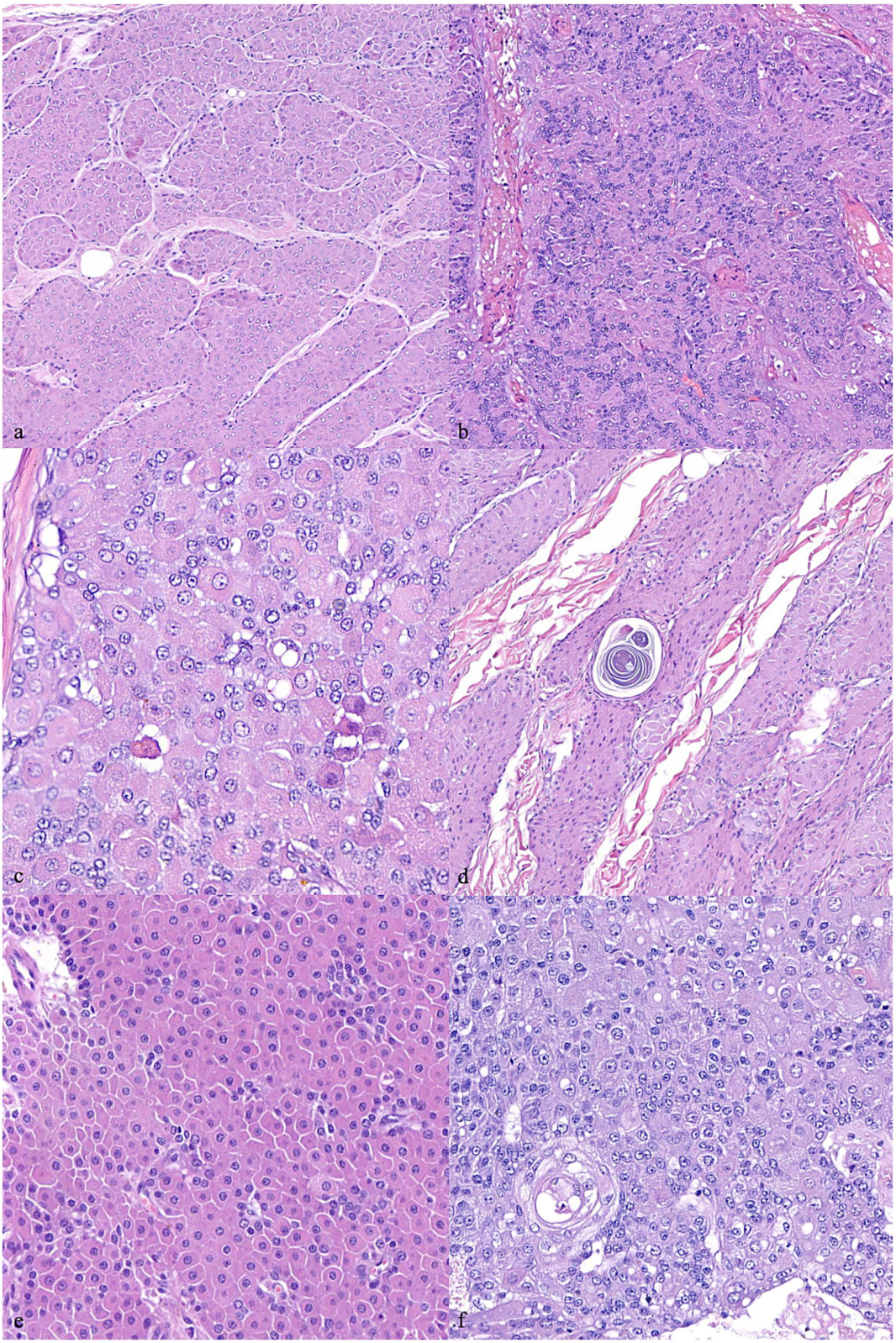

FIGURE 1
Canine hepatoid gland tumors. **(A)** Presence of trabecular/lobular architecture. 200x magnification. **(B)** Loss of trabecular/lobular architecture. 200x magnification. **(C)** Sebaceous differentiation. 400x magnification. **(D)** Ductal differentiation. 400x magnification. **(E)** Cellular pleomorphism assessed as normal – score 0. 400x magnification. **(F)** Cellular pleomorphism assessed as severe – score 2. 400x magnification. Hematoxylin and eosin staining.

TABLE 3 Schematic summary of the new grading model proposed in this study.

Histological feature	Score	*p* value DFI	*p* value OS
Trabecular/lobular architecture	3.02: absence 0: presence	$p = 0.0009$*	$p = 0.003$*
Multinucleated cells	0: absence 2.27: presence	$p = 0.002$*	$p > 0.05$
Cellular pleomorphism	0: regular 2.78: moderate 5.56: severe	$p = 0.002$*	$p = 0.01$*
Mitotic count	0: 0–7 2.21: >7	$p = 0.003$*	$p > 0.05$
Sebaceous differentiation	0: absence 1.92: presence	$p = 0.02$*	$p > 0.05$
Ductal differentiation	0: absence 2.48: presence	$p = 0.015$*	$p = 0.04$*
Total score:	≤ 10: low grade >10: high grade	$p = 0.003$	$p = 0.022$

Each parameter has been correlated with the survival data. *statistically significant association.

cases with a previous diagnosis of adenoma (19 cases), according to the grading system presented herein, the majority were classified as low grade (18/19), with only 1 case being a high grade, based on the grading system proposed herein. The epitheliomas were classified as low grade in 2/7 cases and high grade in 5/7 cases, while the adenocarcinomas were classified as low grade in 18/50 cases and high grade in 32/50 cases. According to this novel grading system, the histological grade was strongly associated with the recurrence (Chi-square test; $p = 0.003$). In particular, three out of 38 dogs (7.9%) with adenocarcinomas classified as low grade and 7 out of 38 (18.4%) dogs with tumors classified as high grade developed a local recurrence. Metastases were confirmed in 3 out of 38 (7.9%) cases with adenocarcinomas classified as low grade and in 4 out of 38 (10.5%) cases classified as high grade. The histological grade was also associated with the patients' outcome ($p = 0.003$ for DFI and a $p = 0.02$ for OS); in particular, a median DFI of 1963 days and a median OS of 1762 days was recorded in dogs bearing a low grade hepatoid gland tumor as compared with a median DFI of 303 days and a median OS of 498 days in those dogs bearing a high-grade tumor (Figure 2). The histological grades in relation to clinicopathological data are summarized in Table 4. In addition, histological grade was applied only to malignant tumors showing it was associated with relapse ($p = 0.04$) but not with survival.

The evaluation of the Ki67 index was available for 75 out of 76 cases; the median value was 4.84. With the cut-off set at 6%, the Ki67 index was not correlated with prognosis (Figure 3).

4 Discussion

In the cohort of cases presented here, the dogs were mainly mixed breeds (39.9%) with a mean age of 11.4 years (SD ± 2.4 years), which, according to the literature (19, 24), is slightly higher than previously reported (3, 25, 26). The clinical features of the hepatoid tumors that were seen in this study mirror those reported in the literature, i.e., perianal tumors, well circumscribed in most cases, having an average diameter between 0.5 and 3 cm (3). Most of the dogs of this study were intact males (85%), and this finding correlates to the development of most low-grade hepatoid tumors with a hormonal influence (3, 4). In particular, it is known that androgenic hormones stimulate the growth of the hepatoid gland cells expressing the receptors. It is also known from the literature that castration alone may induce a substantial cytoreduction of most hepatoid adenomas (27). In intact male dogs, a correlation between perianal adenomas and testicular interstitial cell tumors has been suggested and this support a testosterone stimulation as a causative factor (4, 5). Even in the present cohort of cases, 40.0% of the dogs had a concurrent testicular tumor. However, only 27.5% of these dogs had an interstitial cell tumor and 50% had a seminoma, bearing the remaining a Sertoli cell tumor, or both a Sertoli cell tumor and a seminoma. This phenomenon may indicate that a more complex hormonal change may play a pathogenetic role (28). At present, the standard of care for perianal adenomas is marginal excision associated with castration; conversely, perianal adenocarcinoma should be addressed by a more aggressive surgery, with a minimum margin of 1–2 cm (3, 29). The prognosis for adenocarcinomas seems related to the clinical tumor stage and the completeness of the surgical excision (13). Due to the anatomic contiguity between most of these hepatoid tumors and the external anal sphincter muscle, a wide margin excision is rarely performed in an attempt to preserve fecal continence. Nevertheless, in most of the cases presented in this retrospective study the histologic evaluation of the excision margins indicated a complete surgical excision. Overall, the recurrence rate was 13%, that is comparable to that reported in the literature (2). Currently, the guidelines for the classification of epithelial neoplasms generically divide hepatoid gland tumors into adenoma, epithelioma and adenocarcinoma (without referring to different degrees of differentiation) (15). According to the literature, hepatoid gland adenocarcinomas are characterized by a low rate of both recurrence and metastasis (3, 12); however, to date, a histological

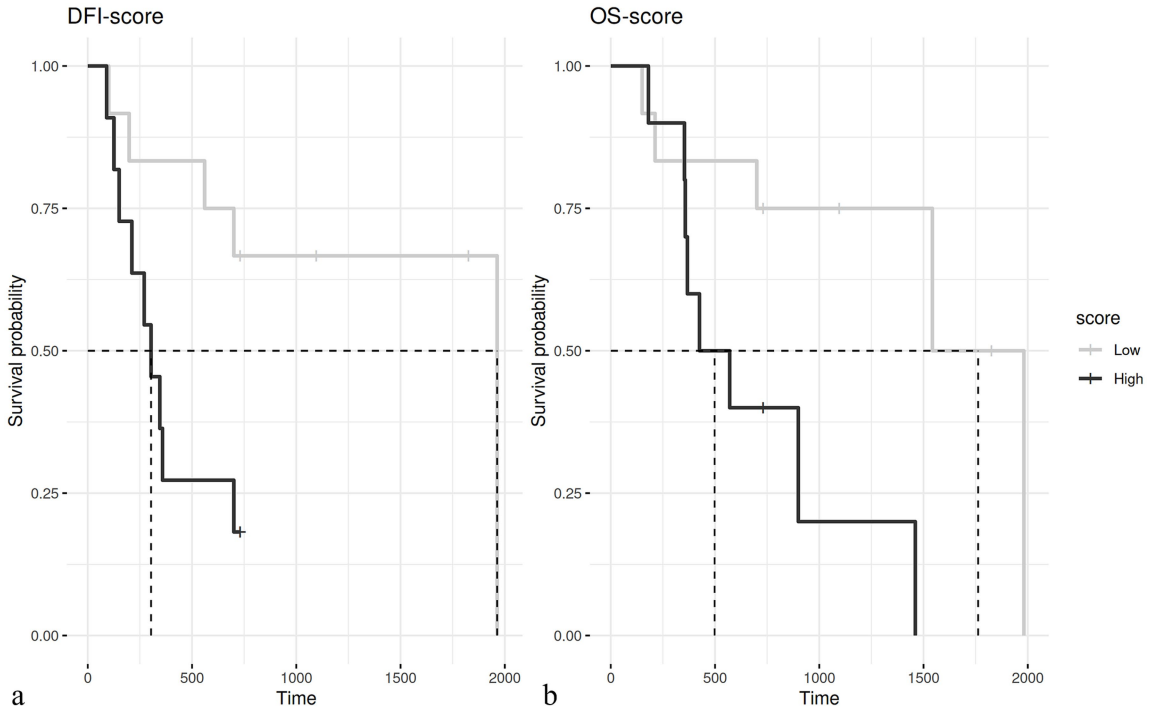

FIGURE 2
(A) Kaplan–Meier curve of the disease-free interval (DFI) in dogs with low grade (median 1963 days) and high grade (median 303 days – $p = 0.003$) tumors. **(B)** Kaplan–Meier curve of overall survival (OS) in dogs with low grade (mean 1762 days) and high grade (mean 498 days – $p = 0.02$) tumors.

TABLE 4 **Histological grade in relation to the clinicopathological data.**

Feature		Low grade (n)	High grade (n)	*p*-value
Sex	M	25	30	0.52
	F	3	1	
	MC	7	4	
	FC	3	3	
Tumor size	T1	25	21	0.56
	T2	10	11	
	T3	3	6	
Testicular tumor	Absent	18	19	0.57
	Present	7	11	
Recurrence	Absent	35	31	0.30
	Present	3	7	
Metastasis	Absent	35	34	1
	Present	3	4	
Ki67 index	≤6	26	24	0.62
	>6	11	14	

grading system capable of identifying cases with a worse prognosis is missing. The literature has reported that a few hepatoid tumors with well-differentiated morphology, in the absence of any clinical tumor staging demonstrating the presence of metastases, would have been diagnosed as adenoma based on cell morphology alone (16); this finding was also confirmed by the present study (unpublished data) and by one case of the present cohort of dogs which developed a metastasis after 198 days, despite a hepatoid tumor with histological features compatible with a benign lesion.

The histological grade proposed in this study was designed to be applicable to all hepatoid neoplasms, either diagnosed as adenomas, epitheliomas, or adenocarcinomas, so that their prognosis could be predicted. The histological parameters that were found to be useful in constructing this histological grading system are largely those that have previously been identified as carcinoma-related.

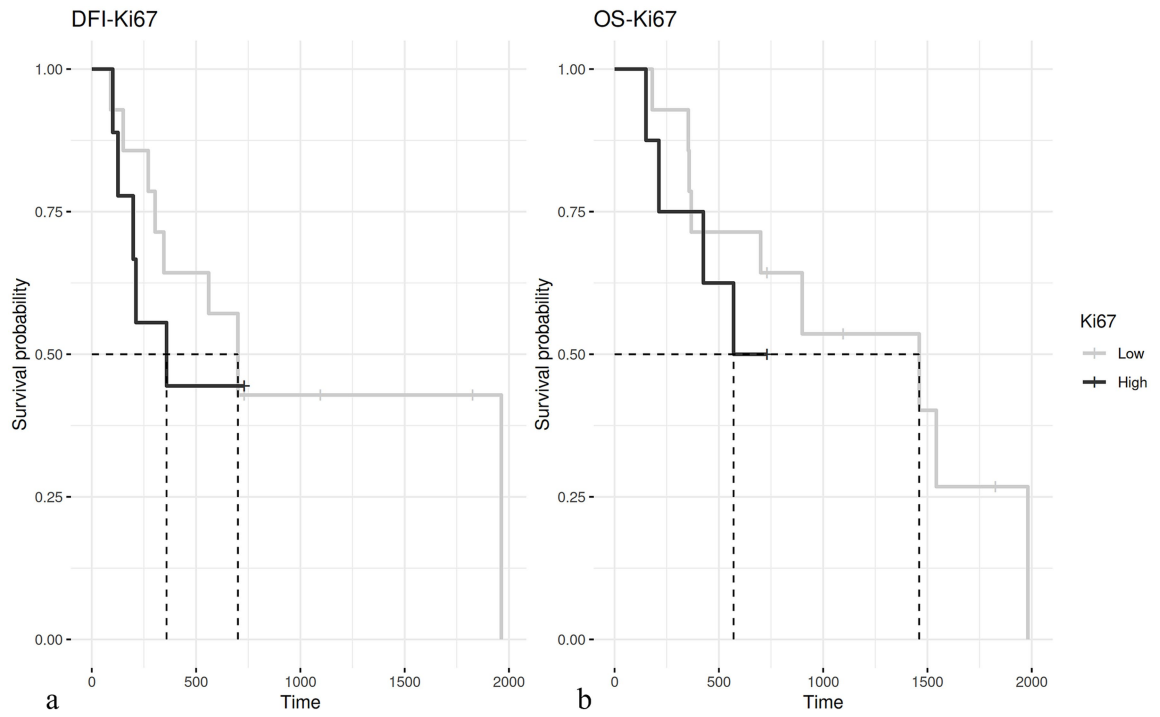

FIGURE 3
(A) Kaplan–Meier curve of disease-free interval (DFI) in dogs having hepatoid gland tumors with a Ki67 ≤ 6% (median 700 days) and > 6% (median 358 days – $p = 0.5$). **(B)** Kaplan–Meier curve of overall survival (OS) in dogs with hepatoid gland tumor with a Ki67 ≤ 6% (median 1,460 days) and > 6% (median 570 days – $p = 0.36$).

Although this grading system offers better assistance in differentiating low-grade from high-grade hepatoid neoplasms, the existence of a small cohort of well-differentiated tumors which may develop metastases needs further consideration. The Ki67 index has been used as a prognostic indicator for some tumors in various studies (30–34); however, the different results that are often obtained may derive from the different immunohistochemical techniques and evaluation methods used. In the present study, the Ki67 index was evaluated using the QuPath software to strongly limit these evaluation bias, but it was not found to be associated with prognosis anyway. This result differs from the study by Pereira et al. (14) who, using a computer-assisted image analysis, found that Ki67 with a cut-off assessed at 9.87% was predictive of recurrence. Therefore, although for many canine cancers, Ki67 seems to be a valuable prognostic factor (30–34), this was not the case for the hepatoid tumors presented in this case cohort. Nonetheless, the Authors encourage its use as an additional prognostic information since a single case diagnosed as adenoma and classified as low-grade by the present study had a Ki67 of 25.37% which was considerably above the cut-off considered by both the authors of this study and Pereira et al. and developed metastasis after 198 days, pointing out that, in selected cases, Ki67 can provide useful prognostic information.

Even if this study has two main limitations due to its retrospective nature and the limited number of cases included, it opens the way to a grading system which may be considered as an important and valid diagnostic tool for formulating a more accurate diagnosis and prognosis of canine hepatoid tumors. Nevertheless, further studies recruiting a larger number of cases are warranted in order to confirm these preliminary results.

5 Conclusion

The histological grading of hepatoid perianal tumors remains a challenge for the veterinary pathologists. Despite the fact that the prognosis for these tumors is often favorable following surgical excision, the Authors emphasize the importance of the collaboration between clinicians and pathologists in the evaluation of the clinical tumor staging, the long-term follow-up, and the histological appearance of these tumors. The Authors believe that the use of the histological scoring system proposed in this study may potentially help the understanding of the clinic-biological behavior of these tumors as additional prognostic information is added; at the same time, the Authors feel that further studies are warranted to confirm these preliminary data.

Data availability statement

The raw data supporting the conclusions of this article will be made available by the authors, without undue reservation.

Ethics statement

Ethical approval was not required for the studies involving animals in accordance with the local legislation and institutional

requirements because it is a retrospective study done on archived histological tissues excised after surgery for removal of tumor with the agreement of the owner. Written informed consent was obtained from the owners for the participation of their animals in this study.

Author contributions

LM: Conceptualization, Investigation, Methodology, Software, Validation, Writing – original draft, Writing – review & editing. MO: Conceptualization, Investigation, Methodology, Project administration, Writing – original draft, Writing – review & editing. LP: Investigation, Methodology, Writing – original draft. PB: Writing – review & editing. EuM: Formal analysis, Methodology, Software, Writing – original draft. GM: Methodology, Software, Writing – original draft. MmM: Writing – review & editing. SI: Writing – review & editing. EmM: Writing – review & editing.

Funding

The author(s) declare that financial support was received for the research, authorship, and/or publication of this article. This research was funded by Department of Veterinary Science of University of Turin, number 1/015/2021 "linea b".

Conflict of interest

The authors declare that the research was conducted in the absence of any commercial or financial relationships that could be construed as a potential conflict of interest.

Publisher's note

All claims expressed in this article are solely those of the authors and do not necessarily represent those of their affiliated organizations, or those of the publisher, the editors and the reviewers. Any product that may be evaluated in this article, or claim that may be made by its manufacturer, is not guaranteed or endorsed by the publisher.

Supplementary material

The Supplementary material for this article can be found online at: https://www.frontiersin.org/articles/10.3389/fvets.2025.1451510/full#supplementary-material

References

1. Moraes JRE, Baretta DC, Zanetti AS, Garrido E, Miyazato LG, Sevarolli AL. Cutaneous tumors in dogs - a retrospective study of ten years. *Vet Not*. (2009) 10:59–68. doi: 10.17582/journal.aavs/2022/10.1.170.182

2. Goldschmidt M.H., and Goldschmidt K. H..Epithelial and Melanocytic Tumors of the Skin. In Tumors in Domestic Animals, D.J. Meuten (Ed.). doi: 10.1002/9781119181200.ch4

3. Liptak J.M, Turek M.M. (2020) Perianal tumors. In Withrow & MacEwen's small animal clinical oncology, edited by D.M. Vail and D.H Thamm. and J.M Liptak. (St. Louis, Missouri: Elsevier), 6th edition, 468–470.

4. Nielsen SW, Attosmis J. Canine perianal gland tumors. *J Am Vet Med Assoc*. (1964) 144:127–35.

5. Maita K, Ishida K. Structure and development of the perianal gland of the dog. *Japanese J Vet Sci*. (1975) 37:349–56. doi: 10.1292/jvms1939.37.349

6. Pisani G, Millanta F, Lorenzi D, Vannozzi I, Poli A. Androgen receptor expression in normal, hyperplastic and neoplastic hepatoid glands in the dog. *Res Vet Sci*. (2006) 81:231–6. doi: 10.1016/j.rvsc.2005.11.001

7. Maxie MG. Jubb, Kennedy, and Palmer's pathology of domestic animals. *Sixth* ed. St. Louis, Missouri: Elsevier (2016).

8. Hayes HM, Wilson GP. Hormone-dependent neoplasms of the canine perianal gland. *Carcer Res*. (1977) 37:2068–71.

9. Ipek E, Epikmen ET, Yildirim F, Ozsoy SY, Tunca R. Immunolabelling of SCF and c-KIT in canine perianal gland tumours. *J Comp Pathol*. (2023) 200:51–8. doi: 10.1016/j.jcpa.2022.11.007

10. Martins AMCRPF, Vasques-Peyser A, Torres LN, Matera JM, Dagli MLZ, Guerra JL. Retrospective – systematic study and quantitative analysis of cellular proliferation and apoptosis in normal, hyperplastic and neoplastic perianal glands in dogs. *Vet Comp Oncol*. (2008) 6:71–9. doi: 10.1111/j.1476-5829.2007.00140.x

11. Owen LN. TNM classification of tumours in domestic animals. *1st* ed. Geneva: World Health Organization (1980).

12. Vail DM, Withrow SJ, Schwarz PD, Powers BE. Perianal adenocarcinoma in the canine male: a retrospective study of 41 cases. *J Am Anim Hosp Assoc*. (1990) 26:329–34.

13. Kessler M. Perianal tumors in world small animal Veterinary Association World Congress Proceedings (2014).

14. Pereira RS, Schweigert A, Fernandes FV, Sueiro FAR, Machado GF. Ki-67 labeling in canine perianal glands neoplasms: a novel approach for immunohistological diagnostic and prognostic. *BMC Vet Res*. (2013) 9:83. doi: 10.1186/1746-6148-9-83

15. Goldschmidt MH, Munday JS, Scruggs JL, Klopfleisch R, Kiupel M. Epithelial tumors of the skin In: Surgical pathology of tumors of domestic animals. Gurnee, IL: Davis Thompson Foundation (2018). 241.

16. McCourt MR, Levine GM, Breshears MA, Wall CR, Meinkoth JH. Metastatic disease in a dog with a well-differentiated perianal gland tumor. *Vet Clin Pathol*. (2018) 47:649–53. doi: 10.1111/vcp.12662

17. Gross TL. Skin diseases of the dog and cat: Clinical and histopathologic diagnosis. *2nd* ed. Oxford: Blackwell Science (2006).

18. Kim S-H, Seung B-J, Cho S-H, Lim H-Y, Park H-M, Sur J-H. Increased p63 expression in canine perianal gland Tumours. *J Vet Res*. (2018) 62:229–35. doi: 10.2478/jvetres-2018-0020

19. Goldschmidt MH, Dunstan RW, Stannard AA, Von Tschargner C, Walder EJ, Yager JA. Melanocytic tumors and tumor-like lesions In: Histological classification of epithelial and melanocytic tumors of skin of domestic animals. Washington D.C.: Yager J.A (1998). 38–40.

20. Meuten DJ, Moore FM, George JW. Mitotic count and the field of view area: time to standardize. *Vet Pathol*. (2016) 53:7–9. doi: 10.1177/0300985815593349

21. Pai R, Karki S, Agarwal R, Sieber S, Barasch S. Optimal settings and clinical validation for automated Ki67 calculation in neuroendocrine tumors with open source informatics (QuPath). *J Pathol Inform*. (2022) 13:100141. doi: 10.1016/j.jpi.2022.100141

22. Boracchi P, Roccabianca P, Avallone G, Marano G. Kaplan-Meier curves, cox model, and P -values are not enough for the prognostic evaluation of tumor markers: statistical suggestions for a more comprehensive approach. *Vet Pathol*. (2021) 58:795–808. doi: 10.1177/03009858211014174

23. Webster JD, Dennis MM, Dervisis N, Heller J, Bacon NJ, Bergman PJ, et al. Recommended guidelines for the conduct and evaluation of prognostic studies in veterinary oncology. *Vet Pathol*. (2011) 48:7–18. doi: 10.1177/0300985810377187

24. Evans HE. The digestive apparatus and abdomen In: Miller's anatomy of the dog, vol. *75*. Philadelphia: Saunder (2012). 324–6.

25. Berrocal A, Vos JH, Ingh TSGAM, Molenbeek RF, Sluijs FJ. Canine perineal Tumours. *J Veterinary Med Ser A*. (1989) 36:739–49. doi: 10.1111/j.1439-0442.1989.tb00787.x

26. Goldschmidt MH, Shofer FS. Skin tumors of the dog and cat. *1st* ed. Oxford, UK: Pergamon Press (1992).

27. Wilson GP, Hayes HM. Castration for treatment of perianal gland neoplasms in the dog. *J Am Vet Med Assoc*. (1979) 174:1301–3.

28. Brodzki A, Łopuszyński W, Brodzki P, Głodkowska K, Knap B, Gawin P. Pharmacological treatment of perianal gland tumors in male dogs. *Animals*. (2023) 13:463. doi: 10.3390/ani13030463

29. Buracco P. Perianal Tumors In: C WTN, RP Cavanaugh, CalfeeEF III, P Buracco and TA Banks, editors. Veterinary surgical oncology. *2nd* ed. Hoboken, NJ USA: John Wiley & Sons (2022). 347–73.

30. Abadie JJ, Amardeilh MA, Delverdier ME. Immunohistochemical detection of proliferating cell nuclear antigen and Ki-67 in mast cell tumors from dogs. *J Am Vet Med Assoc*. (1999) 215:1629–34. doi: 10.2460/javma.1999.215.11.1629

31. Bergin IL, Smedley RC, Esplin DG, Spangler WL, Kiupel M. Prognostic evaluation of Ki67 threshold value in canine Oral melanoma. *Vet Pathol*. (2011) 48:41–53. doi: 10.1177/0300985810388947

32. Buishand FO, Kik M, Kirpensteijn J. Evaluation of clinico-pathological criteria and the Ki67 index as prognostic indicators in canine insulinoma. *Vet J*. (2010) 185:62–7. doi: 10.1016/j.tvjl.2010.04.015

33. Maglennon GA, Murphy S, Adams V, Miller J, Smith K, Blunden A, et al. Association of Ki67 index with prognosis for intermediate-grade canine cutaneous mast cell tumours*. *Vet Comp Oncol*. (2008) 6:268–74. doi: 10.1111/j.1476-5829.2008.00168.x

34. Sierra Matiz OR, Santilli J, Anai LA, Da Silva MCL, Sueiro FA, Sequeira JL, et al. Prognostic significance of Ki67 and its correlation with mitotic index in dogs with diffuse large B-cell lymphoma treated with 19-week CHOP-based protocol. *J Vet Diagn Invest*. (2018) 30:263–7. doi: 10.1177/1040638717743280

frontiers | Frontiers in Veterinary Science

TYPE Case Report
PUBLISHED 24 February 2025
DOI 10.3389/fvets.2025.1542700

Check for updates

OPEN ACCESS

EDITED BY
Yasunaga Yoshikawa,
Kitasato University, Japan

REVIEWED BY
Nicola Zizzo,
Uniba, Italy
Paola Modesto,
Experimental Zooprophylactic Institute for Piedmont, Liguria and Valle d'Aosta (IZSPLVA), Italy

*CORRESPONDENCE
Desheng Li
lidesheng_ccrcgp@163.com
Zhengli Cheng
chzhli75@163.com

†These authors have contributed equally to this work

RECEIVED 10 December 2024
ACCEPTED 21 January 2025
PUBLISHED 24 February 2025

CITATION
Xiong Z, Ling S, Li C, Deng L, Wei T, He M, Wang C, Luo Q, Li D and Cheng Z (2025) Case report: A study on the pathology of mandibular osteosarcoma with hepatic metastasis in a giant panda.
Front. Vet. Sci. 12:1542700.
doi: 10.3389/fvets.2025.1542700

COPYRIGHT
© 2025 Xiong, Ling, Li, Deng, Wei, He, Wang, Luo, Li and Cheng. This is an open-access article distributed under the terms of the Creative Commons Attribution License (CC BY). The use, distribution or reproduction in other forums is permitted, provided the original author(s) and the copyright owner(s) are credited and that the original publication in this journal is cited, in accordance with accepted academic practice. No use, distribution or reproduction is permitted which does not comply with these terms.

Case report: A study on the pathology of mandibular osteosarcoma with hepatic metastasis in a giant panda

Zongliang Xiong[1†], Shanshan Ling[2†], Caiwu Li[2†], Linhua Deng[2], Tingting Wei[1], Ming He[2], Chengdong Wang[2], Qihui Luo[1], Desheng Li[2*] and Zhengli Cheng[1*]

[1]Experimental Animal Disease Model Research Laboratory, School of Veterinary Medicine, Sichuan Agricultural University, Chengdu, China, [2]Key Laboratory of State Forestry and Grassland Administration on the Giant Panda, China Conservation and Research Center for the Giant Panda, Chengdu, China

During routine health examinations, an abnormal growth was detected in the oral cavity of a male giant panda. A malignant tumor, osteosarcoma, was diagnosed through CT (computed tomography) scans and pathological examination of biopsy samples. After two attempts at "tumor reduction surgery" with no improvement, the condition stabilized following particle implantation and arterial infusion interventional therapy. The following year, a CT scan revealed a highly similar mass in the left lumbar muscle, which showed no improvement despite chemotherapy, leading to death 1 month later. Post-mortem examination and tissue pathological diagnosis confirmed osteosarcoma characteristics in the facial, lumbar, and liver masses. The giant panda was diagnosed with osteosarcoma with liver metastasis based on integrated pathological and gross anatomical observations. This case represents the first report of osteosarcoma with liver metastasis in a giant panda, providing valuable data and references for future clinical diagnosis and treatment of tumors in giant pandas.

KEYWORDS

giant panda, osteosarcoma, tumor metastasis, pathology, cheek osteosarcoma

Introduction

The giant panda (scientific name *Ailuropoda melanoleuca*) belongs to the bear family, genus Ailuropoda, and has existed on Earth for at least 8 million years. Known as a "living fossil" and the "national treasure of China," it serves as the emblem of the World Wildlife Fund (WWF) and is a flagship species in global biodiversity conservation. Its disease research is also highly focused. As a severe disease that poses a significant threat to health, the incidence of tumors in giant pandas has correspondingly increased with their extended lifespan. Given the uniqueness of the giant panda, clinical tumor case reports are extremely rare, with only sporadic reports available, such as ovarian cancer, pancreatic ductal adenocarcinoma, seminomas, cutaneous hemangiomas, and conjunctival vascular sarcomas (1–5). This leads to a severe shortage of clinical diagnostic data for tumors in giant pandas, especially lacking in testing data and reports from live sampling.

Osteosarcoma (Osteosarcoma, OS) is a common primary malignant bone tumor (6, 7), and OS is a disease originating from mesenchymal cells, characterized by the proliferation of osteoblast precursor cells and the formation of bone or immature bone (8). It is particularly common in humans and canines (9), and is typically treated with amputation or chemotherapy. Osteosarcoma can arise in any bone, most commonly affecting the long bones of the legs and occasionally the long bones of the arms (10). Osteosarcoma can metastasize from the primary

site to other locations, most frequently to the lungs, the same bone, or another bone, which increases the difficulty of treatment and rehabilitation (11–13). This case represents the first report of osteosarcoma in a giant panda and also the first report of osteosarcoma with liver metastasis in a giant panda, filling a gap in the clinical data of giant panda osteosarcoma and holding significant reference value.

Case presentation

Basic case information

Giant panda "Wugang" (lineage number 502), a male, was rescued in the wild in 1999. CT scans in May 2021 revealed irregular local bone quality in the right zygomatic arch, with adjacent soft tissue swelling and multiple small nodular calcifications; no other significant abnormalities were observed. In February 2023, an abnormal growth was found in its oral cavity, accompanied by symptoms such as bleeding during feeding. After examination and diagnosis, a malignant tumor, osteosarcoma, was confirmed. Two attempts at tumor reduction surgery were made, but the recovery was poor. Due to the astonishing growth rate of the osteosarcoma, the frequency and volume of bleeding increased, leading to severe anemia in the panda. To better control the tumor and reduce bleeding, Wugang underwent interventional chemotherapy, including particle implantation and arterial infusion, which effectively controlled the bleeding and reversed the anemia, stabilizing the condition for a period. In September 2023, a follow-up enhanced CT scan showed the oral tumor to be relatively stable, but a mass approximately 9.8 cm × 7.7 cm was found in the left lumbar muscle, highly similar in nature to the oral tumor (osteosarcoma), with surrounding bone tissue destruction affecting normal walking. After intravenous chemotherapy, the panda's condition did not improve and the panda died at the age of 24. For treatment of tumors, please see the Supplementary material.

Necropsy findings

The body weight was 86 kg, with a total body length of 112 cm, head length of 37 cm, hind limb length of 59 cm, forelimb length of 65 cm, chest circumference of 106 cm, abdominal circumference of 113 cm, and neck circumference of 71 cm. The cadaver appeared clean, emaciated, with dull fur; the right cheek was swollen, and the mouth was draining brown liquid (Figures 1A,B). Upon necropsy, a large bony mass was found in the right cheek and mandible area, with a surface that exhibited a gradient of color from black to grayish-white, resembling a cauliflower-like variation; the central part of the mass was a pinkish bone structure, and the mass occupied the entire right side of the face (Figures 1C,E). There was a mass measuring approximately 10 cm × 10 cm in the left lumbar muscle area, presenting as a solid structure with varying shades of pink (Figure 1F). The stomach was distended with gas, the gastric wall had pinpoint bleeding, there was hemorrhaging in the peritoneum, congestion in the intestinal walls, hepatic edema, multiple pale gray nodules on the

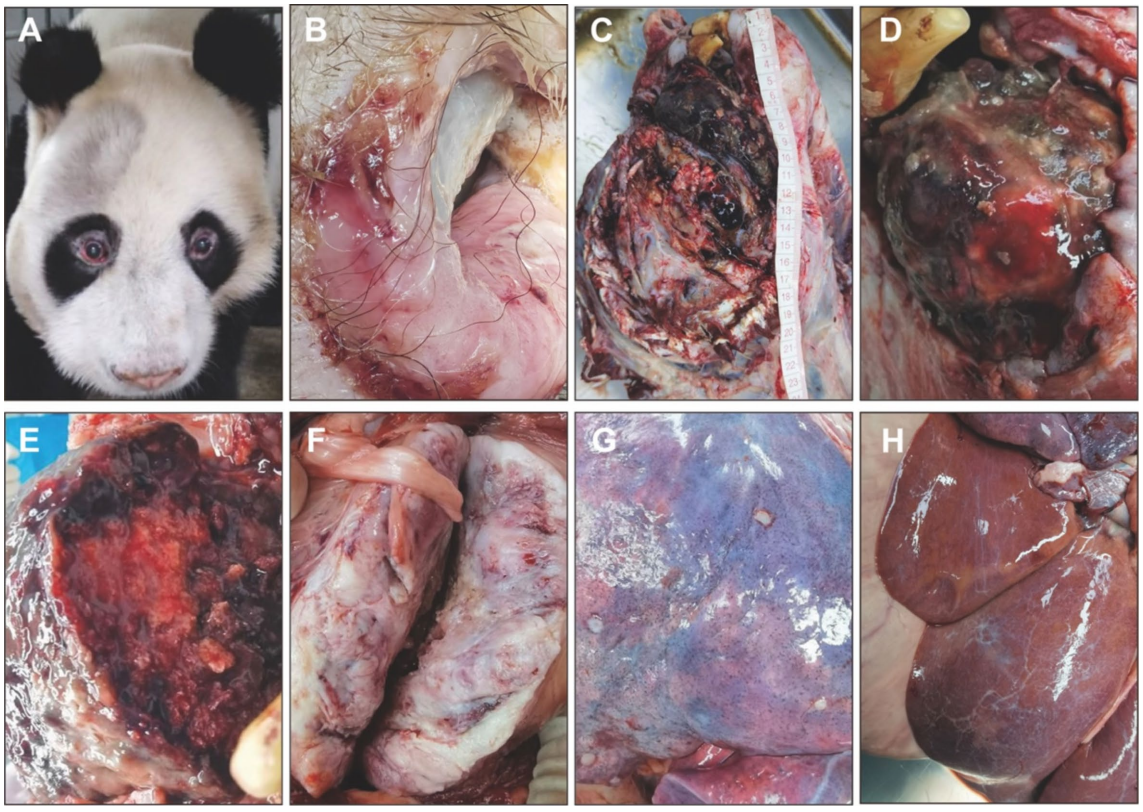

FIGURE 1
Clinical necropsy examination of giant panda Wugang. **(A)** Facial appearance before death. **(B)** Oral margin. **(C)** Location and size of the cheek mass. **(D)** Surface characteristics of the cheek mass. **(E)** Cross-sectional characteristics of the cheek mass. **(F)** Cross-sectional characteristics of the lumbar mass. **(G)** Nodules on the lung surface. **(H)** Pale yellow foci can be seen in the liver.

lung surface, each about 0.5 cm in diameter, and the lungs showed mild atrophy and collapse (Figure 1G). The liver is slightly enlarged, lighter in color, and yellowish foci are visible (Figure 1H).

Imaging examination

CT scans revealed a local mass in the right maxillofacial region extending to the right side of the neck, with the largest dimension measuring approximately 204 × 113 × 124 mm. The lesion had uneven density, with multiple patchy high-density and gas shadows, and showed mild heterogeneous enhancement on contrast scans. The skull and right maxillofacial bones were invaded and destroyed (Figure 2A). CT scans of the thorax and abdomen demonstrated a bulla in the left lower lobe of the lung (Figure 2B); left pleural effusion measuring approximately 20 mm in thickness, and right pleural effusion measuring approximately 10 mm (Figure 2C); degenerative changes in the 12th and 13th thoracic vertebrae and intervertebral discs (Figure 2D); enlargement of the left adrenal gland with multiple calcified foci (Figure 2E); swelling of the left psoas major muscle with an internal mass measuring approximately 98 × 77 mm, uneven density, and patchy non-enhancing shadows. Contrast scans showed peripheral rim enhancement, seemingly with small vessels traversing through, and the internal low-density focus did not enhance, with surrounding bone destruction (Figure 2F).

Pathological examination

Biopsy tissue pathology examination

After the excision of the mass from the right cheek, paraffin sections were prepared and HE (Hematoxylin–Eosin)-stained, with a pathological diagnosis of spindle cell tumor, easily visible mitotic figures (Figure 3A), presence of atypical cartilage and tumorous osteogenesis (Figures 3B,C), and the tissue morphology was that of a high-grade malignant tumor (sarcoma), graded as 3 (G3) by the FNCLCC (French Federation of Comprehensive Cancer Centers) system. The subtype diagnosis, combining tissue morphology and immunohistochemical results, was conventional osteosarcoma (fibroblastic subtype). Surface squamous epithelial ulceration with significant hyperplasia and pseudoepitheliomatous hyperplasia (Figure 3D). Immunohistochemical results: tumor cells showed SATB2(+), Desmin(−), S100(−), SMA(partially +), H3K27Me3(partially lost), ERG(−), Ki-67(MIB-1) (inconclusive) (Figures 3E–L).

Post-mortem tissue pathology examination

After necropsy, tissue samples from the major organs of the giant panda were collected, with bone tissues undergoing decalcification treatment and the remaining tissues undergoing routine dehydration and clarification. Paraffin sections were then prepared, stained with

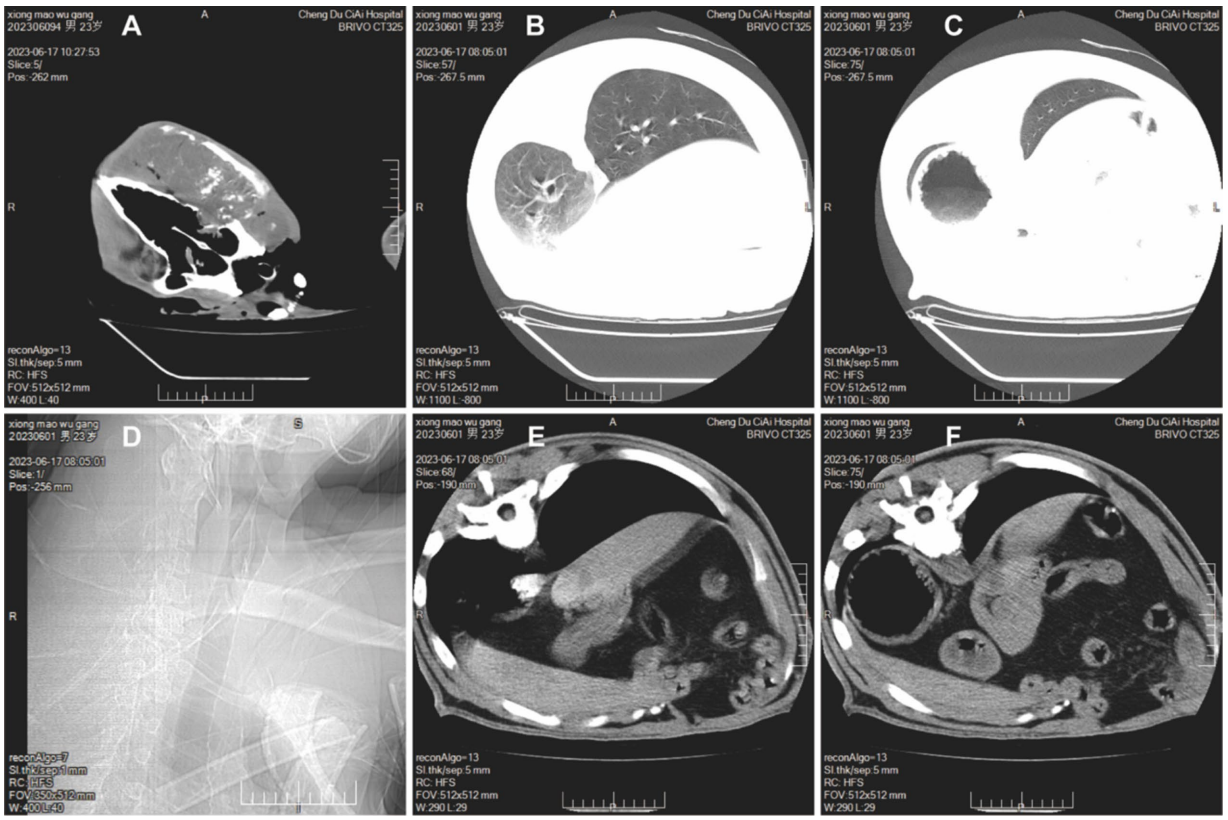

FIGURE 2
CT scans of giant panda Wugang. **(A)** A mass is visible in the right maxillofacial region. **(B)** A bulla is observed in the left lower lobe of the lung. **(C)** Pleural effusion is present. **(D)** Degenerative changes in the vertebrae. **(E)** Enlargement of the left adrenal gland with multiple calcified foci. **(F)** Swelling of the left psoas major muscle with a visible mass.

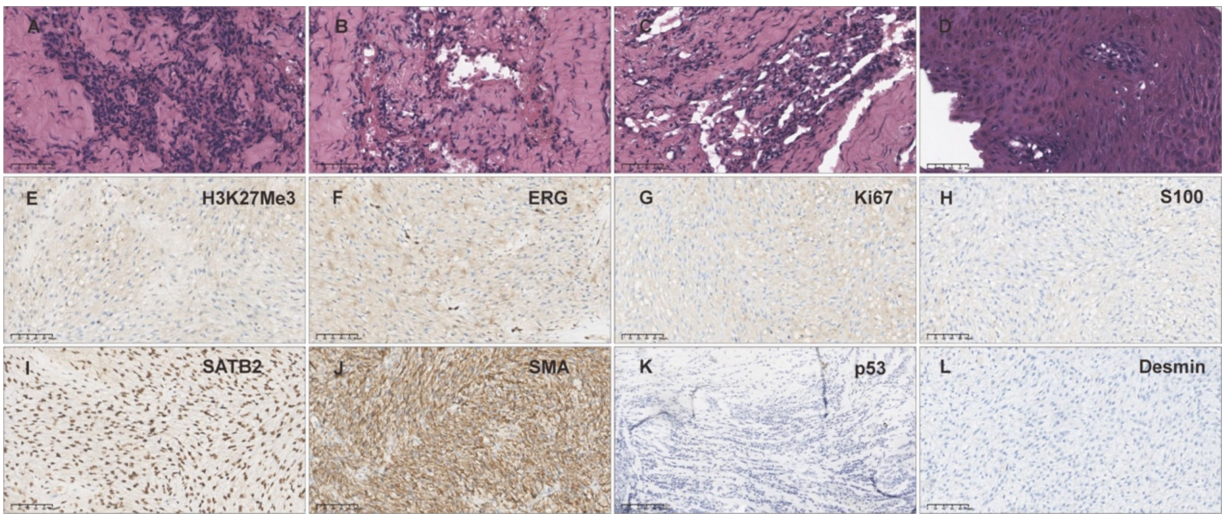

FIGURE 3
Biopsy tissue HE staining and immunohistochemical examination. **(A–D)** HE staining of the biopsy sample from the cheek mass. **(E)** H3K27Me3 staining of the biopsy sample from the cheek mass (partially lost). **(F)** ERG staining of the biopsy sample from the cheek mass (–). **(G)** Ki67 staining of the biopsy sample from the cheek mass (inconclusive). **(H)** S100 staining of the biopsy sample from the cheek mass (–). **(I)** SATB2 staining of the biopsy sample from the cheek mass (+). **(J)** SMA staining of the biopsy sample from the cheek mass (partially +). **(K)** p53 staining of the biopsy sample from the cheek mass (–). **(L)** Desmin staining of the biopsy sample from the cheek mass (–).

HE, and histopathological changes were observed. The results are as follows: Facial mass: The mass tissue is primarily composed of large areas of interlacing neoplastic immature bone or cartilage. There is significant proliferation of fibrous new tissue between the bone plates, accompanied by a large number of blood vessels with vascular congestion. Most cells in the bone plates appear vacuolated. The fibrous tissue exhibits marked cellular pleomorphism, with spindle, oval, or round shapes, and contains a large amount of collagen. Mitotic figures are frequently observed (Figures 4A1–A6). In conjunction with the gross anatomical protruding proliferative mass on the facial surface, a preliminary diagnosis of osteosarcoma is made. Jejunum: Mucosal autolysis/necrosis (Figures 4B1,B2). Lumbar mass: The mass tissue is primarily composed of large areas of interlacing neoplastic immature bone. Between the bone plates, there are mature red blood cells and bone marrow cells, with erythroid hyperplasia. The bone plates contain a high amount of bone collagen, with cellular atypia, round, oval, and spindle shapes, and frequent mitotic figures (Figures 4C1–C4). In conjunction with the gross anatomical protruding proliferative mass, a preliminary diagnosis of osteosarcoma is made. Lungs: The pleura exhibits hyperplasia and hemorrhage. There is alveolar overinflation, rupture of the alveolar septa, and vascular congestion (Figures 4D1,D2). Duodenum: Dilation of intestinal glands, atrophy of intestinal villi, and massive inflammatory cell infiltration (Figures 4E1,E2). Liver: The liver tissue is largely replaced by tumor cells, with hepatocytes being compressed, and the cellular and tissue structure disappearing. The tumor tissue is arranged in sheets, with large cell volume, tight arrangement, obvious atypia, round, oval, and spindle shapes, and a high nuclear-cytoplasmic ratio (Figures 4F1–F6). A preliminary judgment is made for osteosarcoma liver metastasis. Lymph nodes: The lymph nodes show extensive congestion and hemorrhage, tissue structure disorder, almost no mature lymph follicles in the cortical area, a significant reduction in cellular components, and a large number of multinucleated giant cells (Figures 4G1,G2). Spleen: The spleen is atrophied and degenerated, with the structure disappearing, a significant reduction in cellular components, and splenic trabecular hyperplasia (Figures 4H1–H4). Kidneys: Dilation of renal tubules, thinning of tubular walls, and detachment of some renal tubular epithelium. Focal inflammatory cell infiltration is observed (Figures 4I1,I2). Heart: Myocardial cell atrophy, interstitial edema, and brown pigment deposition (Figures 4J1,J2).

Discussion

Giant pandas, due to their unique characteristics, can survive for several decades in captive environments, compared to their wild habitats, they have a longer lifespan. With the extension of the giant panda's lifespan, the incidence of tumors also increases, posing a threat to the lives of elderly giant pandas. Currently, there are few clinical reports of tumors in giant pandas, and there is a severe lack of clinical data. This case is the second tumor case diagnosed pathologically in our laboratory, with both cases having tumors located in the oral cavity (accepted), which may be related to the feeding habits of giant pandas. In canine osteosarcoma cases, tumors are commonly located in the limbs, and the treatment often involves removing the tumor mass while trying to preserve the limb, but sometimes, to eradicate all cancerous lesions, part of the limb may need to be amputated (14, 15). In this case, due to the tumor's location in the maxillofacial region, the treatment methods used in canine osteosarcoma cases could not be applied, and due to the absence of data on giant panda osteosarcoma cases, there were no referable treatment methods. By referring to treatment methods from human medicine, a tumor reduction surgery was first performed, but with poor results; eventually, particle implantation and arterial infusion were used to inhibit further tumor progression.

In canine osteosarcoma cases, osteosarcoma most commonly metastasizes to the lungs, the same bone, or another bone (16, 17). In this case, the maxillofacial osteosarcoma in the giant panda, after being

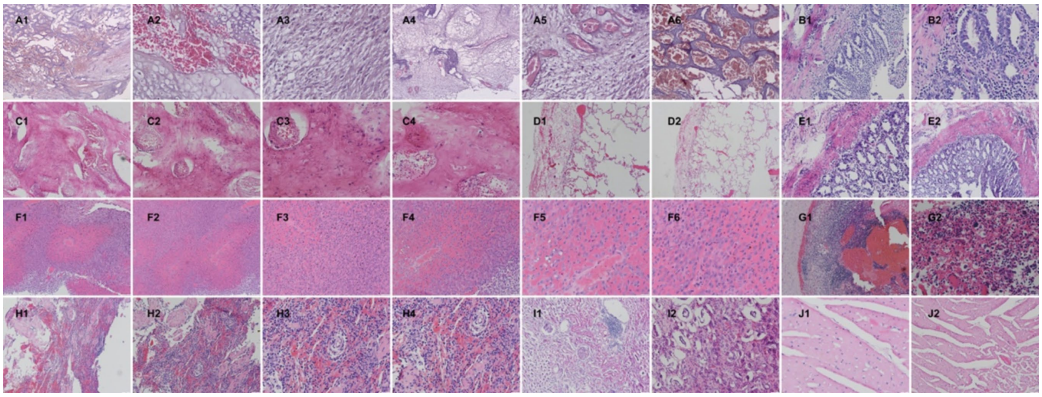

FIGURE 4
Post-mortem tissue sampling with H&E staining for pathological diagnosis. **(A)** Facial mass, with different Arabic numerals indicating different fields and magnifications, A1 40X, A2-A3 400X, A4 100X, A5 400X, A6 200X. **(B)** Jejunal tissue, B1 200X, B2 400X. **(C)** Mass in the lumbar region, C1 100X, C2 200X, C3-C4 400X. **(D)** Lungs, D1 100X, D2 40X. **(E)** Duodenum, E1 200X, E2 400X. **(F)** Liver, F1 100X, F2-F4 200X, F5-F6 400X. **(G)** Lymph node G1 100X, G2 400X. **(H)** Spleen, H1 100X, H2 200X, H3-H4 400X. **(I)** Kidney, I1 100X, I2 200X. **(J)** Heart, J1 400X, J2 200X.

stabilized with interventional treatment, experienced metastasis the following year. However, unlike the spread of canine osteosarcoma, after the stabilization of the maxillofacial osteosarcoma in this case, a mass with the same characteristics as the maxillofacial tumor was observed in the lumbar muscle by CT scan, and post-mortem sampling with H&E staining revealed similar tumor features in the liver tissue. Owing to the scarcity of clinical tumor case data in giant pandas, it is unclear whether this particular pattern of tumor metastasis is an isolated case or a common feature. This case represents the first reported instance of osteosarcoma in giant pandas, establishing a systematic and comprehensive diagnostic approach. The liver metastasis of osteosarcoma in this case also provides valuable reference and clinical data for the treatment of osteosarcoma in giant pandas.

Data availability statement

The original contributions presented in the study are included in the article/Supplementary material, further inquiries can be directed to the corresponding authors.

Ethics statement

The animal study was approved by Sichuan Agricultural University Institutional Animal Care and Use Committee. The study was conducted in accordance with the local legislation and institutional requirements. Informed consent was obtained from the participants for the publication of this case report.

Author contributions

ZX: Data curation, Formal analysis, Writing – original draft, Writing – review & editing. SL: Investigation, Writing – original draft. CL: Resources, Writing – original draft. LD: Resources, Writing – original draft. TW: Formal analysis, Writing – original draft. MH: Project administration, Writing – original draft. CW: Resources, Writing – original draft. QL: Writing – review & editing, Formal analysis. DL: Resources, Writing – original draft. ZC: Funding acquisition, Project administration, Resources, Validation, Writing – review & editing.

Funding

The author(s) declare that financial support was received for the research, authorship, and/or publication of this article. This project was supported by the China Youth Development Foundation Mercedes-Benz Star Fund.

Conflict of interest

The authors declare that the research was conducted in the absence of any commercial or financial relationships that could be construed as a potential conflict of interest.

Generative AI statement

The authors declare that Gen AI was used in the creation of this manuscript. English grammar correction.

Publisher's note

All claims expressed in this article are solely those of the authors and do not necessarily represent those of their affiliated organizations, or those of the publisher, the editors and the reviewers. Any product that may be evaluated in this article, or claim that may be made by its manufacturer, is not guaranteed or endorsed by the publisher.

Supplementary material

The Supplementary material for this article can be found online at: https://www.frontiersin.org/articles/10.3389/fvets.2025.1542700/full#supplementary-material

References

1. Lopez M, Talavera C, Rest JR, Taylor D. Haemangiosarcoma of the conjunctiva of a giant panda. *Vet Rec*. (1996) 138:24.

2. Mauroo NF, Rourke NL, Chan WK. Cutaneous hemangioma in a giant panda (Ailuropoda melanoleuca). *J Zoo Wildl Med*. (2006) 37:59–60. doi: 10.1638/04-098.1

3. Yijiao C, Junhui A, Rong H, Yuliang L, Donghui W, Songrui L, et al. Single-cell mRNA sequencing of giant panda (Ailuropoda melanoleuca) seminoma reveals the cellular and molecular characteristics of tumour cells. *Vet Med Sci*. (2024) 10:e1348. doi: 10.1002/vms3.1348

4. Wang Y, Xia M, Li X, Guo X, Lu Y, Zhao S, et al. A rare case of giant panda cancer: pancreatic ductal adenocarcinoma. *Animal Model Exp Med*. (2022) 5:582–6. doi: 10.1002/ame2.12269

5. Gao Q, Wang C, Li D, Zhang H, Deng L, Li C, et al. A case of giant panda ovarian cancer diagnosis and histopathology. *BMC Vet Res*. (2018) 14:311. doi: 10.1186/s12917-018-1630-x

6. Lacour B, Guyot-Goubin A, Guissou S, Bellec S, Désandes E, Clavel J. Incidence of childhood cancer in France: national children cancer registries, 2000–2004. *Eur J Cancer Prev*. (2010) 19:173–81. doi: 10.1097/CEJ.0b013e32833876c0

7. Ottaviani G, Jaffe N. The epidemiology of osteosarcoma. *Cancer treatment and research*. (2009) 152:3–13. doi: 10.1007/978-1-4419-0284-9_1

8. Rodrigues J, Sarmento B, Pereira CL. Osteosarcoma tumor microenvironment: the key for the successful development of biologically relevant 3D in vitro models. *Models*. (2022) 1:5–27. doi: 10.1007/s44164-022-00008-x

9. Withrow SJ, Powers BE, Straw RC, Wilkins RM. Comparative aspects of osteosarcoma: dog versus man. *Clin Orthop Relat Res*. (1991) 270:159–68. doi: 10.1097/00003086-199109000-00023

10. Gill J, Gorlick R. Advancing therapy for osteosarcoma. *Nat Rev Clin Oncol*. (2021) 18:609–24. doi: 10.1038/s41571-021-00519-8

11. Reich M, Dinart D, Bellio H, Berchoud J, Jean-Denis M, Bonneau M, et al. 1971P metastatic osteosarcoma, patterns of care and outcomes of patients in a real-life setting: the Metabone national observational study. *Ann Oncol*. (2023) 34:S1053. doi: 10.1016/j.annonc.2023.09.1200

12. Sheng G, Gao Y, Yang Y, Wu H. Osteosarcoma and Metastasis. *Front Oncol*. (2021) 11:780264. doi: 10.3389/fonc.2021.780264

13. PDQ® Pediatric Treatment Editorial Board. *PDQ Osteosarcoma and Undifferentiated Pleomorphic Sarcoma of Bone Treatment*. Bethesda, MD: National Cancer Institute (US) (2024). Available at: https://www.cancer.gov/types/bone/hp/osteosarcoma-treatment-pdq

14. Langenbach A, Anderson MA, Dambach DM, Sorenmo KU, Shofer FD. Extraskeletal osteosarcomas in dogs: a retrospective study of 169 cases (1986-1996). *J Am Anim Hosp Assoc*. (1998) 34:113–20. doi: 10.5326/15473317-34-2-113

15. Dailey DD, Hess AM, Bouma GJ, Duval DL. MicroRNA expression changes and integrated pathways associated with poor outcome in canine osteosarcoma. *Front Vet Sci*. (2021) 8:637622. doi: 10.3389/fvets.2021.637622

16. Duffy D, Selmic LE, Kendall AR, Powers BE. Outcome following treatment of soft tissue and visceral extraskeletal osteosarcoma in 33 dogs: 2008–2013. *Vet Comp Oncol*. (2017) 15:46–54. doi: 10.1111/vco.12141

17. Stokes R, Wustefeld-Janssens BG, Hinson W, Wiener DJ, Hollenbeck D, Bertran J, et al. Surgical and oncologic outcomes in dogs with malignant peripheral nerve sheath tumours arising from the brachial or lumbosacral plexus. *Vet Comp Oncol*. (2023) 21:739–47. doi: 10.1111/vco.12938

frontiers | Frontiers in Veterinary Science

TYPE Brief Research Report
PUBLISHED 24 March 2025
DOI 10.3389/fvets.2025.1546872

Check for updates

OPEN ACCESS

EDITED BY
Helen C. Roberts,
Middlesex University, United Kingdom

REVIEWED BY
Carmelo Iaria,
University of Messina, Italy
Nicola Zizzo,
Uniba, Italy
Roberto Senas Cuesta,
University of Arkansas, United States

*CORRESPONDENCE
Karen Power
karen.power@unina.it

RECEIVED 17 December 2024
ACCEPTED 06 March 2025
PUBLISHED 24 March 2025

CITATION
Power K, Leandri R, Federico G, De Vico G and Leonardi L (2025) Ferritinophagy: a possible new iron-related metabolic target in canine osteoblastic osteosarcoma. *Front. Vet. Sci.* 12:1546872. doi: 10.3389/fvets.2025.1546872

COPYRIGHT
© 2025 Power, Leandri, Federico, De Vico and Leonardi. This is an open-access article distributed under the terms of the Creative Commons Attribution License (CC BY). The use, distribution or reproduction in other forums is permitted, provided the original author(s) and the copyright owner(s) are credited and that the original publication in this journal is cited, in accordance with accepted academic practice. No use, distribution or reproduction is permitted which does not comply with these terms.

Ferritinophagy: a possible new iron-related metabolic target in canine osteoblastic osteosarcoma

Karen Power[1]*, Rebecca Leandri[1], Giorgia Federico[2], Gionata De Vico[1] and Leonardo Leonardi[3]

[1]Department of Biology, University of Naples Federico II, Naples, Italy, [2]Department of Molecular Medicine and Medical Biotechnologies, University of Naples Federico II, Naples, Italy, [3]Department of Veterinary Medicine, University of Perugia, Perugia, Italy

Canine osteosarcomas (COS) are the most common bone tumors in dogs, characterized by high metastatic rates, poor prognosis, and poor responsiveness to routine therapies, which highlights the need for new treatment targets. In this context, the metabolism of neoplastic cells represents an increasingly studied element, as cancer cells depend on particular metabolic pathways that are also elements of vulnerability. Among these, tumor cells (TCs) show higher iron requirements to sustain proliferation (so-called iron addiction), which are achieved by increasing iron uptake and/or by activating ferritinophagy, a process mediated by the Nuclear receptor Co-Activator 4 (NCOA4) leading to iron mobilization from ferritin (Ft) deposits. Previous studies have shown that COS cells overexpress Transferrin Receptor 1 (TfR1) to increase iron uptake. In this study we evaluated the immunohistochemical expression of ferritinophagy-related proteins, namely Ferritin Heavy chain (FTH1) and NCOA4, and proliferating cell nuclear antigen (PCNA) in canine normal bone and canine osteoblastic osteosarcoma (COOS) samples. Normal samples revealed negative/weak immunoreactivity for FTH1, NCOA4 and PCNA in <10% of osteocytes. In COOS samples the majority of neoplastic cells showed immunoreactivity to FTH1, NCOA4 and PCNA. Our data suggest that the activation of ferritinophagy by COOS cells responds to the need for feed their "iron addiction." These data, though preliminary, further suggest that targeting iron metabolism represents a new potential strategy worthy of further study to be transferred into clinical practice.

KEYWORDS

bone cancer, canine osteosarcoma, immunohistochemistry, iron metabolism, therapy

1 Introduction

The study of metabolic alterations of neoplastic cells is currently a hot topic, as cancer cells can become addicted to specific metabolic pathways also representing metabolic vulnerabilities against which novel drugs that target them can be developed (1). Among these, the so-called "iron addiction" is one of the most relevant metabolic alterations of neoplastic cells (2). Cancer cells show higher iron requirements than normal cells to sustain proliferation (3) and tissue invasion (4) and tend to satisfy this need by over-expressing a series of proteins involved both in the iron uptake from the bloodstream (5, 6) and in its mobilization from intracellular reserves by so-called "ferritinophagy," a selective form of autophagy that specifically targets intracellular (Ft) for lysosomal degradation (7, 8). Key molecules in iron metabolism are: (1) TfR1, which uptakes and internalizes iron by binding transferrin (Tf)-Fe3+ complex, which is followed by Fe3+ reduction to Fe2+ by ferrireductases in the cytosol (9); (2) the Ft, which represents the storage site of iron in the cytosol, and which also contributes to the physiological

release of iron from reserves to form the cytoplasmic labile iron pool (cLIP) (10–12); and (3) the NCOA4, a selective cargo protein which binds to a conserved C-terminal domain of FTH1 and to autophagy-related proteins to deliver FT to autophagosomes and trigger ferritinophagy (13, 14). Previous studies in human pathology have reported impairment of iron metabolism in different cancers (15–21). This appears to be particularly true in human osteosarcomas (22, 23), the most common primary malignant bone tumor affecting children and adolescents (24, 25). Unfortunately, in veterinary medicine iron metabolism and its alterations connected to cancer are still poorly studied (26–31). The early results presented in a previous study (26) highlighted the relevance of TfR-1 expression in canine osteosarcomas (COS), suggesting therapies involving both TfR-1 and other molecules related to iron metabolisms in dogs with osteosarcoma should be developed, also considering the potential clinical impact for humans. COS represent a well-known preclinical model for human osteosarcoma, particularly for those developing in young people as they share molecular and morphological aspects, as well as prognosis and treatment options (32). COS represent the most frequent primary malignant bone neoplasms of mesenchymal origin in dogs (33, 34), exhibiting local aggressiveness, high metastatic behavior and high mortality rates (35–38). COS originate mainly from appendicular skeleton, with the most frequent localization occurring at the metaphyseal level, while only 20–25% of tumors originate from the axial bone (34). Histological classification of bone tumors of domestic animals describes the presence of six different histotypes, namely: poorly differentiated, osteoblastic (productive and non-productive), chondroblastic, fibroblastic, telangiectatic, giant cell type, with the osteoblastic type being the most frequent (33, 39). To date, therapy is based on surgery (conservative or not) coupled to chemotherapy and radiotherapy, however life expectancy remains low (40–42) and resistance to typical antineoplastic drugs is building up (43–45). Therefore, the need for new targets, new antineoplastic drugs and/or adjuvant antineoplastic compounds for COS is rising. In this context, we recently validated and studied the expression of the NCOA4 and FTH1 in some canine normal and neoplastic tissues (46). In this report, we provide additional evidence for the relevance of iron metabolism alterations in canine osteoblastic osterosacomas (COOS), highlighting the role of ferritinophagy-related molecules NCOA4 and FTH1, thus suggesting that the mechanisms of ferritinophagy could represent a further potential pathway to be targeted to selectively destroy this type of cancer cells.

2 Materials and methods

2.1 Tissue samples

Three normal bone samples (N1-N3) and 20 COOS samples (COOS1-COOS20) were retrieved from the archives of the Department of Veterinary Medicine – University of Perugia. Ethics committee's approval and animal testing request were waived since all animal tissue samples examined in this study were retrieved from archives. Samples had been previously decalcified and processed by routing histological techniques, paraffin-embedded and stained with hematoxylin and eosin (H&E). All samples had been observed by light microscopy for morphological classification of histological subtypes according to the World Health Organization's histologic classification of tumors of domestic (33).

2.2 Immunohistochemistry

For each paraffin-embedded sample 3 µm sections were processed for immunohistochemistry (IHC) as previously described (47) to evaluate expression of proteins involved in ferritinophagy (FTH1, NCOA4), and PCNA to assess proliferation (46). Antibody specification and dilutions are reported in Table 1. Sections were counterstained with hematoxylin, and immunolabeling was revealed with diaminobenzidine-tetrahydrochloride (DAB).

2.3 Scoring of Immunoreactivity

To evaluate the expression of FTH1, NCOA4 and PCNA a semiquantitative score was applied by analyzing the number of positively labelled cells in 1,000 cells in 10 fields at 400x magnification (40x objective 10x ocular) for each specimen by two independent observers (Leonardo Leornardi and Gionata De Vico) under blinded conditions (48). Results were expressed as percentage.

3 Results

3.1 Histopathology results

Breeds, sex, age, tumor localization and histologic classification are summarized in Supplementary Table S1. Normal tissue samples (N1-N3) were characterized by abundant bone matrix in which elliptical osteocytes, showing mildly basophilic cytoplasm and oval nucleus, were immersed (Figure 1A). All COS samples (COOS1-COOS20) were characterized by polyhedral cells with eccentric nuclei and basophilic cytoplasm. Nuclei appeared pleomorphic, presenting hyperchromatic chromatin, and bizarre and atypical mitosis were observed. Osseus matrix was present in moderate to high amounts, often in the pattern of dense sheets (Figure 1B). Considered the histopathological features observed in the COS samples, they were classified as productive COOS.

TABLE 1 Antibodies used in immunohistochemical analysis.

Antibody	Manufacturer/clone	Host species	Dilution	
FTH1	Antibodies/Polyclonal	Rabbit	1:100	Leandri et al. (46)
NCOA4	Abcam ab62495/439CT10.1.2	Mouse	1:100	Leandri et al. (46)
PCNA	Abcam ab18197/PC10	Mouse	1:400	Ersoy et Ozem (68)

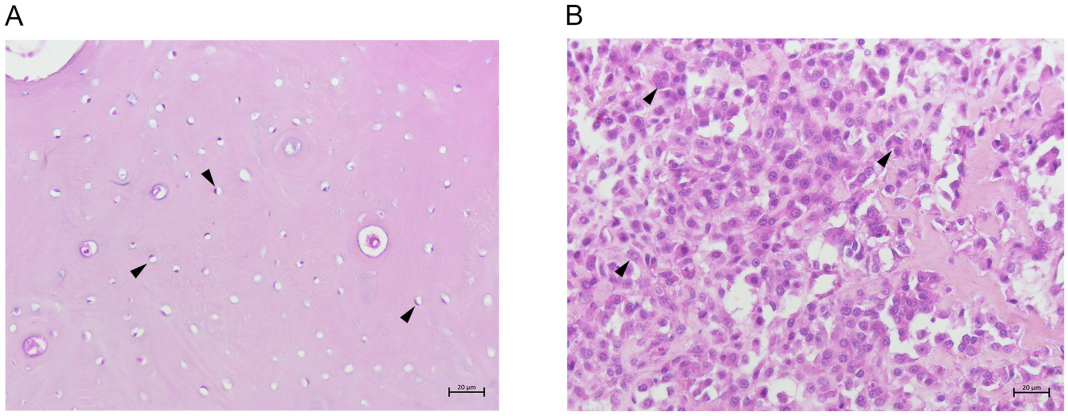

FIGURE 1
(A) Canine normal bone tissue showing osteocytes (arrow heads) and abundant bone matrix. H&E 20x. **(B)** Canine productive osteoblastic osteosarcoma showing many polyhedral cells (arrow heads) and osseus matrix. H&E 20x.

3.2 Immunohistochemistry results

Normal bone samples presented less than 10% of cells positive for all the three tested antibodies (Figures 2A,C,E). On the contrary, in COOS samples 85–95% of neoplastic cells showed a strong cytoplasmic immunostaining for FTH1 (Figure 2B) and NCOA4. (Figure 2D). Moreover, 70–80% of neoplastic cells were strongly labelled at the nuclear level by anti-PCNA (Figure 2F).

4 Discussion

Canine osteosarcomas (COS) are aggressive malignancies of the bone, for which the prognosis of patients still remains relatively poor and survival rates have not significantly improved during the recent decades. COS share biological and clinical similarities with the human counterpart, where a growing research tendency is focusing on the role of iron and its metabolism in both tumor progression and tumor suppression (2, 3, 20). Given the similarities between the two species, we investigated the expression in COOS of key proteins involved in iron metabolism to possibly identify new therapeutical targets for both dogs and possibly humans. Our results show an increased expression of all analyzed proteins in COOS samples compared to normal samples. Previous data on the overexpression of TfR1 in COS (26), supported the idea that iron uptake plays a decisive role in supporting the growth of COOS neoplastic cells and could represent a new therapeutic target. Our study emphasizes for the first time in COOS the role of NCOA4 and FTH1, key molecules involved in ferritinophagy regulation (49). Interestingly, in our study cancer samples showed higher immunoreactivity in neoplastic cells compared to normal ones, in accordance to literature (50, 51). In the classical ferritinophagy pathway NCOA4 interacts with ferritin-heavy chain (FTH1), transferring autophagosomes to lysosomes to degrade FT and release free iron thus increasing cLIP. Physiologically, NCOA4 combined with iron is continuously degraded by ubiquitin-proteasome system or directly by lysosomes (52), explaining why in our study NCOA4 was usually poorly highlighted in normal cells by immunohistochemistry. On the contrary, an intriguing result of our investigation is the strong immunohistochemical detection of NCOA4 coupled with the one of FTH1 in COOS cells, which testify for a deep dysregulation of iron metabolism and in particular of the ferritinophagy pathway. In our case, in fact, it could be hypothesized that the COOS cells are so highly dependent on the availability of iron for their growth and survival (iron addiction), to simultaneously activate different pathways that allow them to maintain high levels of iron in the cytosol, namely iron upload, storage and mobilization from storage. High iron loads and ferritinophagy have also been closely correlated with ferroptosis, a form of iron dependent non-apoptotic programmed cell death linked to oxidation of membrane lipid (53). It is to be believed that COOS cells have developed mechanisms to evade these forms of cell death as already described in other tumor types (54, 55, 69). As a matter of fact, in our cases there was no evidence of characteristic morphological feature of ferroptosis in COS cells, namely cell membrane rupture, cytoplasmic swelling, and moderate chromatin condensation (56). Escaping ferroptotic mechanisms provides further vulnerable possible targets for ferroptosis-based therapy (70). Previous studies in human oncology have described the possibility of using synthetical or natural compounds to target iron metabolism (57–60) and enhance ferroptosis. Artemisin, the main bioactive component of *Artemisia annua* L, has been proven to activate apoptosis, ferroptosis and induce cancer cell death by producing ROS in human osteosarcoma (61, 62) and also in COS cell lines (63). More recently, two studies by Isani et al. (64) and Colurciello et al. (65) showed that COS cells treated with artemisin showed higher mortality rates and lower iron concentrations compared to untreated ones, probably due to ferroptosis. Furthermore, targeting ferritinophagy pathway can also represent mechanisms for some common anticancer drugs. As examples, low-dose cisplatin combined with ursolic acid inhibits cancer cell growth by activating autophagic degradation of Ft and overloading intracellular iron ions (66). The combination of artesunate and the hepatocellular carcinoma first-line drug sorafenib induces ferritinophagy in hepatocellular carcinoma cells and improve the efficacy of single anticancer drugs (67). The results of our study provide relevant, thought preliminary data on the alteration of the iron-metabolic pathway in COOS. Notably, they suggest an increased uptake of iron (26), release of iron from ferritin-storage coupled to a continuous replacement of the used Ft storage. COS appear as

10.3389/fvets.2025.1546872

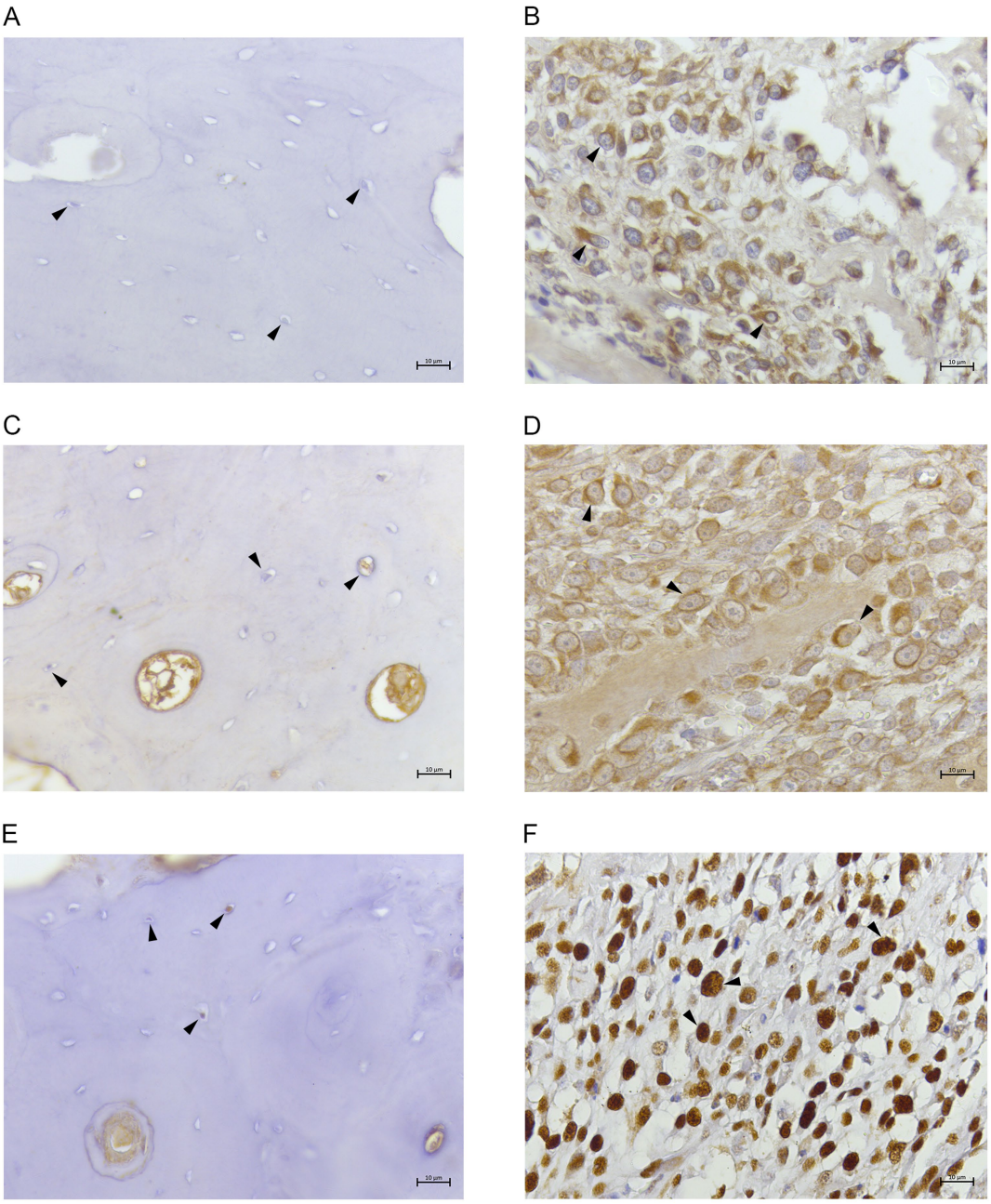

FIGURE 2
(A) Canine normal bone tissue. FTH1. Osteocytes showing no immunolabeling. 40x; **(B)** canine productive osteoblastic osteosarcoma. FTH1. Tumoral cells revealed cytoplasmic immunostaining (arrow heads). 40x; **(C)** canine normal bone tissue. NCOA4. Osteocytes showing no/weak immunolabeling. 40x; **(D)** canine productive osteoblastic osteosarcoma. NCOA4. Tumoral cells revealed cytoplasmic/perinuclear immunostaining (arrow heads). 40x; **(E)** canine normal bone tissue. PCNA. Few osteocytes showing weak nuclear immunolabeling. 40x. **(F)** canine productive osteoblastic osteosarcoma. PCNA. Tumoral cells showing strong nuclear immunolabeling (arrow heads). 40x.

favorable candidates for the use of antineoplastic drugs targeting iron metabolism, ferroptosis and ferritinophagy. Ideally, therapies should on one hand enhance cLIP by increasing NCOA4-induced ferritinophagy and on the other hand use TfR1 as a tool to selectively deliver compounds to tumoral cells and reduce undesired effects on healthy cells. Further studies will help deepen the knowledge about alterations in iron metabolism in COOS. Of particular interest would be correlating the overexpression of these molecules with patient follow-up data to assess their potential prognostic implications, and using 2D cell models hopefully opening the way to possible *in vivo* studies to be transferred into clinical practice.

Data availability statement

The original contributions presented in the study are included in the article/Supplementary material, further inquiries can be directed to the corresponding author.

Ethics statement

The requirement of ethical approval was waived by Institutional review board of the University of Perugia for the studies involving animals because the study was performed on archive paraffine embedded samples, previously used for diagnostic purposes. The studies were conducted in accordance with the local legislation and institutional requirements. Written informed consent was obtained from the owners for the participation of their animals in this study.

Author contributions

KP: Conceptualization, Writing – original draft. RL: Investigation, Methodology, Writing – original draft. GF: Investigation, Writing – original draft. GV: Supervision, Writing – review & editing. LL: Validation, Writing – review & editing.

Funding

The author(s) declare that no financial support was received for the research and/or publication of this article.

Acknowledgments

Authors would like to thank Dr. Claire Power for helping editing the figures in the article. The authors acknowledge the Histopathology and Diagnostics Core at Department of Biology of University of Naples "Federico II for their technical and scientific support.

Conflict of interest

The authors declare that the research was conducted in the absence of any commercial or financial relationships that could be construed as a potential conflict of interest.

Generative AI statement

The authors declare that no Gen AI was used in the creation of this manuscript.

Publisher's note

All claims expressed in this article are solely those of the authors and do not necessarily represent those of their affiliated organizations, or those of the publisher, the editors and the reviewers. Any product that may be evaluated in this article, or claim that may be made by its manufacturer, is not guaranteed or endorsed by the publisher.

Supplementary material

The Supplementary material for this article can be found online at: https://www.frontiersin.org/articles/10.3389/fvets.2025.1546872/full#supplementary-material

References

1. Zaal EA, Berkers CR. The influence of metabolism on drug. *Resp Cancer Front Oncol*. (2018) 8:500. doi: 10.3389/fonc.2018.00500

2. Torti SV, Torti FM. Iron and Cancer: 2020 vision. *Cancer Res*. (2020) 80:5435–48. doi: 10.1158/0008-5472.CAN-20-2017

3. Steegmann-Olmedillas JL. The role of iron in tumour cell proliferation. *Clin Transl Oncol*. (2011) 13:71–6. doi: 10.1007/s12094-011-0621-1

4. Fischer-Fodor E, Miklasova N, Berindan-Neagoe I, Saha B. Iron, inflammation and invasion of cancer cells. *Clujul Med*. (2015) 88:272–7. doi: 10.15386/cjmed-492

5. Aisen P. Transferrin receptor 1. *Int J Biochem Cell Biol*. (2004) 36:2137–43. doi: 10.1016/j.biocel.2004.02.007

6. Candelaria PV, Leoh LS, Penichet ML, Daniels-Wells TR. Antibodies targeting the transferrin receptor 1 (TfR1) as direct anti-cancer agents. *Front Immunol*. (2021) 12:607692. doi: 10.3389/fimmu.2021.607692

7. Sun K, Li C, Liao S, Yao X, Ouyang Y, Liu Y, et al. Ferritinophagy, a form of autophagic ferroptosis: new insights into cancer treatment. *Front Pharmacol*. (2022) 13:1043344. doi: 10.3389/fphar.2022.1043344

8. Wang J, Wu N, Peng M, Oyang L, Jiang X, Peng Q, et al. Ferritinophagy: research advance and clinical significance in cancers. *Cell Death Discov*. (2023) 9:463. doi: 10.1038/s41420-023-01753-y

9. Knutson MD. Steap proteins: implications for iron and copper metabolism. *Nutr Rev*. (2007) 65:335–40. doi: 10.1301/nr.2007.jul.335–340

10. Shesh BP, Connor JR. A novel view of ferritin in cancer. *Biochim Biophys Acta Rev Cancer*. (2023) 1878:188917. doi: 10.1016/j.bbcan.2023.188917

11. Ford GC, Harrison PM, Rice DW, Smith JM, Treffry A, White JL, et al. Ferritin: design and formation of an iron-storage molecule. *Philos Trans R Soc Lond Ser B Biol Sci*. (1984) 304:551–65. doi: 10.1098/rstb.1984.0046

12. Levi S, Luzzago A, Cesareni G, Cozzi A, Franceschinelli F, Albertini A, et al. Mechanism of ferritin iron uptake: activity of the H-chain and deletion mapping of the ferro-oxidase site. A study of iron uptake and ferro-oxidase activity of human liver, recombinant H-chain ferritins, and of two H-chain deletion mutants. *J Biol Chem*. (1988) 263:18086–92. doi: 10.1016/S0021-9258(19)81326-1

13. Mancias JD, Wang X, Gygi SP, Harper JW, Kimmelman AC. Quantitative proteomics identifies NCOA4 as the cargo receptor mediating ferritinophagy. *Nature*. (2014) 509:105–9. doi: 10.1038/nature13148

14. Federico G, Carrillo F, Dapporto F, Chiariello M, Santoro M, Bellelli R, et al. NCOA4 links iron bioavailability to DNA metabolism. *Cell Rep*. (2022) 40:111207. doi: 10.1016/j.celrep.2022.111207

15. Steinbicker AU, Muckenthaler MU. Out of balance--systemic iron homeostasis in iron-related disorders. *Nutrients*. (2013) 5:3034–61. doi: 10.3390/nu5083034

16. Tian Y, Tian Y, Yuan Z, Zeng Y, Wang S, Fan X, et al. Iron metabolism in aging and age-related diseases. *Int J Mol Sci*. (2022) 23:3612. doi: 10.3390/ijms23073612

17. Lee J, Hyun DH. The interplay between intracellular Iron homeostasis and Neuroinflammation in neurodegenerative diseases. *Antioxidants*. (2023) 12:918. doi: 10.3390/antiox12040918

18. Rosenblum SL. Inflammation, dysregulated iron metabolism, and cardiovascular disease. *Front Aging*. (2023) 4:1124178. doi: 10.3389/fragi.2023.1124178

19. Manz DH, Blanchette NL, Paul BT, Torti FM, Torti SV. Iron and Cancer: recent insights. *Ann N Y Acad Sci*. (2016) 1368:149–61. doi: 10.1111/nyas.13008

20. Chen Y, Fan Z, Yang Y, Gu C. Iron metabolism and its contribution to cancer. *Inter J Onc*. (2019) 54:1143–54. doi: 10.3892/ijo.2019.4720

21. Brown RAM, Richardson KL, Kabir TD, Trinder D, Ganss R, Leedman PJ. Altered Iron metabolism and impact in Cancer biology, metastasis, and immunology. *Front Oncol*. (2020) 10:476. doi: 10.3389/fonc.2020.00476

22. Chen H, Han Z, Wang Y, Su J, Lin Y, Cheng X, et al. Targeting Ferroptosis in bone-related diseases: facts and perspectives. *J Inflamm Res*. (2023) 16:4661–77. doi: 10.2147/JIR.S432111

23. Ma Y, Cong L, Shen W, Yang C, Ye K. Ferroptosis defense mechanisms: the future and hope for treating osteosarcoma. *Cell Biochem Funct*. (2024) 42:e4080. doi: 10.1002/cbf.4080

24. Brown HK, Schiavone K, Gouin F, Heymann MF, Heymann D. Biology of bone sarcomas and new therapeutic developments. *Calcif Tissue Int*. (2018) 102:174–95. doi: 10.1007/s00223-017-0372-2

25. Harris MA, Hawkins CJ. Recent and ongoing research into metastatic osteosarcoma treatments. *Int J Mol Sci*. (2022) 23:3817. doi: 10.3390/ijms23073817

26. De Vico G, Martano M, Maiolino P, Carella F, Leonardi L. Expression of transferrin receptor-1 (TFR-1) in canine osteosarcomas. *Vet Med Sci*. (2020) 6:272–6. doi: 10.1002/vms3.258

27. McCown JL, Specht AJ. Iron homeostasis and disorders in dogs and cats: a review. *J Am Anim Hosp Assoc*. (2011) 47:151–60. doi: 10.5326/JAAHA-MS-5553

28. Priest H, McDonough S, Erb H, Daddona J, Stokol T. Transferrin receptor expression in canine lymphoma. *Vet Pathol*. (2011) 48:466–74. doi: 10.1177/0300985810377074

29. Caro JT, Marìn LM, Iazbik MC, Zaldivar-Lopez S, Borghese H, Couto CG. Markers of iron metabolism in retired racing greyhounds with and without osteosarcoma. *Vet Clin Pathol*. (2013) 42:360–3. doi: 10.1111/vcp.12066

30. Ploypetch S, Rungsipipat A, Piyaviriyakul P, Choisunirachon N, Makoom P, Kalpravidh C. Relationships between transferrin and transferrin receptor (TfR) expression in dogs with malignant Oronasal tumors. *Thai J Vet Med*. (2017) 47:61–70. doi: 10.56808/2985-1130.2812

31. Marques O, Canadas A, Faria F, Oliveira E, Amorim I, Seixas F, et al. Expression of iron-related proteins in feline and canine mammary gland reveals unexpected accumulation of iron. *Biotech Histochem*. (2017) 92:584–94. doi: 10.1080/10520295.2017.1369160

32. Simpson S, Dunning MD, de Brot S, Grau-Roma L, Mongan NP, Rutland CS. Comparative review of human and canine osteosarcoma: morphology, epidemiology, prognosis, treatment and genetics. *Acta Vet Scand*. (2017) 59:71. doi: 10.1186/s13028-017-0341-9

33. Slayter MV, Boosinger TR, Pool RR, Dammrich K, Misdrop W, Larsen S. World Health Organization, international histologic classification of tumors of domestic animals, histological classification of bone and joint tumors of domestic animals. Washington, DC: Armed Forces Institute of Pathology American Registry of Pathology (1994).

34. Thompson KG, Pool RR. "Tumors of bones" in tumors in domestic animals. *4th*. ed. Ames, IA: Iowa State Press (2002).

35. Brodey RS, Riser WH. Canine osteosarcoma. A clinicopathologic study of 194 cases. *Clin Orthop Relat Res*. (1969) 62:54–64.

36. Culp WT, Olea-Popelka F, Sefton J, Aldridge CF, Withrow SJ, Lafferty MH, et al. Evaluation of outcome and prognostic factors for dogs living greater than one year after diagnosis of osteosarcoma: 90 cases (1997-2008). *J Am Vet Med Assoc*. (2014) 245:1141–6. doi: 10.2460/javma.245.10.1141

37. Silver KI, Patkar S, Mazcko C, Berger EP, Beck JA, LeBlanc AK. Patterns of metastatic progression and association with clinical outcomes in canine osteosarcoma: a necropsy study of 83 dogs. *Vet Comp Oncol*. (2023) 21:646–55. doi: 10.1111/vco.12927

38. Wright TF, Brisson BA, Belanger CR, Tiessen A, Sabine V, Skowronski K, et al. Quantification of circulating tumour cells over time in dogs with appendicular osteosarcoma. *Vet Comp Oncol*. (2023) 21:541–50. doi: 10.1111/vco.12918

39. Misdorp W, Hart AA. Some prognostic and epidemiologic factors in canine osteosarcoma. *J Natl Cancer Inst*. (1979) 62:537–45. doi: 10.1093/jnci/62.3.537

40. Schmidt AF, Nielen M, Klungel OH, Hoes AW, de Boer A, Groenwold RH, et al. Prognostic factors of early metastasis and mortality in dogs with appendicular osteosarcoma after receiving surgery: an individual patient data meta-analysis. *Prev Vet Med*. (2013) 112:414–22. doi: 10.1016/j.prevetmed.2013.08.011

41. Szewczyk M, Lechowski R, Zabielska K. What do we know about canine osteosarcoma treatment? *Rev Vet Res Commun*. (2015) 39:61–7. doi: 10.1007/s11259-014-9623-0

42. Griffin MA, Mastorakis A, Wustefeld-Janssens B, Martin TW, Duda L, Seguin B, et al. Outcomes in dogs undergoing surgical stabilization and non-stereotactic radiation therapy for axial and appendicular bone tumors. *Front Vet Sci*. (2024) 10:1283728. doi: 10.3389/fvets.2023.1283728

43. Shahi MH, York D, Gandour-Edwards R, Withers SS, Holt R, Rebhun RB. BMI1 is expressed in canine osteosarcoma and contributes to cell growth and chemotherapy resistance. *PLoS One*. (2015) 10:e0131006. doi: 10.1371/journal.pone.0131006

44. Weinman MA, Ramsey SA, Leeper HJ, Brady JV, Schlueter A, Stanisheuski S, et al. Exosomal proteomic signatures correlate with drug resistance and carboplatin treatment outcome in a spontaneous model of canine osteosarcoma. *Cancer Cell Int*. (2021) 21:245. doi: 10.1186/s12935-021-01943-7

45. Hodge MA, Miller T, Weinman MA, Wustefeld-Janssens B, Bracha S, Davis BW. Cellular Transcriptomics of carboplatin resistance in a metastatic canine osteosarcoma cell line. *Genes*. (2023) 14:558. doi: 10.3390/genes14030558

46. Leandri R, Power K, Buonocore S, De Vico G. Preliminary evidence of the possible roles of the Ferritinophagy-Iron uptake Axis in canine testicular Cancer. *Animals*. (2024) 14:2619. doi: 10.3390/ani14172619

47. Paciello O, Passantino G, Costagliola A, Papparella S, Perillo A. Histiocytic sarcoma of the nasal cavity in a horse. *Res Vet Sci*. (2013) 94:648–50. doi: 10.1016/j.rvsc.2013.01.005

48. Martano M, Altamura G, Power K, Restucci B, Carella F, Borzacchiello G, et al. Evaluation of hypoxia-inducible Factor-1 alpha (HIF-1α) in equine sarcoid: an Immunohistochemical and biochemical study. *Pathogens*. (2020) 9:58. doi: 10.3390/pathogens9010058

49. Tang M, Chen Z, Wu D, Chen L. Ferritinophagy/ferroptosis: Iron-related newcomers in human diseases. *J Cell Physiol*. (2018) 233:9179–90. doi: 10.1002/jcp.26954

50. Santana-Codina N, Del Rey MQ, Kapner KS, Zhang H, Gikandi A, Malcolm C, et al. NCOA4-mediated Ferritinophagy is a pancreatic Cancer dependency via maintenance of Iron bioavailability for Iron-sulfur cluster proteins. *Cancer Discov*. (2022) 12:2180–97. doi: 10.1158/2159-8290.CD-22-0043

51. Feng Z, Luan M, Zhu W, Xing Y, Ma X, Wang Y, et al. Targeted ferritinophagy in gastrointestinal cancer: from molecular mechanisms to implications. *Arch Toxicol*. (2024) 98:2007–18. doi: 10.1007/s00204-024-03745-y

52. Le Y, Liu Q, Yang Y, Wu J. The emerging role of nuclear receptor coactivator 4 in health and disease: a novel bridge between iron metabolism and immunity. *Cell Death Discov*. (2024) 10:312. doi: 10.1038/s41420-024-02075-3

53. Dixon SJ, Lemberg KM, Lamprecht MR, Skouta R, Zaitsev EM, Gleason CE, et al. Ferroptosis: an iron-dependent form of nonapoptotic cell death. *Cell*. (2012) 149:1060–72. doi: 10.1016/j.cell.2012.03.042

54. Huang R, Dong R, Wang N, He Y, Zhu P, Wang C, et al. Adaptive changes allow targeting of Ferroptosis for glioma treatment. *Cell Mol Neurobiol*. (2022) 42:2055–74. doi: 10.1007/s10571-021-01092-5

55. Hong X, Roh W, Sullivan RJ, Wong KHK, Wittner BS, Guo H, et al. The Lipogenic regulator SREBP2 induces transferrin in circulating melanoma cells and suppresses Ferroptosis. *Cancer Discov*. (2021) 11:678–95. doi: 10.1158/2159-8290.CD-19-1500

56. Tang D, Chen X, Kang R, Kroemer G. Ferroptosis: molecular mechanisms and health implications. *Cell Res*. (2021) 31:107–25. doi: 10.1038/s41422-020-00441-1

57. Lv H, Zhen C, Liu J, Shang P. β- Phenethyl Isothiocyanate induces cell death in human osteosarcoma through altering Iron metabolism, disturbing the redox balance, and activating the MAPK signaling pathway. *Oxidative Med Cell Longev*. (2020) 2020:5021983. doi: 10.1155/2020/5021983

58. Lin H, Chen X, Zhang C, Yang T, Deng Z, Song Y, et al. EF24 induces ferroptosis in osteosarcoma cells through HMOX1. *Biomed Pharmacother*. (2021) 136:111202. doi: 10.1016/j.biopha.2020.111202

59. Xue Y, Zhang G, Zhou S, Wang S, Lv H, Zhou L, et al. Iron Chelator induces apoptosis in osteosarcoma cells by disrupting intracellular Iron homeostasis and activating the MAPK pathway. *Int J Mol Sci*. (2021) 22:7168. doi: 10.3390/ijms22137168

60. Zhao J, Zhao Y, Ma X, Zhang B, Feng H. Targeting ferroptosis in osteosarcoma. *J Bone Oncol*. (2021) 30:100380. doi: 10.1016/j.jbo.2021.100380

61. Bhaw-Luximon A, Jhurry D. Artemisinin and its derivatives in cancer therapy: status of progress, mechanism of action, and future perspectives. *Cancer Chemother Pharmacol*. (2017) 79:451–66. doi: 10.1007/s00280-017-3251-7

62. Li Z, Ding X, Wu H, Liu C. Artemisinin inhibits angiogenesis by regulating p38 MAPK/CREB/TSP-1 signaling pathway in osteosarcoma. *J Cell Biochem*. (2019) 120:11462–70. doi: 10.1002/jcb.28424

63. Hosoya K, Murahari S, Laio A, London CA, Couto CG, Kisseberth WC. Biological activity of dihydroartemisinin in canine osteosarcoma cell lines. *Am J Vet Res*. (2008) 69:519–26. doi: 10.2460/ajvr.69.4.519

64. Isani G, Bertocchi M, Andreani G, Farruggia G, Cappadone C, Salaroli R, et al. Cytotoxic effects of *Artemisia annua* L. and pure Artemisinin on the D-17 canine osteosarcoma cell line. *Oxidative Med Cell Longev*. (2019) 2019, 2019:1615758. doi: 10.1155/2019/1615758

65. Culurciello R, Bosso A, Di Fabio G, Zarrelli A, Arciello A, Carella F, et al. Cytotoxicity of an innovative pressurised cyclic solid-liquid (PCSL) extract from *Artemisia annua*. *Toxins*. (2021) 13:886. doi: 10.3390/toxins13120886

66. Liu X, Zhang Y, Wu X, Xu F, Ma H, Wu M, et al. Targeting Ferroptosis pathway to combat therapy resistance and metastasis of Cancer. *Front Pharmacol*. (2022) 13:909821. doi: 10.3389/fphar.2022.909821

67. Cui Z, Wang H, Li S, Qin T, Shi H, Ma J, et al. Dihydroartemisinin enhances the inhibitory effect of sorafenib on HepG2 cells by inducing ferroptosis and inhibiting energy metabolism. *J Pharmacol Sci*. (2022) 148:73–85. doi: 10.1016/j.jphs.2021.09.008

68. Ersoy T, Ozmen O. Immunohistochemical detection of caspase 3 and proliferating cell nuclear antigen in the intestines of dogs naturally infected with parvovirus. *Vet Res Forum*. (2022) 13:127–131. doi: 10.30466/vrf.2020.116534.2772

69. Li Z, Hu Y, Zheng H, Li M, Liu Y, Feng R, et al. LPCAT1-mediated membrane phospholipid remodelling promotes ferroptosis evasion and tumour growth. *Nat Cell Biol*. (2024) 26:811–824. doi: 10.1038/s41556-024-01405-y

70. Khan M, Sunkara V, Yadav M, Bokhari SFH, Rehman A, Maheen A, et al. Ferroptosis and Triple-Negative Breast Cancer: A Systematic Overview of Prognostic Insights and Therapeutic Potential. *Cureus*. (2024) 16:e51719. doi: 10.7759/cureus.51719

frontiers | Frontiers in Veterinary Science

TYPE Case Report
PUBLISHED 26 March 2025
DOI 10.3389/fvets.2025.1477063

Check for updates

OPEN ACCESS

EDITED BY
Leonardo Leonardi,
University of Perugia, Italy

REVIEWED BY
Ravikanthreddy Poonooru,
University of Missouri, United States
Hyeona Bae,
Gyeongsang National University,
Republic of Korea
Ha-Jung Kim,
Chonnam National University,
Republic of Korea

*CORRESPONDENCE
Byeong-Teck Kang
✉ kangbt@chungbuk.ac.kr

†These authors have contributed equally to this work

RECEIVED 07 August 2024
ACCEPTED 10 March 2025
PUBLISHED 26 March 2025

CITATION
Wang J, Chae Y, Lee D, Yun T, Kim H and Kang B-T (2025) Case Report: ^{18}F-FDOPA PET in the clinical management of a dog with an intraventricular tumor suspected to be choroid plexus papilloma.
Front. Vet. Sci. 12:1477063.
doi: 10.3389/fvets.2025.1477063

COPYRIGHT
© 2025 Wang, Chae, Lee, Yun, Kim and Kang. This is an open-access article distributed under the terms of the Creative Commons Attribution License (CC BY). The use, distribution or reproduction in other forums is permitted, provided the original author(s) and the copyright owner(s) are credited and that the original publication in this journal is cited, in accordance with accepted academic practice. No use, distribution or reproduction is permitted which does not comply with these terms.

Case Report: ^{18}F-FDOPA PET in the clinical management of a dog with an intraventricular tumor suspected to be choroid plexus papilloma

Juwon Wang†, Yeon Chae†, Dohee Lee, Taesik Yun, Hakhyun Kim and Byeong-Teck Kang*

Laboratory of Veterinary Internal Medicine, College of Veterinary Medicine, Chungbuk National University, Cheongju, Republic of Korea

An 8-year-old neutered male Miniature Poodle, weighing 6.7 kg, was presented with lethargy, anorexia, and single seizure episode. Neurological examination revealed bilaterally absent menace reflexes and an obtunded mental status. Magnetic resonance imaging showed a papilliform shaped mass measuring 1.2 × 1.4 × 1.3 cm in size, with a volume of 1.17 cm^3 in the third ventricle. 3,4-dihydroxy-6-[^{18}F] fluoro-l-phenylalanine (^{18}F-FDOPA) positron emission tomography/computed tomography (PET/CT) was performed 53 days after presentation, revealing a hypermetabolic region in the intraventricular mass with mean and maximal standardized uptake values (SUV_{mean} and SUV_{max}) of 1.2 and 1.42, respectively, and a tumor to normal tissue (T/N) ratio of 1.33. The mass lesion measured 1.3 ×1.4 × 1.2 cm in size, with a volume of 1.09 cm^3 on contrast-enhanced CT images. The metabolic tumor volume (MTV) was 1.184 cm^3. No evidence of brain parenchymal metastases was observed. Therefore, the dog was tentatively diagnosed with a brain tumor, which was suspected to be a choroid plexus papilloma (CPP) and chemotherapy with prednisolone and cyclophosphamide was initiated. As worsening clinical signs were observed, a second ^{18}F-FDOPA PET/CT scan was performed on day 183. The SUV_{mean}, SUV_{max}, and T/N ratio of the lesion were 1.49, 1.85, and 1.62, respectively. The mass lesion measured 1.0 × 1.0 × 1.3 cm in size, with a volume of 0.68 cm^3 on contrast-enhanced CT images, whereas the MTV was increased to 2.217 cm^3. The dog died 186 days after the presentation. To the best of our knowledge, this is the first report describing the ^{18}F-FDOPA PET/CT findings in a dog with an intraventricular brain tumor suspected of having CPP. In the present case, although the lesion size decreased on CT contrast imaging, an increase in the MTV was observed on follow-up ^{18}F-FDOPA PET/CT after chemotherapy. Thus, an increase in MTV post-chemotherapy combined with the worsening clinical signs and limited survival period in dogs correlates with poor prognosis, as previously reported in a human study. This case offers significant diagnostic insights into canine intraventricular tumors within the field of veterinary medicine.

KEYWORDS

canine, dog, ^{18}F-FDOPA, choroid plexus papilloma, positron emission tomography

Introduction

Intraventricular brain tumors in dogs mainly arise from the ependymal cells and the choroid plexus epithelium. Therefore, differential diagnoses for intraventricular tumors in dogs include choroid plexus tumors (CPT), ependymomas, oligodendrogliomas, and astrocytomas (1).

CPTs are mostly found in the intraventricular region, originating from the epithelium of the choroid plexus, wherein the primary mass is mostly located in the lateral or third ventricle (2). They constitute 10% of primary intracranial central nervous system tumors in dogs. Although the definitive diagnosis of CPT relies on histopathological examination, magnetic resonance imaging (MRI) and cerebrospinal fluid (CSF) analysis are used for presumptive clinical diagnosis of brain tumors in dogs. CPT is suspected based on MRI results of an intraventricular mass at or adjacent to anatomical sites of the choroid plexus. Commonly observed features include intraventricular masses characterized by prominent contrast enhancement and ventriculomegaly (3–8). Several treatment modalities are available for CPTs including surgery, radiation therapy, chemotherapy, and palliative treatment with anticonvulsants and steroids (9–14). Conversely, in veterinary medicine, chemotherapy protocols for CPTs remain limited, and a standardized treatment regimen has not been established; however, cyclophosphamide, one of the most effective agents for treating choroid plexus-derived tumors in human medicine is known to cross the blood-brain barrier (BBB) in humans, and may be a treatment option (15).

Positron emission tomography (PET) offers significant advantages over conventional imaging methods, such as computed tomography (CT) or MRI, which primarily focus on anatomical features, by providing functional information about tumors. One of the amino acid analogs used in PET is 3,4-dihydroxy-6-[^{18}F] Fluoro-L-phenylalanine (^{18}F-FDOPA) (16). ^{18}F-FDOPA absorption is facilitated by up-regulated amino acid transporters, which is attributed to the nature of brain tumor (16, 17). Additionally, the efficacy of ^{18}F-FDOPA PET (96%) surpasses that of ^{18}F- Fluoro-2-Deoxyglucose PET (^{18}F-FDG) PET (61%) in visualizing human brain tumors (18).

Previously, human studies have demonstrated the superiority of ^{18}F-FDOPA over MRI in visualizing tumors more accurately and delineating brain tumor margins (19). Moreover, metabolic tumor volume (MTV) obtained from ^{18}F-FDOPA images provides valuable insights into predicting tumor recurrence or progression, assessing treatment response, and predicting the prognosis of human brain tumors (17, 20, 21). However, only a single instance has been reported in dogs, wherein a tumor lesion was detected by ^{18}F-FDG PET but was successfully identified through visual analysis using ^{18}F-FDOPA PET, underscoring the superiority of ^{18}F-FDOPA PET over ^{18}F-FDG PET (22).

Herein, we present a report describing the application of ^{18}F-FDOPA in visualizing an intraventricular brain tumor suspected to be a CPT, particularly choroid plexus papilloma (CPP), in a dog.

Case description

An 8-year-old neutered male Miniature Poodle presented with a lethargy, anorexia, and tonic seizures. On physical examination, the dog weighed 6.7 kg, had a pulse rate of 114 beats per minute, a respiratory rate of 30 breaths per minute, and a rectal temperature of 38.3 °C. Neurological examination revealed bilaterally absent menace reflexes and an obtunded mental status. No other abnormalities were observed, and ocular findings were unremarkable. Complete blood count revealed thrombocytopenia (81 × 10^3/μL; reference interval RI: 148–484 × 10^3/μL), whereas serum biochemical analysis did not show any remarkable abnormalities, except for mildly decreased aspartate transaminase activity (18 mg/dL; RI: 23–66 mg/dL), hypotriglyceridemia (19 mg/dL; RI: 21–116 mg/dL), and hyperlactatemia (2.99 mmol/L; RI: 0.5–2.5 mmol/L). Blood electrolyte analysis revealed mild hypocalcemia (8.5 mg/dL; RI: 9–11.3 mg/dL) and mild hypomagnesemia (1.6 mg/dL; RI: 1.8–2.4 mg/dL), which were clinically insignificant.

Based on clinical signs, neurological, ocular, and laboratory examination results, the lesion was neuroanatomically localized to the forebrain. A brain MRI was performed using 1.5-Tesla unit (Signa Creator; GE Healthcare, Milwaukee, WI, USA). The dog was anesthetized via intravenous administration of 6 mg/kg propofol (Provive, Myungmoon Pharm. Co., Ltd, Seoul, South Korea) and 0.2 mg/kg midazolam (Midazolam, Bukwang Pharm. Co., Ltd., Seoul, South Korea) and maintained by inhalation of 2.0–2.5% isoflurane (Terrell, Piramal Critical Care, Bethlehem, PA, USA) in 100% oxygen in a circle rebreathing circuit. T1-weighted images (WI) (pre- and post-contrast), T2-WI, and fluid-attenuated inversion recovery (FLAIR) images were obtained using transverse, sagittal, and dorsal planes. A papilliform shaped mass lesion measuring 1.2 × 1.4 × 1.3 cm in size, with a volume of 1.17 cm^3 was detected in the third ventricle. Additionally, periventricular and peritumoral edema were observed around the lesion (Figure 1). The papilliform-shaped mass was identified as hyperintense on T2-WI (Figure 1A) and FLAIR images (Figure 1B) and hypointense on T1-WI (Figure 1C). A remarkable enhancement in the papilliform shaped mass on T1-WI was noted after administration of 0.1 mmol/kg gadolinium-diethylenetriamine pentaacetic acid [IV; OmniscanTM, GE Healthcare (Shanghai), Co., Ltd, China], (Figure 1D). However, diagnosis and treatment options involving a surgical approach for the lesion could not be performed due to lack of consent from the owner. Nonetheless, a diagnosis of CPP was strongly suspected based on the patient's history, clinical assessments, and MRI features, even though CSF collection and analysis could not be performed owing to considerations regarding post-seizure intracranial pressure elevation.

Therefore, symptomatic therapy was prescribed with prednisolone 0.5 mg/kg PO q12h (Solondo®, Yuhan, Seoul, South Korea) and zonisamide 10 mg/kg PO q12h (Excegran®, Dong-A, Seoul, South Korea). After 53 days, an ^{18}F-FDOPA PET scan of whole body, including the head, was performed to determine malignancy of the tumor and whether metastasis had occurred. ^{18}F-FDOPA (0.094 mCi/kg) was intravenously administered into the right saphenous vein, followed by 5 mL of 0.9% normal saline to flush residual ^{18}F-FDOPA. CT images (pre- and post-contrast) were acquired before PET scans. Attenuation correction for PET image reconstruction was performed using pre-contrast CT images to prevent potential artifacts from iodine-based contrast agents. The PET scans (Discovery-STE, General Electric Medical Systems, Waukesha, WI, USA) were

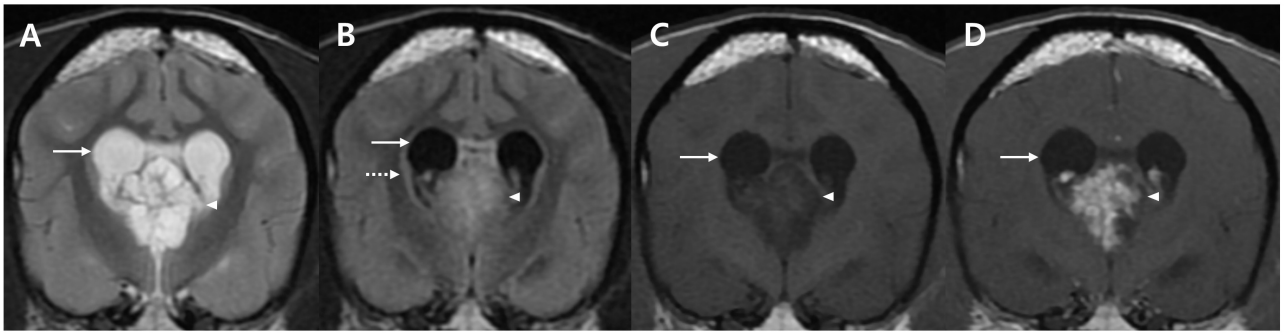

FIGURE 1
MRI characteristics of a dog with an intraventricular tumor suspected to be choroid plexus papilloma presented in the transverse plane. A well-defined solitary papilliform shaped mass is observed in the third ventricle with enlarged lateral ventricle (arrows). The tumor lesion (arrow heads) shows hyperintensity on T2-weighted images (WI) **(A)**, hyperintensity on FLAIR images **(B)** with periventricular edema (dotted arrow), and hypointensity on T1-WI **(C)**. Post-contrast T1-WI **(D)** image shows uniformly remarkable enhancement (arrow). No metastatic findings or brain parenchymal involvement were identified. MRI, magnetic resonance imaging; T1-WI, T1-weighted image; T2-WI, T2-weighted image; FLAIR, fluid-attenuated inversion recovery.

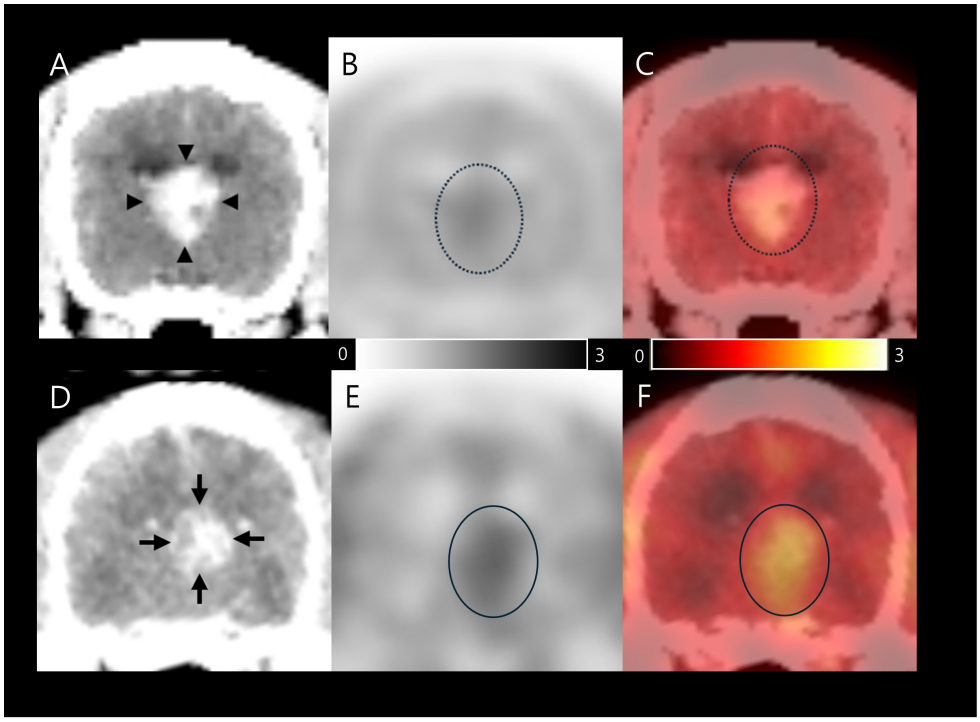

FIGURE 2
^{18}F-FDOPA PET/CT findings in a dog with an intraventricular tumor suspected to be choroid plexus papilloma. The first image was taken on day 53, after initial symptomatic therapy **(A–C)**; Contrast-enhanced CT **(A)** image shows size of 1.3 ×1.4 × 1.2 cm papilliform shaped mass (arrow heads). ^{18}F-FDOPA PET **(B)** and PET/CT fusion **(C)** images showed elevated ^{18}F-FDOPA uptake (dotted circles) with SUV_{mean} 1.2, SUV_{max} 1.42, T/N ratio 1.33, and MTV 1.184 cm^3. The second image was captured on day 117 after initiation of chemotherapy; Contrast-enhanced CT **(D)** image shows size of 1.0 × 1.0 × 1.3 cm papilliform shaped mass (arrows). ^{18}F-FDOPA PET **(E)** and PET/CT fusion **(F)** images demonstrated remarkable elevated ^{18}F-FDOPA uptake in the papilliform shaped tumor lesion (circles) with SUV_{mean} 1.49, SUV_{max} 1.62, T/N ratio 1.62, and MTV 2.217 cm^3. The black and white scale bar represents high ^{18}F-FDOPA uptake in black and low uptake in white (B and E), while the color scale bar represents high ^{18}F-FDOPA uptake in yellow and low uptake in red **(C, F)**. ^{18}F-FDOPA, 3,4-dihydroxy-6-[^{18}F]-fluoro-l-phenylalanine; PET, positron emission tomography; CT, computed tomography; SUV, standard uptake value; T/N, tumor to normal tissue; MTV, metabolic tumor volume.

obtained 10 min after ^{18}F-FDOPA injection (Figures 2A-C) and were analyzed using OsiriX MD v10.0 (Pixmeo Sarl, Geneva, Switzerland).

Based on visual evaluation of the contrast enhanced CT images, the papilliform shaped mass lesion measured 1.3 ×1.4 × 1.2 cm in size, with a volume of 1.09 cm^3 (Figure 2A). An ^{18}F-FDOPA avid

tumor was identified in PET and PET/CT images, with no evidence of metastatic lesions (Figures 2B, C). The regions of interest (ROIs) were manually drawn on the PET/CT fusion images (Figure 2C). The metabolic activity of ROIs was converted to a standard uptake value (SUV) as follows: SUV = concentration of ^{18}F-FDOPA in the ROIs (mCi/kg)/injected dose (mCi) per kilogram of body weight (kg). The mean and maximum SUVs (SUV_{mean} and SUV_{max}) of the tumor were 1.2 and 1.42, respectively. The tumor to normal tissue (T/N) ratio was calculated by dividing the SUV_{max} of the tumor by the SUV_{max} of the normal brain parenchyma using the dorsal plane to evaluate metabolic activity objectively, and was 1.33. All voxels with SUV above the threshold were included to evaluate the MTV based on an SUV threshold determined by the SUV_{mean} of the normal tissue background (17). The MTV was calculated to be 1.184 cm^3. The increase in intracranial pressure was expected to stabilize after medication. Eventually, with the owner's consent, CSF samples were collected via the foramen magnum immediately after the ^{18}F-FDOPA PET scan for differential diagnosis. Cytological evaluation of CSF was conducted within 30 min of collection, with total nucleated cell counts, RBC counts, and differential nucleated cell counts assessed using a standard hemocytometer and methylene blue staining. Total protein concentration was measured using an automated biochemical analyzer (Catalyst One, IDEXX Laboratories, USA). CSF cytology analysis revealed no detectable nucleated cells or red blood cells, with a total protein concentration of 30 mg/dL. Polymerase chain reaction was negative for the following infectious agents: *Bartonella spp., Blastomyces dermatitidis, Coccidioides spp., Cryptococcus spp., Histoplasma capsulatum*, Canine distemper virus, West Nile virus, *Borrelia burgdorferi, Neospora spp., and Toxoplasma gondii.*

On initial evaluation, the dog was suspected to have CPP based on history, clinical assessments, and MRI features. CPP was more strongly presumed to be a tentative diagnosis following additional examinations, including CSF analysis and ^{18}F-FDOPA PET. Chemotherapy with cyclophosphamide 12.9 mg/m^2 PO q12 h, PO (Alkyroxan®, JW-pharma, Seoul, South Korea) and prednisolone 0.5 mg/kg PO q24 h was initiated based on its established efficacy in human cases, its accessibility in veterinary practice, and the owner's decision to proceed with this treatment option (15). Fifteen days after the commencement of chemotherapy, elevated liver enzyme levels were observed without worsening neurological signs, and prednisolone was tapered to 0.5 mg/kg q48 h. However, 100 days after the initiation of chemotherapy, dullness was observed, representing the first deterioration in neurological signs since the commencement of chemotherapy. Consequently, the prednisolone dose was increased to 0.5 mg/kg q24 h. On day 102 after the commencement of chemotherapy, cluster seizures were observed, and prednisolone dose was increased to 0.5 mg/kg q12 h. Additionally, potassium bromide was loaded at 100 mg/kg PO q12h for 2 days and tapered to 17.5 mg/kg PO q12 h as an epileptic drug to control cluster seizures.

A second ^{18}F-FDOPA PET scan was performed to assess the treatment response after 117 days of chemotherapy (Figures 2D–F), employing the same procedure as previously described. A visual evaluation of the contrast enhanced CT image showed that the papilliform shaped mass lesion measuring 1.0 × 1.0 × 1.3 cm in size, with a volume of 0.68 cm^3 was present in the third ventricle (Figure 2D). An ^{18}F-FDOPA avid tumor was identified in the second PET/CT image, without evidence of metastatic lesions (Figures 2E, F). The tumor displayed an SUV_{mean} of 1.49 and SUV_{max} of 1.85. In addition, the T/N ratio was 1.62, and the MTV was 2.217 cm^3. An increase in both ^{18}F-FDOPA avidity and MTV was observed compared with the initial pre-chemotherapy scan results. Unfortunately, the dog died 120 days after the commencement of chemotherapy and 186 days after the initial presentation.

Discussion

In the present case, the dog presented with an intraventricular brain tumor, which was suspected to be CPP, and survived for 186 days after diagnosis and 120 days after chemotherapy with prednisolone and cyclophosphamide. Unfortunately, necropsy could not be performed due to the owner's refusal, therefore, a definitive diagnosis could not be made. Nonetheless, a tentative diagnosis was made based on history, signalment, clinical assessment, MRI features, CSF analysis, and ^{18}F-FDOPA PET scans. This is the first report describing ^{18}F-FDOPA PET findings in a dog presenting with an intraventricular tumor suspected to be CPP. Our case suggests that the findings from ^{18}F-FDOPA PET scans may provide superior clinical insights compared with those from conventional diagnostic methodologies.

Differentiation between CPP, choroid plexus carcinoma (CPC), meningioma, ependymoma, oligodendroglioma, and astrocytoma is essential (1). Both MRI and CSF examinations present distinct characteristics which help differentiate between CPC and CPP. CPPs typically present as a papilliform or globular mass on MRI, with variable T1-WI, contrast enhancement, and hyperintense T2-WI, often accompanied by periventricular edema. In contrast, CPCs exhibit MRI characteristics similar to those of CPP but may display multiform or linear shapes and occasionally metastasize. Additionally, the median CSF protein concentration for CPP is 34 mg/dL, ranging from 32 to 80 mg/dL, whereas that for CPC is 108 mg/dL, ranging from 27 to 380 mg/dL (2). Moreover, discrimination between CPPs and CPCs can be achieved by assessing CSF protein concentration, with a sensitivity of 67% and specificity of 100% when using a threshold of 80 mg/dL (2). Conversely, intraventricular meningiomas are rare, with only one documented case displaying a well-defined mass with T1 isointensity and T2 hyperintensity within the fourth ventricle (23). Whereas ependymomas typically manifest as smooth or lobulated masses on MRI, showing T1 isointensity, T2 hyperintensity, and variable contrast enhancement. Although parenchymal tumors have been described as breaking through the ependymal lining to invade the ventricular space, intraventricular occurrences of oligodendrogliomas are not well documented in veterinary literature (1). In the present case, MRI revealed a papilliform lesion in the third ventricle, demonstrating T1 hypointensity, T2 hyperintensity, and contrast enhancement without metastasis. Parenchymal lesions were not identified, and no signs of ventricular penetration were observed. The CSF protein concentration was 30 mg/dL, below the 80 mg/dL threshold for distinguishing CPP from CPC. Therefore, the patient was tentatively diagnosed with CPP

based on these findings, however, a definitive diagnosis remained inconclusive owing to the lack of histopathological examination.

In the field of human oncology, PET/CT is extensively employed to assess tumor metabolism, metastases, and evaluate residual disease after radiotherapy and surgery (24–26). ^{18}F-FDG, a glucose analog, is a commonly used PET tracer; however, the inherent high physiological glucose metabolism rate of normal brain tissue represents challenge for FDG PET scans in identifying intracranial malignancies (27). In contrast, ^{18}F-FDOPA, an amino acid analog tracer, is advantageous for brain tumor imaging because of its low uptake in normal brain tissue and high uptake within tumor tissue. A previous human study reported that the sensitivity of ^{18}F-FDOPA for the detection of brain tumors was higher than that of ^{18}F-FDG (96% and 61%, respectively) (18, 28).

The detection of brain tumors using ^{18}F-FDOPA has also been reported in veterinary medicine (22, 29). A previous case study involving canine glioma highlighted discrepancies between diagnostic results of ^{18}F-FDG and ^{18}F-FDOPA scans (22). Notably, although the tumor lesion was not detected on the ^{18}F-FDG scan, it was confirmed on the ^{18}F-FDOPA PET scan, which aligns with previous findings in human medicine (17, 29). Although ^{18}F-FDOPA PET can detect tumor lesions with high sensitivity (18, 28), no metastatic tumor lesions were identified on ^{18}F-FDOPA PET in this case. This observation serves as a further point of differentiation from CPC, where metastatic occurrences are prevalent in over half of cases (2).

The findings from the ^{18}F-FDOPA PET scan in the current case suggest several implications. First, ^{18}F-FDOPA PET scans could be used to detect not only brain parenchyma tumors, previously identified in veterinary medicine, but also intraventricular tumors. Second, ^{18}F-FDOPA scans, which are highly sensitive to tumor detection, can determine the presence of metastasis to the brain parenchyma and serve as a distinguishing feature of the tumor. Third, the T/N ratio of the ^{18}F-FDOPA PET scan, which serves as a diagnostic parameter for brain tumors, has demonstrated high sensitivity (96%) and specificity (86%) for identifying brain tumors in humans when its value exceeds 1.3 (18). The T/N ratio in the present case was 1.33 before chemotherapy, which is consistent with the cut-off value reported in human brain tumors; however, it increased to 1.62 at ^{18}F-FDOPA PET/CT follow-up, which was conducted 117 days after chemotherapy with prednisolone and cyclophosphamide. Although it was challenging to diagnose and initiate chemotherapy for the tumor solely based on the results of conventional diagnostic methodologies, such as physical examination, neurological assessment, blood tests, MRI scans, and CSF analysis, with the utilization of T/N ratio results, a provisional diagnosis of brain tumor was made, allowing for the initiation of chemotherapy. Thus, differentiating between tumor and other intracranial conditions is crucial for developing treatment plans for veterinary patients presenting with brain abnormalities. Although biopsy remains an essential diagnostic tool for differential diagnosis in veterinary patients with brain lesions, its invasiveness and potential for complications limit its use. In such cases, ^{18}F-FDOPA PET scans are a noninvasive diagnostic modality for identifying of brain tumors, including metastasis to brain parenchyma. Thus, our findings serve as important points for differentiating between different diagnoses, thereby effectively guiding the course of treatment. However, while ^{18}F-FDOPA PET provides valuable metabolic insights, its limitations in distinguishing benign from malignant tumors and the lack of established evidence for detecting extracranial metastases suggest that it should not be solely relied upon for diagnosis. Consequently, a comprehensive evaluation incorporating other diagnostic modalities is essential (18).

Additionally, the MTV on ^{18}F-FDOPA PET increased from 1.184 cm^3 to 2.217 cm^3 despite observed tumor volume upon MRI being 1.17 cm^3 and on contrast-enhanced CT scans decreasing from 1.09 cm^3 to 0.68 cm^3 in the present case. A study in human medicine suggested that the response rate of MTV at follow-up examinations may serve as a prognostic indicator for brain tumor chemotherapy (17). This association is due to the increased amino acid uptake by the tumor, which may be due to the impairment of BBB integrity, suggesting tumor-induced BBB disruption (17). Moreover, this indicates that the normalization of BBB permeability leads to a decrease in the MTV in cases where the treatment response is favorable, whereas BBB permeability remains abnormal in cases where the treatment response is unfavorable (16). Although the median survival time for CPP is not well known due to the limited number of reports, a survival period of 388 days has been reported for dogs treated with lomustine and hydroxyurea (30). In addition, a survival of 15 months with symptomatic treatment alone has been reported (31). In this case, the dog died 186 days after diagnosis and 120 days after the start of chemotherapy. This coincides with a previously reported human study showing that non-responder MTV after treatment indicates a poor prognosis. Therefore, follow-up ^{18}F-FDOPA PET scans could be helpful for monitoring treatment effects and evaluating prognosis after the treatment of intracranial tumors in veterinary medicine.

To the best of our knowledge, this is the first report to describe ^{18}F-FDOPA PET findings in a clinical case of a dog with an intraventricular brain tumor suspected to have CPP. This case offers significant diagnostic insights into canine intraventricular tumors within the field of veterinary medicine. Nevertheless, further studies are required to establish diagnostic criteria using ^{18}F-FDOPA PET scans, such as SUV_{max} or T/N ratio cut-off, for canine intraventricular tumors. In the present case, although the lesion size decreased on follow-up CT contrast imaging, an increase in the MTV was observed on the ^{18}F-FDOPA PET/CT after chemotherapy. Consequently, integrating findings from other diagnostic modalities is important for a more comprehensive evaluation. Combining this with worsening clinical signs and a limited survival period suggests that increased MTV post-chemotherapy correlates with poor prognosis, as reported in human studies. Thus, MTV measurements from pre- and post-chemotherapy ^{18}F-FDOPA scans could be valuable prognostic factors beyond lesion size assessments from contrast-enhanced CT images. However, this was a single case study; therefore, investigations involving larger populations are required to confirm these findings.

Data availability statement

The raw data supporting the conclusions of this article will be made available by the authors, without undue reservation.

Ethics statement

Ethical approval was not required for the studies involving animals in accordance with the local legislation and institutional requirements because Ethical approval was not necessary for the animal studies as they adhered to local laws and institutional guidelines. This case study was conducted retrospectively using data collected for clinical purposes, and all procedures were part of standard care. Informed consent was obtained from the owners for all data included in our manuscript. Written informed consent was also obtained from the participants for the publication of this case report. Written informed consent was obtained from the owners for the participation of their animals in this study.

Author contributions

JW: Writing – original draft. YC: Writing – original draft. DL: Data curation, Formal analysis, Investigation, Writing – review & editing. TY: Writing – review & editing. HK: Writing – review & editing. B-TK: Writing – review & editing.

Funding

The author(s) declare that financial support was received for the research and/or publication of this article. This work was supported by the National Research Foundation of Korea (NRF) grant funded by the Korean Government (MSIT) (No. RS-2024-00337663), and the Korea Institute of Planning and Evaluation for Technology in Food, Agriculture, Forestry (IPET) through the Companion Animal Life Cycle Industry Technology Development Program (322095-04), and Agriculture and Food Convergence Technologies Program for Research Manpower development (RS-2024-00398561) funded by the Ministry of Agriculture, Food, and Rural Affairs (MAFRA).

Conflict of interest

The authors declare that this study was conducted in the absence of any commercial or financial relationships that could be construed as potential conflicts of interest.

Publisher's note

All claims expressed in this article are solely those of the authors and do not necessarily represent those of their affiliated organizations, or those of the publisher, the editors and the reviewers. Any product that may be evaluated in this article, or claim that may be made by its manufacturer, is not guaranteed or endorsed by the publisher.

References

1. Wisner ER, Dickinson PJ, Higgins RJ. Magnetic resonance imaging features of canine intracranial neoplasia. *Vet Radiol Ultrasound.* (2011) 52:S52–61. doi: 10.1111/j.1740-8261.2010.01785.x

2. Westworth DR, Dickinson PJ, Vernau W, Johnson EG, Bollen AW, Kass PH, et al. Choroid plexus tumors in 56 dogs (1985–2007). *J Vet Intern Med.* (2008) 22:1157–65. doi: 10.1111/j.1939-1676.2008.0170.x

3. Hammer AS, Couto CG, Getzy D, Hunter W. Magnetic resonance imaging in a dog with a choroid plexus carcinoma. *J Small Anim Pract.* (1990) 31:341–4. doi: 10.1111/j.1748-5827.1990.tb00826.x

4. Ohashi F, Kotani T, Onishi T, Katamoto H, Nakata E, Fritz-Zieroth B. Magnetic resonance imaging in a dog with choroid plexus carcinoma. *J Vet Med Sci.* (1993) 55:875–6. doi: 10.1292/jvms.55.875

5. Lipsitz D, Levitski RE, Chauvet AE. Magnetic resonance imaging of a choroid plexus carcinoma and meningeal carcinomatosis in a dog. *Vet Radiol Ultrasound.* (1999) 40:246–50. doi: 10.1111/j.1740-8261.1999.tb00356.x

6. Snyder JM, Shofer FS, Van Winkle TJ, Massicotte C. Canine intracranial primary neoplasia: 173 cases (1986–2003). *J Vet Intern Med.* (2006) 20:669–75. doi: 10.1111/j.1939-1676.2006.tb02913.x

7. Thomas WB, Wheeler SJ, Kramer R, Kornegay JN. Magnetic resonance imaging features of primary brain tumors in dogs. *Vet Radiology Ultrasound.* (1996) 37:20–7. doi: 10.1111/j.1740-8261.1996.tb00807.x

8. Kraft SL, Gavin PR, Dehaan C, Moore M, Wendling LR, Leathers CW. Retrospective review of 50 canine intracranial tumors evaluated by magnetic resonance imaging. *J Vet Intern Med.* (1997) 11:218–25. doi: 10.1111/j.1939-1676.1997.tb00094.x

9. Rossmeisl JH. New treatment modalities for brain tumors in dogs and cats. *Vet Clin North Am Small Anim Pract.* (2014) 44:1013–38. doi: 10.1016/j.cvsm.2014.07.003

10. Miller AD, Miller CR, Rossmeisl JH. Canine primary intracranial cancer: a clinicopathologic and comparative review of glioma, meningioma, and choroid plexus tumors. *Front Oncol.* (2019) 9:1151. doi: 10.3389/fonc.2019.01151

11. Dickinson PJ. Advances in diagnostic and treatment modalities for intracranial tumors. *J Vet Intern Med.* (2014) 28:1165–85. doi: 10.1111/jvim.12370

12. Rossmeisl JH Jr, Jones JC, Zimmerman KL, Robertson JL. Survival time following hospital discharge in dogs with palliatively treated primary brain tumors. *J Am Vet Med Assoc.* (2013) 242:193–8. doi: 10.2460/javma.242.2.193

13. Dolera M, Malfassi L, Bianchi C, Carrara N, Finesso S, Marcarini S, et al. Frameless stereotactic radiotherapy alone and combined with temozolomide for presumed canine gliomas. *Vet Comp Oncol.* (2018) 16:90–101. doi: 10.1111/vco.12316

14. Van Meervenne S, Verhoeven PS, de Vos J, Gielen IM, Polis I, Van Ham LM. Comparison between symptomatic treatment and lomustine supplementation in 71 dogs with intracranial, space-occupying lesions. *Vet Comp Oncol.* (2014) 12:67–77. doi: 10.1111/j.1476-5829.2012.00336.x

15. Berrak SG, Liu DD, Wrede B, Wolff JE. Which therapy works better in choroid plexus carcinomas? *J Neurooncol.* (2011) 103:155–62. doi: 10.1007/s11060-010-0372-9

16. Laverman P, Boerman OC, Corstens FHM, Oyen WJG. Fluorinated amino acids for tumour imaging with positron emission tomography. *Eur J Nucl Med Mol Imaging.* (2002) 29:681–90. doi: 10.1007/s00259-001-0716-y

17. Schwarzenberg J, Czernin J, Cloughesy TF, Ellingson BM, Pope WB, Grogan T, et al. Treatment response evaluation using 18F-FDOPA PET in patients with recurrent malignant glioma on bevacizumab therapy. *Clin Cancer Res.* (2014) 20:3550–9. doi: 10.1158/1078-0432.CCR-13-1440

18. Chen W, Silverman DHS, Delaloye S, Czernin J, Kamdar N, Pope W, et al. 18F-FDOPA PET imaging of brain tumors: comparison study with 18F-FDG PET and evaluation of diagnostic accuracy. *J Nucl Med.* (2006) 47:904–11.

19. Ponisio MR, McConathy JE, Dahiya SM, Miller-Thomas MM, Rich KM, Salter A, et al. Dynamic ^{18}F-FDOPA-PET/MRI for the preoperative evaluation of gliomas: correlation with stereotactic histopathology. *Neurooncol Pract.* (2020) 7:656–67. doi: 10.1093/nop/npaa044

20. Zaragori T, Ginet M, Marie PY, Roch V, Grignon R, Gauchotte G, et al. Use of static and dynamic [^{18}F]-F-DOPA PET parameters for detecting patients with glioma recurrence or progression. *EJNMMI Res.* (2020) 10:56. doi: 10.1186/s13550-020-00645-x

21. Ledezma CJ, Chen W, Sai V, Freitas B, Cloughesy T, Czernin J, et al. 18F-FDOPA PET/MRI fusion in patients with primary/recurrent gliomas: initial experience. *Eur J Radiol.* (2009) 71:242–8. doi: 10.1016/j.ejrad.2008.04.018

22. Yun T, Koo Y, Kim S, Lee W, Kim H, Chang D, et al. Characteristics of ^{18}F-FDG and ^{18}F-FDOPA PET in an 8-year-old neutered male Yorkshire Terrier dog with glioma: long-term chemotherapy using hydroxyurea plus imatinib with prednisolone and immunoreactivity for PDGFR-β and LAT1. *Vet Q.* (2021) 41:163–71. doi: 10.1080/01652176.2021.1906466

23. Salvadori C, Pintore MD, Ricci E, Konar M, Tartarelli CL, Gasparinetti N, et al. Microcystic meningioma of the fourth ventricle in a dog. *J Vet Med Sci.* (2011) 73:367–70. doi: 10.1292/jvms.10-0337

24. Delbeke D, Martin WH, Sandler MP, Chapman WC, Wright JK Jr, Pinson CW. Evaluation of benign vs malignant hepatic lesions with positron emission tomography. *Arch Surg.* (1998) 133:510–5. doi: 10.1001/archsurg.133.5.510

25. Nakamoto Y, Higashi T, Sakahara H, Tamaki N, Kogire M, Doi R, et al. Delayed (18)F-fluoro-2-deoxy-D-glucose positron emission tomography scan for differentiation between malignant and benign lesions in the pancreas. *Cancer.* (2000) 89:2547–54. doi: 10.1002/1097-0142(20001215)89:12<2547::AID-CNCR5>3.0.CO;2-V

26. Weder W, Schmid RA, Bruchhaus H, Hillinger S, von Schulthess GK, Steinert HC. Detection of extrathoracic metastases by positron emission tomography in lung cancer. *Ann Thorac Surg.* (1998) 66:886–92. doi: 10.1016/S0003-4975(98)00675-4

27. Olivero WC, Dulebohn SC, Lister JR. The use of PET in evaluating patients with primary brain tumours: is it useful? *J Neurol Neurosurg Psychiatry.* (1995) 58:250–2. doi: 10.1136/jnnp.58.2.250

28. Wardak M, Schiepers C, Cloughesy TF, Dahlbom M, Phelps ME, Huang SC. ^{18}F-FLT and ^{18}F-FDOPA PET kinetics in recurrent brain tumors. *Eur J Nucl Med Mol Imaging.* (2014) 41:1199–209. doi: 10.1007/s00259-013-2678-2

29. Lee D, Yun T, Kim S, Koo Y, Chae Y, Kim S, et al. Case Report: 18F-fluoro-L-phenylalanine positron emission tomography findings and immunoreactivity for L-type amino acid Transporter 1 in a dog with meningioma. *Front Vet Sci.* (2022) 9:899229. doi: 10.3389/fvets.2022.899229

30. Jung DI, Kim HJ, Park C, Kim JW, Kang BT, Lim CY, et al. Long-term chemotherapy with lomustine of intracranial meningioma occurring in a miniature schnauzer. *J Vet Med Sci.* (2006) 68:383–6. doi: 10.1292/jvms.68.383

31. Itoh T, Uchida K, Nishi A, Shii H, Nagayoshi T, Sakamoto H. Choroid plexus papilloma in a dog surviving for 15 months after diagnosis with symptomatic therapy. *J Vet Med Sci.* (2016) 78:167–9. doi: 10.1292/jvms.15-0330

frontiers | Frontiers in Veterinary Science

TYPE Brief Research Report
PUBLISHED 27 March 2025
DOI 10.3389/fvets.2025.1552415

Check for updates

OPEN ACCESS

EDITED BY
Yasunaga Yoshikawa,
Kitasato University, Japan

REVIEWED BY
Gashaw Getaneh Dagnaw,
University of Gondar, Ethiopia
Prasanna K. S.,
KVASU, India

*CORRESPONDENCE
Kozo Ohkusu-Tsukada
✉ tkd-oks@nvlu.ac.jp

RECEIVED 28 December 2024
ACCEPTED 10 March 2025
PUBLISHED 27 March 2025

CITATION
Tsumoto S, Tamura K, Nakazawa Y, Fujita M and Ohkusu-Tsukada K (2025) Detection of bimodal survivin expressions in canine cancer types by flow cytometry compared to immunohistochemistry.
Front. Vet. Sci. 12:1552415.
doi: 10.3389/fvets.2025.1552415

COPYRIGHT
© 2025 Tsumoto, Tamura, Nakazawa, Fujita and Ohkusu-Tsukada. This is an open-access article distributed under the terms of the Creative Commons Attribution License (CC BY). The use, distribution or reproduction in other forums is permitted, provided the original author(s) and the copyright owner(s) are credited and that the original publication in this journal is cited, in accordance with accepted academic practice. No use, distribution or reproduction is permitted which does not comply with these terms.

Detection of bimodal survivin expressions in canine cancer types by flow cytometry compared to immunohistochemistry

Shohei Tsumoto[1], Kyoichi Tamura[2], Yuta Nakazawa[3], Michio Fujita[3] and Kozo Ohkusu-Tsukada[1]*

[1]Laboratory of Veterinary Pathology, School of Veterinary Medicine, Nippon Veterinary and Life-Science University (NVLU), Tokyo, Japan, [2]Laboratory of Veterinary Clinical Pathology, School of Veterinary Medicine, Nippon Veterinary and Life-Science University (NVLU), Tokyo, Japan, [3]Laboratory of Veterinary Radiology, School of Veterinary Medicine, Nippon Veterinary and Life-Science University (NVLU), Tokyo, Japan

Animal practice requires both convenience for the owner and risk management for the animal's health. Deterioration due to cancer may associate with poor prognosis under general anesthesia, which need to partial excision for pathological diagnosis. This study aimed to establish rapidly detecting the expression of survivin antigens for cancer vaccines or molecular targeted therapies via flow cytometry (FCM) using the intracellular staining method in tumor samples obtained via needle biopsy without anesthesia. Therefore, survivin expression patterns in each cell lines of canine melanomas, a murine mast cell tumor, a murine colon carcinoma, and a murine melanoma was analyzed by FCM and immunofluorescence microscopy, and compared with immunohistochemical analysis and western blot method. Interestingly, FCM results of the bimodal expression pattern of survivin were suggested to reflect the high fluorescence intensity of its nuclear–cytosol localization and the weak fluorescence intensity of its cytosol alone localization. In a case of canine cancer disease, it was confirmed that survivin expression patterns can be detected via FCM using needle biopsy samples in actual clinical settings. In this study, a novel method via FCM was proposed to quickly determine also survivin localization not only whether the survivin is expressed in cancer cells. The application of cancer vaccine or chemical therapy via this technology can be expected to contribute to improved animal care due to the "one-day first program," which has been proposed in convenience for owners.

KEYWORDS

survivin, flow cytometry, CMM2, CMeC2, LMeC, p815, CT26, B16F10

1 Introduction

Survivin (BIRC5, API4) is known for its dual biological role in apoptosis inhibition and mitotic progression (proliferative response) in many cancers (1). Five splice variants of survivin have been reported, namely, survivin-2α, survivin-3α, survivin-2B, survivin-3B, and survivin-δ-Ex3, in addition to the survivin wild type (2). These heterogeneous or homogenous dimerization results in the determination of nuclear or cytoplasmic

localization and the functions of apoptosis inhibition and mitotic progression (3). Survivin-δ-Ex3 has antiapoptotic functions (inhibits caspase-3) and promotes cell cycle progression via nucleolar localization signals and degradation signals (4). It has also been shown that not only survivin dimers but also survivin monomers participate in regulating apoptosis (5). In highly malignant cancers where the splicing of survivin is progresses, more survivin-δ-Ex3 of five splice variants are formed, which leads to the nuclear localization of the survivin molecule. On the contrary, it was also reported that survivin-2B expression (in cytoplasm) was dominant in benign brain tumors in comparison with the malignant ones (6).

In canine cancer, survivin expression is recognized in various malignant tumors, such as lymphoma (7), malignant melanoma (8), mast cell tumors (9), hemangiosarcomas (10), transitional cell carcinoma (11), osteosarcoma (12), cutaneous squamous cell carcinomas (13), histiocytic sarcoma (14), nasal carcinoma (15), prostatic carcinoma (16), and canine hemangiopericytomas (17). Therefore, the molecular targeted agents using such as 3-cyanopyridine, YM-155, Debio1143, EM1421, LQZ-7I, or TL32711 (18), and immunotherapies as cancer vaccines (19), targeting survivin molecules have been highlighted recently.

In previous cancer treatments for dogs, the pathological diagnosis will take on 5 to 7 days after tumor collection, and surgical treatment will be 1 month later for reasons of hospital's reservation and owner schedule, resulted in tumor growth and metastasis. If a rapid diagnosis of survivin expression can be made today, it will enable measures to be taken immediately to slow the progression of cancer and may contribute to reduce the tumor volume and the metastasis risk before surgical treatment.

In this study, we propose a novel method via FCM to quickly determine whether survivin is expressed in cancer cells. Cancer vaccine or chemotherapy by applying this technology will contribute to also solving problems related to human convenience focused on the field of animal medicine.

2 Method

2.1 Mice

An intradermal allograft model or xenograft model using murine or canine cell lines was generated by using NOD/SCID mice (female, 8–12 weeks old). All the mice were kept on clean racks under appropriate air conditioning, room temperature, humidity, and a 12-h light cycle in accordance with the ethical guidelines of the Nippon Veterinary and Life Science University.

2.2 Cell lines

A total of six cell lines were used: canine malignant melanoma lines [CMM2, CMeC2, LMeC; provided by Dr. Takayuki Nakagawa, Department of Veterinary Surgery, University of Tokyo; (20)], the murine malignant melanoma line B16F10, the murine mast cell tumor line p815, and the murine colon cancer line CT26 (distributed for a fee by the JCRB Cell Bank).

2.3 Immunohistochemical analysis (IHC)

After the cell line xenograft or allograft models were prepared, the removed tissue samples were embedded in paraffin blocks, sectioned at 3 μm, deparaffinized in xylene, and rehydrated. Endogenous peroxidase was subsequently treated with 3% H_2O_2 solution for 30 min, and antigen retrieval was subsequently performed by autoclaving at 105°C for 25 min (pH 9.0 EDTA). After cooling at room temperature, the samples were washed three times for 3 min with phosphate-buffered saline (PBS). Next, milk blocking was performed, and a rabbit anti-survivin monoclonal antibody (mAb; 1:300, ab134170, Abcam) was applied and incubated overnight at 4°C. After being washed three times for 3 min with PBS, the sections were incubated with an HRP-labeled anti-rabbit secondary antibody (1:300; G0418, Tokyo Chemical Industry, Japan) for 1 h at 37°C. After washing three times for 3 min each, the sections were stained with DAB for 10 min and counterstained with hematoxylin for 1 min.

2.4 Western blotting (WB)

WB was performed via standard methods to examine total cellular components and cytosolic fraction components. First, various cell lines were dissolved in a neutral detergent, a portion was centrifuged at 10,000 × g to adjust the total protein amount of the cytosolic fraction, and the total cellular components and cytosolic fraction components were prepared by diluting them in the same ratio. The proteins were separated and subjected to 10% SDS–PAGE. After being transferred to polyvinylidene difluoride (PVDF) membranes treated with 99% methanol, the membranes were incubated with 5% skim milk in PBS-T (10 mM sodium phosphate, 0.15 M NaCl, 0.05% Tween-20, pH 7.5) for 1 h to block non-specific binding. Anti-survivin mAb (1:500, ab134170, Abcam, USA) and anti-β-actin mAb (1:1000, W16197A, BioLegend, USA) were then incubated overnight at 4°C. The membrane was then incubated with an HRP-conjugated anti-rabbit secondary mAb (1:5,000). Survivin or β-actin protein was visualized via an enhanced chemiluminescence (ECL) detection system (GE Healthcare Bio-Sciences). The density of the plot was measured via ImageJ software, and the density ratio of cytosolic survivin was fitted on the basis of total survivin corrected for β-actin density.

2.5 Flow cytometry (FCM)

First, the cultured cells or needle biopsy sample cells were treated with 0.25% trypsin-EDTA for 5 min, and the cells were allowed to accumulate. For the intracellular staining method, the cells were fixed with 4% Parafolaldehyde for 60 min. Next, they were reacted with 0.05% Triton-X for 30 min to treat the cell membrane. Finally, they were reacted with an APC-labeled survivin mAb (1:200, ab134170, Abcam) for 30 min and then analyzed via a flow cytometer (Beckman, CytoFLEX).

Abbreviations: IHC, Immunohistochemistry; FCM, Flow cytometry; WB, Western blot; IM, Immunofluorescence microscopy.

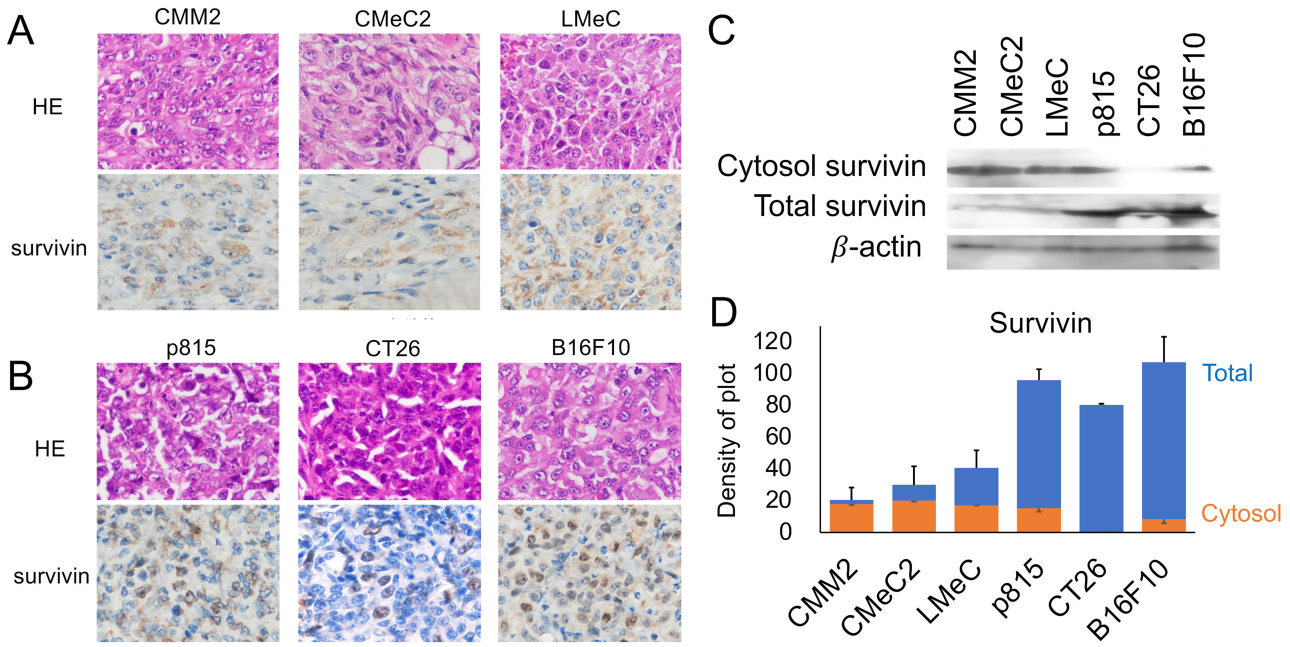

FIGURE 1
Analysis of survivin expression sites by IHC and WB. **(A)** Images of HE staining and survivin expression via IHC in canine melanoma cell lines (CMM2, CMeC, and LMeC) are shown. **(B)** Images of HE staining and survivin expression via IHC in murine cell lines (p815, CT26, and B16F10) are shown. **(C)** The cytosol and total survivin expression patterns via WB are indicated. **(D)** The expression levels of total survivin (blue bar) and cytosolic survivin (orange bar) corrected on the basis of β-actin expression are shown via density of plot analysis via ImageJ software.

2.6 Immunofluorescence microscopy (IM)

The cells were seeded in 96-well glass-bottom plates (GP96000, Matsunami, Osaka, Japan). Adherent cells were fixed with 4% paraformaldehyde and treated with 0.05% Triton, followed by APC-conjugated survivin mAb (1:200, ab134170, Abcam) treatment. Nuclei were counterstained with DAPI (SeraCare, Milford, IA). Images of the sections were captured via a BZ-X800 fluorescence microscope (Keyence Corporation; Tokyo, Japan) at 400 × magnification to measure the survivin (red) area. The images are displayed in Z-axis slices.

2.7 Statistical analysis

The data are expressed as the means ± SEMs. Statistical analysis was performed via one-way ANOVA. A $p < 0.05$ was considered statistically significant.

3 Results

3.1 Analysis of survivin expression sites by IHC or WB

The expression of survivin in the tumor mass from each cell line in the intradermal allograft model or xenograft model in NOD/SCID mice was analyzed via IHC. In canine melanoma cell lines (CMM2, CMeC, LMeC), granular expression of survivin was observed in the cytosol, with little expression in the nucleus. In murine cell lines (p815, CT26, and B16F10), survivin was relatively strongly localized to the nucleus and was expressed in both the cytosol and nucleus in the mast cell tumor line p815 and the melanoma line B16F10. On the other hand, in the colon cancer line CT26, survivin was specifically expressed in the nucleus (Figures 1A, B). The expression of survivin in the total or cytosolic cell fraction was compared with the adjusted total protein amount using β-actin via WB analysis (Figures 1C, D). The amount of total survivin was significantly 2–3 times greater in the murine cell lines than in the canine melanoma cell lines. There were no significant differences between p815 and B16F10 ($p = 0.447$, one-way ANOVA), but CT26 was significantly lower than p815 or B16F10 ($p < 0.05$, one-way ANOVA). The amount of cytosol-localized survivin expression was observed in all the analyzed cell lines except CT26.

3.2 Analysis of survivin expression patterns via FCM and IM

The FCM results indicate that the fluorescence intensity of each individual cell is different but that survivin is detected in total cells, including both the cytosol and nucleus. Histogram analysis via FCM revealed that survivin expression was bimodal in each individual cell line. Although the canine melanoma cell

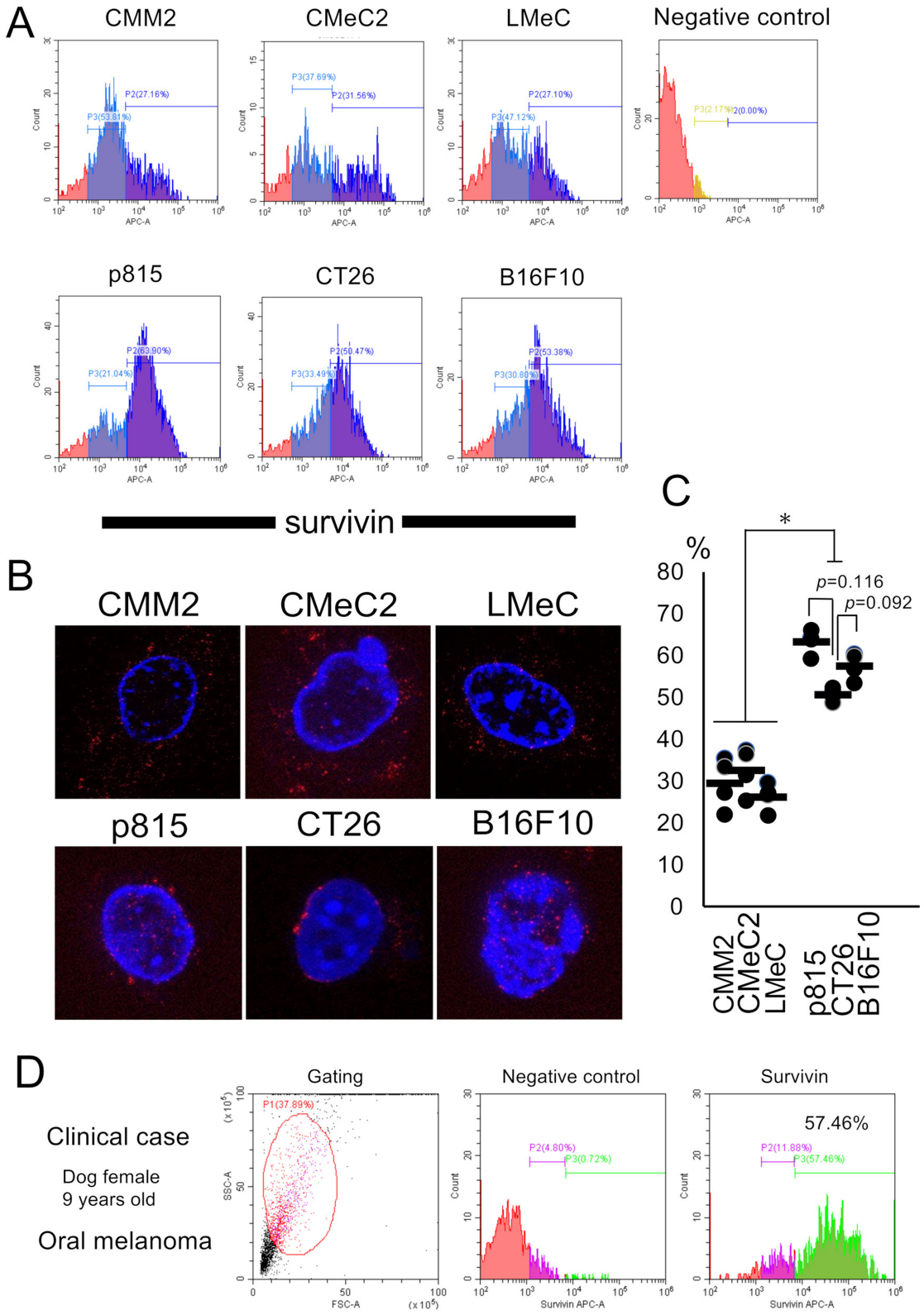

FIGURE 2
Analysis of survivin expression patterns by FCM and IM and the tests in a clinical case. **(A)** The fluorescence intensity of APC-survivin in each cell line detected by FCM is shown. **(B)** Representative survivin expression patterns in each cell line by IM are shown. **(C)** The percentages of high fluorescence intensity of survivin expression in each cell line are indicated. *$p < 0.05$, one-way ANOVA. **(D)** Survivin expression after needle biopsy in a clinical case of canine oral melanoma (female, 9 years old) was analyzed via FCM. The percentage of cells with high fluorescence intensity was 57.46%. Similar findings were detected in four other cases of oral melanoma.

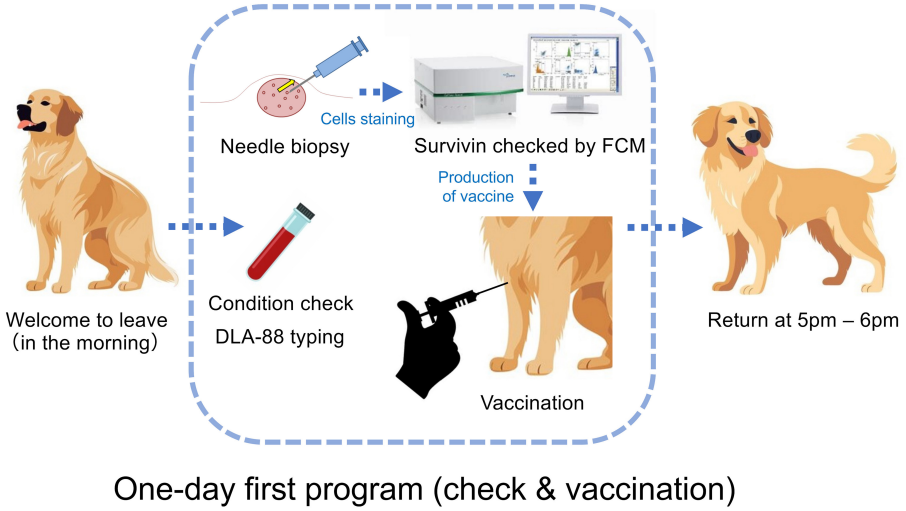

FIGURE 3
"One-day first program" for a cancer check and vaccination. At the university's veterinary hospital, after an interview and an informed consent form (ICF) with the owner in the morning, the patient dog is taken in, and a general CBC blood test is performed to check its health condition. Needle biopsy will be performed on the tumor, the cells will be stained via an APC-conjugated anti-survivin mAb after detergent treatment following cell membrane fixation, and the presence or absence of survivin expression will be examined by FCM. If the tumor expresses survivin, the vaccine after production will be administered intradermally, such as through the axilla. After confirming that there is no anaphylactic reaction, the patient's dog waits until the owner returns to pick up after 5 p.m.

lines (CMM2, CMeC2, and LMeC) expressed survivin mainly in the cytosol were few as 27.2, 31.6, and 27.1%, respectively, in percentage of relatively high fluorescence intensities. On the other hand, the murine cell lines (p815, CT26, and B16F10) expressed mainly in nucleus–cytosol or nucleus alone localization were many as 63.9, 50.4, and 53.4%, respectively, in percentage of relatively high fluorescence intensities (Figures 2A, C). The bimodal expression pattern suggested a high fluorescence intensity of nuclear—cytosol localization and a weak fluorescence intensity of cytosol alone localization. The survivin expression in CT26 cells (nuclear alone localization) tended to be lower than that in p815 and B16F10 cells (nuclear—cytosol localization), but the difference was not significant ($p = 0.116$ and $p = 0.092$, one-way ANOVA). The IM results revealed that the expression pattern of survivin in terms of both nuclear localization and cytosolic localization was granular in each individual cell line; however, interestingly, that in CT26 cells was restricted to the nuclear membrane (Figure 2B). These results suggest that survivin expression detected by FCM is not inconsistent with the results of IHC and WB (expression in the cytosol, nucleus, or both in each cell line) and is reasonably consistent.

3.3 Survivin expression detected via FCM using needle biopsy samples

A clinical case of canine oral melanoma (female, 9 years old) was evaluated for survivin expression via FCM (Figures 2D). This histogram analysis revealed a bimodal pattern, similar to the FCM analysis using each individual cell line, with high fluorescence expression (57.46%). This survivin expression pattern was similar to that of both the cytosol and nucleus, such as p815 or B16F10 cell line.

3.4 "One-day first program" for cancer screening and vaccination

A cancer screening and therapy program that is highly convenient for dog owners is important. The "one-day first program" proposed here is possible to be implemented immediately by avoiding the owner's schedule issues (Figure 3).

The pathological diagnosis will take on 5 to 7 days after tumor collection, and surgical treatment will be performed 1 month later for reasons of hospital's reservation and owner schedule. During this time, the tumor volume increases ~4fold, and both the difficulty of surgery and the risk of metastasis increase. The "one-day first program" as therapy strategy that utilizes and applies the technology established in this study, whose introduction will contribute to simplifying surgical therapy 1 month later by reducing the tumor volume and the risk of metastasis. Thus, depending on the various cases, cancer vaccines using this program can be used not only for (1) the purpose of preventing recurrence but also for (2) active treatment purposes, such as achieving complete or partial remission, and for (3) the purpose of improving poor prognosis when recurrence has occurred after surgery, chemotherapy, radiation therapy, etc., and retreatment is difficult.

4 Discussion

A 2006 study of canine mast cell tumors reported no association between the nuclear or cytosol localization of survivin and prognostic survival rates (9). In a recent study of canine hemangiopericytomas, nuclear survivin expression was observed in all 41 cases (100%), but the proportion of nuclear survivin-expressing cells in the entire tumor mass ranged from 1 to 12%. In contrast, cytoplasmic survivin expression was observed in 31/41

cases (76%), and the proportion of cytoplasmic survivin-expressing cells in the entire tumor mass was 75% or greater. However, the important point of this report is that a statistical association was demonstrated in which every 1% increase in nuclear survivin in the tumor mass was associated with a 1.15-fold increase in the risk of immediate mortality (17). Future research should focus not only on the presence or absence of survivin expression for each type of cancer but also on the localization of survivin in the nucleus and cytoplasm to verify the prognosis.

In this study, the bimodal expression pattern of survivin was suggested to reflect the high fluorescence intensity of its nuclear–cytosol localization and the weak fluorescence intensity of its cytosolic alone localization resulting from FCM in various cell lines. This makes it possible to use FCM technology on clinical specimens obtained via needle biopsy to determine whether the survivin of cancer cells is localized in the cytoplasm alone or both nucleus and cytoplasm. Previous reports (6) have shown that of the five splice variants of survivin, survivin-δ-Ex3 (expressed in the nucleus) is expressed in highly malignant tumors, whereas survivin-2B (expressed in the cytosol) tends to be expressed in relatively benign tumors. In the future, when fluorescent-labeled anti-survivin-2B mAbs and anti-survivin-δ-Ex3 mAbs become available to canine tumor cells, the test via FCM may be able to reflect the prognostic status.

5 Conclusions

In this study, a novel method via FCM was proposed to quickly determine also survivin localization not only whether the survivin is expressed in cancer cells. The application of cancer vaccine or chemotherapy via this technology can be expected to contribute to improved animal care due to the "one-day first program." This technology is also expected to be applicable to other proteins involved in cancer progression.

Data availability statement

The datasets presented in this study can be found in online repositories. The names of the repository/repositories and accession number(s) can be found in the article/Supplementary material.

Ethics statement

The animal studies were approved by the Veterinary Medical Teaching Hospital of Nippon Veterinary and Life Science University Institutional Review Board. The studies were conducted in accordance with the local legislation and institutional requirements. Written informed consent was obtained from the owners for the participation of their animals in this study.

Author contributions

ST: Data curation, Formal analysis, Investigation, Methodology, Writing – review & editing. KT: Formal analysis, Methodology, Project administration, Supervision, Writing – review & editing. YN: Formal analysis, Methodology, Project administration, Writing – review & editing. MF: Project administration, Resources, Supervision, Writing – review & editing. KO-T: Conceptualization, Data curation, Formal analysis, Funding acquisition, Investigation, Methodology, Project administration, Resources, Software, Supervision, Validation, Visualization, Writing – original draft, Writing – review & editing.

Funding

The author(s) declare that financial support was received for the research and/or publication of this article. This work was supported by a Grant-in-Aid for Scientific Research (KAKEN) (B) (19H0312) from the Japan Society for the Promotion of Science (JSPS).

Acknowledgments

We thank Dr. Takayuki Nakagawa, Ph.D. DVM. Department of Veterinary Surgery, University of Tokyo, for kindly providing the canine malignant melanoma lines CMM2, CMeC2, and LMeC. The authors would like to thank the International Council for Laboratory Animal Science (ICLAS) Monitoring Center, Central Institute for Experimental Animals, for the microbiological monitoring of the mice.

Conflict of interest

The authors declare that the research was conducted in the absence of any commercial or financial relationships that could be construed as a potential conflict of interest.

Generative AI statement

The author(s) declare that no Gen AI was used in the creation of this manuscript.

Publisher's note

All claims expressed in this article are solely those of the authors and do not necessarily represent those of their affiliated organizations, or those of the publisher, the editors and the reviewers. Any product that may be evaluated in this article, or claim that may be made by its manufacturer, is not guaranteed or endorsed by the publisher.

Supplementary material

The Supplementary Material for this article can be found online at: https://www.frontiersin.org/articles/10.3389/fvets.2025.1552415/full#supplementary-material

References

1. Wheatley SP, Altieri DC. Survivin at a glance. *J Cell Sci.* (2019) 132:jcs223826. doi: 10.1242/jcs.223826

2. Garg H, Suri P, Gupta JC, Talwar GP, Dubey S. Survivin: a unique target for tumor therapy. *Cancer Cell Int*. (2016) 16:49. doi: 10.1186/s12935-016-0326-1

3. Noton EA, Colnaghi R, Tate S, Starck C, Carvalho A, Ko Ferrigno P, et al. Molecular analysis of survivin isoforms: evidence that alternatively spliced variants do not play a role in mitosis. *J Biol Chem.* (2006) 281:1286–95. doi: 10.1074/jbc.M508773200

4. Song Z, Wu M. Identification of a novel nucleolar localization signal and a degradation signal in survivin-deltaEx3: a potential link between nucleolus and protein degradation. *Oncogene.* (2005) 24:2723–34. doi: 10.1038/sj.onc.1208097

5. Pavlyukov MS, Antipova NV, Balashova MV, Vinogradova TV, Kopantzev EP, Shakhparonov MI. Survivin monomer plays an essential role in apoptosis regulation. *J Biol Chem*. (2011) 286:23296–307. doi: 10.1074/jbc.M111.237586

6. Islam A, Kageyama H, Hashizume K, Kaneko Y, Nakagawara A. Role of survivin, whose gene is mapped to 17q25, in human neuroblastoma and identification of a novel dominant-negative isoform, survivin-beta/2B. *Med Pediatr Oncol.* (2000) 35: 550–3. doi: 10.1002/1096-911x(20001201)35:6<550::aid-mpo12>3.0.co;2-y

7. Rebhun RB, Lana SE, Ehrhart EJ, Charles JB, Thamm DH. Comparative analysis of survivin expression in untreated and relapsed canine lymphoma. *J Vet Intern Med*. (2008) 22:989–95. doi: 10.1111/j.1939-1676.2008.0143.x

8. Bongiovanni L, D'Andrea A, Porcellato I, Ciccarelli A, Malatesta D, Romanucci M, et al. Canine cutaneous melanocytic tumours: significance of β-catenin and survivin immunohistochemical expression. *Vet Dermatol.* (2015) 26:270–e59. doi: 10.1111/vde.12211

9. Scase TJ, Edwards D, Miller J, Henley W, Smith K, Blunden A, et al. Canine mast cell tumors: correlation of apoptosis and proliferation markers with prognosis. *J Vet Intern Med*. (2006) 20:151–8. doi: 10.1111/j.1939-1676.2006.tb02835.x

10. Murakami M, Sakai H, Kodama A, Mori T, Maruo K, Yanai T, et al. Expression of the anti-apoptotic factors Bcl-2 and survivin in canine vascular tumours. *J Comp Pathol.* (2008) 139:1–7. doi: 10.1016/j.jcpa.2008.02.001

11. Rankin WV, Henry CJ, Turnquist SE, Turk JR, Beissenherz ME, Tyler JW, et al. Comparison of distributions of survivin among tissues from urinary bladders of dogs with cystitis, transitional cell carcinoma, or histologically normal urinary bladders. *Am J Vet Res.* (2008) 69:1073–8. doi: 10.2460/ajvr.69.8.1073

12. Fossey SL, Liao AT, McCleese JK, Bear MD, Lin J, Li PK, et al. Characterization of STAT3 activation and expression in canine and human osteosarcoma. *BMC Cancer*. (2009) 9:81. doi: 10.1186/1471-2407-9-81

13. Bongiovanni L, Colombi I, Fortunato C, Della Salda L. Survivin expression in canine epidermis and in canine and human cutaneous squamous cell carcinomas. *Vet Dermatol.* (2009) 20:369–76. doi: 10.1111/j.1365-3164.2009.00822.x

14. Yamazaki H, Takagi S, Hoshino Y, Hosoya K, Okumura M. Inhibition of survivin influences the biological activities of canine histiocytic sarcoma cell lines. *PLoS ONE*. (2013) 8:e79810. doi: 10.1371/journal.pone.0079810

15. Fu DR, Kato D, Watabe A, Endo Y, Kadosawa T. Prognostic utility of apoptosis index, Ki-67 and survivin expression in dogs with nasal carcinoma treated with orthovoltage radiation therapy. *J Vet Med Sci*. (2014) 76:1505–12. doi: 10.1292/jvms.14-0245

16. Bongiovanni L, Caposano F, Romanucci M, Grieco V, Malatesta D, Brachelente C, et al. Survivin and Sox9: potential stem cell markers in canine normal, hyperplastic, and neoplastic canine prostate. *Vet Pathol.* (2019) 56:200–7. doi: 10.1177/0300985818794161

17. Godizzi F, Armando F, Boracchi P, Avallone G, Stefanello D, Ferrari R, et al. Survivin, β-catenin, and ki-67 immunohistochemical expression in canine perivascular wall tumors: preliminary assessment of prognostic significance. *Vet Pathol.* (2024) 61:912–27. doi: 10.1177/03009858241246981

18. Wadhwa R, Wang J, Shefrin S, Zhang H, Sundar D, Kaul SC. Molecular insights into the anticancer activity of withaferin-A: the inhibition of survivin signaling. Cancers. (2024) 16:3090. doi: 10.3390/cancers16173090

19. Kondapuram SK, Ramachandran HK, Arya H, Coumar MS. Targeting survivin for cancer therapy: strategies, small molecule inhibitors and vaccine based therapeutics in development. *Life Sci.* (2023) 335:122260. doi: 10.1016/j.lfs.2023.122260

20. Endo Y, Saeki K, Watanabe M, Miyajima-Magara N, Igarashi M, Mochizuki M, et al. Spindle assembly checkpoint competence in aneuploid canine malignant melanoma cell lines. *Tissue Cell.* (2020) 67:101403. doi: 10.1016/j.tice.2020.101403

frontiers | Frontiers in Veterinary Science

TYPE Original Research
PUBLISHED 25 April 2025
DOI 10.3389/fvets.2025.1486786

Check for updates

OPEN ACCESS

EDITED BY
Yasunaga Yoshikawa,
Kitasato University, Japan

REVIEWED BY
Claudio Gustavo Barbeito,
National University of La Plata, Argentina
Eva-Maria Packeiser,
University of Veterinary Medicine Hannover, Germany
Ana Files,
Universidade de Trás os Montes e Alto Douro, Portugal

*CORRESPONDENCE
Omid Nekouei
✉ omid.nekouei@cityu.edu.hk
Antonio Giuliano
✉ dr.giuliano@hvoc.com.hk

RECEIVED 26 August 2024
ACCEPTED 04 April 2025
PUBLISHED 25 April 2025

CITATION
Chu KT, Nekouei O and Giuliano A (2025) Treatment outcomes of dogs with transitional cell carcinoma.
Front. Vet. Sci. 12:1486786.
doi: 10.3389/fvets.2025.1486786

COPYRIGHT
© 2025 Chu, Nekouei and Giuliano. This is an open-access article distributed under the terms of the Creative Commons Attribution License (CC BY). The use, distribution or reproduction in other forums is permitted, provided the original author(s) and the copyright owner(s) are credited and that the original publication in this journal is cited, in accordance with accepted academic practice. No use, distribution or reproduction is permitted which does not comply with these terms.

Treatment outcomes of dogs with transitional cell carcinoma

Ka To Chu[1], Omid Nekouei[2]* and Antonio Giuliano[1,3]*

[1]Veterinary Medical Centre, City University of Hong Kong, Kowloon, Hong Kong SAR, China, [2]Department of Infectious Diseases and Public Health, Jockey Club College of Veterinary Medicine and Life Sciences, City University of Hong Kong, Kowloon, Hong Kong SAR, China, [3]Department of Veterinary Clinical Science, Jockey Club College of Veterinary Medicine and Life Sciences, City University of Hong Kong, Kowloon, Hong Kong SAR, China

Transitional cell carcinoma (TCC) is the most prevalent cancer of the urinary tract in dogs. The prognosis is often poor, and the optimal standard treatment has not been established. The objectives of this study were to (1) describe the clinical outcomes of dogs with TCC, and (2) determine the potential effects of tumor locations and treatment modalities on the survival times of patients. Electronic records of client-owned dogs with TCC treated with different modalities in a large veterinary hospital in Hong Kong (2005–2024) were evaluated. Of 84 confirmed cases included in the study, 49 (58.3%) died or were euthanized due to TCC. Tumors were located in the bladder neck or trigone region (41), apex (26), prostate (10), and urethra (7). Metastases were detected in 10 patients (12%) at diagnosis, including 4 peripheral lymph nodes, 4 lungs, and 2 in the lumbar spine. Of 84 cases, 4 (4.8%) did not receive any treatments, 14 (16.7%) underwent surgery, 25 (29.7%) received metronomic chemotherapy with chlorambucil with/without methotrexate, 27 (32.1%) received COX-2 inhibitors alone, and 14 (16.7%) received conventional chemotherapy, of which, 5 were later switched to metronomic chemotherapy. The overall median survival time was 233 days. There was no statistically significant difference in patients' survival between tumor locations ($p > 0.05$), aside from tumors involving the prostate that had the shortest MST (88 days). Metronomic chemotherapy led to a significantly longer survival time (median of 303 days) than the other treatment groups ($p < 0.05$), with the lowest incidence of adverse events. Metronomic chemotherapy using chlorambucil was well-tolerated and can be considered as a single modality treatment or as adjunctive therapy to conventional chemotherapy in dogs with TCC.

KEYWORDS

canine, chlorambucil, metronomic chemotherapy, TCC, transitional cell carcinoma, urinary bladder mass

Introduction

Canine transitional cell carcinoma (TCC), also referred to as urothelial carcinoma, is the most common malignant neoplasm of the urinary tract in dogs, accounting for about 1.5 to 2% of all canine cancers (1, 2). Certain breeds, such as Scottish terriers, Shetland sheepdogs, and West Highland white terriers (1, 3) are predisposed to TCC (1, 3). The tumor is aggressive, invading the urinary bladder wall, and often metastasizes to the regional lymph nodes and distant organs, with the metastatic disease found in more than half of the patients at necroscopy (4, 5). However, most dogs are usually euthanized due to the progression of the local disease and/or lower urinary tract obstruction (6). The clinical signs of TCC are nonspecific and include haematuria, dysuria, pollakiuria, stranguria, and urinary obstruction (2, 4).

The prognosis of canine TCC is generally poor, with most patients surviving less than a year despite treatment (7, 8). The most common treatment options for canine TCC consist of

chemotherapy often with mitoxantrone, carboplatin, gemcitabine, doxorubicin and vinblastine (9–15). Non-steroidal anti-inflammatory drugs (NSAIDs) with cyclooxygenase-2 (COX-2) inhibiting properties, especially piroxicam and meloxicam are often used alone or in combination with chemotherapy (11, 15–19). The role of surgery in the treatment of TCC is still controversial (4, 20). Most canine TCCs are located in the trigonal region of the urinary bladder where surgery is usually not feasible (10). Even when the tumor is located away from the trigone and resected with complete margins, recurrence is often seen due to urinary bladder field cancerization (21, 22). Despite surgery alone is unlikely to be effective, a combination of surgery and chemotherapy has shown some promising results (2, 4, 6–8, 11, 16, 17). Unfortunately, the aforementioned therapies are all accompanied by a common incidence of adverse events, impacting the patient's quality of life, which is one of the major reasons patients were elected to be euthanized in some of the cases.

In addition to conventional chemotherapy agents, metronomic chemotherapy has emerged as a promising alternative or adjunctive treatment for canine TCC. Metronomic chemotherapy refers to a continuous and repetitive administration of a chemotherapeutic agent at a lowered dose, contrasting to a conventional regime, where agents are usually administered at maximum tolerated dose as boluses with longer intervals. Chlorambucil is an alkylating agent that inhibits DNA synthesis and functions by cross-linking with cellular DNA (23–25). It has direct anti-tumor effects, inhibiting angiogenesis and immunomodulatory properties that suppress tumor growth (23). In a prospective study on metronomic chemotherapy on canine TCC patients, chlorambucil showed 70% clinical benefit, with a good safety profile, as only 23% of dogs developed mild adverse events (25).

Currently, there is little data on canine tumor cell carcinoma and its treatment options in Asia, and no literature comparing the efficacy and adverse events of metronomic chlorambucil with other approaches. This retrospective study analyzed dogs with TCC treated at a Hong Kong veterinary hospital (2005–2024) to (1) describe their clinical outcomes and assess the impact of tumor location (bladder apex, bladder neck/trigone, prostate, urethra) and (2) treatment modalities (surgery, COX-2 inhibitors, conventional and metronomic chemotherapy) on patient survival.

Methods

Data collection

The electronic database of a tertiary referral veterinary hospital was searched for all canine patients diagnosed with TCC between January 2005 and March 2024. After complete data extraction, all patients meeting the following criteria were included in our study: (1) dogs with confirmed TCC diagnosis by a board-certified pathologist using cytology, histopathology, or CADET BRAF mutation test by a reference laboratory, (2) complete records including the date of birth and death, record of TCC diagnosis, record of surgery in our hospital or dispensation of TCC therapies, and (3) at least one revisit following the initial consultation on the medical records, with the documentation of adverse events between visit(s). Collected data included age at the time of diagnosis, breed, sex, neuter status, the location of TCC, type of treatment, dose, and number of chemotherapy treatments administered, observed adverse events, clinical response, objective response, and patient outcomes.

Treatments

For statistical analysis, administered treatments to the study cases were categorized into five groups: (1) surgery plus COX-2 inhibitors, (2) conventional chemotherapy alone, (3) metronomic chemotherapy alone, (4) metronomic following conventional chemotherapy (patients who responded well to chemotherapy and their stable disease status were maintained with metronomic chemotherapy), and (5) COX-2 inhibitors alone.

Surgery consisted of a partial cystectomy to remove tumors with as wide margins as possible. Long-term COX-2 inhibitors were prescribed following surgery. The most common agent used was oral piroxicam (0.3 mg/kg once daily). Chemotherapy agents in this study included various intravenous administration of mitoxantrone (5–6 mg/m^2 every 21 days), carboplatin (200–300 mg/m^2, with a lower dose in smaller patients), and vinblastine (2 mg/m^2). Based on the clinician's preference, each protocol had chemotherapy agents in different orders. Metronomic chemotherapy consisted of the oral administration of chlorambucil at home, commonly in combination with a reduced dose of a COX-2 inhibitor. The chlorambucil dosage was 4 mg/m^2 every 24 h, or every other day, often in combination with the standard dose of meloxicam 0.1 mg/kg, with/without the combination of oral methotrexate 2.5 mg weekly or biweekly, adjusted based on the weight of the dog and clinician's preference. Metronomic following conventional chemotherapy referred to the group who switched to metronomic chemotherapy after the initiation of conventional chemotherapy. In the group of COX-2 inhibitors alone, oral piroxicam as a single agent (0.3 mg/kg once daily or every other day) was the most used agent. When administered in the metronomic setting, most dogs received meloxicam (0.1 mg/kg once daily), while the most common adjuvant COX-2 inhibitor given after surgery or a single agent was piroxicam (0.3 mg/kg once daily). Table 1 has summarized the treatment options for comparison.

Tumor locations

The location of TCC is determined by imaging, most commonly with abdominal ultrasonography, sometimes with computed tomography when full staging was performed. Locations were categorized into four groups, namely bladder apex, neck, prostate, and urethra. If a tumor demonstrated a diffuse pattern or neoplastic lesions were found in more than one location, the largest measurable lesion represented the location of this tumor.

Response to therapy

Evaluation of the response was based on the Veterinary Cooperative Oncology group's RECIST response in solid tumors (26). The assessment of the response to treatment and subsequent monitoring were conducted

Abbreviations: CBR, clinical benefit rate; CR, complete response; CRR, clinical response rate; COX-2, cyclooxygenase-2; MST, median survival time; NSAIDS, Non-steroidal anti-inflammatory drugs; ORR, objective response rate; PD, progressive disease; PFS, progression-free survival; PR, partial response; SD, stable disease; TCC, Transitional cell carcinoma.

TABLE 1 Summary of treatment groups.

Treatment group	Treatment description	Specific doses
Surgery	Partial cystectomy + long term oral COX-2 inhibitors	Oral piroxicam, 0.3 mg/kg SID
Conventional chemotherapy	Intravenous administration of a single or combination of chemotherapeutic agents	Mitoxantrone (5–6 mg/m^2 every 21 days), carboplatin (200–300 mg/m^2, with a lower dose in smaller patients), and vinblastine (2 mg/m^2); variable
Metronomic chemotherapy	Oral administration of chlorambucil at home	Oral chlorambucil at 4 mg/m^2 SID/EOD, +/− oral meloxicam 0.1 mg/kg SID, +/− oral methotrexate 2.5 mg weekly or biweekly
Metronomic following conventional chemotherapy	Metronomic chemotherapy after the completion of a full course of chemotherapy	As above
COX-2 inhibitors only	Utilize COX-2 inhibitors as the only therapeutic agents	Oral piroxicam as a single agent (0.3 mg/kg SID/EOD) or meloxicam (0.1 mg/kg SID) most commonly

using clinical examination, diagnostic imaging, and ultrasonography. The response was assessed by measuring the mass/masses/lesions before and during the regular follow-up. Complete response (CR) was defined as the resolution of all clinical and imaging-based evidence of the disease; partial response (PR) was defined as a decrease of at least 30% in tumor diameter with no new lesions; stable disease (SD) was defined as neither sufficient shrinkage to qualify as PR nor sufficient increase to qualify as progressive disease (PD). Progressive disease was defined as an increase in tumor diameter greater than 20% or the development of new lesions. Objective response rate (ORR) was defined as CR + PR. Clinical benefit rate (CBR) was defined as CR + PR + SD. A clinical response rate (CRR) was also calculated based on the improvement in clinical signs. For all patients included in the study, the progression-free survival was calculated in days from the date of the first chemotherapy treatment to the date of disease progression. Survival time for each patient was calculated from the TCC diagnosis to the date of death, euthanasia, or loss at follow-up. All observed adverse events were graded based on the Veterinary Cooperative Oncology Group Common Terminology Criteria for Adverse Events (VCOG-CTCAE v2) (27).

Statistical analyses

All statistical analyses were conducted using Stata v18 (StataCorp LLC, College Station, United States). Descriptive statistics (e.g., median and range) for the survival times of patients were calculated and tabulated by the available explanatory variables. In survival analyses, death due to TCC was defined as the outcome of interest. Kaplan–Meier survival curves were created to visualize the survival of patients by tumor locations and treatment groups. The survival time and progression-free survival (PFS) were compared across tumor locations and treatment groups using the Wilcoxon–Breslow test. The PFS was defined as the time from the diagnosis until PD. Survival time was defined as the time from the diagnosis until death. To control the potential confounding effect of tumor location on treatment outcomes, the survival times of patients in different treatment groups were also compared in dogs that had TCC only in their bladder apex using the Wilcoxon-Breslow test.

Results

Initially, 134 cases with suspected transitional cell carcinoma (TCC) were identified, but only 84 cases met the selection criteria. The majority of the excluded cases never had a definitive diagnosis nor returned for rechecks after the initial consultation. Cases without complete documentation of clinical response or tests performed were not included in this study. The frequency distribution of all cases by signalments, tumor location, and treatment modality has been presented in Table 2. Of the 84 patients, 46 were males (55%) and 38 females (45%), with 90.5% being neutered and 93% being purebred (Table 2). Patients were between 7 and 17.5 years old at the time of diagnosis, with a median of 12 years. Of the 84 patients, 41 had TCC in their bladder neck or trigone region, 26 in the apex, 10 in the prostate, and the remaining 7 had urethral involvements. Some forms of staging were performed in all cases but using different modalities. Abdominal ultrasound was performed in all cases. Thoracic radiography and CT-scan were conducted on 19 and 7 cases, respectively. Metastases were detected in 10 patients (12%) at diagnoses, of which, 4 had metastasis in peripheral lymph nodes, 4 had pulmonary metastasis and 2 had metastatic lesions in their lumbar spine. Among these 10 metastatic patients, 6 dogs had TCC in their trigone, 2 in the apex, and 2 in the prostate. A table showing all the patients, including but not limited to outcomes, treatment groups, location groups and adverse events, is provided as a Supplementary material to this study.

Patient outcome

Of the 84 dogs, 49 cases (58.3%) died or were euthanized due to TCC (11 with metastases and 38 due to the local progression). Twelve patients (14.3%) died of other diseases unrelated to TCC. Until the end of the study (March 2024), 10 patients (11.9%) were still alive, and 13 (15.5%) were lost to follow-up. The survival time of patients ranged between 1 and 1,184 days with a median of 233 days. The PFS ranged from 1 to 862 with a median of 177.5 days. The Kaplan–Meier survival curve for all patients by the four tumor locations is illustrated in Figure 1.

Treatments

Of the 84 cases, 4 (4.8%) did not receive any treatments, and 25 (29.8%) received metronomic chemotherapy with chlorambucil, with/without methotrexate. Twenty-seven patients (32.1%) only received COX-2 inhibitors. Of the patients receiving metronomic chemotherapy, 82% also received COX-2 inhibitors. All 9 patients undergoing conventional chemotherapy (10.7%) also received adjunct

TABLE 2 Frequency distribution of 84 dogs with TCC in the study by available explanatory variables.

Variable	Category	Number	%
Sex/Neuter status	Spayed female	35	41.7
	Intact female	3	3.6
	Castrated male	41	48.8
	Intact male	5	6.0
Breed	Poodle	11	13.1
	Schnauzer	7	8.3
	Yorkshire terrier	7	8.3
	Shetland sheepdog	6	7.1
	Pomeranian	6	7.1
	Mongrel	6	7.1
	Shih Tzu	5	6.0
	Others[a]	36	42.9
Age group (year)	7 to <10	16	19.0
	10 to 13	39	46.4
	>13 to 17.5	20	23.8
Tumor location	Urethra	7	8.4
	Bladder neck/trigone	41	48.8
	Prostate	10	11.9
	Bladder apex	26	30.9
Treatment	No treatment	4	4.8
	Surgery	14	16.7
	Conventional chemotherapy	9	10.7
	Metronomic chemotherapy	25	29.8
	Metronomic following conventional chemotherapy	5	5.9
	COX-2 inhibitors	27	32.1

[a]Includes all other pure breeds with low numbers (<4).

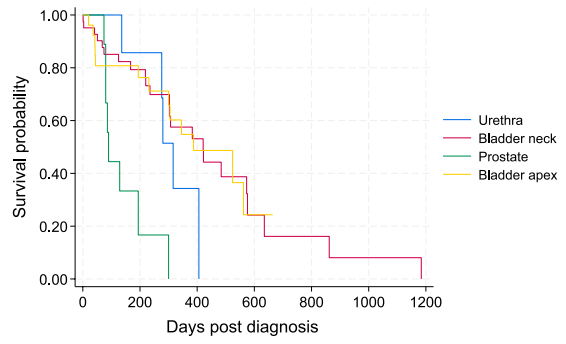

FIGURE 1
Kaplan–Meier survival curve for all 84 study dogs with TCC by tumor location.

COX-2 inhibitors. Five patients (5.9%) received metronomic chemotherapy following conventional chemotherapy. Among these 5 cases, 3 switched because of tumor progression, and 2 received metronomic when stable disease was achieved. Of the 14 patients undergoing surgery, 4 had incomplete excision and 10 had complete excision confirmed in histopathology. Of these 14 cases, 10 also received adjunct COX-2 inhibitors, and 4 received no other treatments.

Responses of all patients to the treatment groups are detailed in Table 3. Patients receiving conventional chemotherapy alone had an ORR of 22% and a CBR of 55%. For the metronomic chemotherapy group, ORR and CBR were 0 and 83.3%, respectively. For patients treated with COX-2 inhibitors alone, ORR was 7.4% and CBR was 85.2%. The five patients treated with metronomic chemotherapy following conventional chemotherapy had ORR and CBR of 0 and 40%, respectively. The CRR was 100% for all three chemotherapy groups, while CRRs for surgery and COX-2 inhibitor groups were 71.4 and 81.5%, respectively (Table 3). The owners of all 4 patients who received no treatments reported worsening clinical signs, one patient remained stable and 3 had progressive diseases.

Adverse events

Among the 14 surgery patients, 8 (57.1%) developed gastrointestinal adverse events, including vomiting, diarrhea, melena

TABLE 3 Responses of 84 study dogs with TCC to the four treatment groups.

Treatment[a]	No. of patients	Complete response (CR)	Partial response (PR)	Stable disease (SD)	Progressive disease (PD)	Objective response rate (ORR)	Clinical benefit rate (CBR)	Clinical response rate (CRR)
Conventional chemotherapy	9	0	2 (22.2%)	3 (33.3%)	4 (44.5%)	2 (22.2%)	5 (55.5%)	9 (100%)
Metronomic chemotherapy	25	0	0	22 (83.35)	3 (16.7%)	0	22 (83.3%)	25 (100%)
Metronomic following conventional chemotherapy	5	0	0	2 (40%)	3 (60%)	0	2 (40%)	5 (100%)
COX-2 inhibitors	27	0	2 (7.4%)	21 (77.8%)	4 (14.8%)	2 (7.4%)	23 (85.2%)	22 (81.5%)

[a]Surgery was not included in the table as the only outcomes were complete or incomplete excision, so response could not be measured.

and hyporexia (Veterinary Cooperative Oncology Group Common Terminology Criteria for Adverse Events Grade 1), 2 (14.3%) dogs died of postoperative complications, and the remaining 4 (28.6%) had no reported adverse events.

Of the 9 conventional chemotherapy cases, 2 (22.2%) developed Grade 1 GI adverse events, 3 (33.4%) had Grade 2 adverse events, such as hematemesis or mild neutropenia, and 2 (22.2%) developed Grade 3 adverse effects, such as lethargy or thrombocytopenia. The remaining 2 cases (22.2%) experienced no adverse events.

Of the 25 patients receiving metronomic chemotherapy, 12 (48%) dogs experienced no adverse events, 10 (40%) showed Grade 1 adverse events, 3 (12%) developed Grade 2 adverse events, including lethargy and listlessness, and no Grade 3 toxicity was reported. Of the 5 patients who received a combination of metronomic and conventional chemotherapy, 2 (40%) had Grade 1 adverse events, 1 (20%) had Grade 2 adverse events, 1 (20%) had Grade 3 adverse events, and 1 (20%) had no adverse events.

Among the 27 patients receiving COX-2 inhibitors alone, 12 (44.5%) dogs had no adverse events, 13 (48.1%) developed Grade 1 GI adverse events, 1 (3.7%) had Grade 2 adverse events, and 1 (3.7%) showed Grade 3 adverse events (azotemia).

Location effects

Patients with TCC in their prostates had significantly shorter survival times than those with tumors in the other three locations in the Wilcoxon tests ($p < 0.05$). There was no statistically significant difference in survival of patients between bladder neck/trigon, apex, and urethra (Figure 1). The Kaplan–Meier curve for PFS of patients by tumor location is depicted in Figure 2. The PFS of patients was significantly shorter in the prostate cases (PFS = 61.5 days) compared to the urethra and bladder neck (178 and 222 days, $p = 0.044$ and $p = 0.003$, respectively), but not significantly different than the apex ($p = 0.104$). There was no significant difference in PFS between the urethra, bladder neck, and apex (all $p > 0.05$).

The four tumor locations were further categorized into two main groups based on their likelihood for early urinary obstruction and to allow a more meaningful comparison: the apex of the bladder (the location considered less likely to cause an early urinary obstruction) versus other locations combined, including the bladder neck, prostate, and urethra (i.e., locations with a higher likelihood of causing early urinary obstruction) (Figure 3). There was no statistically significant difference in the survival of patients between the bladder apex and other locations in the Wilcoxon test ($p = 0.573$).

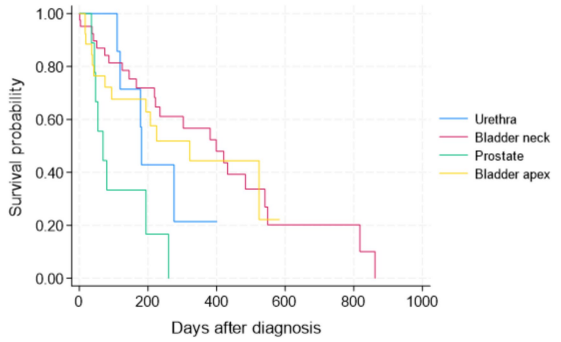

FIGURE 2
Kaplan–Meier progression-free survival (PFS) curve for all 84 study dogs with TCC by tumor location.

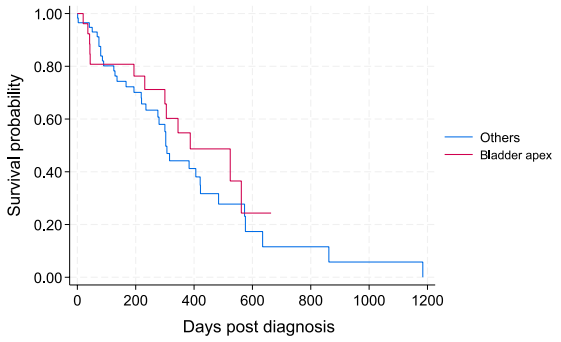

FIGURE 3
Kaplan–Meier survival curve for study dogs with TCC by two main locations; i.e., the apex of urinary bladder versus other locations (bladder neck, prostate, urethra).

Treatment effects

To better assess the potential effects of treatments on the survival of patients, the 5 cases that received metronomic chemotherapy following conventional chemotherapy were removed from the comparisons, as there is potential carryover effect on the metronomic component from the conventional chemotherapy. The Kaplan–Meier survival curve for the four main treatment groups (surgery plus COX-2, conventional chemotherapy, metronomic chemotherapy, and COX-2 inhibitors alone) is presented in Figure 4. There was a statistically significant difference in the survival of patients between the metronomic chemotherapy and the other three treatment groups in the Wilcoxon tests ($p < 0.05$). There was no statistically significant difference between surgery, conventional chemotherapy alone, and COX-2 inhibitors groups (Figure 4). The Kaplan–Meier curve for PFS of patients under the four treatments is depicted in Figure 5. Similarly, the only statistically significant difference in PFS of patients was due to the difference between the metronomic chemotherapy group and the others ($p < 0.05$).

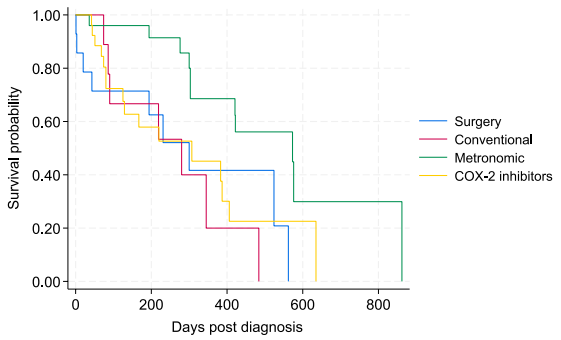

FIGURE 4
Kaplan–Meier survival curve for study dogs with TCC under four types of treatment, including surgery (plus COX-2 inhibitors), conventional chemotherapy alone, metronomic chemotherapy, and COX-2 inhibitors alone.

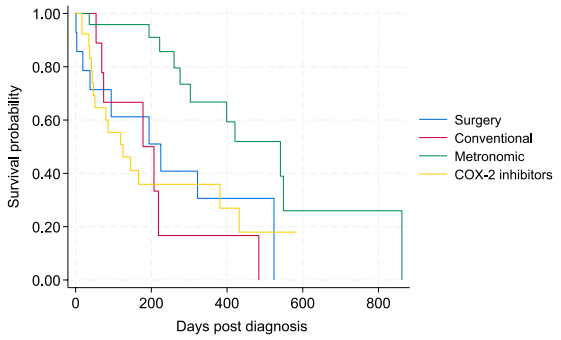

FIGURE 5
Kaplan–Meier progression-free survival (PFS) curve for study dogs with TCC under four types of treatment, including surgery (plus COX-2 inhibitors), conventional chemotherapy alone, metronomic chemotherapy, and COX-2 inhibitors alone.

The medians of survival time and PFS for dogs who died of TCC are presented by tumor locations and treatments in Table 4, indicating MST was the longest for the three chemotherapy groups, especially for those dying after metronomic chemotherapy (303 days). Survival times for the 4 patients who did not receive any treatments were 41, 305, 276, and 316 days.

To account for any potential confounding effect of location, the survival time comparison between the four treatments was restricted to dogs with TCC on their bladder apex only ($n = 25$), no significant difference between the treatments was observed ($p = 0.738$).

Discussion

This study compiled all canine TCC patients treated in a large veterinary hospital, including 84 confirmed cases treated with different modalities. We aimed to describe the clinical outcomes and assess the impact of tumor location and treatment modalities on patient survival.

In our study, metronomic chemotherapy using chlorambucil, with or without methotrexate, resulted in longer survival compared to other treatment options, with a median survival time (MST) of 303 days, consistent with findings reported in previous studies (25). As mentioned above, metronomic administration of chlorambucil offers anti-angiogenesis and immunomodulatory effects to reduce tumor growth. Growth of solid tumor is often accompanied by angiogenesis. A low-dose, continuous administration of chemotherapeutic agents was found to have sustained apoptotic effects on endothelial cells of tumors, thus disrupting and destroying the vascular tumor bed, achieving antitumor effects (28). Moreover, the immunomodulating effects of metronomic chemotherapy might

TABLE 4 Distribution of survival time (ST) and progression-free survival (PFS) of study dogs who died of TCC by tumor location and treatment group.

Variable	Category	No. of death	Median ST (range)	Median PFS (range)
Tumor location	Urethra	5	280 (136–406)	178 (110–276)
	Bladder neck/trigone	23	303 (1–1,184)	222 (1–862)
	Prostate	8	88 (74–300)	61.5 (35–260)
	Bladder apex	13	231 (20–562)	75 (17–524)
Treatment	Surgery (plus COX-2 inhibitors)	9	194 (1–562)	94 (1–524)
	Conventional chemotherapy	7	219 (74–484)	178 (54–484)
	Metronomic chemotherapy	11	303 (36–862)	303 (36–862)
	Metronomic following conventional	3	235 (136–1,184)	235 (110–818)
	COX-2 inhibitors	16	127 (42–635)	65.5 (17–432)

potential benefit its antitumor function: by acting on immunosuppressive cells and allowing T cell and NK cells to infiltrate and attack tumors (29). Metronomic chlorambucil can offer TCC canine patients a promising alternative to traditional chemotherapy or COX-2 inhibitors. Furthermore, metronomic chemotherapy led to the longest PFS compared to other treatment options, indicating that it might offer longer survival in combination with a good quality of life. Potentially, dogs with advanced muscle invasive TCC can be considered a model for similar tumors in humans. Metronomic chemotherapy could also be investigated to be a treatment strategy that could be used in advanced bladder tumors in people when standard treatment have failed.

We initially expected that the combination of metronomic and conventional chemotherapy would result in longer survival than metronomic chemotherapy alone. However, our findings showed the opposite, with a shorter survival time in this group. Nonetheless, the small number of patients in the combined group could be the reason for this observation; therefore, we did not include this group in our direct statistical comparisons. The combined group only included 5 patients with 3 deaths, of which, 3 switched to metronomic chemotherapy due to progression or metastasis, suggesting a more aggressive tumor or a more advanced stage of disease that could have reduced the overall survival time in this group. The remaining 2 patients (of 5) that were switched to metronomic chemotherapy after achieving stable disease over conventional chemotherapy protocol had longer survival times of 401 and 1,184 days, and PFS of 401 and 818 days, respectively. Well-designed prospective studies with a larger number of cases are required to enable a robust comparison of patients' outcomes between metronomic chemotherapy alone and a sequential combination of conventional and metronomic chemotherapy.

We hypothesized that the tumor location could affect the survival of patients with TCC. Iwasaki et al. (5) stated that patients with TCC in their bladder had significantly longer survival than urethra. In their study, urethral TCCs were found to have a significantly higher metastatic rate than TCCs in the bladder, thus shorter survival. Although full tumor staging was not performed in our patients, we can still hypothesize that TCC in the bladder apex may have a better prognosis than urethra and trigone as it is less likely to grow in an area of the bladder that would cause a more rapid urine outflow obstruction (10). Furthermore, complete surgical excision is more likely for apical masses compared to locations like the trigone. When comparing patient outcomes across different tumor locations, no significant difference in survival was observed. However, prostatic carcinomas had a significantly lower survival rate compared to tumors in other locations, a finding previously reported in the literature (1). It is often difficult to differentiate primary prostatic carcinoma from bladder TCC invading the prostate and it is possible that some of these tumors were prostatic adenocarcinoma rather than TCC. It is well known that prostatic adenocarcinoma has a poor prognosis both due to local rapid invasion causing early clinical signs of urinary obstruction and a higher metastatic rate (30). In our study, we also found that patients with prostate tumors had a higher metastatic rate (20%) compared to apex (7.7%), trigone (14.6%), and urethra (0%).

Tumor location could dictate the treatment offered by the clinicians (surgical versus non-surgical). To further account for any potential confounding effect of tumor location on the survival of treatment groups, we specifically compared the survival of patients between treatment groups only in apically located tumors which resulted in no significant difference in MST or PFS of the patients. The latter could suggest different types of treatment did not affect the survival of dogs with apical TCC, but this finding was not statistically robust and must be interpreted with caution due to the low number of cases within each treatment group (e.g., only one case in the conventional chemotherapy group) once we limited our data to the 26 cases of apical TCC only. When we specifically compare apically located masses with all other locations (non-apical masses), no significant difference in survival between the two main locations was found.

Because none of our surgery cases received adjuvant conventional or metronomic chemotherapy, we could not assess the potential additive effects of chemotherapy on surgery. According to Bradbury et al. (4), patients receiving a combination of partial cystectomy and medical therapy, which included chemotherapeutic agents and COX inhibitors, survived significantly longer than those who received medical therapy alone. Also, Molnár et al. reported that a combination of chemotherapy and surgery resulted in longer survival than chemotherapy or surgery alone (31). It would be interesting to compare our current treatment groups with surgical patients who also received chemotherapy, be it conventional or metronomic, and see if there is a survival benefit for a hybrid approach. Nonetheless, there are some risks of performing surgery in patients with TCC. Common complications of partial cystectomy in TCC post-operation include hematuria, pollakiuria, urinary incontinence, and dehiscence, with a reported complication rate of 43 to 81% in two studies (4, 32). Tumor seeding from partial cystectomy can also contribute to rapid regrowth or metastasis in patients who received surgery, leading to a poorer survival and outcome. One of the patients with trigonal TCC in this study was euthanized 1 day after surgery due to uroabdomen and dehiscence despite two revisit surgeries. There was another dog who received a partial cystectomy and passed away 3 days post-surgery at home due to an unknown reason. Another patient who had a complete excision, as confirmed by histopathology, died 20 days post-surgery due to immediate regrowth of the mass and spinal metastasis.

Most of the dogs who underwent surgical removal of TCC were administered COX-2 inhibitors as an adjuvant therapy. Theoretically, COX-2 inhibitors could delay the regrowth of the tumor by its antitumor effect as post-surgical adjuvant treatment (11). Although the MST of surgery plus COX-2 group (194 days) was higher than COX-2 alone (127 days) in our study, this difference was not statistically significant. Marvel et al. (20) reported that the MST of patients receiving daily administration of piroxicam combined with partial cystectomy reached 772 days, which was significantly longer than the survival times in TCC patients who underwent surgery alone. The paper pointed out that adding an adjuvant therapy to surgery might bring survival benefits to patients, but it is also worthwhile to consider the huge discrepancy in MST between our surgical patients and those in Marvel et al. Besides the difference in sample sizes, one of the theories is case selection. As previously mentioned, only a fraction of our sample was fully staged. There was a possibility that clients selected surgery for patients with metastasis or advanced disease, thus poor outcomes. In fact, one of the surgical patients in our study lived up to 562 days, which implied the importance of case selection when it comes to canine TCC (31). Considering the promising antitumoral effect of metronomic chemotherapy, future studies on the use of adjunct metronomic

chemotherapy in surgical patients may offer an alternative to adjuvant COX-2 inhibitors alone.

Ravicini et al. (33) reported that dogs receiving a combination of chemotherapy and COX-2 inhibitors had significantly longer survival times than those receiving COX-2 inhibitors alone. Knapp et al. (11) stated that dogs receiving cisplatin had an MST of 338 days while dogs receiving only firocoxib had an MST of 152 days, but the difference was not statistically significant. Although not directly comparable, in a clinical trial by Schrempp et al. (25), the MST for dogs with TCC receiving chlorambucil was 221 days, whereas the MST of dogs receiving only COX-2 inhibitors in another study was 181 days (16). TCC often causes obstruction in locations such as trigone, ureter, or with invasion into the prostate, and most patients had deteriorated quality of life and were euthanized when obstruction occurred (9). Chemotherapy and metronomic chemotherapy offer better outcomes compared to COX-2 inhibitors alone. Nevertheless, COX-2 inhibitors remain a sensible choice of treatment for cases who cannot receive or decline chemotherapy.

Metronomic chemotherapy with chlorambucil with or without methotrexate led to the lowest occurrence of adverse events among all treatment groups in our study. In Schrempp et al. (25), metronomic chemotherapy with chlorambucil as a treatment for TCC yielded a low rate of adverse events of 23%. Despite a higher rate of adverse events in this study (52%), the majority of the adverse events are low-grade and no grade 3 or above adverse event was reported (25). In another prospective study by Leach et al. (23), using chlorambucil in treating different cancers, metronomic chemotherapy rarely caused adverse events, and they were limited to grade 1 or 2. Our study echoes the previous studies in terms of safety profile in long-term use in our canine patients. COX-2 inhibitors can cause adverse renal or GI events; for example, melena, hematochezia, and hematemesis, especially when piroxicam is used for a long time (34, 35). Conventional chemotherapy resulted in the highest adverse events, including Grade 3 adverse events, such as lethargy and neutropenia, which were often resolved by postponing the next dose of injection (36). The lower rate of adverse events following metronomic chemotherapy not only can lead to a better life quality in patients but also allows better continuity and client compliance without treatment delay, resulting in potentially better outcomes. In addition to a safer toxicity profile, metronomic chemotherapy entails easier oral administration than conventional injectable chemotherapies, thus reducing the number of treatments and revisits and consequently lowering costs. Nearly half of the patients who received metronomic chlorambucil also received oral methotrexate in our study. Methotrexate is an oral antimetabolite chemotherapy mainly excreted by the urine and used in people with bladder cancer (37). Despite methotrexate being given at low doses, concentration in the urine for a long period could increase the cancer control rate for bladder TCC in dogs. Nonetheless, the fact that only 12 patients were treated with this combination precluded robust statistical comparison; therefore, further studies are needed to verify this assumption.

In our study, metronomic chemotherapy was associated with longer survival. However, no statistically significant difference was found between other treatment groups, such as COX-2 inhibitors alone and conventional chemotherapy. The potential benefit of continuing low doses of chemotherapy instead of high pulsatile doses of conventional chemotherapy, in slow-growing tumors, such as the case in some bladder TCC, is reasonable. However, a larger prospective study comparing metronomic, conventional, and metronomic plus conventional chemotherapies is needed to validate our findings. It should be noted that chlorambucil had a poor ORR for canine TCC in our study. Indeed, none of the dogs receiving chlorambucil had a measurable response upon therapy, indicating that metronomic chemotherapy can effectively slow the tumor growth, but its efficacy in reducing the size in extensive disease with partial or complete obstruction is limited and the selection of the treatment on a case-by-case basis is paramount. In advanced TCC affecting the urethra/trigonal area, conventional chemotherapy could be more likely to produce a favorable outcome or measurable response (8, 11, 17).

We had a group of patients ($n = 4$) who received no treatment in this study. It is emphasized that treatment options were recommended for these cases based on each patient's condition, but the owners declined. Under normal circumstances, no treatment is discouraged for animal welfare reasons. These 4 dogs had various survival times of 41, 305, 276, and 316 days. The relatively long survival times in three of these patients could have been due to being in the early stages of the disease. According to medical records, the patient who survived 41 days had evidence of metastasis in the lumbar spine whereas the remaining patients had no signs of metastasis on staging by radiography and ultrasonography.

There were some potential limitations to our study. The retrospective nature of the study does not allow for drawing strong inferences about the location and treatment effects and controlling for potential biases. As mentioned earlier, the low number of cases in some groups did not allow for robust statistical comparisons. For example, although we tried, we were not able to use more sophisticated survival analysis tests, such as the Cox proportional-hazards model to conduct multivariable analyses, as the underlying assumptions (e.g., proportional hazards) were not met. Staging and restaging of tumors were mainly done by ultrasound and the size and amount of urine were not standardized for comparison, hence the RR could have been under or overestimated. However, it should be noted that repeated CT scans for restaging, including general anesthesia, are rarely performed and carry extra costs for the owners. Although we have tried to eliminate the confounding effect of location and treatment, there is still a confounding factor we could not address due to the number of treatment categories and locations. Besides, the low number of observations with non-censored outcomes in some categories in age, breeds, and sub-categories made it impossible to completely eliminate confounders. Despite the outlined potential limitations, we believe including 84 TCC cases from nearly 20 years and handling the data with the ultimate care in this study have resulted in reliable and interesting findings, further contributing to the limited body of evidence on canine TCC topic and setting the stage for well-designed prospective studies (preferably clinical trials) addressing the highlighted gaps.

In conclusion, prostatic TCCs had significantly shorter survival time than TCC in other locations. Metronomic chemotherapy led to longer survival and PFS and the lowest occurrences of adverse events compared to other treatment options in our study. For tumors located in the bladder apical region, surgery in combination with COX-2 inhibitors resulted in comparable survival to metronomic

chemotherapy. Metronomic chemotherapy had relatively lower costs as a long-term control for canine TCC. While metronomic chemotherapy is promising as a relatively safe and effective treatment option for canine TCC, well-designed clinical trials are still recommended to establish the most effective treatment option/s by specific tumor location.

Data availability statement

The raw data supporting the conclusions of this article will be made available by the authors, without undue reservation.

Ethics statement

Ethical approval was not required for the studies involving animals in accordance with the local legislation and institutional. This is a retrospective study, with animals treated with the aim of minimal pain and suffering. No detrimental intervention was given for the purpose of this study. Written informed consent was not obtained from the owners for the participation of their animals in this study because Clients consented the use of patients' data when they agreed to terms at our tertiary veterinary service.

Author contributions

KC: Conceptualization, Data curation, Investigation, Methodology, Project administration, Resources, Validation, Writing – original draft, Writing – review & editing. ON: Data curation, Formal analysis, Methodology, Software, Validation, Visualization, Writing – original draft, Writing – review & editing. AG: Conceptualization, Investigation, Methodology, Project administration, Resources, Supervision, Validation, Writing – original draft, Writing – review & editing.

Funding

The author(s) declare that no financial support was received for the research and/or publication of this article.

Conflict of interest

The authors declare that the research was conducted in the absence of any commercial or financial relationships that could be construed as a potential conflict of interest.

The author(s) declared that they were an editorial board member of Frontiers, at the time of submission. This had no impact on the peer review process and the final decision.

Publisher's note

All claims expressed in this article are solely those of the authors and do not necessarily represent those of their affiliated organizations, or those of the publisher, the editors and the reviewers. Any product that may be evaluated in this article, or claim that may be made by its manufacturer, is not guaranteed or endorsed by the publisher.

Supplementary material

The Supplementary material for this article can be found online at: https://www.frontiersin.org/articles/10.3389/fvets.2025.1486786/full#supplementary-material

References

1. Mutsaers AJ, Widmer WR, Knapp DW. Canine transitional cell carcinoma. *J Vet Intern Med*. (2003) 17:136–44. doi: 10.1111/j.1939-1676.2003.tb02424.x

2. Norris AM, Laing EJ, Valli VEO, Withrow SJ, Macy DW, Ogilvie GK, et al. Canine bladder and urethral tumors: a retrospective study of 115 cases (1980–1985). *J Vet Intern Med*. (1992) 6:145–53. doi: 10.1111/j.1939-1676.1992.tb00330.x

3. Glickman LT, Schofer FS, McKee LJ, Reif JS, Goldschmidt MH. Epidemiologic study of insecticide exposures, obesity, and risk of bladder cancer in household dogs. *J Toxicol Environ Health*. (1989) 28:407–14. doi: 10.1080/15287398909531360

4. Bradbury ML, Mullin CM, Gillian SD, Weisse C, Bergman PJ, Morges MA, et al. Clinical outcomes of dogs with transitional cell carcinoma receiving medical therapy, with and without partial cystectomy. *Can Vet J*. (2021) 62:133–40.

5. Iwasaki R, Shimosato Y, Yoshikawa R, Goto S, Yoshida K, Murakami M, et al. Survival analysis in dogs with urinary transitional cell carcinoma that underwent whole-body computed tomography at diagnosis. *Vet Comp Oncol*. (2019) 17:385–93. doi: 10.1111/vco.12483

6. McKenna C, Poirier VJ, Oblak ML, Nykamp S, Mutsaers AJ. Reason for euthanasia in dogs with urothelial carcinoma treated with chemotherapy or radiation therapy or both: a retrospective observational study. *J Vet Intern Med*. (2024) 38:1127–34. doi: 10.1111/jvim.16994

7. Henry CJ. Management of transitional cell carcinoma. *Vet Clin N Am Small Anim Pract*. (2003) 33:597–613. doi: 10.1016/S0195-5616(03)00032-9

8. Ghisoni G, Foglia A, Sabattini S, Agnoli C, Dondi F, Perfetti S, et al. A retrospective Clinico-pathologic study of 35 dogs with urethral transitional cell carcinoma undergoing treatment. *Animals*. (2023) 13:2395. doi: 10.3390/ani13142395

9. Fulkerson CM, Knapp DW. Management of transitional cell carcinoma of the urinary bladder in dogs: a review. *Vet J*. (2015) 205:217–25. doi: 10.1016/j.tvjl.2015.01.017

10. Knapp DW, Glickman NW, DeNicola DB, Bonney PL, Lin TL, Glickman LT. Naturally-occurring canine transitional cell carcinoma of the urinary bladder a relevant model of human invasive bladder cancer. *Urol Oncol*. (2000) 5:47–59. doi: 10.1016/S1078-1439(99)00006-X

11. Knapp DW, Henry CJ, Widmer WR, Tan KM, Moore GE, Ramos-Vara JA, et al. Randomized trial of cisplatin versus Firocoxib versus cisplatin/Firocoxib in dogs with transitional cell carcinoma of the urinary bladder. *J Vet Intern Med*. (2013) 27:126–33. doi: 10.1111/jvim.12013

12. Abbo AH, Jones DR, Masters AR, Stewart JC, Fourez L, Knapp DW. Phase I clinical trial and pharmacokinetics of Intravesical Mitomycin C in dogs with localized transitional cell carcinoma of the urinary bladder. *J Vet Intern Med*. (2010) 24:1124–30. doi: 10.1111/j.1939-1676.2010.0569.x

13. Culp WTN, Weisse C, Berent AC, Reetz JA, Krick EL, Jackson DE, et al. Early tumor response to Intraarterial or intravenous Administration of Carboplatin to treat naturally occurring lower urinary tract carcinoma in dogs. *J Vet Intern Med*. (2015) 29:900–7. doi: 10.1111/jvim.12594

14. Arnold EJ, Childress MO, Fourez LM, Tan KM, Stewart JC, Bonney PL, et al. Clinical trial of vinblastine in dogs with transitional cell carcinoma of the urinary bladder. *J Vet Intern Med*. (2011) 25:1385–90. doi: 10.1111/j.1939-1676.2011.00796.x

15. Robat C, Burton J, Thamm D, Vail D. Retrospective evaluation of doxorubicin–piroxicam combination for the treatment of transitional cell carcinoma in dogs. *J Small Anim Pract*. (2013) 54:67–74. doi: 10.1111/jsap.12009

16. Knapp DW, Richardson RC, Chan TCK, Bottoms GD, Widmer WR, DeNicola DB, et al. Piroxicam therapy in 34 dogs with transitional cell carcinoma of the urinary bladder. *J Vet Intern Med*. (1994) 8:273–8. doi: 10.1111/j.1939-1676.1994.tb03232.x

17. Allstadt SD, Rodriguez CO, Boostrom B, Rebhun RB, Skorupski KA. Randomized phase III trial of Piroxicam in combination with Mitoxantrone or carboplatin for first-line treatment of urogenital tract transitional cell carcinoma in dogs. *J Vet Intern Med*. (2015) 29:261–7. doi: 10.1111/jvim.12533

18. Henry CJ, McCaw DL, Turnquist SE, Tyler JW, Bravo L, Sheafor S, et al. Clinical evaluation of mitoxantrone and piroxicam in a canine model of human invasive urinary bladder carcinoma. *Clin Cancer Res*. (2003) 9:906–11.

19. Khan KNM, Knapp DW, Denicola DB, Harris RK. Expression of cyclooxygenase-2 in transitional cell carcinoma of the urinary bladder in dogs. *Am J Vet Res*. (2000) 61:478–81. doi: 10.2460/ajvr.2000.61.478

20. Marvel SJ, Séguin B, Dailey DD, Thamm DH. Clinical outcome of partial cystectomy for transitional cell carcinoma of the canine bladder. *Vet Comp Oncol*. (2017) 15:1417–27. doi: 10.1111/vco.12286

21. Saeki K, Fujita A, Fujita N, Nakagawa T, Nishimura R. Total cystectomy and subsequent urinary diversion to the prepuce or vagina in dogs with transitional cell carcinoma of the trigone area: a report of 10 cases (2005–2011). *Can Vet J*. (2015) 56:73–80.

22. Millanta F, Impellizeri J, McSherry L, Rocchigiani G, Aurisicchio L, Lubas G. Overexpression of HER-2 via immunohistochemistry in canine urinary bladder transitional cell carcinoma – a marker of malignancy and possible therapeutic target. *Vet Comp Oncol*. (2018) 16:297–300. doi: 10.1111/vco.12345

23. Leach TN, Childress MO, Greene SN, Mohamed AS, Moore GE, Schrempp DR, et al. Prospective trial of metronomic chlorambucil chemotherapy in dogs with naturally occurring cancer. *Vet Comp Oncol*. (2012) 10:102–12. doi: 10.1111/j.1476-5829.2011.00280.x

24. Lee GW, Kang MH, Jeon JH, Song DW, Ro WB, Kim HS, et al. Case report: long-term survival of a dog with chronic lymphocytic leukemia treated with Chlorambucil, prednisolone, and Imatinib. *Front Vet Sci*. (2022) 8:8. doi: 10.3389/fvets.2021.625527

25. Schrempp DR, Childress MO, Stewart JC, Leach TN, Tan KM, Abbo AH, et al. Metronomic administration of chlorambucil for treatment of dogs with urinary bladder transitional cell carcinoma. *J Am Vet Med Assoc*. (2013) 242:1534–8. doi: 10.2460/javma.242.11.1534

26. Nguyen SM, Thamm DH, Vail DM, London CA. Response evaluation criteria for solid tumours in dogs (v1.0): a veterinary cooperative oncology group (VCOG) consensus document. *Vet Comp Oncol*. (2015) 13:176–83. doi: 10.1111/vco.12032

27. LeBlanc AK, Atherton M, Bentley RT, Boudreau CE, Burton JH, Curran KM, et al. Veterinary cooperative oncology group-common terminology criteria for adverse events (VCOG-CTCAE v2) following investigational therapy in dogs and cats. *Vet Comp Oncol*. (2021) 19:311–52. doi: 10.1111/vco.12677

28. Browder T, Butterfield CE, Kräling BM, Shi B, Marshall B, O'Reilly MS, et al. Antiangiogenic scheduling of chemotherapy improves efficacy against experimental drug-resistant cancer. *Cancer Res*. (2000) 60:1878–86.

29. Zitvogel L, Apetoh L, Ghiringhelli F, André F, Tesniere A, Kroemer G. The anticancer immune response: indispensable for therapeutic success? *J Clin Invest*. (2008) 118:1991–2001. doi: 10.1172/JCI35180

30. Gibson EA, Culp WTN. Canine prostate Cancer: current treatments and the role of interventional oncology. *Vet Sci*. (2024) 11:169. doi: 10.3390/vetsci11040169

31. Molnár T, Vajdovich P. Clinical factors determining the efficacy of urinary bladder tumour treatments in dogs: surgery, chemotherapy or both? *Acta Vet Hung*. (2012) 60:55–68. doi: 10.1556/avet.2012.005

32. Stone EA, George TF, Gilson SD, Page RL. Partial cystectomy for urinary bladder neoplasia: surgical technique and outcome in 11 dogs. *J Small Anim Pract*. (1996) 37:480–5. doi: 10.1111/j.1748-5827.1996.tb01745.x

33. Ravicini S, Baines SJ, Taylor A, Amores-Fuster I, Mason SL, Treggiari E. Outcome and prognostic factors in medically treated canine prostatic carcinomas: a multi-institutional study. *Vet Comp Oncol*. (2018) 16:450–8. doi: 10.1111/vco.12400

34. Shaevitz MH, Moore GE, Fulkerson CM. A prospective, randomized, placebo-controlled, double-blinded clinical trial comparing the incidence and severity of gastrointestinal adverse events in dogs with cancer treated with piroxicam alone or in combination with omeprazole or famotidine. *J Am Vet Med Assoc*. (2021) 259:385–91. doi: 10.2460/javma.259.4.385

35. Harirforoosh S, Jamali F. Renal adverse effects of nonsteroidal anti-inflammatory drugs. *Expert Opin Drug Saf*. (2009) 8:669–81. doi: 10.1517/14740330903311023

36. Rippy SB, Gardner HL, Nguyen SM, Warry EE, Portela RF, Drost WT, et al. A pilot study of toceranib/vinblastine therapy for canine transitional cell carcinoma. *BMC Vet Res*. (2016) 12:257. doi: 10.1186/s12917-016-0882-6

37. Natale RB, Yagoda A, Watson RC, Whitmore WF, Blumenreich M, Braun DW. Methotrexate: an active drug in bladder cancer. *Cancer*. (1981) 47:1246–50. doi: 10.1002/1097-0142(19810315)47:6<1246::AID-CNCR2820470603>3.0.CO;2-G

frontiers | Frontiers in Veterinary Science

TYPE Original Research
PUBLISHED 10 July 2025
DOI 10.3389/fvets.2025.1570720

Check for updates

OPEN ACCESS

EDITED BY
Carlos Eduardo Fonseca-Alves,
Paulista University, Brazil

REVIEWED BY
Mikio Shimada,
Tokyo Institute of Technology, Japan
Rui Ma,
Huazhong Agricultural University, China

*CORRESPONDENCE
Yasunaga Yoshikawa
✉ yyoshika@vmas.kitasato-u.ac.jp

RECEIVED 04 February 2025
ACCEPTED 20 June 2025
PUBLISHED 10 July 2025

CITATION
Kitano T, Zhu Z, Minami N, Orino K and Yoshikawa Y (2025) Enhanced sensitivity, robust p21 activation, and sustained DNA repair responses to interstrand crosslinks in elephant cells compared to humans. *Front. Vet. Sci.* 12:1570720. doi: 10.3389/fvets.2025.1570720

COPYRIGHT
© 2025 Kitano, Zhu, Minami, Orino and Yoshikawa. This is an open-access article distributed under the terms of the Creative Commons Attribution License (CC BY). The use, distribution or reproduction in other forums is permitted, provided the original author(s) and the copyright owner(s) are credited and that the original publication in this journal is cited, in accordance with accepted academic practice. No use, distribution or reproduction is permitted which does not comply with these terms.

Enhanced sensitivity, robust p21 activation, and sustained DNA repair responses to interstrand crosslinks in elephant cells compared to humans

Taisuke Kitano, Zida Zhu, Naoya Minami, Koichi Orino and Yasunaga Yoshikawa*

Laboratory of Veterinary Biochemistry, School of Veterinary Medicine, Kitasato University, Aomori, Japan

Elephants exhibit remarkable resistance to cancer, and understanding these mechanisms has focused on their potential applications in cancer prevention and treatment in humans. A genome-wide comparative analysis identified that the accelerated regions in elephants are enriched in Fanconi anemia (FA) complementation group L (FANCL), a ubiquitin E3 ligase that mediates the monoubiquitylation of FANCD2 as an essential step in the FA pathway. The FA pathway plays a crucial role in DNA interstrand crosslink (ICL) repair, contributing substantially to genome stability and cancer resistance. In this study, we investigated the differences in ICL repair via the FA pathway, including the function of FANCL, as well as the DNA damage response to ICLs between elephants and humans. We found that elephant fibroblasts exhibited higher sensitivity to ICL-inducing treatments, such as mitomycin C and trimethylpsoralen plus UVA (PUVA), than human fibroblasts, while showing comparable or reduced sensitivity to other DNA-damaging agents, such as doxorubicin and bleomycin. Functional analyses revealed that elephant and human FANCL performed similarly in mediating FANCD2 monoubiquitylation and cell viability following mitomycin C treatment. Interestingly, elephant fibroblasts exhibited a more potent and prolonged activation of p21 and sustained DNA repair responses, such as FANCD2 monoubiquitylation and increased RAD51expression, following ICL-induced treatments. Moreover, elephant fibroblasts showed significantly greater RAD51 foci formation than human fibroblasts after PUVA treatment, even under comparable levels of DNA damage. These findings suggest that elephants efficiently repair ICLs in growth-arrested cells likely through robust p21 activation. This study provides new insights into the cancer resistance mechanisms of elephants and offers novel approaches for cancer prevention and therapy.

KEYWORDS

elephant, p21, FANCL, interstrand crosslink repair, comparative molecular biology, RAD51

1 Introduction

Elephants are known for their remarkable resistance to cancer. Despite their large size and long lifespan, their cancer incidence and mortality rates are estimated to be <5%, which is significantly lower than the >20% observed in humans (1, 2). The mechanism of cancer resistance in elephants has been the focus of much research because of its potential application in cancer prevention and treatment in humans (3). As a key mechanism, the elephant genome encodes 20 copies of the tumor suppressor gene *TP53*, which enhances the apoptotic response following DNA damage (1, 4). Additionally, p21 (Waf1/Cip1), a primary downstream target of p53, is strongly upregulated in elephant cells following DNA damage (1). Moreover, elephants possess additional leukemia inhibitory factor (LIF) genes such as *LIF6*, which are upregulated by p53 and further promote apoptosis in response to DNA damage (5). Thus, elephants have evolved mechanisms to resist cancer by activating systems that efficiently eliminate aberrant cells. Interestingly, a genome-wide comparative analysis of accelerated regions revealed that these regions in elephants were uniquely enriched near DNA damage response genes, and the top hotspot was observed in Fanconi anemia (FA) complementation group L (FANCL), a master regulator of the FA DNA repair pathway (6).

The FA pathway plays a crucial role in the repair of DNA interstrand crosslinks (ICLs), which are highly cytotoxic DNA lesions that interfere with critical cellular processes such as DNA replication and transcription (7). Importantly, ICLs can naturally arise within the body due to exposure to endogenous aldehydes generated during normal cellular metabolism as well as from exogenous aldehydes and environmental factors (8, 9). In the FA pathway, at least 22 FA proteins sequentially contribute to the repair of ICLs through distinct steps, including the removal or unhooking of ICLs (which generates DNA double-strand breaks) and subsequent repair via homologous recombination (10). In these steps, FANCL, which functions as a ubiquitin E3 ligase in the core complex with other FA proteins, mediates the monoubiquitylation of FANCD2 and FANCI, which constitutes an essential step in the FA pathway (11). Notably, cancer predisposition is one of the primary symptoms in patients with FA caused by homozygous germline mutations in the FA genes, and somatic mutations and copy number variations in these genes are frequently observed in various human cancers (12, 13). These findings highlight that the FA pathway plays a substantial role in maintaining genomic stability and is crucial for cancer resistance.

Based on these findings, we hypothesized that the characteristics of FANCL, along with the FA pathway and DNA damage responses to ICLs, contribute to cancer resistance mechanisms in elephants. However, limited research has focused on the FA pathway and DNA repair mechanisms in elephants. In this study, we aimed to investigate the differences in ICL repair via the FA pathway, including the function of FANCL, as well as the DNA damage responses to ICLs between elephants and humans as a step toward understanding their unique cancer resistance mechanisms.

2 Materials and methods

2.1 Chemicals and treatments

Mitomycin C (MMC; product no. 20898-21) was purchased from NACALAI TESQUE (Kyoto, Japan). Trimethylpsoralen (product no. T6137) was purchased from Merck (Darmstadt, Germany). Doxorubicin (DOX; product no. 15007) was purchased from Cayman Chemical (Ann Arbor, MI, USA). Bleomycin (product no. HY-17565) was purchased from MedChemExpress (Monmouth Junction, NJ, USA). All drugs were diluted in culture medium and applied to the cells. Psoralens plus UVA (PUVA) treatment was conducted by pre-incubation with trimethylpsoralen for 4 h followed by UVA (0.1 J/cm^2, delivered over ∼10 s) exposure. For Western blotting and immunostaining, the antibodies against FANCL (Product No. sc-137076), and p21 (product no. sc-271610) were purchased from Santa Cruz Biotechnology (Dallas, TX, USA). Antibodies against β-actin (product no. PM053), α-tubulin (product no. M175-3), and lamin B1 (product no. PM064) were purchased from MEDICAL and BIOLOGICAL LABORATORIES (Tokyo, Japan). Antibody against FANCD2 (product no. EPR2302) was purchased from Abcam (Cambridge, UK). Antibody against RAD51 (product no. 70-012) was purchased from BioAcademia (Osaka, Japan). Antibody against FLAG-tag (DYKDDDDK) (product no. KO602-L) was purchased from TransGenic (Tokyo, Japan). Antibody against phospho-histone H2A.X (Ser139) (γH2AX; product no. 05-636) was purchased from Merck.

2.2 Cell cultures and generation of cell lines

Fibroblasts isolated from the ear skin of African elephants (LACF-NaNaII) were provided by the RIKEN Cell Bank (Ibaraki, Japan) through the National BioResource Project of MEXT. Human oral mucosal fibroblasts (hOMF100) were purchased from the Cell Research Corporation (Singapore). Both cells were cultured in α-minimum essential medium (NACALAI TESQUE) supplemented with 10% fetal bovine serum (FBS). Human HeLa cells were purchased from the RIKEN Cell Bank and cultured in Dulbecco's modified Eagle's medium (FUJIFILM Wako Pure Chemical, Osaka, Japan) supplemented with 10% FBS. All cells were maintained at 37°C in a humidified incubator with 5% CO_2.

The FANCL-knockout (KO) HeLa cells were generated by CRISPR-Cas9 using the gRNA sequence 5′-CGGTCGAAAACCGTGTATGA-3′ in the pSpCas9(BB)-2A-Puro (PX459) V2.0 vector (Addgene plasmid no. 190542). Exogenous expression of human or elephant FANCL in LACF-NaNaII and HeLa cells was achieved using retroviral transduction and magnetic sorting. Retroviruses were obtained from Phoenix A cells transfected with a pOZ-N vector carrying human or elephant FANCL. All plasmid DNA transfections were performed using FuGENE HD (Promega, Madison, WI, USA) according to the manufacturer's instructions.

2.3 Cell viability and proliferation assay

Cells were seeded into 96-well plates at 1,000 cells/well and incubated for 24 h. For cell viability assay, cells were treated with drugs for 96 h and then incubated with 10 μL of Cell Counting Kit-8 solution (DOJINDO, Kumamoto, Japan) for 3 h. Absorbance was measured at 450 nm using a microplate reader, and cell viability was calculated as the ratio of absorbance to non-treated cells. For the cell proliferation assay, at each time points of 24, 48, 96, and 120 h after seeding, the cells were incubated with Cell Counting Kit-8 solution for 3 h, and the absorbance was measured in the same way. The cell proliferation rate was calculated as the ratio of the absorbance of the cells at 24 h after seeding.

2.4 Western blotting

Cells were lysed in an equal volume of Benzonase buffer (20 mM Tris-HCl, pH 8.0; 2 mM $MgCl_2$; 1% Triton X-100; 10% glycerol; and >12.5 U/ml Benzonase) at 4°C for 10 min and then treated with the same volume of 2% SDS to extract the total proteins. The lysates were mixed with 4× LDS loading buffer (Thermo Fisher Scientific, Waltham, MA, USA) and 10× reducing agent (Thermo Fisher Scientific). The samples were separated by 4–15% SDS-PAGE and transferred onto nitrocellulose membranes (Cytiva, Tokyo, Japan). The membranes were blocked with 5% skimmed milk and then incubated overnight at 4°C with the primary antibodies. Next, the membranes were incubated with horseradish peroxidase-conjugated secondary anti-mouse or anti-rabbit antibodies (MEDICAL & BIOLOGICAL LABORATORIES) for 1 h at room temperature. Immunoreactive bands were visualized using Immunostar Zeta or Immunostar LD (for higher-sensitivity detection) (FUJIFILM Wako Pure Chemical) and detected using a C-DiGit Blot Scanner (LI-COR, Lincoln, NE, USA). Band intensities were measured using the Image Studio Software (LI-COR).

2.5 Immunostaining and image analysis

Cells were cultured on coverslips (Matsunami Glass, Osaka, Japan) and treated with PUVA (0.1 μg/mL TMP). At 0, 3, 6, 12, 24, and 48 h after treatment, cells were fixed with 4% paraformaldehyde for 5 min at room temperature. Following permeabilization with phosphate-buffered saline (PBS) containing 1% Triton X-100 for 10 min, cells were incubated with PBS containing 5% bovine serum albumin (BSA) at room temperature for 1 h. Subsequently, cells were incubated overnight at 4°C with anti-γH2AX and anti-RAD51 antibodies diluted in PBS with 5% BSA. After washing, cells were stained for 1 h at room temperature with Alexa Fluor 488-conjugated goat anti-mouse IgG and Alexa Fluor 568-conjugated goat anti-rabbit IgG (Thermo Fisher Scientific), along with 4′,6-diamidino-2-phenylindole (DAPI; Thermo Fisher Scientific), all diluted in PBS containing 5% BSA. Coverslips were mounted using VECTASHIELD® Antifade Mounting Medium (Vector Laboratories, Newark, CA, USA). Cells were imaged using a confocal laser scanning microscope (Carl Zeiss AG, Oberkochen, Germany) equipped with ZEN software (Carl Zeiss AG). Nuclear γH2AX and RAD51 foci were analyzed in >70 cells per group using Cellpose3 (14) and ImageJ software (National Institutes of Health, Bethesda, MD, USA). Briefly, individual nuclei were segmented based on DAPI staining using Cellpose3, and the resulting outlines were used as nuclear regions of interest (ROIs) for subsequent analyses. Foci in the γH2AX and RAD51 channels were identified by subtracting a Gaussian-blurred background image, followed by local auto-thresholding using the "Bernsen" method and conversion to binary masks. The area fraction (%) of γH2AX and RAD51 foci was quantified within each nuclear ROI. Additionally, the percentage of RAD51-positive area within γH2AX foci was calculated for nuclei with a γH2AX area fraction >1.5%.

2.6 Data analysis

Data are expressed as mean ± standard error of the mean (SEM) (n = number of independent experiments). Two-group comparisons were performed using Welch's t-tests or the exact Wilcoxon rank-sum test (also known as the Mann-Whitney U test). Multiple comparisons were performed using one-way ANOVAs followed by Tukey's HSD test, Dunnett's test, or Steel's test (with control group), as appropriate. Statistical significance was set at $p < 0.05$. All statistical analyses were performed using the JMP Pro software (SAS, Cary, NC, USA). Comparisons between the control and treatment, as well as between elephant and human cells, were analyzed based on independent hypotheses; therefore, no correction was applied. All graphs were constructed using Excel (Microsoft, Redmond, WA, USA).

3 Results

3.1 Elephant fibroblasts exhibited higher sensitivity to ICL-inducing treatments compared to human fibroblasts

To compare the properties in the viability to ICLs between human and elephant cells, we examined the effects of ICL-induced treatment on the viability of human and elephant cells. Human (hOMF100) and African elephant (LACF-NaNaII) fibroblasts were used because these cells exhibit comparable proliferative capacities under identical culture conditions (Figure 1A). MMC, a major DNA crosslinking agent, reduced the viability of LACF-NaNaII cells in a dose-dependent manner, with a significantly greater effect than on hOMF100 cells (Figure 1B). A similar differential sensitivity to MMC was also observed in the clonogenic assay (Supplementary Figure S1). Moreover, LACF-NaNaII cells exhibited a higher sensitivity to trimethylpsoralen plus UVA (PUVA) treatment, which induces ICLs more effectively and specifically (15) (Figure 1C). Consistent with these findings, cell cycle analysis revealed a pronounced G2/M arrest in LACF-NaNaII cells following MMC treatment (Supplementary Figure S2). In contrast, this increased sensitivity in LACF-NaNaII cells was not observed with other DNA-damaging agents such as DOX, which intercalates into the DNA and inhibits topoisomerase II, or bleomycin, which induces DNA double-strand breaks

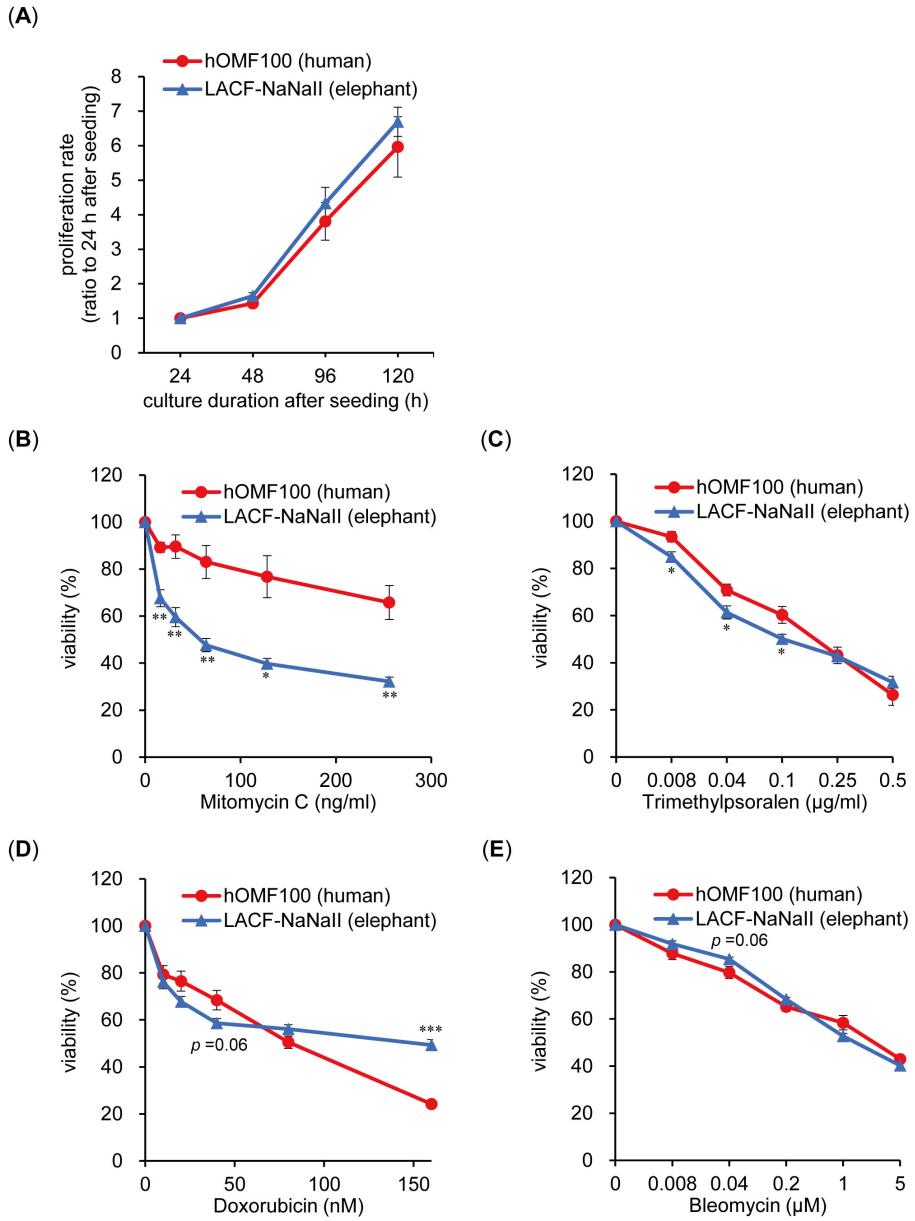

FIGURE 1
Elephant fibroblasts exhibit higher sensitivity to DNA ICL treatments compared to human fibroblasts. **(A)** Proliferation rate of hOMF100 and LACF-NaNaII cells at 24–120 h after seeding ($n = 6–9$). **(B–E)** Viability of hOMF100 and LACF-NaNaII cells at different concentrations of mitomycin C ($n = 5$) **(B)**, trimethylpsoralen (plus UVA [0.1 J/cm^2]: PUVA) ($n = 6$) **(C)**, doxorubicin ($n = 7$) **(D)** or bleomycin ($n = 9$) **(E)**. *$p < 0.05$, **$p < 0.01$ vs. hOMF100 cells (Welch's *t*-tests). All data are presented as mean ± SEM.

(Figures 1D, E). In contrast, LACF-NaNaII cells exhibited lower sensitivity to higher DOX concentrations (160 nM). These results suggest that elephant cells are more sensitive to ICLs than are human cells.

3.2 Comparable function of elephant and human FANCL in ICL repair

FANCL locus has been identified as a genomic hotspot of elephant-accelerated regions (6). Elephant genomic DNA information has been reported, but the sequence of *FANCL* mRNA has not been confirmed. Therefore, we first determined the full-length elephant FNACL cDNA (Accession No. LC858708). The open reading frame consisted of 1,119 base pairs, and the predicted protein length was 372 amino acids, which was three amino acids shorter than that of human FANCL. Moreover, amino acid sequence alignment between elephant and human FANCL revealed three substitutions in elephant FANCL at functionally significant positions: I136F, F252R, and I265L (Supplementary Figure S3). These residues are critical for FANCL folding or the monoubiquitylation of FANCD2, as reported in studies on human FANCL

mutations (16). Thus, we investigated the functional differences between elephant and human FANCL and their potential relationship with the enhanced sensitivity of elephant cells to ICLs.

To compare FANCL functions, we generated FANCL-KO HeLa cells and reconstituted them with either human or elephant FANCL (Figure 2A). FANCL-KO cells exhibited significantly increased sensitivity to MMC, which was restored to a similar extent by exogenous expression of both human and elephant FANCL (Figure 2B). Furthermore, we examined the functional differences between human and elephant FANCL in the monoubiquitylation of FANCD2 after treatment with MMC (160 ng/mL) for 12 or 24 h (Figure 2C). The change in the ratio of monoubiquitylated FANCD2 levels was not significantly different between parental cells and cells expressing human or elephant FANCL (Figure 2D). Nuclear FANCD2 foci formation after MMC treatment was also restored in these cells (Supplementary Figure S4). These results indicate that the function of elephant FANCL in ICL repair is comparable to that of human FANCL when expressed in human cells. To investigate whether higher expression levels of FANCL rescued the enhanced sensitivity of elephant cells to ICLs, we generated LACF-NaNaII cells expressing exogenous human or elephant FANCL (Figure 2E). MMC sensitivity was not influenced by exogenous expression of either human or elephant FANCL (Figure 2F), suggesting that the heightened sensitivity of elephant cells to ICLs is not attributable to differences in FANCL function or expression levels.

3.3 Elephant fibroblasts exhibit a potent p21 response to ICL-inducing agents compared to human fibroblasts

Elephant fibroblasts exhibit increased p21 protein expression and reduced viability following ionizing radiation exposure compared to human fibroblasts (1). To investigate the mechanism underlying the higher sensitivity of elephant cells to ICL treatment, we compared the ICL damage response following MMC treatment of hOMF100 and LACF-NaNaII cells (Figure 3A). Treatment with MMC (256 ng/mL) for 12 and 24 h enhanced the monoubiquitylation of FANCD2 in both cell lines. Higher levels of FANCD2 were detected in LACF-NaNaII cells than in hOMF100 cells. Additionally, even after MMC treatment, the proportion of non-ubiquitylated FANCD2 relative to ubiquitylated FANCD2 was higher in LACF-NaNaII cells than in hOMF100 cells. The change in the ratio of monoubiquitylated FANCD2 following MMC treatment was not significantly different between these cells (Figure 3B), suggesting a comparable ICL repair response between elephant and human cells. Interestingly, treatment with MMC for 24 h increased p21 expression in LACF-NaNaII cells but not in hOMF100 cells (Figure 3C). In contrast, DOX (80 nM) and bleomycin (5 μM) increased p21 expression to the same level in both cell lines (Figures 3D, E), consistent with their comparable effects on cell viability, as shown in Figure 1. These results suggest that ICLs induce a more potent p21 response in elephant cells than in human cells.

3.4 Prolonged and robust p21 activation and sustained DNA repair responses following ICL-inducing treatment in elephant fibroblasts

We further investigated time-dependent differences in the monoubiquitylation of FANCD2 and p21 expression between human and elephant cells following ICL induction using PUVA treatment, which induces ICLs more specifically at the precise time of UVA exposure (Figure 4A). In addition to FANCD2 and p21, we also examined the expression of RAD51 recombinase (also known as FANCR), which is essential for homologous recombination following the removal of ICLs during ICL repair (17). PUVA treatment (trimethylpsoralen [0.1 μg/mL] plus UVA [0.1 J/cm^2]) enhanced the monoubiquitylation of FANCD2 in both cells starting 6 h after treatment. In LACF-NaNaII cells, even after PUVA treatment, the proportion of non-ubiquitylated FANCD2 relative to ubiquitylated FANCD2 was higher than that in hOMF100 cells. Interestingly, increased levels of monoubiquitylated FANCD2 following PUVA treatment were sustained for up to 48 h in LACF-NaNaII cells; however, they were not sustained and instead decreased in hOMF100 cells (Figure 4B). Consistent with the results of MMC treatment, an increase in p21 expression was observed in LACF-NaNaII cells following PUVA treatment, starting at 24 h post-treatment and persisting for up to 48 h, whereas no such increase was observed in hOMF100 cells (Figure 4C). Moreover, PUVA treatment increased RAD51 expression in both cell lines starting at 12 h after treatment. Similar to monoubiquitylated FANCD2, this increase was sustained for up to 48 h post-treatment in LACF-NaNaII cells, and decreased by 48 h in hOMF100 cells (Figure 4D). These results indicate that ICLs induce a more prolonged and robust activation of p21, along with sustained DNA repair responses, in elephant cells than in human cells. To investigate whether these long-lasting responses to ICLs in elephant cells are dependent on the level of ICLs, specifically whether the prolonged responses result from higher levels of ICLs, we performed PUVA treatment using lower concentrations (0.04 and 0.008 μg/ml) of trimethylpsoralen and evaluated the responses in LACF-NaNaII cells (Figure 5A). These concentrations exerted similar or less effects on the viability of LACF-NaNaII cells compared to the effect of 0.1 μg/ml trimethylpsoralen on hOMF100 cells. PUVA treatment increased the levels of monoubiquitylated FANCD2 (Figure 5B), p21 (Figure 5C), and RAD51 (Figure 5D) in a dose-dependent manner 24 h post-treatment. These responses were sustained by 48 h. Together, these results suggest that prolonged p21 activation and sustained DNA repair responses in elephant cells are independent of ICL levels.

3.5 Enhanced DNA repair responses under comparable levels of DNA damage after ICL-inducing treatment in elephant fibroblasts

To elucidate the differences in DNA damage and repair responses—and their relationship—following ICL induction

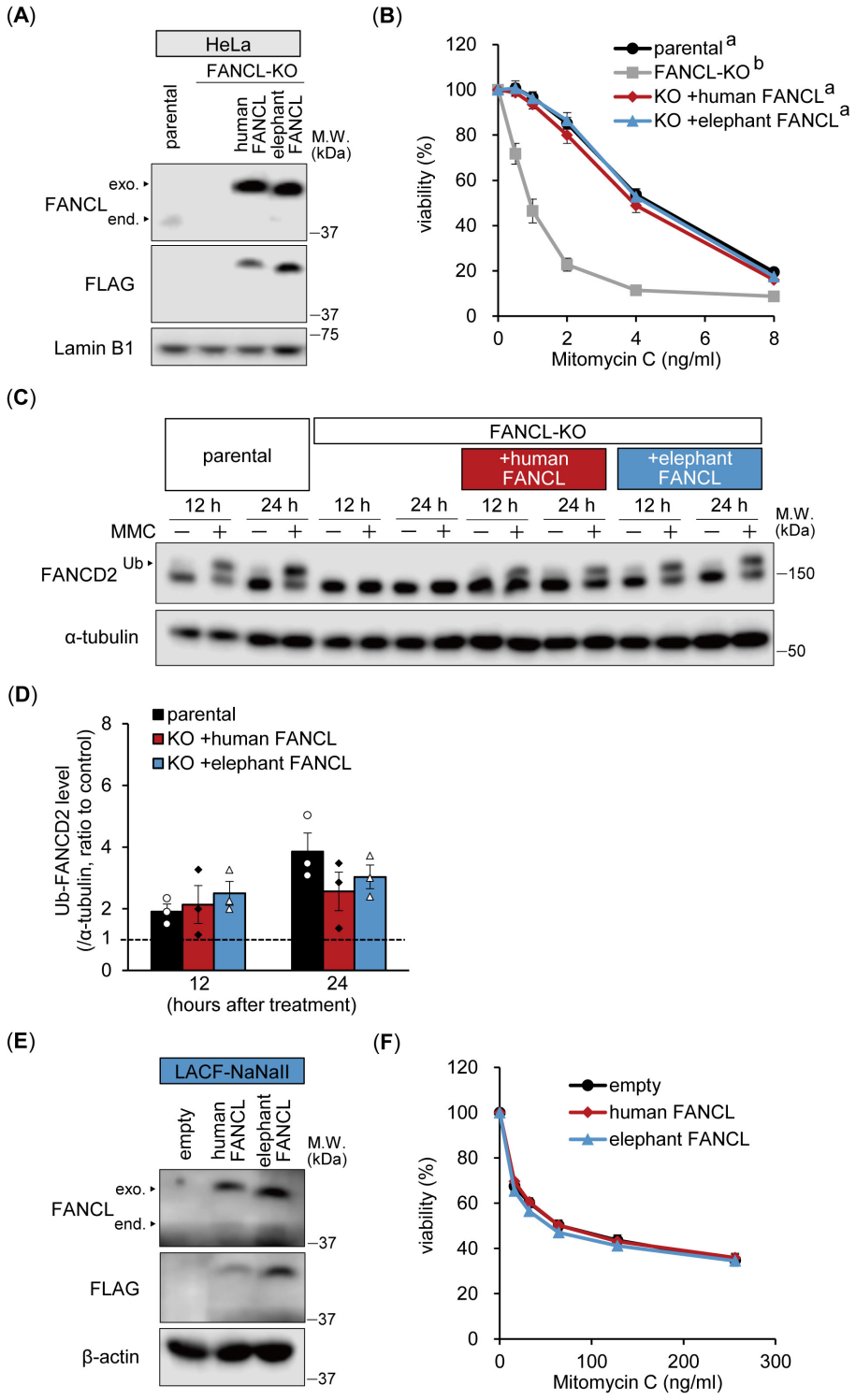

FIGURE 2
Functional comparison between human and elephant FANCL. **(A, B)** Expression levels of endogenous (end.) FANCL and exogenous (exo.) FLAG-HA-fused human or elephant FANCL in four types of HeLa cells: parental, FANCL knockout (KO), and FANCL-KO cells expressing exogenous human or elephant FANCL, were analyzed via Western blotting using anti-FANCL and FLAG antibodies **(A).** Viability of these cells at different concentrations of mitomycin C (MMC) was examined ($n = 5$) **(B).** Different letters indicate statistically significant differences ($p < 0.01$, Tukey's HSD test) at all concentrations. **(C, D)** Monoubiquitylation (Ub) of FANCD2 at 12 or 24 h after treatment with MMC (160 ng/mL) in parental, FANCL-KO HeLa cells, and FANCL-KO cells expressing exogenous human or elephant FANCL, were evaluated via Western blotting using anti-FANCD2 antibody **(C).** Change ratio of Ub-FANCD2 levels with MMC treatment were quantified ($n = 3$) **(D). (E, F)** Expression levels of endogenous FANCL and exogenous FLAG-HA-fused human or elephant FANCL in LACF-NaNaII cells, transduced with empty vector or vector carrying human or elephant FANCL, were observed via Western blotting using anti-FANCL and FLAG antibodies **(E).** Viability of these cells at different concentrations of MMC was examined ($n = 6$) **(F)**. All data are presented as mean ± SEM with or without individual data points.

10.3389/fvets.2025.1570720

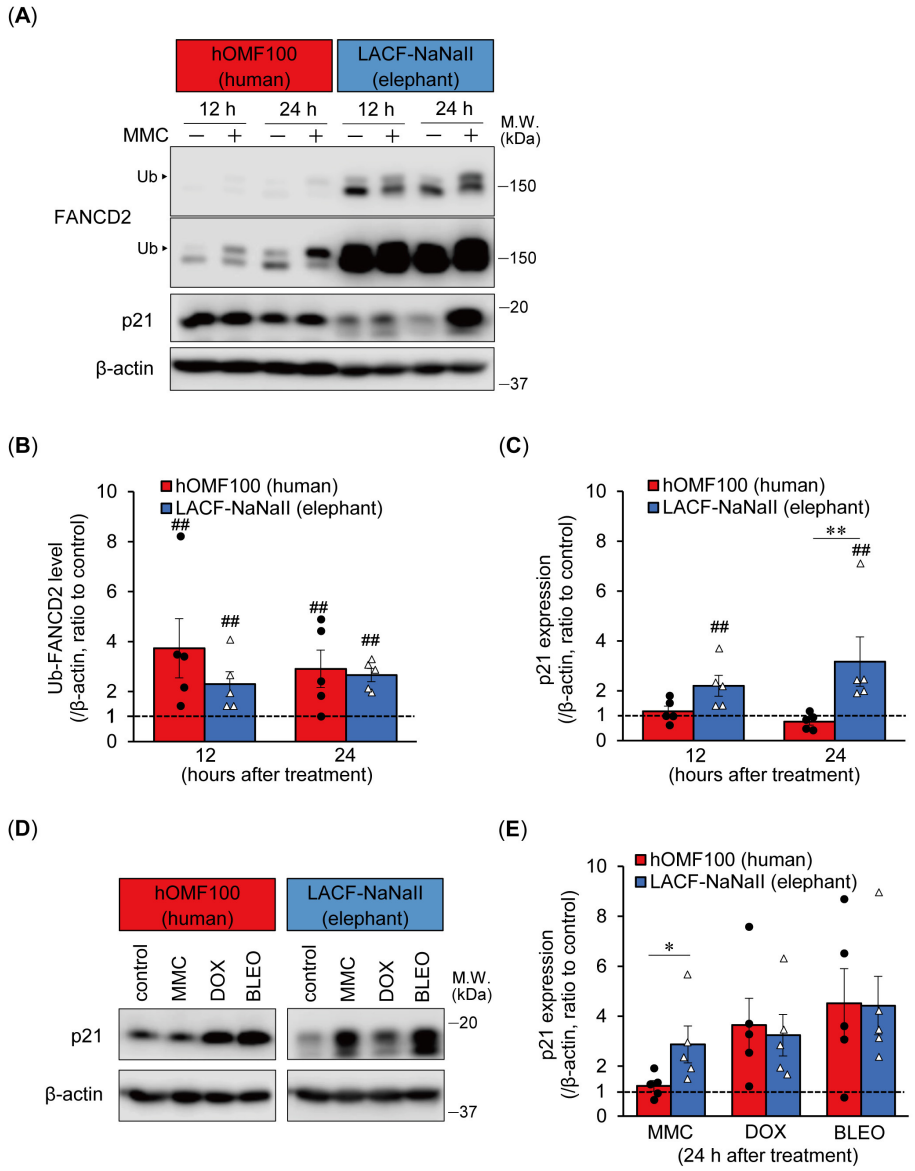

FIGURE 3
Elephant fibroblasts exhibit potent p21 response to DNA ICL agent. **(A–C)** Monoubiquitylation (Ub) of FANCD2 and p21 expression levels at 12 or 24 h after treatment with mitomycin C (MMC; 256 ng/mL) in hOMF100 and LACF-NaNaII cells were observed via Western blotting using anti-FANCD2 and p21 antibodies **(A).** Change ratio of Ub-FANCD2 levels **(B)** and p21 expression levels **(C)** with MMC treatment were quantified ($n = 5$). Two images of same membrane with different contrast settings for FANCD2 are shown. $^{\#\#}p < 0.01$, control vs. MMC treatment (exact Wilcoxon rank-sum test). $^{**}p < 0.01$, hOMF100 vs. LACF-NaNaII cells (exact Wilcoxon rank-sum test). **(D, E)** p21 expression levels at 24 h after treatment of MMC (256 ng/mL), doxorubicin (DOX; 80 nM), or bleomycin (BLEO; 5 μM) in hOMF100 and LACF-NaNaII cells were analyzed via Western blotting using anti-p21 antibody **(D)**. Change ratio of p21 expression with drug treatments were quantified ($n = 5$) **(E)**. $^{*}p < 0.05$, hOMF100 vs. LACF-NaNaII cells (exact Wilcoxon rank-sum test). All data are presented as mean ± SEM with individual data points.

between human and elephant cells, we further examined the time-dependent formation of nuclear γH2AX foci, a highly sensitive marker of ICL-associated DNA damage (18, 19), as well as RAD51 foci following PUVA treatment (Figure 6A). Although the basal level of γH2AX foci was higher in LACF-NaNaII cells than in hOMF100 cells, PUVA treatment induced a continuous increase in γH2AX foci formation up to 48 h post-treatment to a similar extent in both cells (Figure 6B). These results suggest that PUVA treatment causes comparable levels of DNA damage in both human and elephant fibroblasts. RAD51 foci also tended to be higher at the basal level in LACF-NaNaII cells (Figure 6C). Although PUVA treatment induced RAD51 foci formation in hOMF100 cells, the levels at all time points remained significantly lower than those in LACF-NaNaII cells. Furthermore, the RAD51-positive area within γH2AX foci was (tended to be) higher in LACF-NaNaII cells compared to hOMF100 cells across all time points (Figure 6D). These findings suggest that elephant cells may exhibit a more robust RAD51-mediated DNA repair response under comparable levels of DNA damage.

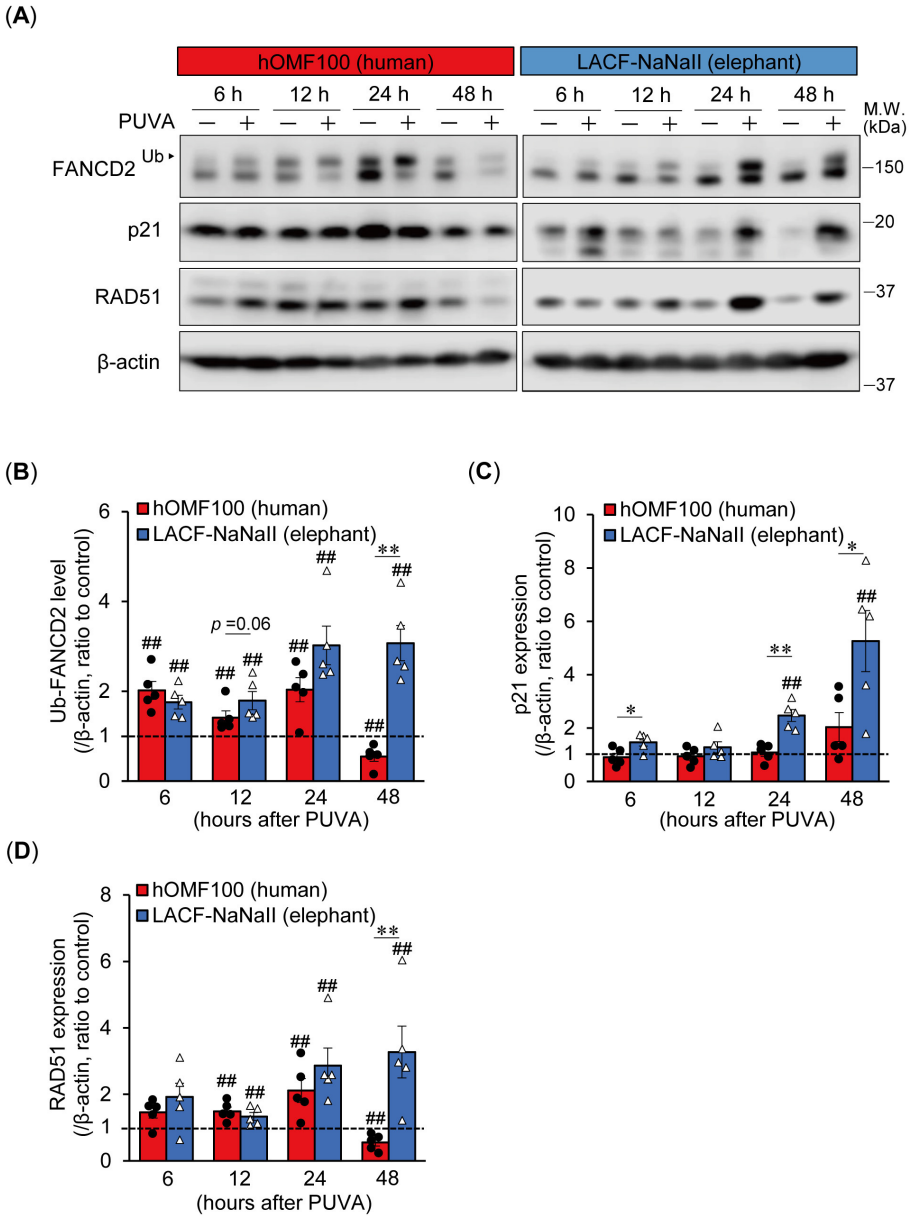

FIGURE 4
Elephant fibroblasts exhibit prolonged and robust p21 activation along with sustained DNA repair responses following ICL treatment compared to human fibroblasts. **(A–D)** Monoubiquitylation (Ub) of FANCD2 and expression levels of p21 and RAD51 at 6, 12, 24, or 48 h after treatment with trimethylpsoralen (0.1 μg/mL) plus UVA (0.1 J/cm^2) (PUVA) in hOMF100 and LACF-NaNaII cells were analyzed via Western blotting using anti-FANCD2, p21, and RAD51 antibodies **(A).** Change ratio of Ub-FANCD2 levels **(B)** and expression levels of p21 **(C)** and RAD51 **(D)** with PUVA treatment were quantified ($n = 5$). $^{\#\#}p < 0.01$, control vs. PUVA treatment (exact Wilcoxon rank-sum test). $^{*}p < 0.05$, $^{**}p < 0.01$, hOMF100 vs. LACF-NaNaII cells (exact Wilcoxon rank-sum test). All data are presented as mean ± SEM with individual data points.

4 Discussion

In this study, we observed that elephant cells exhibited enhanced sensitivity, prolonged and robust p21 activation, and sustained DNA repair responses (monoubiquitylation of FANCD2, increased expression of RAD51 and prominent formation of nuclear RAD51 foci), specifically following ICL-inducing treatment, compared to human cells. The comparable induction of nuclear γH2AX foci in both species following ICL-inducing treatment suggests that the differences in cellular responses are not due to differences in the extent of DNA damage. Furthermore, the similar functions of elephant and human FANCL suggest that their function is not likely to contribute to these differences.

Our results are consistent with those of a previous report that showed greater p21 upregulation following irradiation in elephant fibroblasts than in human fibroblasts (1). p21 is a critical mediator of cell-cycle arrest and is upregulated by p53 activation in response to DNA damage (20). Considering previous reports of more robust p53 signaling in elephant cells after DNA damage (1, 4), it is speculated that ICL-induced treatments strongly activate the p53-p21 pathway in elephant cells, leading to a more pronounced reduction in cell viability than in human

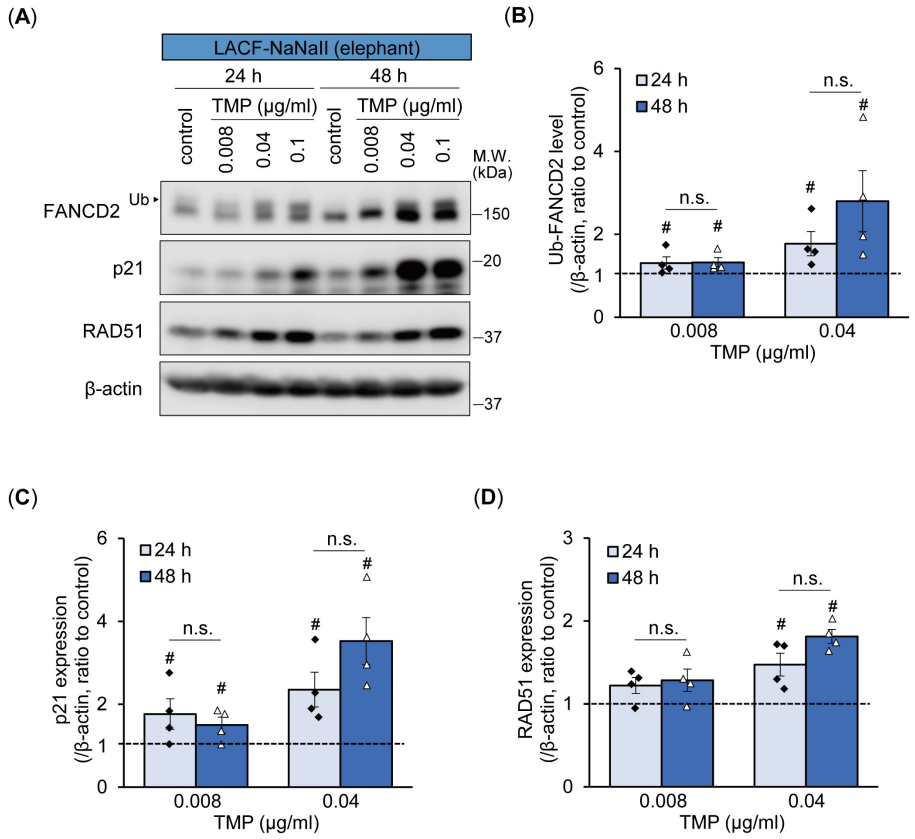

FIGURE 5
Prolonged p21 and sustained DNA repair responses in elephant fibroblasts appear to be independent of ICL levels. **(A–D)** Monoubiquitylation (Ub) of FANCD2 and expression levels of p21 and RAD51 at 24 or 48 h after treatment with different concentrations of trimethylpsoralen (TMP) plus UVA (0.1 J/cm^2) (PUVA) in LACF-NaNaII cells were evaluated via Western blotting using anti-FANCD2, p21, and RAD51 antibodies **(A).** Change ratio of Ub-FANCD2 levels **(B)** and expression levels of p21 **(C)** and RAD51 **(D)** with PUVA treatment were quantified (n = 4). $^{\#}p < 0.05$ vs. control (Steel's test). Not significant (n.s.), 24 h vs. 48 h after PUVA treatment (exact Wilcoxon rank-sum test). All data are presented as mean ± SEM with individual data points.

cells. However, the specificity of the enhanced p21 response to ICLs in elephant cells may not be solely explained by the p53 mechanism, as enhanced p53 signaling in elephant fibroblasts has also been observed in response to other DNA-damaging treatments, such as DOX and UVC, in addition to MMC (although not directly compared with human fibroblasts) (4). Several studies have identified p53-independent mechanisms for the upregulation of p21, notably involving breast cancer susceptibility gene 1 (BRCA1, also known as FANCS), which functions as a component of the FA pathway (20, 21). In addition, increased p21 expression in FA pathway-deficient cells (with knockdown of FANCA or FANCD2) is partially mediated by microphthalmia-associated transcription factor and nucleophosmin 1 in a p53-independent manner (22). Unfortunately, in this study, we were unable to evaluate the expression of elephant p53 because it was not detected by western blotting using various commercially available anti-p53 antibodies (DO-1, DO-7, A-1, and C-11) (data not shown). The relationship between p53 signaling and enhanced p21expression in elephant cells in response to ICLs should be addressed in future studies.

In contrast to sustained FANCD2 monoubiquitylation and a sustained increase in RAD51 expression in elephant cells following ICL induction, these DNA repair responses disappeared 48 h after induction in human cells. Both FANCD2 and RAD51 are cleaved by caspase 3 and undergo proteolytic degradation during DNA damage-induced apoptosis (23–25). Additionally, p53 downregulates FA proteins, including FANCD2 and RAD51, by activating p21 (26). These mechanisms are likely to contribute to the reduction in the expression of monoubiquitylated FANCD2 and RAD51 following ICL induction in human cells. However, it seems unlikely that p53 signaling and the apoptotic response were strongly induced in human cells compared to elephant cells, given the lower sensitivity of human fibroblasts to PUVA in terms of viability, and previous reports indicate higher p53 signaling and caspase 3/7 activity in elephant cells in response to DNA damage (1, 4). Negative regulatory mechanisms affecting the expression of FANCD2 and RAD51 may be less active in elephant cells. Suzuki et al. have reported that p21 mediates the inactivation of caspase 3 (27, 28). Furthermore, p21 promotes MMC-induced FANCD2/I monoubiquitylation, likely through the transcriptional repression of the USP1, a deubiquitylating enzyme for FANCD2/I (29). Thus, the prolonged and robust activation of p21 following ICL induction may contribute to the sustained monoubiquitylation of FANCD2 and a sustained increase in RAD51 expression in elephant cells. Higher levels of FANCD2 were detected in elephant cells than in human cells. Additionally, even after ICL-inducing treatments, the proportion of non-ubiquitylated FANCD2 relative to ubiquitylated FANCD2 in elephant cells remained higher than that in human cells, despite a similar

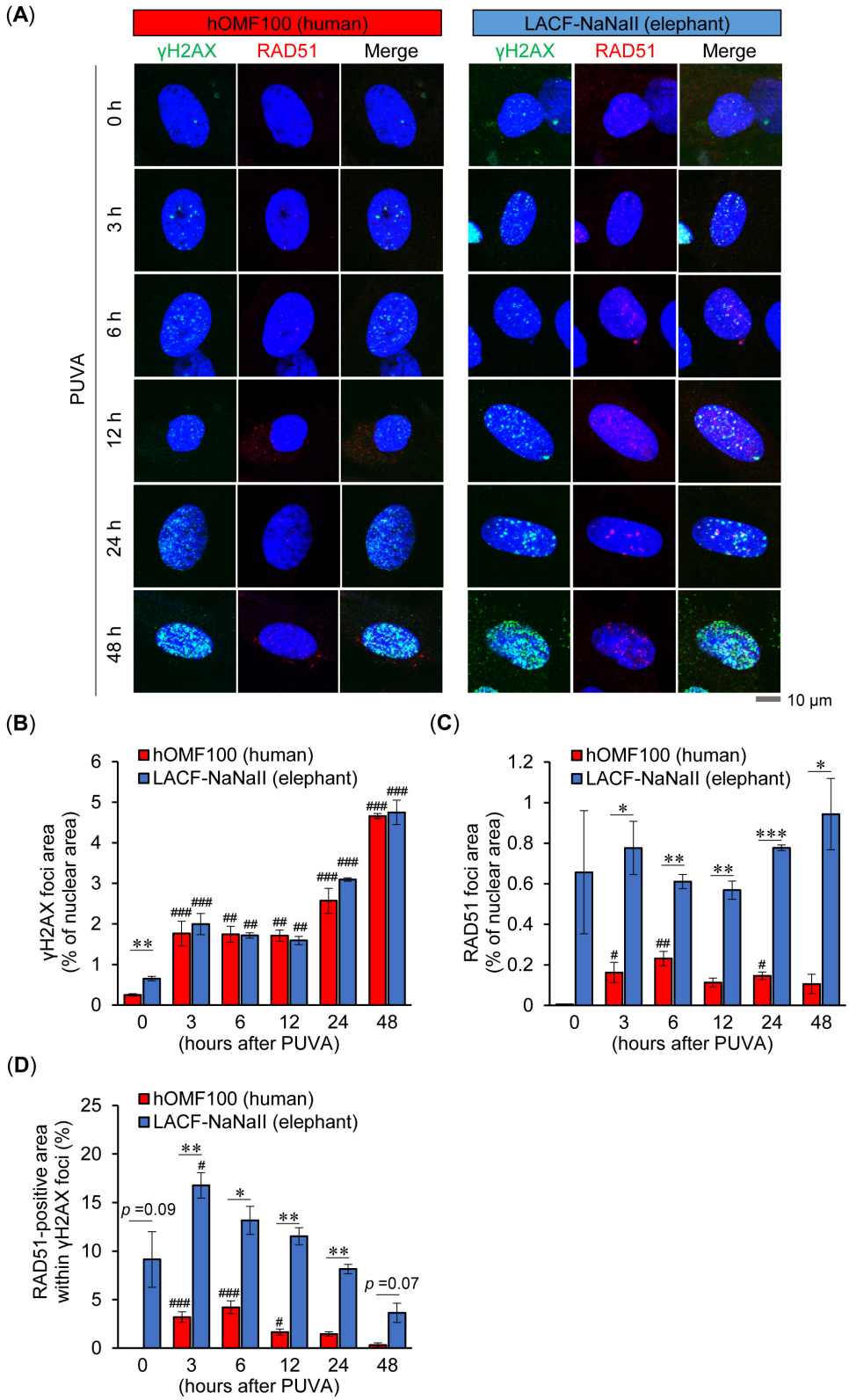

FIGURE 6
Elephant fibroblasts exhibit higher RAD51 foci formation than human fibroblasts under comparable levels of DNA damage. **(A)** Formation of γH2AX (green) and RAD51 (red) foci in DAPI-stained nuclei (blue) at 0, 3, 6, 12, 24 and 48 h after treatment with trimethylpsoralen (0.1 μg/mL) plus UVA (0.1 J/cm^2) (PUVA) in hOMF100 and LACF-NaNaII cells were evaluated via immunostaining. Representative images of a single cell at each timepoint are shown. Scale bar = 10 μm. **(B–D)** Percentage of γH2AX **(B)** and RAD51 **(C)** foci area in nuclei, and RAD51-positive area within γH2AX foci **(D)** were quantified ($n = 3$). #$p < 0.05$, ##$p < 0.01$, ###$p < 0.001$ vs. 0 h (Dunnett's test). *$p < 0.05$, **$p < 0.01$, ***$p < 0.001$, hOMF100 vs. LACF-NaNaII cells (Welch's t-tests). All data are presented as mean ± SEM.

induction ratio of ubiquitylated FANCD2 in both cells. These observations suggest that elephant cells exhibit a higher overall expression of FANCD2, which may contribute to the sustained levels of monoubiquitylated FANCD2 following ICL induction. RAD51 plays a crucial role in homologous recombination and is essential for ICL repair (17). Monoubiquitylated FANCD2 promotes homologous recombination during ICL repair by interacting with CtIP, which is involved in DNA end resection (30–32). Moreover, regardless of monoubiquitylation, FANCD2 plays a crucial role in the stabilization of RAD51 in single-stranded DNA and promotes strand exchange activity, an important process in homologous recombination (33). Given this role, the higher expression of FANCD2 in elephant cells may partly account for the elevated formation of RAD51 foci. Taken together, sustained FANCD2 monoubiquitylation, along with the prolonged increase in RAD51 expression and nuclear foci formation in elephant cells, likely contribute to the error-free repair of ICLs and maintenance of genome stability. However, further investigations are needed to determine whether homologous recombination or other error-free repair pathways are indeed more active in elephant cells, and how these mechanisms influence cellular fate following ICL-induced DNA damage.

Our findings suggest that elephant cells may not only indiscriminately eliminate abnormal cells through apoptosis mediated by potent p53 signaling but also exhibit a remarkable ability to arrest cell proliferation via robust p21 signaling (likely regulated by p53), enabling efficient repair of DNA damage. Supporting this hypothesis, previous studies have demonstrated that p21 expression is positively associated with RAD51 expression and foci formation (34), and that p21 promotes error-free replication-coupled repair of DNA double-strand breaks (35). Although further research is necessary to confirm whether our findings are universally applicable to elephant cells, this strategy may explain the exceptional cancer resistance of elephants, allowing them to sustain numerous cells in their large bodies over a long lifespan. The modulation of p53 signaling by various mechanisms, depending on the type and extent of DNA damage, determines the cell fate, including apoptosis, cell cycle arrest, and DNA repair (36). Understanding how p53 signaling orchestrates these cell fates in elephants is particularly intriguing and may hold the key to uncovering the molecular basis of cancer resistance. This study provides new insights into the cancer resistance mechanisms of elephants, potentially offering novel approaches for cancer prevention and therapy in humans.

Data availability statement

The datasets presented in this study can be found in online repositories. The names of the repository/repositories and accession number(s) can be found in the article/Supplementary Material.

Ethics statement

Ethical approval was not required for the studies on humans in accordance with the local legislation and institutional requirements because only commercially available established cell lines were used. Ethical approval was not required for the studies on animals in accordance with the local legislation and institutional requirements because only commercially available established cell lines were used.

Author contributions

TK: Conceptualization, Data curation, Formal analysis, Investigation, Methodology, Validation, Visualization, Writing – original draft, Writing – review & editing. ZZ: Formal analysis, Investigation, Writing – review & editing. NM: Data curation, Investigation, Writing – review & editing. KO: Conceptualization, Supervision, Writing – review & editing. YY: Conceptualization, Data curation, Project administration, Supervision, Writing – review & editing, Writing – original draft.

Funding

The author(s) declare that financial support was received for the research and/or publication of this article. This work was partially supported by the Japan Society for the Promotion of Science KAKENHI, under Grant No. 21K05960 (to KO). The funding bodies played no role in study design, data collection, analysis, interpretation, or manuscript writing.

Acknowledgments

We appreciate Nobutaka Sato and Gen Bando at Asahiyama Zoo, who prepared LACF-NaNaII cells.

Conflict of interest

The authors declare that the research was conducted in the absence of any commercial or financial relationships that could be construed as a potential conflict of interest.

The author(s) declared that they were an editorial board member of Frontiers, at the time of submission. This had no impact on the peer review process and the final decision.

Generative AI statement

The author(s) declare that Gen AI was used in the creation of this manuscript. This manuscript was edited for grammar and expression with the assistance of ChatGPT (OpenAI). The authors reviewed, revised, and approved all AI-generated suggestions to ensure accuracy and integrity.

Publisher's note

All claims expressed in this article are solely those of the authors and do not necessarily represent those of

their affiliated organizations, or those of the publisher, the editors and the reviewers. Any product that may be evaluated in this article, or claim that may be made by its manufacturer, is not guaranteed or endorsed by the publisher.

Supplementary material

The Supplementary Material for this article can be found online at: https://www.frontiersin.org/articles/10.3389/fvets.2025.1570720/full#supplementary-material

References

1. Abegglen LM, Caulin AF, Chan A, Lee K, Robinson R, Campbell MS, et al. Potential mechanisms for cancer resistance in elephants and comparative cellular response to DNA Damage in Humans. *JAMA J Am Med Assoc.* (2015) 314:1850–60. doi: 10.1001/jama.2015.13134

2. Bray F, Laversanne M, Sung H, Ferlay J, Siegel RL, Soerjomataram I. Global cancer statistics 2022: GLOBOCAN estimates of incidence and mortality worldwide for 36 cancers in 185 countries. *CA Cancer J Clin.* (2024) 74:229–63. doi: 10.3322/caac.21834

3. Seluanov A, Gladyshev VN, Vijg J, Gorbunova V. Mechanisms of cancer resistance in long-lived mammals. *Nat Rev Cancer.* (2018) 18:433–41. doi: 10.1038/s41568-018-0004-9

4. Sulak M, Fong L, Mika K, Chigurupati S, Yon L, Mongan NP. TP53 copy number expansion is associated with the evolution of increased body size and an enhanced DNA damage response in elephants. *Elife.* (2016) 5:e11994. doi: 10.7554/eLife.11994.032

5. Vazquez JM, Sulak M, Chigurupati S, Lynch VJ, A. Zombie LIF Gene in Elephants Is Upregulated by TP53 to Induce Apoptosis in Response to DNA Damage. *Cell Rep.* (2018) 24:1765–76. doi: 10.1016/j.celrep.2018.07.042

6. Ferris E, Abegglen LM, Schiffman JD, Gregg C. Accelerated Evolution in Distinctive Species Reveals Candidate Elements for Clinically Relevant Traits, Including Mutation and Cancer Resistance. *Cell Rep.* (2018) 22:2742–55. doi: 10.1016/j.celrep.2018.02.008

7. Rodríguez A, D'Andrea A. Fanconi anemia pathway. *Curr Biol.* (2017) 27:R986–8. doi: 10.1016/j.cub.2017.07.043

8. Stonez MP, Cho YJ, Huang H, Kim HY, Kozekov ID, Kozekova A, et al. Interstrand DNA cross-links induced by α,β-unsaturated aldehydes derived from lipid peroxidation and environmental sources. *Acc Chem Res.* (2008) 41:793–804. doi: 10.1021/ar700246x

9. Voulgaridou GP, Anestopoulos I, Franco R, Panayiotidis MI, Pappa A, DNA. damage induced by endogenous aldehydes: Current state of knowledge. *Mutat Res.* (2011) 711:13–27. doi: 10.1016/j.mrfmmm.2011.03.006

10. Peake JD, Noguchi E. Fanconi anemia: current insights regarding epidemiology, cancer, and DNA repair. *Hum Genet.* (2022) 141:1811–36. doi: 10.1007/s00439-022-02462-9

11. Tan W, Deans AJ. The ubiquitination machinery of the Fanconi Anemia DNA repair pathway. *Prog Biophys Mol Biol.* (2021) 163:5–13. doi: 10.1016/j.pbiomolbio.2020.09.009

12. Nalepa G, Clapp DW. Fanconi anaemia and cancer: an intricate relationship. *Nat Rev Cancer.* (2018) 18:168–85. doi: 10.1038/nrc.2017.116

13. Niraj J, Färkkilä A, D'Andrea AD. The fanconi anemia pathway in cancer. *Annu Rev Cancer Biol.* (2019) 3:457–78. doi: 10.1146/annurev-cancerbio-030617-050422

14. Stringer C, Pachitariu M. Cellpose3: one-click image restoration for improved cellular segmentation. *Nat Methods.* (2025) 22:592–9. doi: 10.1038/s41592-025-02595-5

15. Lopez-Martinez D, Liang CC, Cohn MA. Cellular response to DNA interstrand crosslinks: the Fanconi anemia pathway. *Cell Mol Life Sci.* (2016) 73:3097–114. doi: 10.1007/s00018-016-2218-x

16. Frost MG, Aboukheili AMM, Toth R, Walden H. Characterization of FANCL variants observed in patient cancer cells. *Biosci Rep.* (2020) 40:BSR20191304. doi: 10.1042/BSR20191304

17. Long DT, Räschle M, Joukov V, Walter JC. Mechanism of RAD51-dependent DNA interstrand cross-link repair. *Science.* (2011) 333:84–7. doi: 10.1126/science.1204258

18. Mogi S, Oh DH. γ-H2AX formation in response to interstrand crosslinks requires XPF in human cells. *DNA Repair.* (2006) 5:731–40. doi: 10.1016/j.dnarep.2006.03.009

19. Clingen PH, Wu JYH, Miller J, Mistry N, Chin F, Wynne P, et al. Histone H2AX phosphorylation as a molecular pharmacological marker for DNA interstrand crosslink cancer chemotherapy. *Biochem Pharmacol.* (2008) 76:19–27. doi: 10.1016/j.bcp.2008.03.025

20. Karimian A, Ahmadi Y, Yousefi B. Multiple functions of p21 in cell cycle, apoptosis and transcriptional regulation after DNA damage. *DNA Repair.* (2016) 42:63–71. doi: 10.1016/j.dnarep.2016.04.008

21. Mullan PB, Quinn JE, Harkin DP. The role of BRCA1 in transcriptional regulation and cell cycle control. *Oncogene.* (2006) 25:5854–63. doi: 10.1038/sj.onc.1209872

22. Renaudin X, Al Ahmad Nachar B, Mancini B, Gueiderikh A, Louis-Joseph N, Maczkowiak-Chartois F, et al. Contribution of p53-dependent and -independent mechanisms to upregulation of p21 in Fanconi anemia. *PLoS Genet.* (2024) 20:e1011474. doi: 10.1371/journal.pgen.1011474

23. Sakai W, Sugasawa K. FANCD2 is a target for caspase 3 during DNA damage-induced apoptosis. *FEBS Lett.* (2014) 588:3778–85. doi: 10.1016/j.febslet.2014.08.027

24. Huang Y, Nakada S, Ishiko T, Utsugisawa T, Datta R, Kharbanda S, et al. Role for Caspase-Mediated Cleavage of Rad51 in Induction of Apoptosis by DNA Damage. *Mol Cell Biol.* (1999) 19:2986–97. doi: 10.1128/MCB.19.4.2986

25. Brown ET, Robinson-Benion C, Holt JT. Radiation enhances caspase 3 cleavage of Rad51 in BRCA2-defective cells. *Radiat Res.* (2008) 169:595–601. doi: 10.1667/RR1129.1

26. Jaber S, Toufektchan E, Lejour V, Bardot B, Toledo F. P53 downregulates the Fanconi anaemia DNA repair pathway. *Nat Commun.* (2016) 7:11091. doi: 10.1038/ncomms11091

27. Suzuki A, Tsutomi Y, Miura M, Akahane K. Caspase 3 inactivation to suppress Fas-mediated apoptosis: identification of binding domain with p21 and ILP and inactivation machinery by p21. *Oncogene.* (1999) 18:1239–44. doi: 10.1038/sj.onc.1202409

28. Suzuki A, Kawano H, Hayashida M, Hayasaki Y, Tsutomi Y, Akahane K. Procaspase 3/p21 complex formation to resist Fas-mediated cell death is initiated as a result of the phosphorylation of p21 by protein kinase A. *Cell Death Differ.* (2000) 7:721–8. doi: 10.1038/sj.cdd.4400706

29. Rego MA, Harney JA, Mauro M, Shen M, Howlett NG. Regulation of the activation of the Fanconi anemia pathway by the p21 cyclin-dependent kinase inhibitor. *Oncogene.* (2012) 31:366–75. doi: 10.1038/onc.2011.237

30. Nakanishi K, Yang Y-G, Pierce AJ, Taniguchi T, Digweed M, D'Andrea AD, et al. Human Fanconi anemia monoubiquitination pathway promotes homologous DNA repair. *Proc Nat Acad Sci.* (2005) 102:1110–5. doi: 10.1073/pnas.0407796102

31. Murina O, von Aesch C, Karakus U, Ferretti LP, Bolck HA, Hänggi K, et al. FANCD2 and CtIP cooperate to repair DNA interstrand crosslinks. *Cell Rep.* (2014) 7:1030–8. doi: 10.1016/j.celrep.2014.03.069

32. Unno J, Itaya A, Taoka M, Sato K, Tomida J, Sakai W, et al. FANCD2 binds CtIP and regulates DNA-end resection during DNA interstrand crosslink repair. *Cell Rep.* (2014) 7:1039–47. doi: 10.1016/j.celrep.2014.04.005

33. Liu W, Polaczek P, Roubal I, Meng Y, Choe WC, Caron MC, et al. FANCD2 and RAD51 recombinase directly inhibit DNA2 nuclease at stalled replication forks and FANCD2 acts as a novel RAD51 mediator in strand exchange to promote genome stability. *Nucleic Acids Res.* (2023) 51:9144–65. doi: 10.1093/nar/gkad624

34. Raderschall E, Bazarov A, Cao J, Lurz R, Smith A, Mann W, et al. Formation of higher-order nuclear Rad51 structures is functionally linked to p21 expression and protection from DNA damage-induced apoptosis. *J Cell Sci.* (2002) 115:153–64. doi: 10.1242/jcs.115.1.153

35. Mauro M, Rego MA, Boisvert RA, Esashi F, Cavallo F, Jasin M, et al. P21 promotes error-free replication-coupled DNA double-strand break repair. *Nucleic Acids Res.* (2012) 40:8348–60. doi: 10.1093/nar/gks612

36. Hafner A, Bulyk ML, Jambhekar A, Lahav G. The multiple mechanisms that regulate p53 activity and cell fate. *Nat Rev Mol Cell Biol.* (2019) 20:199–210. doi: 10.1038/s41580-019-0110-x

Frontiers in Veterinary Science

Transforms how we investigate and improve animal health

The third most-cited veterinary science journal, bridging animal and human health with a comparative approach to medical challenges. It explores innovative biotechnology and therapy for improved health outcomes.

Discover the latest Research Topics

See more →

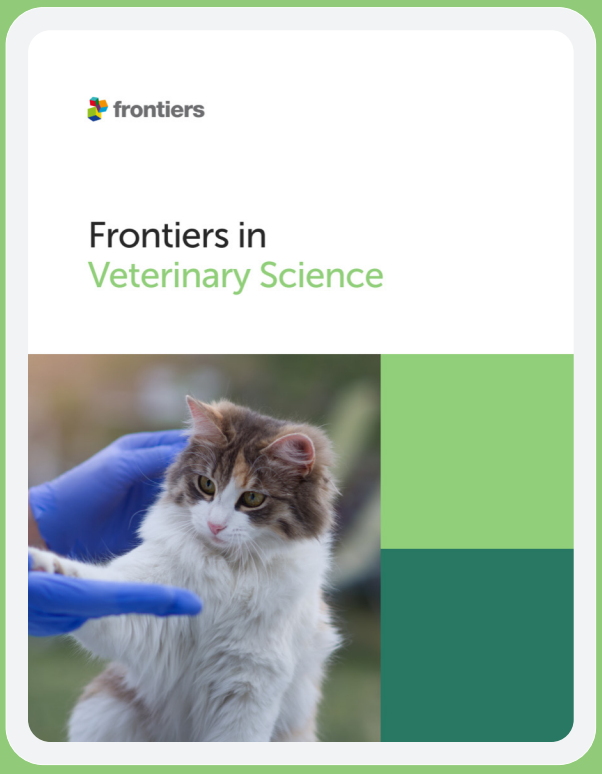

Frontiers

Avenue du Tribunal-Fédéral 34
1005 Lausanne, Switzerland
frontiersin.org

Contact us

+41 (0)21 510 17 00
frontiersin.org/about/contact